Surfactant Migration on Polymeric Substrates

A dissertation submitted to Imperial College London for the degree of Doctor of Philosophy

By

JONA RAMADANI

Department of Chemical Engineering

Imperial College London South Kensington

United Kingdom

SW7 2AZ

May 2022

COPYRIGHT DECLARATION

Jona Ramadani

May 2022

DECLARATION OF ORIGINALITY

I hereby declare that this thesis has been written solely by myself and that it has not been submitted in any previous application for a degree at any other university. All the work in this thesis were designed and planned by me and the experiments were performed by myself unless indicated otherwise. Information presented based on the published and unpublished work used have been acknowledged appropriately and referenced.

Jona Ramadani

May 2022

ACKNOWLEDGEMENTS

ABSTRACT

Many industrial nonwoven polymeric fabrics are coated with surfactants to provide improved wettability which is an essential attribute for disposable hygiene products, like facemasks, wipes, absorbent materials and baby nappies. These surfactant coatings on polyolefinic nonwovens appear to be typically not permanent and this fugitive nature of the surfactants is a concern for the industry. However, the interaction between organic species and complex semi-amorphous polymers as used in nonwoven products is an industrially important but poorly understood research area. Experimental studies reported here have established the mechanisms by which surfactants interact with polyolefinic surfaces, provide visualisation of 3D surfactant distributions on these nonwovens as well as their wettability, and report on the processes responsible for surfactant migration/loss from polyolefins.

A novel confocal microscopy method is reported here for the non-invasive imaging of the 3D distributions of surfactants on polymeric nonwovens. Optical contrast was achieved by introducing a fluorescent dye via vaporisation at elevated temperatures, which preferentially dissolves into the hydrophilic surfactant regions of the nonwoven sample. The method is quantitative and allows the patch wise heterogenic distribution of surfactant coatings on complex 3D nonwoven materials to be visualised.

To understand the interaction between surfactants and nonwoven polyolefins, several chemical properties and physicochemical descriptors of nonwoven materials were determined including wettability, specific surface area, surface energy, solvent sorption kinetics, and their surface elemental composition. Specific surface area BET measurements demonstrated that industrial nonwovens are characterised by generally low specific surface area values, in the range 0.1 - 4 m^2/g and that inverse gas chromatography (IGC) offered best sensitivity and precision. The wettability of polyolefin surfaces is well described by the dispersive contribution of surface free energy γ_s^D. Alkane probes are normally used for measuring γ_s^D but dissolve in polyolefins invalidating the method. A new method using a series of normal alcohols was developed as part of this work, yielding γ_s^D values in the range 20 - 40 mJ/m^2. XPS analysis confirmed the hydrocarbon nature of polyolefinic nonwoven materials and the polar elements present responsible for the hydrophilic nature when the nonwovens were coated with surfactants, confirming surfactant treatment was not permanent.

The solubility interactions between organic solutes and a range of amorphous and semicrystalline PP and PE were investigated by DSC, pycnometry, dynamic vapour sorption

(DVS) and ellipsometry. The work confirmed that the presence of crystalline regions decreased the sorption of organic solutes in polyolefins. DVS studies of the sorption and desorption kinetics for small organic molecules in polyolefin films demonstrated that temperature increased diffusion rates and the amounts of solutes sorbed. However, increasing molecular size, or polarity, of the solute decreased the solubility.

DVS combined with ellipsometry was used to determine the processes responsible for surfactant loss in thin polyolefin films. The amount of water sorbed by a polyolefin material was used here for the first time as a proxy for the amount of surfactant present on the polyolefin surface. DVS studies confirmed very slow mass losses due to surfactant evaporation from the surfactant coated polymers. However, the total rate of surfactant mass loss from the polymer surface was 10 times higher than the evaporative losses. The significant solubility of the non-polar surfactants and organic solutes in different polymer analogues was experimentally estimated. Based on these studies the hypothesis was that there are two processes causing surfactant loss from the polyolefin surface:

- slow surface evaporation of the surfactants into the surrounding environment
- a faster concurrent dissolution of the surfactant into the bulk polyolefin

In summary, this thesis, provides new experimental insights into the interaction between liquid solutes, including surfactants, with semi-amorphous polyolefin materials including nonwoven fabrics.

PUBLICATIONS

Manuscripts in preparation/ submission/ review

Ramadani, J., Claussen, J., Williams, D.R. 3D Confocal Imaging and Quantification of Surfactant Distributions on Polymeric Porous Media. submitted to Journal of Colloid and Interface Science. (2021)

Ramadani, J., Williams, D.R. Studies on the Diffusion Characteristics of Small Molecules into Polyolefins. submitted to Analytical Chemistry (2022)

Ramadani, J., Williams, D.R. IGC Characterisation of Polyolefin Materials using Polar Probes. submitted to Journal of Chromatography A (2022)

Valsecchi, M., **Ramadani, J**., Galindo, A., Jackson, G., Williams, D.R. The effects of tie-chains and microstructure on the solubility of gases in semi-crystalline, in preparation to Macromolecules. (2022)

CONFERENCE PAPERS / ORAL PRESENTATIONS

Ramadani, J., Williams, D.R., Caputi, M., Ambrogio, I. *An Investigation of Surfactant Migration in Polymeric Substrates*. 8th Pacific Basin Conference on Adsorption Science and Technology (PBAST-8). Sapporo, Japan. 3 - 6 September 2018. Oral and poster presentation.

Ramadani, J., Williams, D.R., Caputi, M., Ambrogio, *Mapping of Surfactants on Polymeric Substrates using Confocal Fluorescence Microscopy*. Procter & Gamble Chemical Engineering Symposium, Imperial College London 27 September 2018. Oral and poster presentation.

Ramadani, J., Williams, D.R., Caputi, M., Ambrogio, I. *Surfactant Migration on Polymeric Substrates*. Society of Chemical Industry (SCI) Postgraduate Scholars' Showcase London, 3 July 2019. Oral and poster presentation.

Ramadani, J., Claussen, J., Williams, D.R. *A Novel Method for Determining Surfactant Distribution on Polymers using Confocal Laser Scanning Fluorescence Microscopy.* AICHE Annual Meeting, Orlando, 10-15 November 2019. Oral presentation.

Ramadani, J. *Using science to create better nappies!* SCI's 139th Annual General Meeting (AGM) 2020 - Society of Chemical Industry (SCI) London, 1st July 2021. Online Oral presentation.

TABLE OF CONTENTS

TABLE OF FIGURES

xxi

ABBREVIATIONS

AFM	Atomic force microscopy
aPP	Atactic polypropylene
AU	Airy unit
BET	Brunauer–Emmett–Teller theory
CA	Contact angle
CMC	Critical micelle concentration
CLSM	Confocal laser scanning microscopy
CFM	Confocal microscopy
DIM	Diiodomethane
DSC	Differential scanning calorimetry
DVS	Dynamic vapor sorption
FTIR	Fourier transform infrared spectroscopy
FID	Flame ionisation detector
HDPE	High-density polyethylene
RH	Relative humidity
IGC	Inverse gas chromatography
iPP	Isotactic polypropylene
IR	Infrared spectroscopy
LDPE	Low-density polyethylene
MDPE	Medium-density polyethylene
PE	Polyethylene
PP	Polypropylene
Peak COM	Centre of mass of peak
Peak Max	The time which belongs to the maximum FID signal
Relative STD	Relative standard deviation
SEM	Scanning electron microscopy
STD	Standard deviation
SSA	Specific surface area
TOF-SIMS	Time-of-flight secondary ion mass spectroscopy
XRD	X-ray diffraction
XPS	X-ray photoelectron spectroscopy

1 Introduction

1.1 Background

A journey back in history highlights materials as an important aspect of civilizations such that entire periods of time have been defined by the critical material used e.g., the "Stone Age, Bronze Age and the Iron Age". The prehistoric men and women had a limited number of materials at their disposal, stones, bones, leather, natural fibres, grasses, and wood. In rare instances metals like gold and copper were found directly from the Earth by some ancient cultures. However, these metals are soft, and they were mostly used for jewellery, decorative and cooking items, rather than tools. For over 2 million years, humans lived using only these naturally occurring and easily obtained materials in a period known as the Stone Age. Around 5,000 years ago, humans discovered that adding other elements to copper, particularly tin, made it much stronger, and therefore allowed much stronger and more durable tools to be produced than had been possible before. This alloy of copper and tin is called bronze and so the Stone Age became the Bronze Age. Nearly two thousand years later, humans learned to turn iron oxide into iron and steel by smelting, and the Bronze Age became the Iron Age. The smelting technique uses heat and chemical reactions to produce metal from the more complex mixture of minerals found in ore. Much of this focused on the manufacture of weaponry, (swords, shields, armour etc) from steels. Early metallurgists found that very small additions of carbon to iron, combined with heat treatments, lead to massive increases in strength.

As cultures grew more technologically capable, they gradually developed some of the familiar tools and technologies we know today. The earliest method for producing glass from the melting of sand and other quartz-based minerals, developed around 2500 BCE. The introduction of paper to Europe (first developed in China around 200 CE) and invention of the printing press in 1450 were important technological developments. The Industrial Revolution began around 1760 and marked the introduction of a new period of scientific and technological breakthroughs, including the development of steam power, factory manufacturing and the use of iron and cement as structural materials. In 19th century scientists modified colloids and natural polymers to form new materials. John Wesley Hyatt, an American inventor, produced a new material called celluloid from natural cellulose which was used to make movie films and billiard balls. Soon after, scientists moved on from simply mixing and modifying natural polymer materials to making man made macromolecules. Humans created an entirely new class of materials by manipulating the structure of the carbon bond, and forming catenated molecular structures, polymers. This era was inaugurated in 1907 by Leo H. Baekeland, the inventor of the first synthetic plastic, Bakelite. He took two ordinary chemicals, phenol and formaldehyde,

mixed them in a sealed vessel, and subjected them to heat and pressure. This was the first man made plastic to be created entirely from organic chemicals.

Bakelite featured extraordinarily high resistance to electricity, heat, and chemicals and therefore was a suitable material for the emerging electrical and automobile industries. It found a place in almost every area of modern life, from jewellery to radios and telephones. Baekeland's new material opened the door to the Age of Plastics. In 1920, Hermann Staudinger postulated that materials such as natural rubber have very high molecular weights. In a paper entitled "Über Polymerisation[1]" Staudinger[2] introduced the process of polymerisation for creating macromolecules by linking together, (via covalent bonds) many small molecules. This new concept covered both synthetic and natural polymers and was the key to a wide range of modern polymeric materials and innovative applications. The early 1900s was the pinnacle for development of new synthetic polymers. Scientists were synthesizing new monomers from abundant and inexpensive raw materials. Earlier examples include the large-scale production of vinyl-chloride resins in 1927, the invention of polystyrene in 1930, and nylon in 1938.

While improvements have taken place in all areas of materials over the last 100 years, it is the field of polymers that has experienced arguably the largest upsurge in progress. Polymers have transitioned from being cheap substitutes for natural products to providing high-quality and high-performance options for a wide range of applications, becoming the material of choice for many high technology and low technology applications. Nowadays, polymers are widely utilised advanced materials, found almost in every product used in our daily life such as clothing[3], food packaging, medicines, transportation and building equipment, cosmetics and hygiene products, the list [4-10] is endless. Among all synthetic polymers in use globally, olefin polymers such as polypropylene (PP) and polyethylene (PE) are the most popular thermoplastic polymers[4] used for a variety of applications, as depicted in Figure 1. 1.
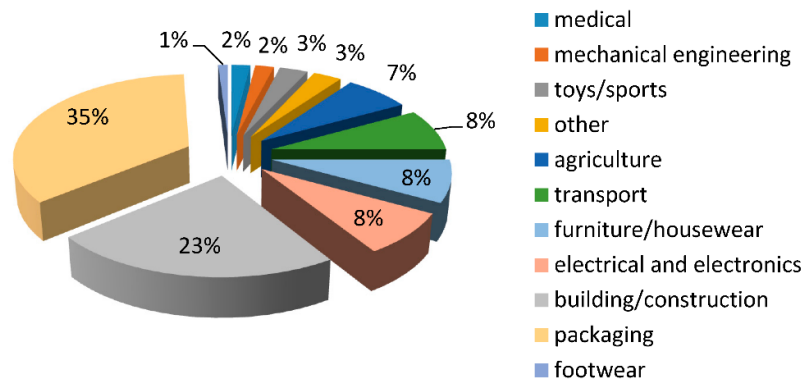
Figure 1. 1 Industrial applications of polyolefins[11].

It is a remarkable fact that the world's most ubiquitous thermoplastic PE was invented by accident during high-pressure experiments conducted in 1933 by ICI scientists, Fawcett and Gibson. PE has many useful properties including its strength and hardness, highly ductile, water resistant and durable, good electric insulator, low cost, low density and almost all forms can be recycled. However, PE has a few disadvantages. Like many other plastics, it takes a long time to naturally break down in the environment, and as such can end up in landfill for decades. Producing PE takes a large amount of energy and leads to high emissions of carbon dioxide, a greenhouse gas contributing to global warming and climate change. The second most used thermoplastic in the world is polypropylene (PP). This material is a rigid, semi-crystalline thermoplastic that was first polymerised in 1951. Its popularity is due to its highly flexible properties, toughness, low density, and ability to adapt to a range of fabrication techniques. PP is waterproof and extremely resistant to moisture absorption. Like PE, it also has the same key disadvantages when it comes to the wider environment and preservation of global resources.

Virtually all polymers used are from petroleum-based products, and although they are durable in use, they are also durable in waste. An estimated 60% of global plastic waste is used only once before it is discarded, producing a stream of waste in waterways and landfill. Figure 1. 2 show that the share of global plastic waste that is discarded, recycled or incinerated from 1980 through to 2015. It was the plastics industry that offered recycling as a solution in the 1980s. Recycling is a process that breaks down and reuses some types of plastics and other materials to make new products. However, recycling is far from perfect. This is an energy-consuming process and subsequently only about 20% of all plastics are recycled, shown in Figure 1. 2 ; most plastics still end up in landfills.
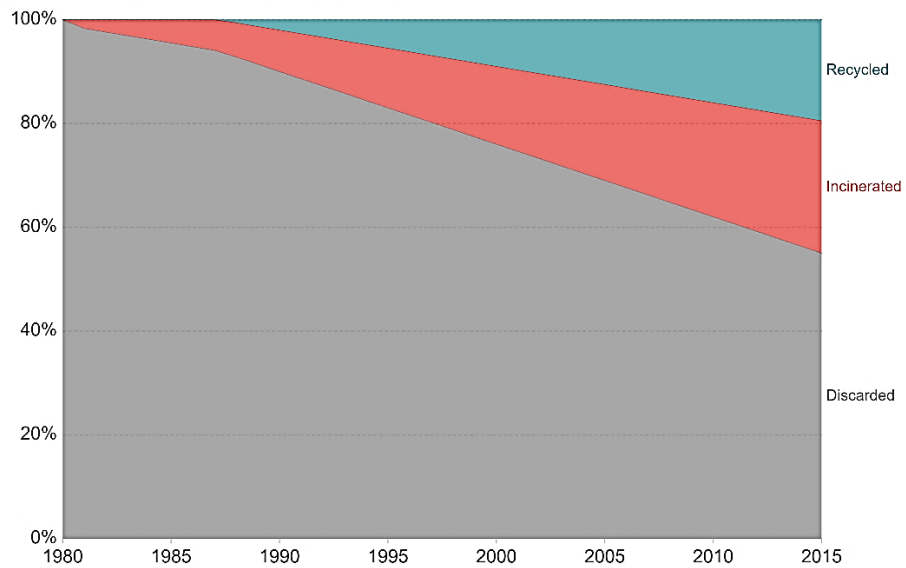
Figure 1. 2 Estimated global plastic waste by disposal method, 1980 to 2015[12].

The numbers found on the underside of many plastic products are used to sort them for recycling. These are the ASTM International Resin Identification Coding System, often abbreviated RIC. The numbers and letters correspond to specific polymer types and are used to facilitates an efficient recycling process. The system for categorising plastics was first introduced by the Society of the Plastics Industry (SPI) and Table 1. 1 displays the seven pictograms of the code numbers associated with the different plastic materials used in industry.

Table 1. 1 The code numbers for various types of plastics established by the SPI along with use examples.

Code	Examples of use
1 PET	Source: stevegalloway.mycouncillor.org.uk
2 HDPE	Source: keeptruckeegreen.org
3 PVC	Source: omnexus.specialchem.com
4 LDPE	Source: ldpebag.com
5 PP	Source: hyosungchemical.com
6 PS	Source: styrofoamdensifier.org
7 Other	Source: recyclenation.com

The past decade has seen an increased interest on development of materials that are biodegradable and are made from renewable resources such as plants. A query on PubMed shows that there has been an increase in the number of publications on biodegradable polymers, presented in Figure 1. 3. This surge in research will undoubtably pave the way for the transfer of the science from the laboratory and into the mass production of biodegradable materials.
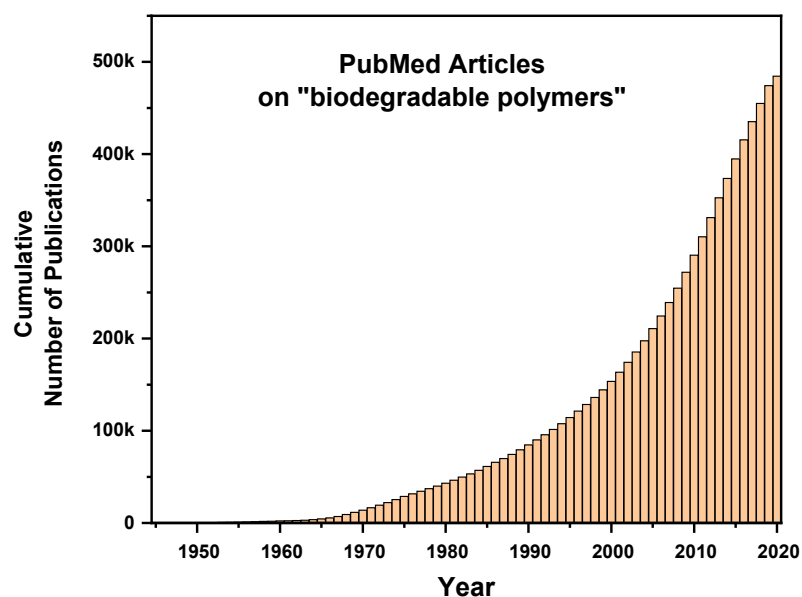
Figure 1. 3 Publication history on biodegradable polymers (information obtained from PubMed).

Polymers based on natural starch are already in the market as is synthetic polylactide (PLA), which is made from lactide or lactic acid derived from biological sources and may be found in products from tea bags to medical implants. But sustainable polymers still make up less than 10% of the total plastics. A key hurdle is that they cost too much, and another is that they do not always perform as well as traditional polymers. Material scientists hope that these new class of plastics will have equivalent properties to petroleum-based plastics, but with environmental benefits. One alternative approach is to blend sustainable polymers such as PLA with conventional polymers to make them tougher. Other alternatives involve learning to use natural polymers directly. Some innovators are developing bioplastics, which are made from starch (e.g., polylactide), bacterial polymers (polyhydroxyalkanoates), cellulose, and compositions based on shellac, zein and other pro-ecological ingredients[13, 14] Others are searching for ways to make recycling more efficient, and they even hope to perfect a process that converts plastics back into the fossil fuels from which they were derived. In the current era of sustainability all these innovators recognise that man made plastics are not perfect, but that they are an important and necessary part of our future so, this remains an evolving area of material engineering.

The increasing global demand for personal and health-care products, (due in part to a steady growth in global human population), has resulted in strong competition for unique and improved absorbent products and materials. Personal care hygiene products represent a multibillion-dollar business[15]. This constitutes the growing basic care needs of hundreds of millions of

6

infants, children, hospital patients as well as millions of women using feminine hygiene products, and adults suffering from incontinence worldwide.

The unique properties of PP and PE make them excellent candidate base materials for manufacturing nonwoven fabrics for use in disposable hygiene products including facemasks, wipes, absorbent materials as well as other personal care products. A typical example is the disposable nappy. The basic structure and composition consists of four main functional layers as shown in Figure 1. 4, most of which are coated with surfactant(s) to aid the transfer of fluids to the absorbent internal layers. The top sheet is composed of soft, porous polypropylene or polyethylene, or PE/PP blended non-woven fabric. The core cover is made of a porous polymer non-woven fabric that are both soft and hydrophilic, being effective at quickly absorbing the liquid and transferring it to the absorbent layer, which is the storage layer of the nappy. Then there is the outer cover of the nappy, the back sheet which is water-proof typically made of soft textured, polypropylene laminated with a polyethylene film [16] to help prevent wetness from transferring outside the nappy.
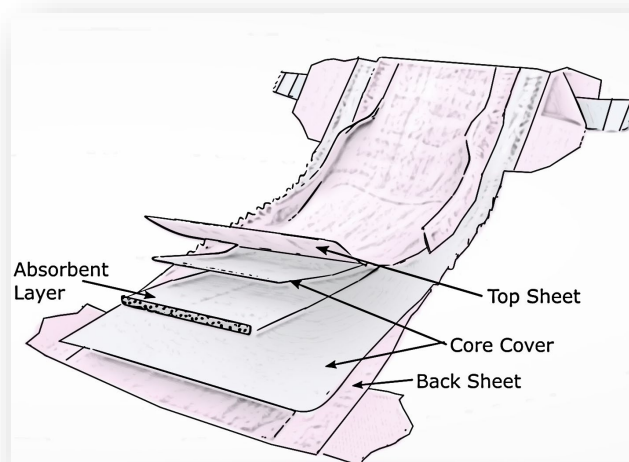
Figure 1. 4 Typical disposable nappy design. Adapted from Bostik.com[17]

Polyolefins are commonly used in the hygiene industry alongside natural and synthetic fibers such as cotton and polyamide (nylon) because they have ideal melt rheological characteristics essential for fiber formation with high crystallinity. Although, nonwoven fibers are manufactured by high speed and low-cost processes [3], they are versatile materials which can be engineered to deliver a diverse range of properties. PP and PE fibres, and their copolymers, are the predominant raw material used in the nonwoven industry accounting for 63%[3] of all production. The success can be associated with properties such as their low density, low cost, chemical stability, good fluid handling, mechanical strength and abrasion resistance. When a nonwoven

fabric is formed from a hydrophobic polymer, it is often desirable to modify the surface of the nonwoven to increase the wettability, transforming a hydrophobic nonwoven into a fabric which readily assimilates and distributes aqueous fluids. Several effective methods have been developed to convert PE/PP nonwovens into hydrophilic materials including plasma/corona treatment[18-23], grafting modification[24-26], and blending/coating with hydrophilic materials[27-31]. All of the nonwoven materials used in this research are made hydrophilic by coating with surfactants, converting them into wettable materials, and thus allow water to pass through them. Coating nonwoven fabrics with surfactants changes their wetting characteristics making them hydrophilic. This characteristic is obvious if two samples, one surfactant coated and another uncoated, are placed into an aqueous solution, as shown in Figure 1. 5. The uncoated, hydrophobic sample, (right), floats on top of the solution whereas the coated, hydrophilic, sample, (left) immerses into the solution. This phenomenon is easy to see but difficult to quantify.
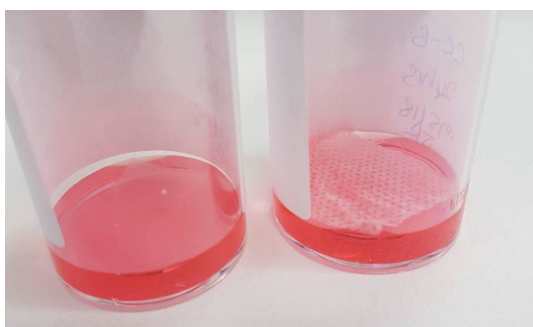
Figure 1. 5 Photograph of coated, (left) and uncoated, (right) nonwoven samples immersed in basic red 14 aqueous solution.

It is a common industrial experience that the surface hydrophilicity of these industrial coated polyolefinic materials is time dependent and significant losses in the surface concentrations of surfactants are observed[32]. The decreasing amount of surfactant on polyolefinic nonwovens reduces their hydrophilicity and compromises their performance. Therefore, maintaining the amount of surfactant on some of these nonwovens rigorously is a critical product attribute. Consequently, studying and understanding how the surfactants interact with solid state polyolefins and their fugitive nature of surfactants in complex 3D polyolefinic fiber networks is of paramount importance for the successful manufacturing of many classes of personal care and related hygiene products.

1.2 Thesis Outline

Chapter 1 charts the overall progress of man-made materials including the developments in man-made polymers over the last 100 years, leading on to the world's two most popular

polymers PP/PE and describing their transition into the materials of choice for the manufacture of personal and hygienic care products. Key attributes of these materials are briefly discussed.

Chapter 2 forms the literature review of this thesis. It starts with an introduction to properties and structures of the materials relevant to this research. Polyolefins in nonwoven forms and the surfactants used to coat nonwoven materials are reviewed. It also presents the different manufacturing approaches for controlling surface properties of these polymeric fibers for the intended industrial purposes. Surfactant-polymer systems such as coatings/films, mixtures and the interactions at interfaces have also been explored together with solubility of solutes and surfactants in polyolefins. Finally, this Chapter concludes with a gap analysis of the research underpinning the underlying research questions arising from the literature. It also presents the aims and objectives of the overall thesis.

Chapter 3 provides details of the wide-ranging experimental materials and methodology utilised in this thesis.

Chapter 4 focuses on the experimental characterisation of the surface properties of polyolefin-based nonwovens, including those coated with surfactants manufactured via standard high speed, low-cost coating processes used for production of disposable baby nappies. To understand the interaction between surfactants and polyolefins, several chemical properties and physicochemical descriptors of these materials were investigated including wettability, specific surface area, surface energy, sorption kinetics, and their elemental composition. Techniques such as IGC, BET, and contact angle were used to determine surface properties, including the determination of surface thermodynamics and related physiochemical properties of polymeric nonwovens. XPS, was also used to measure the surface elemental composition of the substrate to establish chemical differences between surfactant coated and uncoated samples and image surfactant distribution/heterogeneity across the material surface.

Chapter 5 details a novel method developed as part of this research for visualising in 3D and quantifying surfactant distributions on complex polymeric nonwoven fabrics using confocal laser scanning microscopy (CLSM). In this method solid-state fluorophores are introduced to the samples via vapor phase staining. Since polyolefinic non-woven materials comprise of a web of fibres with voids and intersections randomly oriented, then unavoidably the surfactant coating is also randomly distributed throughout the non-woven network. This Chapter, in line with wettability studies, confirmed the patch wise topographical heterogeneity of the surfactant coated nonwovens.

Chapter 6 and 7, focuses on understanding the fugitive nature of surfactants in polyolefins. These Chapters provide comprehensive experimental studies using characterisation methods such as DSC, pycnometry, DVS and ellipsometry to study bulk properties of amorphous and semicrystalline PP and PE, as well as for these polymers in contact with solutes including surfactants. Specifically, Chapter 6 outlines experimental studies to investigate the solubility of small molecules in polyolefins which involves mainly DVS experiments. Chapter 7 provides a series of systematic experimental results which reveal the processes responsible for surfactant losses in polyolefins, including surfactant losses from industrially relevant polyolefinic nonwovens. The amount of water dissolved in the material was used here for the first time as a proxy to the amount of surfactant present on the polymer sample surface. Techniques such as DVS, Ellipsometry, DSC, and helium pycnometry and were utilised for studying thin polyolefin films casted on SiO_2 wafers (via spin coating) and alumina (via dip coating) which were used as model substrates for this research.

Chapter 8 provides a discussion summarising the results and findings from this thesis. It also offers explanations of the fundamental understanding of the mechanism by which surfactants are lost. This Chapter concludes by providing recommendations for future work in this area.

1.3 Project Management

All the experiments were carried out at Imperial College London under the supervision of Professor Daryl Williams except the Confocal Laser Scanning Microscopy experiments which were carried out at P&G in Egham & Reading sites in the UK. All the nonwoven and woven based materials used in this research were provided by P&G Germany. The customised sample preparation units made of brass were designed in collaboration with Jonathon Henton from the Chemical Engineering workshop at Imperial College London who then fabricated them.

2 Literature Review

2.1 Introduction

As discussed briefly in the first Chapter of this thesis, human history is shaped by the materials we develop and use, and today we are faced with a bewildering choice of materials. As scientists and engineers, a clear understanding of materials and their properties is vital in order to select the right material for an application, assess product liability, develop and automate production techniques, design for recyclability, solve problems, challenge and replace traditional materials with the ultimate aim to improve products and their performance while sustaining our natural habitat and resources. Therefore, this Chapter explores the literature around the materials relevant to this research and discusses the experimental methods relevant for studying such materials. This Chapter concluded by identifying the current gaps in the research landscape in the context of this research topic, and subsequently sets out the overall aims and objectives of this thesis.

In 2019, the production of plastics totalled around 368 million metric tons worldwide.[33] Their success results mainly from their ease of production and processing, low costs as well as from the diversity of their properties. Polymers today are widely used advanced materials, which are found almost in every product we use in our daily life. The word "polymer" comes from Greece and it means "many parts". They are long chain molecules that can be naturally occurring or synthetic. A polymer is a large molecule, (macromolecule) composed of repeating structural units known as monomers[34]. Monomers are generally simple organic molecules with an intrinsic chemical reactivity which allows links with each other to form long molecular chains. These chemically form in a repetitive linear fashion in some cases and in other cases the chains are branched or interconnected to form 3D networks. Polymers both natural and synthetic, are created via the polymerisation of monomers which are covalently bonded, forming long chains or a network. The use of polymers for different purposes is guided by various molecular and bulk properties. Numerous polymer classifications exist, and one common way to classify synthetic polymers is based on their thermal response and their molecular structure, such as crosslinking, crystallinity and amorphicity, which lead to 3 major classes of polymers as shown in Figure 2. 1.

Polymers
├── Thermoplastics
│   ├── Crystalline
│   └── Amorphous
├── Thermosets
└── Elastomers
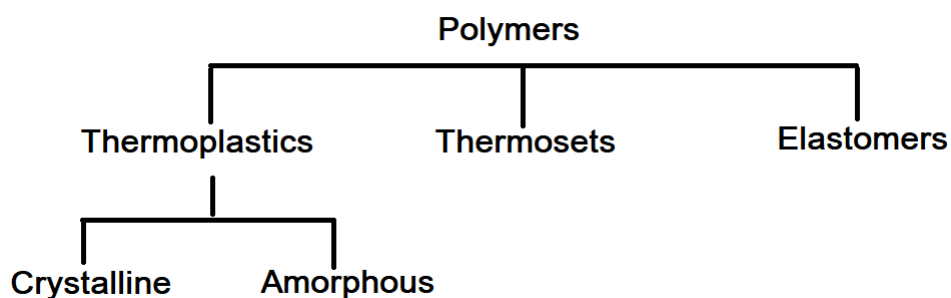
Figure 2. 1 Classification of polymers.

Thermoplastic polymers can be either amorphous[35] (random arrangement of the chains) or crystalline[36] (regular arrangement of the chains) or semi-crystalline. Their linear long chain molecules are held together by weak intermolecular forces; van der Waals forces[34]. The glass transition temperature can be considered as the temperature at which the intramolecular forces for amorphous materials are overwhelmed by thermal motions, resulting in local polymer flow. Thermoplastics can be melted and reformed on heating allowing them to be easily recycled.

Thermoset polymers are crosslinked. They normally exist as solids at room temperature, and if heated sufficiently will take on the behaviour of a crosslinked elastomer. Elastomers are rubbery polymers that can be stretched with a low cross-link density. At room temperature the polymer chains have sufficient thermal energy to overcome some of the secondary van der Waals bonds, thus have some viscoelastic freedom to move. However, the cross-links that exist in the structure act to recover the elastomer back to its original form following deformation.

A major feature of all these polymers is their large molecular weights from 10,000 to 1,000,000 daltons (Da) are common[37]. Unlike small molecules such as octane or cyclohexane a synthetic polymer has no single, fixed molecular weight but a distribution of molecular weights so an average molecular weight is quoted for these materials rather than a single value[38].

Around 90% of the total demand for all polymers by weight is accounted for by five main so called commodity plastics: polypropylene (PP), polyethylene (PE), polyvinyl chloride (PVC), polystyrene (PS) and polyethylene terephthalate (PET). This thesis is concerned with PP and PE thermoplastic polyolefins.

2.2 Polyolefins

2.2.1 Polypropylene structure, properties, and applications

Polyolefins are the most widely used synthetic polymers. They can be divided into two main types, PP and PE, which are subdivided into several grades for different applications[39]. They are produced mainly from oil and natural gas based chemicals by the polymerisation of propylene and ethylene respectively. Several factors have been principally responsible for the great success that polyolefins have enjoyed: an abundant supply of cheap and simple monomers; advances in reactor engineering and catalysis; and the ability to compound these polymers with fillers and other polymers. For example, the discovery of Ziegler Natta catalysts[40] in the 1950s, which reduces the reaction activation energy, accelerated the popularity of these polyolefins because it made their synthesis easier, at low costs, with higher yield and with better molecular mass control.

In 1954, Giulio Natta discovered PP which is a tough, rigid and semi-crystalline thermoplastic produced from propene (or propylene) monomer as shown in Figure 2. 2. The propene molecule, $CH_2 = CH(—CH_3)$, is unsymmetrical with a methyl group appended to one of the carbons in the carbon-carbon double bond. The methyl group has a relatively larger size which occupies space such that it imposed a degree of steric hindrance to one side of the π(pi) bond in the molecule.
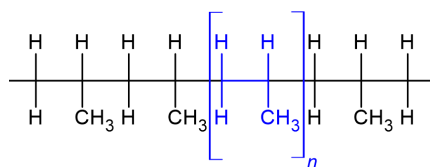
Figure 2. 2 Molecular structure of PP.

Olefin molecules that contain one unique side group, such as polypropylene, possesses an asymmetric carbon centres[41]. The position of these asymmetric centres defines the tacticity of the polymer which in turn affects its bulk physical properties. Polypropylene is found in three stereo specific configurations: isotactic, (methyl groups on one side of polymer backbone), syndiotactic, (methyl groups alternate on both sides) and atactic, (irregular arrangement of methyl group) as shown in Figure 2. 3. Atactic PP is amorphous and has the least commercial value. Both isotactic and syndiotactic PP are semicrystalline polymers with high melting temperatures, but it is the isotactic PP which dominates the market because of the arrangement of methyl groups oriented on one side of the carbon backbone creating a greater degree of crystallinity which results in a stiffer material that is resistant to creep.

13

Isotactic : methyl groups occur on the same side

H H H H H H H H H

CH_3 CH_3 CH_3 CH_3 CH_3 CH_3 CH_3 CH_3 CH_3

Syndiotactic: methyl groups alternate

H CH_3 H CH_3 H CH_3 H CH_3 H

CH_3 H CH_3 H CH_3 H CH_3 H CH_3
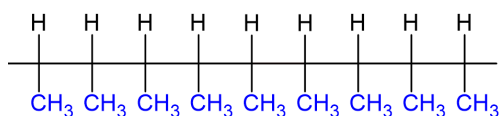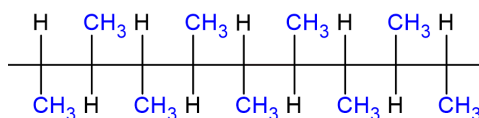
Atactic: methyl groups irregularly distributed

CH_3 CH_3 H CH_3 H CH_3 CH_3 CH_3 H

H H CH_3 H CH_3 H H H CH_3
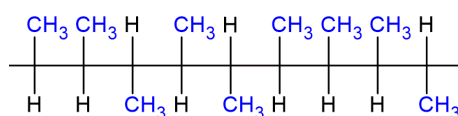
Figure 2. 3 Stereochemical structures of PP.

There are three major sources of propylene: from steam cracking of naphtha, gasoline refining process and propane dehydrogenation technology. For industrial applications, PP is made from polymerization of propene monomer by Ziegler-Natta polymerization or metallocene catalysis polymerization. Metallocenes are single-site catalysts that are used to make PP with uniform microstructures different to those made with Ziegler–Natta and Phillips catalysts[42]. Melting point of isotactic PP is 171°C, but syndiotactic PP (30% crystallinity) has a melting point of 130°C. Isotactic PP has a crystalline structure with a high level of stiffness and a high melting point compared to other commercial thermoplastics. PP is a lightweight polymer with a low density of ~ 0.90 g/cm^3, chemical inertness and crystallinity of PP is typical between 40-60%. Different microstructures structures of PP are possible by using fillers, reinforcing agents or by blending PP with other polymers which can yield superior performance. In addition, PP is a low-cost thermoplastic polymer with excellent properties like flame resistance, transparency, high heat distortion temperature, stability, low water absorption, good electrical resistance, a lightweight, high impact strength, a non-toxicity property and recyclability making it ideal for a wide range of short and long-life applications. These range from automobile components to packaging, from construction products to consumer goods and medical applications. PP is used to produce clothes and personal care hygiene products like nappies or sanitary products where, once it is treated, it is a key component for these liquid management products. It is this later application which this thesis will focus on.

2.2.2 Polyethylene structure, properties, and applications

Another common plastic type is PE which consists of ethene (or ethylene) monomers, $CH_2 = CH_2$, as shown in Figure 2. 4.
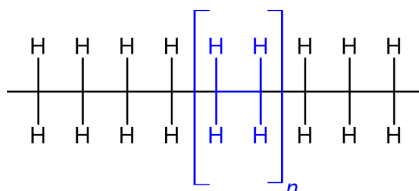
Figure 2. 4 Molecular structure of PE.

There are several types of PE. The most known and studied PEs are linear low density (LLDPE), low density (LDPE), medium density (MDPE) and high density (HDPE). This traditional classification distinguishes each polyethylene type according to its density, which ranges between 0.910 - 0.970 g/cm^3, although these limits may vary slightly among different sources. In general, HDPE and LDPE are the most commonly used PE. HDPE is a cost-effective thermoplastic with linear structure and no or a low degree of chain branching. It is manufactured at low temperature (70-300°C) and pressure (10-80 bar) and derived from either modifying natural gas (a methane, ethane, propane mix) or the catalytic cracking of crude oil into gasoline. High density polyethylene is flexible, translucent/waxy, weather resistant, and displays toughness at very low temperatures. LDPE is a semi-rigid and translucent polymer. Compared to HDPE, it has a higher degree of short and long sidechain branching. It is produced at high temperature (80-300°C) and pressure (1000-3000bar) via free radical polymerisation processes. PE's including LDPE and HDPE are non-biodegradable in nature and contribute significantly to the world's plastic waste products. Both these forms are recyclable and can be used to produce bottles for non-food items, plastics for outdoor applications, compost bins, etc. In a solid form PE is generally considered to be safe and non-toxic, but could be toxic if consumed, as in the current global concern around microplastics. HDPE contains low levels of chain branching which confers intermolecular forces, crystallinity levels and tensile strength which is higher than in LDPE. LDPE has high degree of short and long chain branching. Furthermore, HDPE has a physical structure that can withstand higher temperatures (120 °C) and it is harder and opaque whereas, LDPE supports temperatures at 80–95 °C for a short time, being considered non-reactive at room temperature.

In PE, local chain structure is sufficiently regular to give rise to a crystalline phase. Entanglement of chains, chain branching, and the presence of end groups prevents complete

crystallisation of a polymer. Polymeric materials which contain crystallinity are always described by a multi-phase model, i.e., semicrystalline, which includes an amorphous and crystalline phase in coexistence. LDPE contains a low crystalline and high amorphous component, (<50% crystalline) whereas HDPE is characterised by high crystalline and low amorphous elements, (>60%). A critical discussion of the meaning and measurement of crystallinity in polymers was given by Kavesh and Schultz[43].

European studies have described that in the last 15 years the use of PE has been growing at about 12% per year, with approximately 140 million tons of synthetic polymer produced annually worldwide. Some of the uses of HDPE include packaging applications, consumer goods, fibres and textiles, construction, automotive industry, and telecommunications. LDPE uses majorly revolve around manufacturing household appliances, electronics, automobiles, and various laboratory equipment. The most popular application of LDPE is plastic bags.

2.2.3 Mixtures and copolymers

Polymerisation of organic compounds has been known for over 100 years, however, simultaneous polymerization, (co-polymerisation) of two or more monomers is a more recent discovery. For example when copolymers of olefins and diolefins were found to have rubbery properties and were more useful than homopolymers made from single monomers. When two or more polymers are mixed, the product is known as a polymer blend. Polymer blending is a simple and economically viable route to develop composite materials with superior properties than the parent homopolymer phases. There are several driving forces for blending two or more existing polymers. The goal is to achieve a material having a combination of the properties unique to each of the components, such as chemical resistance and toughness but at lower cost for example. So, a high-performance material can be blended with a lower-cost polymer to expand market opportunities. Blending polymers of different types such as adding elastomeric filler materials to rigid and brittle polymers for the purpose of toughening is another example. However, sometimes when polymers are blended, some critical properties may be severely weakened because of incompatibility[44, 45]. The area of polymer blends is one of the routes to new materials that is most actively pursued by the polymer industry. However, due to inherent immiscibility with other macromolecules, the desired properties are often not realised by mere blending[46]. For example, polymeric membranes, in general, are derived from phase inversion process track etching or by solvent free methods like stretching melt-cast polymer films.

A wide range of improved mechanical properties may be achieved using copolymerisation, blending, and additives. Propene and ethene may be copolymerised using metallocene catalysts to provide a range of polymer structures that are essentially elastomeric copolymers[47]. The PP copolymer family with different monomer types can be divided into random copolymers and block copolymers produced by polymerising of propene and ethene. Random copolymers (RCP) are ethylene/propylene copolymers that are produced in a single reactor by copolymerising propylene and small amounts of ethylene. Impact resistant copolymers (IRCP) are physical mixtures of a homopolymer PP, (one monomer type) and elastomer particles. The ethene content in most of these blends is reported[48] to be less than 20% and so in some respects these copolymers have the desirable properties of isotactic PP[49] in terms of relatively low cost, good chemical resistance and ease of manufacture, but with much improved impact behavior[44]. Structurally the propene repeat units along the polymer chain are predominantly in an isotactic arrangement which leads to crystalline thermoplastic zones. If such copolymers have high levels of crystallinity, they are more likely to be thermoplastic isotactic PP and are not elastomers. Isotactic PP has been blended with various types of PE[50], (HDPE, LDPE, LLDPE), as well as with PET to increase strength, polystyrene improves both the rigidity and creep resistance of the blend, with other polypropylenes of different isotactic content, tacticity or molar mass to improve interfacial adhesion and with polylactic acid (PLA) to produce partially biodegradable materials. Amongst many other applications these copolymers are finding use in the production of nonwoven fabrics[51].

2.3 Nonwovens

All nonwoven materials are made from fibres or continuous filaments which are laid down to form a web which is then bonded using chemical, heat or mechanical processes[52]. PP and PE are widely used in nonwoven manufacturing and result in products with a complex 3D structure. They are highly porous due to the very large void space with a complex non-flat surface structure and have a low aerial density. Figure 2. 5 shows an image of a typical spun-laid polypropylene nonwoven made via thermo bonding.
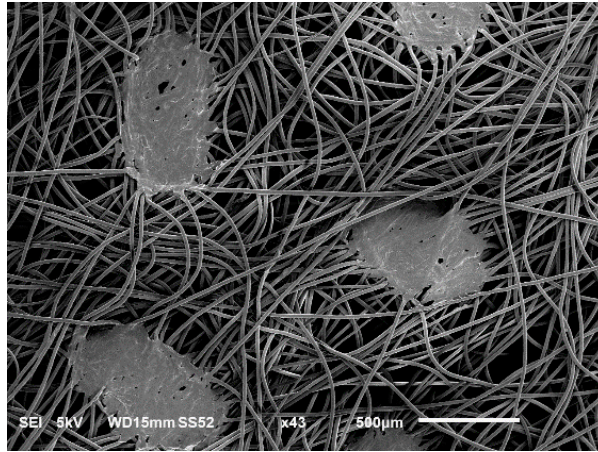
Figure 2. 5 SEM image of a spun-laid polypropylene nonwoven

2.3.1 Manufacturing approaches

According to The European Disposables and Nonwovens Association (EDANA) [3] a nonwoven is defined as "a manufactured sheet, web or batt of directionally or randomly orientated fibres, bonded by friction, and/or cohesion and/or adhesion" excluding woven materials, such as paper etc. However, the International Organization for Standardization, (ISO 9092:2019) defines nonwovens as "an engineered fibrous assembly, primarily planar, which has been given a designed level of structural integrity by physical and/or chemical means, excluding weaving, knitting or paper making". Virtually all kinds of fibres can be used to produce nonwoven fabrics[53], natural, (e.g., cotton, jute, linen), synthetic, (PP, PE, PET, Nylon, polyester, PLA) or regenerated, (e.g., Bamboo, Tencel, modal) fibres. Although different fibres can be used to produce nonwovens, synthetic man-made polymers account for the largest portion of the raw material used in manufacturing nonwovens. PP and PE fibres, and their copolymers, account for 63%[3] of all production in the nonwoven industry because of properties such as their low density, low cost, chemical stability, good fluid handling, mechanical strength and abrasion resistance.

Traditionally fabrics have been produced by weaving and knitting, which involve conversion of fibres into yarns and subsequently yarns into two-dimensional fabric structures. The nonwoven manufacturing process is fundamentally different from weaving and knitting and does not require conversion of the fibres into yarn. Nonwoven manufacturing processes include fibre selection, (the raw material) and preparation, web formation, web bonding, enhancement and finishing. In most cases, the first three stages are combined into a continuous process. Majority of the nonwoven products are used by consumers either as single or one-time use or short life products. As a result, disposability is becoming a major issue. In these situations, natural fibres

18

such as cotton, wool, jute, flax and hemp have become the fibre of choice. Several producers are trying to make degradable nonwovens or, respectively, films using raw materials[6, 11] such as thermoplastic cellulose, polylactide products, polylactide/starch blends, and thermoplastic starch. It is expected that natural fibres might enjoy more favourable market conditions in the future because of the increasing concern with global environmental issues. However, there are also many environmental benefits which result from nonwovens use, e.g., in air and oil filtration, oil absorption, protective workwear, geotextiles, agriculture etc.

The production of nonwovens involves two major steps as shown in Figure 2. 6: web formation and web bonding. There are three main web formation methods[53] : dry/air laid, wet laid, and polymer laid. These can be further subdivided into spun laid and melt blown web formation which apply particularly to synthetic polymers. There are strong similarities between wet-laid technology and conventional papermaking processes. A key differentiation between the papermaking and nonwoven forming is that the later employs a substantial content of fibres with lengths greater than 3mm, the typical length of fibres in softwood pulp[54]. The concept of melt blowing of thermoplastics to form microfibres (<10 microns) was first demonstrated back in 1954 by Van A. Wente, of the Naval Research Laboratories, who were interested in developing such fibres to collect radioactive particles in the upper atmosphere to monitor worldwide testing of nuclear weapons[55]. In the late 1960's and early 1970's, Exxon Research, who commercialised PP, were the first to demonstrate, patent, publicise and license the use of the Wente concept as a very practical process to produce unique types of nonwoven webs from polyolefins[56]. Consolidation of the web after its formation is the second step in the nonwoven manufacturing process. The main web consolidating methods are classified into mechanical, chemical, and thermal bonding, based on raw material fibres, end-use applications, and web formation technology. Mechanical bonding can be further categorised as needle punching, stitch bonding, and spun lacing[57] and so can chemical and thermal bonding be further sub-categorised as shown in Figure 2. 6. Frequently, a combination of different bonding methods is used to achieve a product with specific properties. Nonwovens can be made absorbent, breathable, flame resistant, heat sealable, light, lint-free, mouldable, soft, stable, stiff, tear resistant, water repellent, if needed. Obviously though, not all the properties mentioned can be combined in a single nonwoven, particularly those that are mutually exclusive.

Nonwoven

Web Forming — Dry/Air Laid — Wet Laid — Polymer Laid — Spun Laid, Melt Blown, Flush Spun

Web Bonding — Chemical (Impregnating, Coating, Spraying) — Mechanical (Needling, Looping, Entangling) — Thermal (Calendering, Air Blowing, Welding)
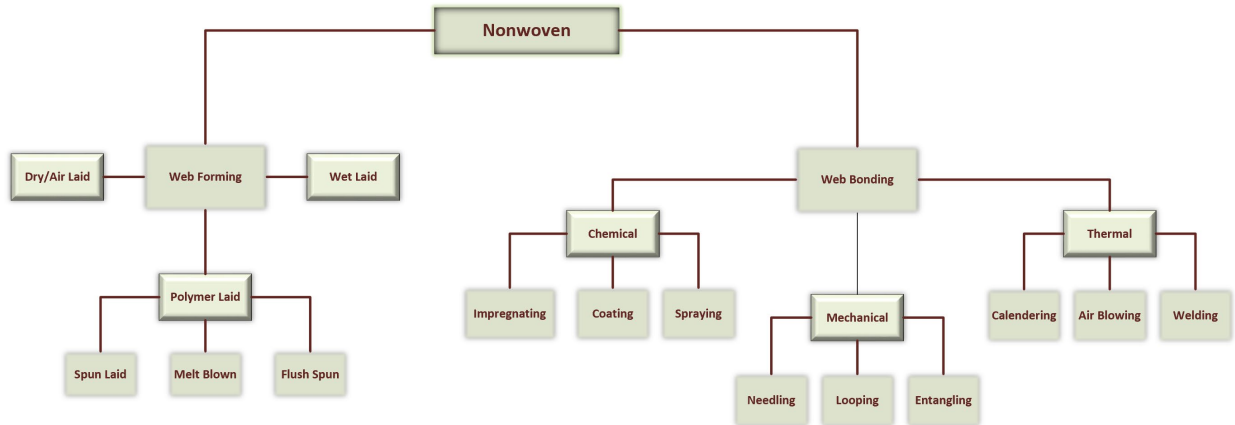
Figure 2. 6 Nonwoven manufacturing process and approaches.

Compared with traditional fabric-forming processes[58], the production processes of nonwovens are much shorter, faster, and more economical due to the motivation for fabric-like attributes and paper-like rates of production. A comprehensive view of what nonwovens are, their manufacturing processes, and their applications is provided by Albrecht et. al.[53]. Economic advantages has been the primary driver behind the rapid development of nonwovens since the 1930s.[52] However, modern nonwovens have become much more technologically driven due to the flexibility of the processes and products. Nonwovens nowadays form a multi-billion-dollar industry[3] and examples of their uses can be listed as follows:

- Personal care and hygiene - nappies, feminine hygiene products, adult incontinence items, dry and wet pads.
- Healthcare - operation gowns and dressings, packs, face masks, and swabs
- Clothing - interlinings, insulation and protection clothing, industrial workwear, chemical defence suits, shoe components, etc.
- Home - wipes and dusters, tea and coffee bags, fabric softeners, food wraps, filters, bed and table linen, etc.
- Automotive - boot liners, shelf trim, oil and cabin air filters, moulded bonnet liners, heat shields, airbags, tapes, decorative fabrics, etc.
- Building - roofing and tile underlay, thermal and noise insulation, drainage, etc.
- Engineering - asphalt overlay, soil stabilization, drainage, sedimentation, and erosion control, etc.
- Filtration - air and gas filters
- Industrial - cable insulation, abrasives, reinforced plastics, battery separators, satellite dishes, artificial leather, air conditioning, coating.

The manufacturing process used to make synthetic fibres incorporates, in addition to the raw materials, many other ingredients and additives[53]. Some are added to provide special design features and others are necessary to assist the processes of manufacturing. Examples include additives such as UV and chemical stabilisers, pigments[53], binders[53], delusturing agents, (e.g. titanium dioxide) optical brighteners, (which convert short-wave rays into longer visible rays making fibres look whiter) antistatic agents, (usually organic additives) light-proofing agents, (e.g. bivalent manganese compounds and phosphates) flame-retardant agent, (which contain phosphorus, nitrogen and usually halogens) to property modifiers, added to change their physical and chemical properties. There are also spin finishes[53] applied in the form of oils during nonwoven production to improve processing performance of these nonwovens. Other functional materials used include bonding agents, gliding agents, emulsifiers, anti-splash and thread cohesion agents, bactericides, wetting and moisture retaining agents as well as corrosion inhibitors. Whilst in the past mineral oils of various degrees of purity, natural fats and oils played a dominant role in the range of spin finishes, these are today supplemented by silicones, ester oils, phosphoric ester and polyalkylene glycol ether in their simplest forms, with ethylene and propylene oxides[53]. Finally, the application of surfactants to achieve good fibre distribution in the nonwoven production processes has been documented in the literature by Cai et al.[59] and a list, shown in Table 2. 1, of some examples was provided by Hubbe et al. [54].

Table 2. 1 Examples of surfactants used to enhance wetting of hydrophobic fibres in wet-laid manufacturing processes.

TYPE	EXAMPLE	NOTES
EO/PO/EO tri-block	Pluronic® F108	Stabiliser, Low foam
EO/alkyl	Triton® X-114	High wetting
EO/terephthalate	Milease® T	For polyester fibers
Silicone-based	Q2® 5211	High wetting
Alkyl sulfosuccinate	Aerosol® OT	Anionic low foam

Key: EO = ethylene oxide, PO = propylene oxide

Nonwoven materials for purposes of manufacturing are characterised in terms of fabric weight, thickness, density, uniformity, porosity, and fibre orientation/distribution typically. The weight of nonwoven fabrics is expressed in grams per square meter (gsm). Parameters such as fabric density and porosity are important for understanding the mechanisms of the transport of fluids through the fabric. Porosity of nonwovens is defined as the ratio of the non-solid volume (voids) to the total volume of the fabric and the majority of nonwoven fabrics have porosities of >50%[3]. It is known that nonwovens weight and thickness varies in different locations along and across

a sample and that such variations are of a recurring nature and are very process dependant.[3] Therefore, it is always necessary to sample different regions of the fabric when making any kind of measurements on such materials. The fibres in a nonwoven are rarely completely randomly orientated, they are aligned in different directions mostly in plane.[3] Nonwovens are also termed anisotropic; their uniformity is directionally dependent within the structure.

2.3.2 Surface Modification Methods

The end-use of nonwovens is determined by the properties of the fibres they are made from, the fabric structure, and other functionalities, such as absorbency, hydrophobicity, wettability, and antimicrobial properties are some key examples. Surface modifications can be applied to add value to the nonwoven fabric by enhancing the functional performance of the final product. For example, the presence of surface hydroxyl groups makes their surfaces hydrophilic which is not an inherent property of all polyolefin based nonwoven fabrics. Thus, surface modification is necessary to transform these inexpensive materials into valuable finished products. Hence, polyolefin nonwovens need to undergo chemical treatments to facilitate their use in select industrial applications.

Several effective surface modification methods have been developed and applied over the years not only for improving polyolefin nonwovens but many other polymeric based materials. A wide array of surface modification techniques[60], ranging from simple to sophisticated, wet to dry, and vacuum to nonvacuum, are available. In general, the surface modification of polymers can be classified into physical methods, chemical methods, or the combination of both. They include chemical[61] etching, physical[62] methods, and more advanced non-invasive processes such as UV/ozone irradiation[63-66], corona/plasma treatment[18-23, 67], laser induced patterning techniques[60], grafting modification[24-26], and blending/coating with hydrophilic materials[27-31]. Plasma treatments and exposure to radiations are generally gas phase methods, while chemical treatments are generally carried out with oxidants or other finishing agents performed in the liquid phase, followed by thermal treatments. These modifications processes can impart a wide range of characteristics on the material surface, the most common being to modulate the surface energy and surface roughness, thus increasing or decreasing its adhesive, wetting, absorbing, or releasing properties[68]. To do so the polymer could be subjected to chemical, ionic, or light-based treatment processes which involve the addition of different functional groups to the material[68]. Desirable surface properties can be tailored by the various methods mentioned above, the main ones being discussed in the sections that follow. All the nonwoven

materials used in this research are made hydrophilic utilising surfactants to convert them into materials that are wettable and allow water to pass through them.

2.3.2.1 Surface Modification by Physical Routes

Typical physical surface treatments involve surface roughening, such as with sandpaper or emery cloth, adhesive abrading, and media blasting. The effect of the physical treatment depends on the type of abrading material, the plastic, the original surface quality, and the process parameters. For thermoplastic polymers, the physical modification generally is performed as a part of the surface fabrication itself[60]. While it cannot change the inherent chemical nature of the polymer, modifying the polymer surface by physical methods alters its wettability by inducing surface roughness at both micro and nanoscales. Altering the surface roughness can lead to a transition from hydrophilic to a more hydrophobic state[69]. For example Xu et al.[70] fabricated superhydrophobic polymer surfaces by laminating PE films against woven wire mesh templates. The resulting texture of the polymer film required no chemical modification to exhibit super hydrophobicity.

Apart from low costs, the main advantages of the physical modifications over other methods are their relative simplicity, low costs, scalability, and robustness. They are considered eco-friendly because they do not require the use of any chemicals, and thereby there is no disposal of the waste liquids. In addition, the polymers modified by physical methods do not exhibit ageing or deterioration as the generated surface roughness rarely effects the polymer surface chemistry. Moreover, thermoplastic polymers can be physically processed in their solid or molten states, without altering their bulk properties such as mechanical strength and elasticity. However, physical modification are not effective for many types of plastics and adhesives or coatings. For many applications, simply increasing surface area/roughness is insufficient for the adhesion requirements, and commonly chemical surface modifications are required.

2.3.2.2 Chemical Treatments

Chemical surface modification involves exposing the surface of a polymer to a chemical which reacts with molecules on the surface to create new surface functional groups. Chemical surface modification of polymers is useful in areas where other methods are insufficient to meet the needs of the industry, e.g. for biomedical applications where the enhanced properties are desired without altering the surface roughness[60]. Most chemical surface treatment methods involve wet procedures where the polymer is dipped or coated/

sprayed with a chemical to enhance its surface properties and sometimes to remove debris and microbes from the surface to facilitate a sterile environment, suitable for biomedical applications too. Chemical modifications help to increase the surface energy by localising oxidised functional groups on the surface via different organic reactions such as hydrolysis, aminolysis, reduction and oxidation. These reactions allow the introduction of surface carboxylic, hydroxyl or amide groups. Some polymers include oxidised functionalities in their backbone such as ester or carbonyl groups, and these groups can be reduced with standard reducing reagents to provide alcohol groups that can undergo further modifications. Chemical treatments are associated with some degradation of the surface and are mostly used to provide different polymer surfaces with biocompatibility or antifouling properties[71].

In the early 80s Haridoss and Perlman[72] chemically modified the surfaces of LDPE, HDPE and PP films by oxidising with permanganic acid. Permanganic acid removed amorphous and defective chemical regions of the polymer surfaces, exposing more crystalline regions and crystalline-amorphous boundaries, both of which provided trapping sites, producing better charge storers than the untreated materials. More recently, PLA, an important biodegradable polymer used in agricultural films, biomedical devices, packaging, and automotive industries, has been hydrolysed by both chemical reagents and by enzymes to increase the number of hydroxyl and carboxylic groups on the outer polymer surface. Literature shows that PLA can also be aminolysed, a process which provides a surface bonded with positively charged amino groups able to interact directly with collagen, a modification which makes PLA substrate suitable for cartilage repair[73]. PET, a common thermoplastic polymer used in fibres for clothing, containers for liquids and foods, and in combination with glass fibre for engineering resins has been chemically modified by reduction, hydrolysis and transesterification[71] to display an increased number of –OH and -COOH groups on its surface. Acid oxidation of polymer surfaces involves application of acid to a surface to induce surface oxidation and increase surface energy. This approach has been utilised for the modification of polyolefins such as PP and PE which present C–H groups only therefore, strong oxidants are necessary for their oxidation. One investigation[74] used concentrated chromic acid solution at high temperatures ~ 75°C. Such extreme conditions lead to the etching of the surface and the formation of surface carbonyl derivatives thus increasing the hydrophilicity of the polymer.

The main advantages of wet chemical treatments include the wide range of reagents available to select for treatment of polymers at large scale with minimum cost. Chemicals in the liquid phase can penetrate pores more effectively than other types of surface modification techniques[75]. However, they require a careful approach as the rate of reaction is dependent

on the strength of the reagents, material composition, and time of treatment. Furthermore, rinsing, washing, and drying are essential before further processing of the polymer. These generate significant amounts of chemical hazardous waste during chemical surface modification. Therefore, surface modification through wet chemical routes is desirable as long as the application does not create too much waste, and has minimal side effects such as etching, and changes in the bulk crystalline phase of the material are not of major concern in the end-application[60].

2.3.2.3 Plasma Treatments

The term plasma was first used in 1926 by Irving Langmuir to describe the inner region of an electrical discharge. A plasma is an ionised gas made up of electrons, protons, neutrons, radicals, ionic particles, photons, and neutrals. Plasmas are produced by exciting a gas with electrical energy and it is often known as the "fourth state of matter"; see Figure 2. 7. This description is because it does not fit into the classic categories of solids, liquids, and gases. Gas, for example, is in an overall neutral state with an equal density of positive and negative charges and it can conduct electricity. Plasma is an intensely reactive process where positive and negative ions, electrons and radicals react and collide as long as an electric potential difference exists, which is precisely the reason why it can be used to modify surfaces.
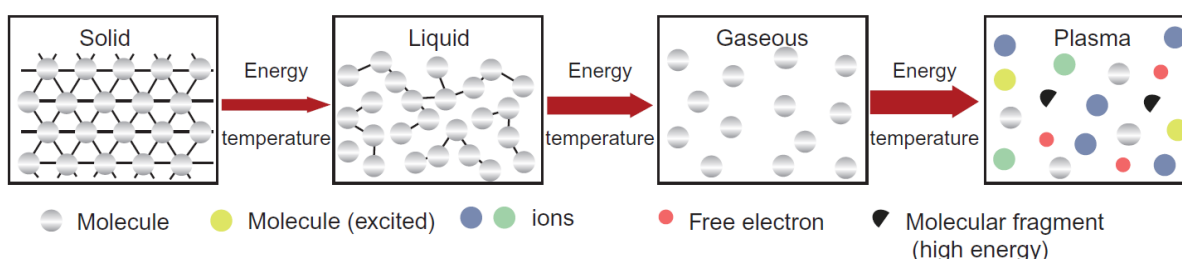
Figure 2. 7 States of mater[76]

Plasmas can be used to modify surfaces either by activating the surface for polymer grafting[77], i.e., by surface treatment (via depositing atoms or molecules onto a surface), by surface etching[78] or by polymerising a brand-new polymer onto the surface of any object resulting in a chemical coating which is so thin that it seems invisible. Plasma treatment or functionalisation in general involves the addition new functional groups to the surface (amines, alcohols, ketones, esters), or by making free radicals on a surface such that the object can undergo grafting. These lead to changes, (lowering/raising) the surface energy of the substrate. The other plasma-based process is surface etching which results in roughening of a surface by chemical erosion. Other methods use liquid acids to etch patterns in the films, however, this

has limitations because the etching is as isotropic. Plasma etching works by two mechanisms ion bombardment at the surface, (removing the material required to form trenches) and the gas monomer present in the plasma reactor can react with the substrate molecules forming volatile by products which are then vaporised. Plasmas are considered to be more environmentally friendly than solution-based acid etching for example and can produce eroded regions for increased surface roughness.

The final plasma method process is plasma polymerisation which involves forming a new polymer coating on a surface. Plasma polymerisation is another method for the addition of certain functional groups onto a surface via a polymer layer. However, it is different in the sense that the functional groups being added are all connected as they are part of a polymer which is formed *in situ* and coats every single surface layer. These polymer coatings can be very thin, and nm thick layers are not uncommon.

Plasma polymerisation works by activating monomers under a vacuum. Generation of radiofrequency radiation produces the plasma. Like in surface functionalisation, electron impact causes fragmentation and excitation of the monomer. However, here the excited monomers can react with each other as well as the substrate to be coated so a series of propagation steps occur polymerising the monomer as well as bonding them to the substrate surface. These mechanisms of polymerisation can be difficult to control leading to rearrangements and polymers with very different chemical composition to the monomer. In the mid-1990s an alternative to continuous wave plasmas was developed which revolutionised the field of plasma surface functionalisation. Scientists discovered that using pulsed plasma which involves applying the electric field across the gas in microsecond pulses rather than continuously, led to much more controllable polymerisation. This enabled polymer surfaces which were structurally more like the parent molecule, (compared to continuous wave plasma) because there was less fragmentation of the monomers. Plasma processes with surfaces are summarised in Figure 2. 8.
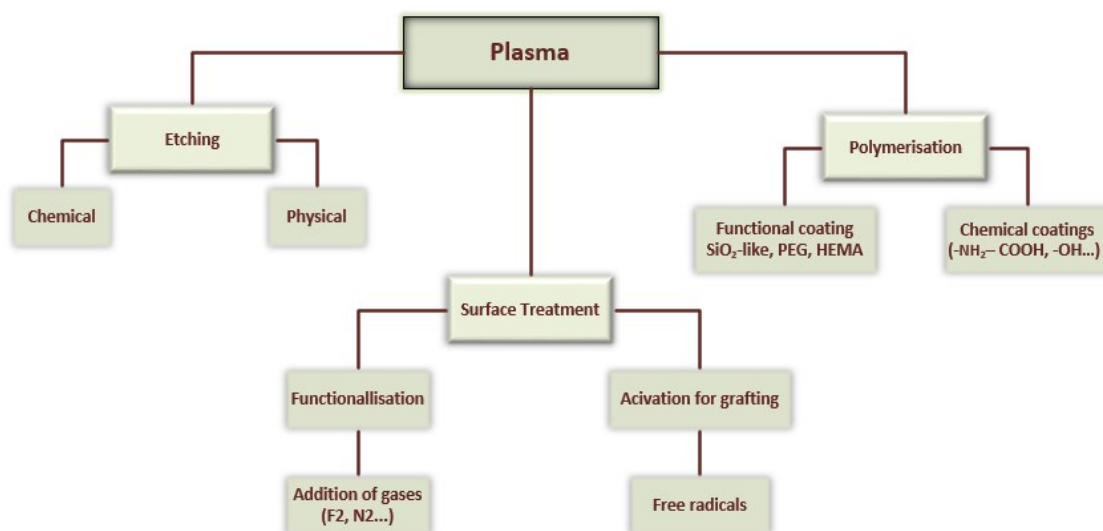
Figure 2. 8 Plasma processes of interactions with surfaces.

Plasmas have been grouped into two major categories: thermal plasmas (very high temperature) and non-thermal plasmas (close to room temperature). Only cold plasmas are suitable for surface modifications of temperature sensitive polymeric materials. Cold plasmas can be further classified into atmospheric pressure plasmas (APPs)[79] and low-pressure plasmas (LPPs)[80-82]. Cold plasmas are produced by applying an electric field which transmits energy to the gas electrons, which are accelerated and collide with neutral gas molecules or atoms.[83] Although most of the plasma applications on polymeric materials, including textiles, have been studied using LPP, APP technique has demonstrated to be the most interesting tool for large-scale applications on textiles[68]. There are different technical solutions for obtaining plasma at atmospheric pressure, including corona discharge, dielectric barrier discharge, atmospheric pressure glow discharge, and plasma jet. Corona discharge is a process in which a current develops between two opposing electrically conductive electrodes separated by a gap containing a gas, usually air. By applying a high voltage, an electric field develops and current flows from the electrode to the neutral gas which becomes ionised and plasma is generated. The process introduces polar groups that significantly improve the surface energy, which also effects the surface roughness, adhesion properties and wettability. Recently, Zhang et al.[84] report a novel methodology for producing high performance air filters by combining melt blown technique with corona charging treatment. Novak et.al[85] has modified iPP and LDPE surfaces using a corona discharge plasma. They highlight that the chemical changes on the modified surfaces affected the surface and the adhesive properties of the studied materials.

Using plasmas, different types of reactions are possible. Polymer surfaces can be cleaned or etched[86], mostly using nonpolymerisable gases such as O_2, N_2, H_2, the noble gases, or gas mixtures[13]. By controlling variables, such as the nature of gas, gas composition, discharge power, pressure, and exposure time, a great variety of surface properties can be improved such as cleaning, wettability, hydrophobic and oleophobic properties for soil release, adhesion of coatings, enhance dyeability and printability, introduce flame resistance[80] and addition of antibacterial/fungicidal properties. However, the effects induced by non-thermal plasma activation treatments are not always permanent. Surface energy of treated samples can deteriorates with storage time. This aging process is driven by the reorientation and diffusion of induced polar groups into the bulk with the rate of deterioration depending on the external temperature and humidity[87]. Borcia et al. [88] reported that plasma treated PE and polyimide were more stable to aging, while the PP samples exhibited faster aging. Plasma treated PET and PS featured moderate/low stability[60, 89]. It is believed that the hydrophobic recovery of polymers occurs due to their inherent nature to decrease their surface energies for attaining equilibrium[60] and that this reduction happens because of variety of processes such as rearrangement of chemical groups on the exposed surface to plasma treatment, oxidation, and degradation of the plasma-treated surface.

The degradation is a result of exposure to air including moisture as well as the diffusion of low molecular weight products from the surface to the bulk to reach a thermodynamically more stable state[85]. Penetration of plasma into solid substrate matter is very limited, but R Väänänen et al[22] found that plasma penetrated through three nonwoven layers without mechanical properties of the material being affected, mainly due to the porous nature of these materials. The modification induced by plasma treatment on a polymeric film is easily measured by contact angle determination with the sessile drop method. In the case of textile materials, contact angle determinations are severely compromised by the complex material topography and local contact geometry with the test liquid droplets. The porosity of the fabrics can often determine an imbibing effect on the water drop, preventing the contact angle determination. An exhaustive book on the applications of plasma technologies to textiles was published by Shishoo[82], whereas the surface modifications by plasma treatments were reviewed by Radu et al.[90] and Morent et al. [33]. Reviews on atmospheric plasma treatments for textile surface modification were published by Kale et al.[91], Wolf[92] and more recently by Peran et al[79].

Plasma treatments are popular methods of surface functionalisation because they offer many benefits over other coating possibilities. Some advantages[79] of using plasma treatments to modify polymer surface are the high efficiency and the short treatment time necessary to reach

a sufficient degree of surface modification. Also, plasma functionalisation is a low-energy method due to its room temperature conditions and the treatment is conformal, meaning that all the surfaces throughout the 3D object get treated. It is well documented in literature that non-thermal plasmas can significantly change the substrate's surface chemistry and topography without altering the bulk. Moreover, plasmas does not involve addition of toxic and/or hazardous chemicals and it have minimal waste, thereby making it environmentally friendly. Some disadvantages[79] of this type of surface treatment are its inability to generate active species uniformly on polymer with complex structures, hence it is only commonly used for polymer films, and the equipment for plasma treatment are usually expensive and of large scale. Another major drawback of plasma treatment is it complexity; specific control of the polymer molecular weights or creation of well-defined chemical surface architectures are difficult to achieve. Moreover, the surface aging or hydrophobic recovery of plasma-modified polymers is the major drawback because most of the free radicals remaining on the treated surface are reacted away when exposed to air oxygen.

2.3.2.4 Ultraviolet (UV)/Ozone Treatment

UV treatments are typically performed for curing light-sensitive polymers[93], for increasing the surface adhesiveness by increasing hydrophilicity[94] and for functionalising the surface by photoinitiated polymer grafting[95]. The UV light initiates a photochemical reaction that generates a cross-linked network of polymers changing its structural and chemical properties[96]. In UV irradiation the polymer degrades and breaks into free radicals which then react with atmospheric oxygen or ozone to form carbonyl and carboxyl hydrophilic groups. Ozone is a strong oxidant agent, which can be produced synthetically, as well as is being naturally available in the atmosphere. Christian Schönbein described "ozein" odor during electrolysis of water in 1839. Thomas Andrews found out that ozone was formed only by oxygen in 1856 and it was Soret in 1863 who defined the relationship between oxygen and ozone. He determined that 3 volumes of oxygen produce 2 volumes of ozone and that ozone is thermodynamically unstable and spontaneously reverts to oxygen. This means ozone must be generated "in situ" and cannot be stored and transported. The basic methods for generating ozone artificially are a) photochemical ozone generation, b) electrolytic ozone generation, c) radiochemical ozone generation, and d) ozone generation by corona discharge. The extent of surface modification can be controlled by tuning the irradiation time, monomer concentration, photoinitiator, and solvent. In addition to the generation of above oxygen-containing polar functional groups, the UV oxidation also creates nanoscale roughness (RMS ~ 3–5 nm) on a polymer surface contributing to the enhancement in the surface adhesiveness.

Combining UV with ozone is a more effective treatment than ozone or UV light alone according to some studies[97]. The ultraviolet light and ozone gas, (UVO) treatment[98, 99] relies on UV light and ozone gas, the latter supplied either by a separate ozone generator or from UV-induced gas-phase reactions. Ozone is constantly formed and destroyed by the action of 183 nm and 254 nm wavelength light, respectively, with both processes involving free atomic oxygen, (with strong oxidising ability), shown by the following reaction:

$$O_2 \longrightarrow O + O$$
$$O + O_2 \longrightarrow O_3$$

UVO is a common cleaning process accepted as an effective method used in the semiconductor industry[100] where the atomic oxygen reacts with contaminant molecules to form simpler volatile molecules, such as CO_2, H_2O, N_2 etc. The first UVO surface modification study to add supplemental ozone, from an external ozone generator, to the UVO treatment was done by Strobel et al.[97] who studied PP and PET films, obtaining increased wettabilities and surface oxidation with both polymers after treatment times of only 3 min. Lin et al.[99] presented long-term stability data for UVO-treated thermoplastics for up to 16 weeks and showed that the storage conditions has a significant impact on the surface stability recommending thus dehumidified or vacuum conditions for storing these treated thermoplastics.

Ozone on its own has found use for treatment of textile materials[101] as an ecofriendly[63] alternative to traditional wet processing methods that consume large amounts of electricity, fuel, and water. Eren and Öztürk[102] investigated the ozonation of cotton fabrics and found that the water absorbency of cotton samples increased following ozonation. Hydrophilicity of synthetic polymer surfaces can be accomplished by ozone which treats not only the surface but penetrates through the polymer bulk[103]. Yang et al.[104] studied the effect of ozone on aramid fibres. They found that ozonation process extracts foreign matters from the surface of the fibre and establishes oxygen-containing functional groups. Moreover, ozone has been utilised as a pre-treatment for introducing active groups on polymer surfaces, which would act as initiator for graft polymerisation. Ozonation works as pre-treatment method by attacking the surface of polymer and introducing peroxide groups, alcohol groups and carbonyl groups[105] too. This work shows that ozone can not only be combined with UV radiation but with plasma methods too to improve efficiency[106].

A common goal of polymer surface modification is to increase the hydrophilicity of the naturally inert or hydrophobic polymer surface. It is well documented in the literature that ozone on its own or combined with other techniques can achieve this goal. Some of the advantages[105] of using UV/ozone for surface modification are the relatively low operational cost, and its ability to introduce an uniform treatment even on complex 3D structures. The process can be carried out at atmospheric pressure, with simple and in-expensive equipment. Because of the relatively fast decomposition of ozone, it does not form any toxic products, which is particularly important for treating polymers in biomedical applications. Polymer surface modification by UV treatments is a scalable and environmentally friendly method, requiring no chemical reagents other than compressed gas, and the ozone gas, which is inactivated readily, and it produces no polluting waste by-products. Though the modified polymers recover to their inherent surface properties due to aging, it can be delayed by incorporating relevant reactive chemical vapours or by depositing semiconductor nanoparticles onto the surface[107].

The main disadvantages[66] of ozone treatment are the long treatment times needed and the reaction of ozone on the polymer backbone, which may cause polymer degradation, with mechanical properties being compromised. For the UV treatments, the polymers must be photoactive to absorb the UV light for any surface modification. UV treated polymers tend to revert to their original hydrophobic surface, the so called "hydrophobic recovery", over time. This ageing effect is due to the formation of free siloxanes and/or reorientation of polar groups according to Hillborg et al.[108] It is also possible for the polymers to deteriorate when exposed to the UV light, due to UV-stimulated photo-oxidative reactions such as C-C bond scission, photolysis, and/or dissociation of side groups[109].

2.3.2.5 Surface Modification through Laser Patterning

Laser surface patterning involves direct treatment of the polymer surface with a laser beam. The laser radiation is absorbed by the polymer surface which heats up causing local melting or even vaporisation. Selective material removal is achieved, and the surface topography is modified. If the surface of the material melts, bumps or dimples can be formed creating regular or irregular patterns. Removal of material is mainly produced by the vaporisation or thermal decomposition, but some melting or thermal degradation can also occur. Moreover, if the laser beam photons are sufficiently energetic, they can break chemical bonds. Such non-thermal processing is associated with ultrafast lasers which can produce dimples and grooves modifying thus the surface chemistry of the material without undesirable thermal effects[110]. Laser texturing can be performed using a stationary laser beam or providing a relative

movement between the laser beam and the surface. The first approach requires the utilisation of a mask with the desired pattern, production of which is a time-consuming process. The second method involving the relative motion of the laser beam produces a pattern by moving either the laser beam or the sample. The latter is more commonly used due to its versatility and throughput.

A wide range of laser wavelengths (198, 248, 355, 532, 1064nm, and 10.6µm)[111, 112] can be used for laser surface texturing, to create micro-channels, improve tribological properties[113], increase surface roughness, modify surface chemistry which simultaneously changes the wettability and surface energy of polymers[114, 115]. Such techniques can modify polymeric surfaces at a macro-, micro-, and nano-size scale with a high spatial and temporal resolution[110]. Given the non-contact nature of the process, the contamination of the substrate is minimised which is very important for biomedical applications[110, 116]. For example, polyetheretherketone (PEEK) is used as structural material in orthopaedic applications and was laser treated by Laurens et al.[117] to increase its polar oxygen containing groups and its surface roughness, resulting thus increased wettability. Okoshi et al.[118] studied the utilisation of femto-second laser sources to ablate and modify the surface of PE sample, successfully producing PE surfaces rich with carbonyl polar groups. Riveiro et al. [119] studied the effect of laser textured PP surfaces and demonstrated the ability of nano-second lasers to successfully modify PP surfaces resulting on increased roughness and the formation of PP surfaces rich with carbonyl and hydroxyl groups.

Laser surface modifications offer a great number of advantages, including potential modification of surface roughness and chemistry in one step without using any toxic substances. Therefore, laser surface modification is considered environmentally friendly. It is a fast and relatively cheap method which can be used in mass fabrication processes. However, laser radiation can produce a lot of heat and as a result undesirable thermal effects (e.g., generation of a heat affected zone) can occur.

Literature shows that UV radiation is preferred over the IR radiation because of its ability to ionise and decompose polymers without the substantial melting produced by IR radiation.

2.3.2.6 Surfactant coatings/blending

Surface coatings, often based on surfactants, can also be used to change the surface characteristics of polymers. Surfactants' amphiphilic nature makes them particularly favourable

to reside at interfaces and significantly change the interfacial physics and chemistry of materials; hence they are termed surface-active agents. They are used as coatings to facilitate emulsification and emulsion polymerisation, as well as to improve wetting and dispersion. Different types of surfactants have been used to achieve a good distribution/dispersion of hydrophobic PP and PE fibres in aqueous media in wet-laid nonwoven processing[59] methods. In this process, the way the surfactant interacts with the surfaces of hydrophobic solids in an aqueous suspension is based on their characteristic molecular structure which contains both hydrophilic and hydrophobic components. The hydrophobic parts of the surfactant tend adsorb on the hydrophobic solid surfaces, while the hydrophilic portions of the molecule to preferentially interact with the aqueous phase [54]. Thus, the aqueous fluid with surfactant present can coat the fibres rendering them hydrophilic and thus facilitating their suspension in an aqueous solution. An alternative route to modify the polymer properties via surfactants is by dissolving these molecules into the polymer. Silicone or siloxane based surfactants are occasionally used as additives in plastics or as a surface coating on pigment dispersants which are used in latex paints[75].

A major use of surfactants in the coating industry is as wetting agents. Zhang et al. [120] studied the effects of the wettability of 16 additives introduced into the nonwoven fibres produced by the melt-blown process. They found that the additive with the best performance in reducing surface tension was a surfactant of the family of the polyethers modified with trisiloxane. Antunes et al.[121] evaluate the effect of the addition of polyether siloxane in a PP film and found that it increased the hydrophilic characteristics, allowing the sorption of polar materials, such as water. Additionally, Yang et al.[122] employed surfactants to tune the hydrophilicity of degradable polyesters, an important characteristic for such materials when used for bone tissue engineering and repair. They designed porous biodegradable polymer scaffolds with improved hydrophilicity, while maintaining mechanical, thermal, and degradation properties, by introducing the surfactant Tween 80 via direct blending.

Previous studies have indicated that surfactants, such as HTAB, SDS, Triton X-100, could improve the compatibility of hydrophilic and hydrophobic polymers[123, 124] especially when employed with nanofillers for the preparation of polymer nanocomposites. The presence of surfactants in polymer nanocomposites improved the compatibility, wettability and enhanced final product properties[125]. Moreover, polymeric nanoparticles surface modified with surfactants are commonly used in the pharmaceuticals industry for controlled drug release purposes. These surfactants significantly influences nanoparticles properties including, morphology, surface chemistry and surface hydrophobicity [126].

For applications in personal hygiene products, hydrophilic nonwovens are required. However, commonly used polymer nonwoven fabrics, such as PP, PE or PET are significantly hydrophobic. To address this problem different methods for making these surfaces hydrophilic exist. A common solution is topical treatments with surfactant coatings. WO 93/04113, WO 95/25495 and numerous other patents describe similar industrial methods and related inventions. Current state-of-the-art in topical surface treatment is represented by the application of commercial spin-finishes by kiss roll deposition, shown in Figure 2. 9, spraying, dipping the nonwoven in a treatment bath, or similar application processes[127, 128]. For example, during the coating process via kiss roll deposition the surfactant is applied as an emulsion of the surface-active agent in water onto a roller which in turn contacts, kisses, the moving nonwoven fabric. These are considered external hydrophilic surfactant coatings. Factors to be considered during the coating process including the amount of coating that adheres to the roll's surface, the roll speed, the web speed, the web tension, the web wrap angle and the surface characteristics of the web[129]. Table 2. 2 shows the typical operating speeds, coating application rates and coating viscosity for a kiss coater. An alternative approach is blending an internal hydrophilic surfactant with the polymer used to form the nonwoven web, which later migrates to the surface after the nonwoven web is formed. Only samples prepared using the former method (external hydrophilic surfactant coatings) are studied within this thesis.
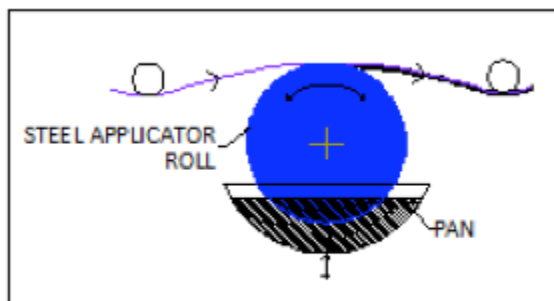
Figure 1 – Kiss Coater

Photo 1 – Kiss Coater with Metering Rolls

Figure 2. 9 Schematic of 'kiss roll' coating process[129]

Table 2. 2 Typical operating conditions for a kiss coater

Kiss Coating		
Speed (Maximum)	915 fpm	300 mpm
Coating Thickness (Wet)	0.2 – 0.5 mils	5 – 12 µm
Coating Viscosity	15 – 500 cps	0.015 – 0.5 Pa.s

The amphiphilic nature of the surfactants allows them to orient themselves when applied to a hydrophobic polyolefin surface in a way that the hydrophobic side is facing towards the surface

and the hydrophilic side facing away from it, creating thus a surface with hydrophilic properties. Surfactant compositions having both durability and a faster rate of wetting are desirable for a variety of reasons. Therefore, hydrophilic organosilicone surfactants having a relatively broad molecular weight distribution, which imparts both durability and a fast rate of wetting to the nonwoven fabric are normally used. Commercial spin-finishes commonly applied to nonwovens in personal hygiene industry are typically performed using proprietary blends of synthetic surfactant solutions commercially available, for example, from Schill & Seilacher AG (e.g. Silastol PHP 26, Silastol PHP 90, & Silastol 163), and Pulcra Chemicals (e.g. Stantex S6327, Stantex S6087-4, & Stantex PP602)[130]. For cost and other reasons, it is usually desired to use the minimum amount of surfactant that will produce the desired effect with an acceptable degree of uniformity. Surfactants are typically applied to nonwovens in the range of 0.004-0.006 gm solids/gm nonwoven (i.e., 0.4-0.6% wt/wt). Other types of surfactants used are based on fatty acid polyethylene glycol esters.

Nonwovens coated with surfactants via these spin finishes methods have the advantage of being relatively inexpensive to coat and are quick to manufacture. A drawback of these methods is that the surfactants and/or other coatings are easily washed off when the nonwoven is exposed to an aqueous solution because the coating is not permanent. However, the major disadvantage of such coating processes is the tendency of the surfactant coating to migrate and disappear over time from the polymer surface, causing low coating durability upon storage. Thus, hydrophilicity decreases over time which could lead to reduced aqueous liquid management performance. Accordingly, there is a need for more research which helps understand the polymer-surfactant interaction and how these develop over time and under different environmental conditions. Understanding the fugitive nature of these hydrophilic coatings will facilitate the development of more durable hydrophilic surfactant coatings for polyolefin nonwovens, that does not migrate easily when dry or subjected to elevated temperature during storage and are not easily washed off when wetted or when fluid passes through them.

2.3.3 Applications in hygiene sector

This thesis will investigate polyolefins, in particular polyethylene (PE) and isotactic polypropylene (i-PP), which are widely used in our everyday life for a wide range of applications. The application focus here is the hygiene sector although they are used in other applications such as building and construction[131], biomedicals [60], consumer goods [132], electronics [60], electrical and automotive industries[133]. The unique properties of polyolefins

make them excellent candidates for one time use as disposable hygiene products[134]. The steady growth in global human population, and the more recent COVID19 pandemic, has led to increasing global demand for disposable personal and health-care products resulting thus in strong competition for unique and improved absorbent products and materials. Personal care hygiene products represent a $40B business[15]. This includes the growing basic care needs of hundreds of millions of children, millions of women using feminine hygiene products, and adults suffering from incontinence worldwide. Statistics on the market growth for such products demonstrates a steady upward trend; see Figure 2. 10.
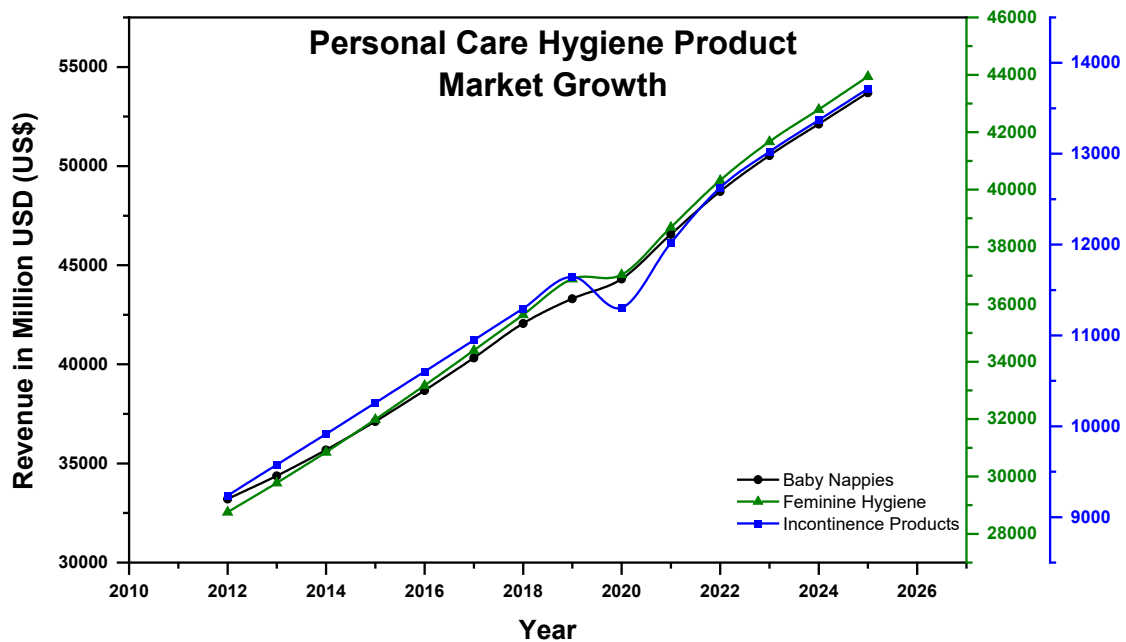
Figure 2. 10 Global market revenue statistics for personal care hygiene products.
(Source - Statista Ltd. - Forecast adjusted for expected impact of COVID-19)

With respect to fibres in general, natural fibres tend to be hydrophilic, especially when natural oils have been removed from them. However, virtually all thermoplastic fibres are innately hydrophobic due to the dominantly hydrocarbon nature of the base polymers. As discussed previously there is not currently a commercially viable way for PE/PP fibres to be made sufficiently hydrophilic long term to meet the application requirements in the personal hygiene industry. This problem is further exacerbated by the fact that the time dependence loss of performance is not currently understood. Despite this, polyolefin-based fibres are preferred to natural fibres such as cotton and synthetic fibres such as polyamide (nylon) for manufacturing of hygiene products, because they are cheap and have ideal rheological characteristics essential for fibre formation with high crystallinity.

36

Nonwoven fibres are versatile materials[135] which can be engineered to deliver a diverse range of properties via surface coating processes. They are produced by high speed and low-cost processes[3] and are made hydrophilic utilising surfactants which converts them into wettable materials that allow water to pass through them. A typical example is spunlaid nonwovens which are used for manufacturing baby nappies[136]. The first disposable nappies into the market in the 30s were cellulose based[53]. These were followed by two-component nappies, in which a nonwoven film was used as a casing for the cellulose layer. In the 80s the "all in one" nappies with superabsorbent polymers were developed. It is estimated that the total number of disposable nappies used during the babies first 3 years is 4600- 4800 [16]. The basic structure and composition of a modern nappy have been previously reviewed [137]. It consists of four main functional polymeric layers as shown in Figure 2. 11, most of which are coated with surfactant(s).
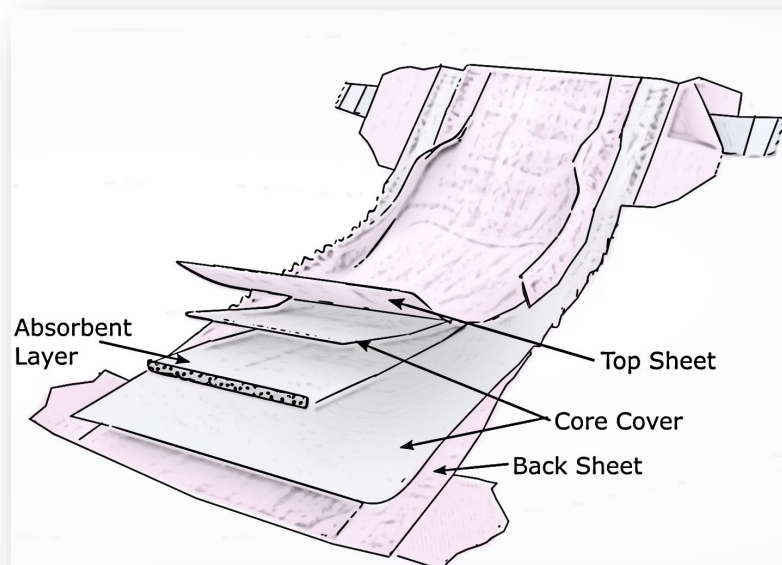
Figure 2. 11 Typical disposable nappy design. Modified from[17].

So how does a nappy work? Baby waste liquids are first channelled through a protective inner liner, called a top sheet (TS). The TS is composed of soft, porous PP/PE surfactant coated nonwoven fabric, either alone or as a blend. This layer is in direct contact with the skin therefore, it includes a mild lotion (emollient) to help protect baby's skin from hydration and irritation[138]. This fabric layer must facilitate the quick passage of liquid through to the interior of the nappy functioning as a 'one-way valve', whilst restricting passage of the liquid back through in the reverse direction, achieving a dry and soft fibrous surface to the skin. The waste then passes through the core cover (CC) which facilitates the movement of fluid away from the skin to distribute it evenly to the nappy absorbent layer. The CC is made of porous polymer fibres

that are effective at quickly absorbing the liquid and transferring it to the absorbent layer, which is the storage layer of the nappy. The absorbent layer is made of super absorbent gel, which looks like sugar, but turns into a gel as it absorbs liquid. Finally, the outer cover of the nappy, known as the back sheet, functions as a barrier to prevent fluid from leaking out of the nappy. The back sheet is water-proof typically made of cloth-like PP laminated with a PE film[16].

TS and CC are often made from polypropylene (PP). Liquid handling performance is one of the main functions of TS and CC materials in a nappy and is strongly influenced by the amount of surfactant present on these layers. The surfactants are needed because otherwise the CC and TS would be an effective barrier to fluid due to capillary repulsion coming from the hydrophobic polymer. Decreasing amount of surfactant on these layers could lead to leakages. Controlling the amount of surfactant on nonwovens rigorously is therefore very important for product performance. The hygiene market defines product success based on three factors; form, fit and function. Form has been achieved through the incorporation of superabsorbents[134], which make products thinner. Fit is achieved through use of elastics and stretchable materials. While form and fit are important, they cannot surpass function in performance. After all, what is the point of hygiene material, if it does not achieve its function? For baby nappies, this means no leaking and less frequent nappy changes, for adult incontinence, this means a more active lifestyle and for feminine hygiene, this means discretion. It is a common industrial experience that the surface hydrophilicity of these coated materials is time dependent and significant losses in surface concentrations of surfactants are observed. It is therefore important to study how the surfactants interact with the polymer and their fugitive nature, so the performance of many surfactant coated polymeric nonwovens-based products is improved.

2.4   Surfactants - properties and structure

Surfactants also known as 'surface active agents' are compounds that reduce the surface tension between interfaces[139]. To understand the relationship between the surface activity of a material and its chemical composition, it is necessary to understand the chemistry of the individual molecular components in the material that produce the observed phenomena. This Section discusses surfactants their structure and physicochemical properties.

Surfactants are amphiphilic organic compounds, meaning they contain both hydrophobic, their tails, and hydrophilic groups, their heads, as shown in Figure 2.17. So, a surfactant contains both a water-insoluble section and a water-soluble section. Considering water as a

polar solvent, when surfactant molecules are in water at low concentrations, they will be solubilised as monomers. The hydrophobic group distorts the structure of water, increasing thus the free energy of the system. To decrease the free energy, the hydrophobic tails need to be excluded from the solvent. As the surfactant concentration increases, the molecules will align at the surface since the attractive forces between the hydrocarbon tails are greater than those between the tails and water. As a result, surfactants tend to accumulate at interfaces, arranging themselves in a way that both sections of the molecule are in a favourable environment, reducing the free energy of the system. The polar head will be immersed in the polar phase and the tail in the non-polar phase. Based on the chemistry of their head groups, surfactants are classified into four basic classes; non-ionic, anionic, cationic, and amphoteric as depicted in Figure 2. 12.
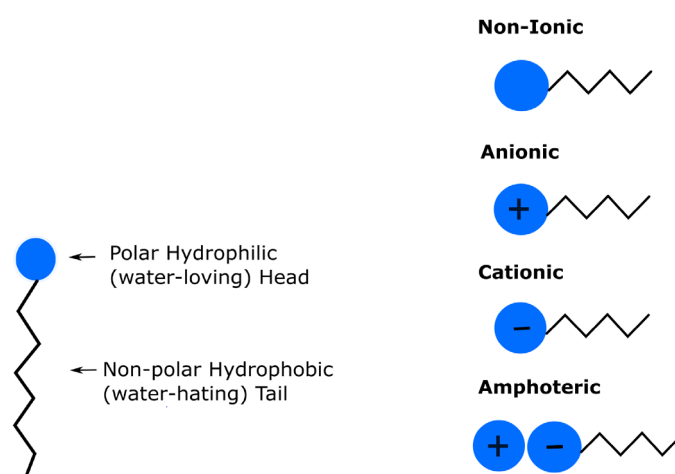
Figure 2. 12 Schematic of a typical surfactant structure (LHS) and the different types of surfactants (RHS), non-ionic (top), anionic, cationic and amphoteric (bottom).

A fundamental property of surfactants is that in solution they tend to associate into ensembles, called micelles[140, 141]. In a micelle, polar head groups form an outer shell in contact with water, while nonpolar tails are organised in the micelle interior. A schematic structure of a micelle is shown in Figure 2. 13.
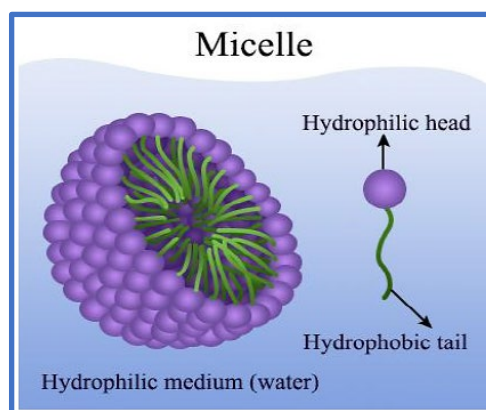
Figure 2. 13 Micelle formation[142].

The micelles can form in various shapes; spherical to rod- or disc- like to lamellar[140, 143-145]. They start to form at a solution concentration called critical micelle concentration (CMC) which is an important point since surfactants behave very differently depending on whether they are present in micelles or as free monomers. Only surfactant monomers contribute to surface and interfacial tension lowering and therefore wetting properties depend on the concentration of free monomers in solution[141]. Ionic surfactants tend to form smaller micelles than nonionic surfactants because of the greater electrostatic repulsion between ionic head groups compared to the steric repulsion between non-ionic head groups. The solubility of micelle forming surfactants increases above a certain temperature, termed the Krafft point (KP). The KP is the temperature at which the solubility of surfactant becomes equal to its CMC[142]i.e. the alkyl chains melt resulting in the dissolution of surfactant crystals into micelles and monomers. Nonionic surfactants often do not exhibit a KP, instead, the solubility of these surfactants decreases with increasing temperature and they begin to lose their surface active properties above a transition temperature referred to as the Cloud point[142]. At elevated temperatures non-ionic surfactants containing ethylene oxide segments display a clouding behaviour in water.

2.4.1 Non-ionic

Non-ionic surfactants do not have a charged head-groups. The major subgroups of this class of surfactants are alcohol ethoxylates, alkyl phenol ethoxylates, fatty acid ethoxylates, monoalkaolamide, ethoxylates, sorbitan ester ethoxylates, fatty amine ethoxylates, ethylene oxidepropylene, oxide copolymers, and glycol esters[143]. The most common nonionic surfactants are those based on ethylene oxide, referred to as polyethyleneoxide-based surfactants, (PEO)[143]. Their hydrophilicity comes from a water-soluble group which partially ionises, e.g., the hydroxy group, (R-OH) in polyethyleneoxide 4 lauryl ether, the structure of

which is depicted in Figure 2. 14. The presence of several oxygen atoms helps to form hydrogen bonds with water molecules contributing to the polarity of these surfactants.
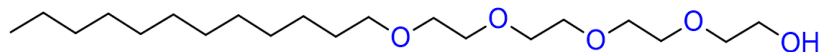
Polyoxyethylene 4 lauryl ether

Figure 2. 14 Molecular structures of a non-ionic surfactant.

An interesting characteristic of many non-ionic surfactants is their inverse temperature–solubility relationship[143]; as the solution temperature is increased, their solubility in water decreases. This effect is attributed to the disruption of hydrogen bonding between the water and the PEO units in the molecule. The temperature at which components of the PEO surfactant begin to precipitate from solution is defined as the "cloud point." Nonionics tend to have maximum surface activity near to the cloud point. They are cheap to produce, but some can suffer from the problem of poor biodegradability and potential toxicity. For example when the by-product of degradation is a nonyl phenol which has considerable toxicity for fish and mammals[143]. Other advantages of these surfactants include their ability to solubilise species in both aqueous and nonaqueous media, as well as good emulsification and dispersion properties. They are also compatible with other surfactants and have good chemical stability in many formulations[139]. An example of an industrial non-ionic surfactant is Stantex produced by Pulcra Chemicals. This material is a blend of synthetic surfactants made of ethoxylated fatty acid esters which is used for coating the top sheet layer of disposable nappies. Such surfactants are often applied to nonwovens using solution concentrations in the range of 0.4%-6% which have surface tension in the range of 31-37 mN/m [130]. The low surface tension promotes wetting of the hydrophobic polypropylene based nonwovens and thus enables the nonwoven to spontaneously imbibe the surfactant solution.

2.4.2 Anionic

Anionic surfactants contain negatively charged head groups, such as sulfonates, phosphates, sulphates and carboxylates. The straight hydrophobic chain is a saturated/unsaturated C12-C18 aliphatic group. The surfactant solubility in water is determined by the presence of double bonds and the anionic head group. Figure 2. 15 shows the structure of a common anionic surfactant, sodium dodecyl sulfate, with anionics constituting ~70% of total worldwide surfactant consumption[143].
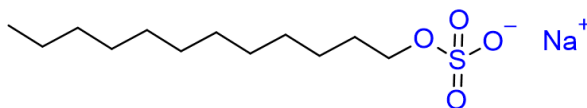
Sodium dodecyl sulfate (SDS)

Figure 2. 15 Molecular structures of an anionic surfactant.

The most used anionic surfactants have sulfate headgroups, which are produced by the esterification of an alcohol with sulfuric acid. Their widespread usage is due to properties such as good water solubility and surface activity, chemical stability, their low manufacturing costs, relatively simple manufacturing processes and natural availability of starting materials from agricultural and petroleum sources. Anionic surfactants are used in practically every type of detergent, either on their own or in combination with other surfactants. They are compatible with non-ionic, amphoteric and some cationic surfactants [139].

2.4.3 Cationic

Cationic surfactants have positively charged head groups, the most common examples typically contain an ammonium ion. Two most common classes of cationics are the alkyl trimethyl ammonium chlorides, and dialkyl dimethyl ammonium chlorides which contain two long chain alkyl groups[141]. They are produced by reacting a tertiary amine with an organic halide or organic sulfate[143]. Cationic surfactants are generally stable over a range of pHs, including very acidic to alkaline environments[146]. Cetyltrimethylammonium bromide (CTAB) is an example of cationic surfactant; see Figure 2. 16.
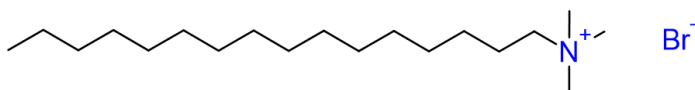
Cetyltrimethylammonium bromide (CTAB)

Figure 2. 16 Molecular structures of a cationic surfactant.

Cationic surfactants represent a relatively minor part of worldwide surfactant production, accounting for probably less than 10% of total production[143]. Similarly, to anionic and nonionic surfactants, commercial cationic surfactants are usually produced as a mixture of homologues. They are incompatible with most anionic surfactants, but they are compatible with nonionics [139]. Cationic surfactants can also kill or inhibit the growth of many microorganisms. Their germicidal properties make them important to the textile industry as fabric softeners, waterproofing and dye-fixing agents. The cationic surfactants are also useful in flotation

processing, lubrication, and corrosion inhibition, and they are gaining importance as surface modifiers for the control of surface tribological properties, especially electrostatic charge control. Silastol PHP 26 produced by Schill & Seilacher is an example of a commercially available cationic surfactant. It is made of fatty quaternary ammonia compounds (dialkylquats), and cationically modified poly-dimethylsiloxane (PDMS). Silastol PHP 26 solutions with concentrations in the range of 6% are used to produce coatings for durable hydrophilic spunbonded nonwoven fibres suitable for core cover layers of disposable nappies[130].

2.4.4 Amphoteric or zwitterionic

Amphoteric surfactants, also known as zwitterionic surfactants, contain or have the potential to form, both positive/cationic and negative/anionic charged head groups. The cationic part is based on primary, secondary, or tertiary amines or quaternary ammonium cations while the anionic part can vary to include carboxylate, sulphate, or sulphonate[142]. Imidazoline derivatives, betaines and sulfobetaines, amino acid derivatives, and lecithin and related phosphatides are the most commonly encountered subgroups of amphoteric surfactants[142]. A typical example of zwitterionic surfactant is alkyl betaine, depicted in Figure 2. 17.
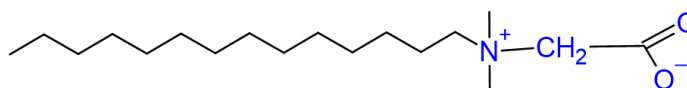
Alkyl betaine

Figure 2. 17 Molecular structures of a zwitterionic surfactant.

They show good compatibility with all other classes of surfactants and are soluble and effective in the presence of high concentrations of acids and alkalis[139]. Amphoteric surfactants can behave as anionic or cationic surfactants depending on solution pH. They are less common than anionic, cationic, and non-ionic surfactants due to their high cost of manufacture but are characterised by excellent dermatological properties and skin compatibility, and therefore are commonly used in shampoos, cosmetics, and household cleaning products[142].

2.4.5 Speciality surfactants

Concerns about the use of "synthetic" surfactants, produced from petroleum and other "nonrenewable" raw materials, as well as related possible risks to human health and the environment, have triggered an interest in a new class of surfactants referred to as "natural"

surfactants or "biosurfactants". These materials are isolated from plants, animal, microbial, fungal, or yeast and are of interest for applications in personal care products, food and pharmaceuticals[141]. Because of their biological origin, they do not fit into the classic chemical categories for surfactants. In particular, the natures of their hydrophobic and hydrophilic groups are often much more complicated than the simple synthetic materials mentioned above[147]. These surfactants are attractive because of properties such low toxicity, functionality under extreme conditions, extensive "recycling" potential, and a rapid biologically degradable nature. The commercialisation of these eco-friendly surfactants is currently limited by low productivity and expensive processes but in the future[143], it is expected that better reactor design and product isolation and purification technology would lower production costs and increase yields making biosurfactant production ecologically and economically favoured. One of the first commercial biosurfactants on the market was sophorolipids[148], produced from a naturally occurring yeast found in honey.

2.5 Surfactant - Polymer Interactions

Surfactants and polymers have extensive uses and applications in day-to-day life as mentioned in detail elsewhere. A comprehensive understanding of such mixed systems is essential for the continued improvement of current materials, development of new ones and efficient industrial development. Surfactant polymer systems are found generally in three physical forms: thin films, solution mixtures and solid-state systems, as depicted in Figure 2. 18.
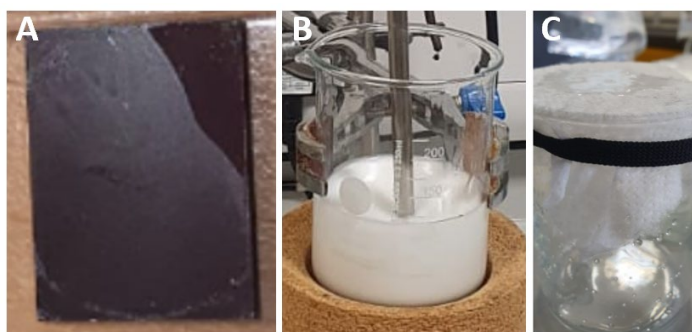
Figure 2. 18 Different physical forms of surfactant polymer systems, A) thin polypropylene layer coated on silicon wafer, B) polypropylene-surfactant solution, and C) surfactant coated polypropylene based nonwoven fabric).

Literature reports highlight numerous studies on surfactant-polymer interactions important to the success of product formulations in many areas[149]. Most researchers have studied surfactant-polymer adsorption interactions in solution[8, 150, 151] where various micellar structures including spherical, cylindrical, and bilayer, as seen in Figure 2. 19.
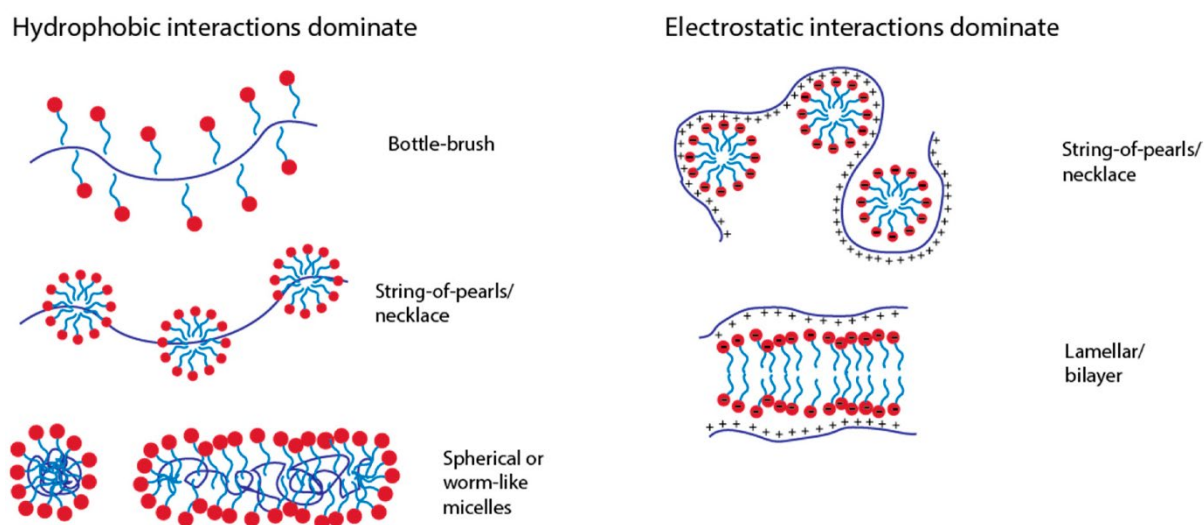
Figure 2. 19 Typical micellar or micelle-like structures formed with polyelectrolytes[152].

There have been many studies which have investigated how surfactants adsorb onto solid substrates too, including nonwoven fabrics, from aqueous solution[153-155] with Elaissari et al.[156] detailing methods for studying such mechanisms. Like most natural surfaces, nonwovens have a complicated surface structure, with their intrinsic surface irregularities and heterogeneity making it a difficult material class to study. Surfactant adsorption from aqueous solutions onto nonwoven fabrics exhibit a range of complex adsorption behaviour. Some adsorption is Langmuir adsorption, but at the same time, multilayer or colloid adsorption phenomena also exist[153]. Most adsorption isotherms reported in the literature are based on the ethoxylated type surfactants. The adsorption isotherm of nonionic surfactants are in many cases Langmuirian, and adsorption is generally reversible. Surfactant-surfactant interactions are reported to be negligible, and the literature suggests that adsorption occurs mainly through van der Waals interactions. On a hydrophobic surface, the interaction is dominated by the hydrophobic portion of the surfactant molecule[153]. Ivanova et al.[157] state that ionic surfactants such as SDS and CTAB exhibit stronger interactions with polymers than non-ionic surfactants such as Pluronics® .

However, a limited number of studies have looked at surfactant-polymer interactions in the solid state[153, 158, 159] including specifically the migration of surfactants coated onto nonwovens[32]. These are likely to be governed by hydrophobic interaction between the alkyl chain of the surfactant and the hydrophobic nonwoven polymers. There is a lack of studies investigating why the hydrophilicity of surfactant coated polyolefin degrades with time, and the process by which surfactants interact with polyolefins when coated onto nonwovens is poorly understood. The limited amount of literature available indicates a research gap in this area of science which

warrants further investigation. Although the basic mechanisms of interaction in the solution state are well understood, even in this scenario there is still disagreement on the surfactant–polymer interactions principles at the molecular level. Regardless of the exact molecular processes, one thing is for certain, surfactants do change interfacial, rheological, spectroscopic, and other physicochemical properties of these polymeric systems, significantly altering the macroscopic characteristics and the end-use functionality. It is generally accepted that surfactant–polymer interactions occur between individual surfactant molecules and the polymer chain usually initialled via simple surface adsorption. Surfactant–polymer interactions may also via the formation of polymer–surfactant aggregate complexes between the polymer chain and micelles[143]. Often described as resulting from the formation of "hemi-micelles" along the polymer chain, the formation of which is often illustrated as resembling a string of pearls. It could, therefore, be hypothesised that hemi-micelle structures potentially may form on solid surfaces too, especially heterogeneous surfaces that offer variations in the hydrophobic–hydrophilic environments available to surfactant molecules. However, the existence of these hemi-micelles is still speculative. Generally speaking, the basic forces governing surfactant interactions with polymers are the same as those involved in other interfacial properties of amphiphilic systems, namely, van der Waals and dispersion forces, the hydrophobic effect, dipole and acid–base interactions, and electrostatic interactions.

Literature[160] indicates that surfactant adsorption at hydrophobic surfaces is concentration dependant. At very low concentrations the surfactants adsorb with their hydrocarbon chain laying down at a hydrophobic surface, whereas at higher concentrations a monolayer is formed as depicted in Figure 2. 20. The driving force for the adsorption in this example is the hydrophobic effect.

Figure 2. 20 Illustration of adsorption of surfactants at a hydrophobic surface for a) low and b) high concentrations[143].

In solution, surfactants tend to associate into micellar structures. In many cases, such assemblies can transform from one morphology to another because of changes in solution conditions such as (i) the concentration, (ii) the addition of new components, (iii) changes in solvent composition, (iv) the addition of electrolytes or other solutes, (v) temperature changes, (vi) changes in solution pH, and (vii) unspecified influences from internal and external sources[143]. Assuming similar conditions, it can be hypothesised that surfactants in solid state potentially behave is a similar fashion when for example found coated onto hydrophobic materials, (e.g., surfactant coated polymeric nonwovens), such that they change/immobilise

because of changes in temperature and humidity which inadvertently affect residual concentrations, probably not in the same way or to the same extent as in liquid systems but following the same basic concepts that govern surfactant self-association or aggregation.

Surfactant layers/coatings on solid polymer surfaces are important in many technologies especially when the solid has a high surface to volume ratio, e.g., surfactant coated nonwoven fibres. The properties of the solid such as hydrophilicity, hydrophobicity, wetting, friction, and electrostatics are influenced by such layers/coatings. The theoretical understanding of the processes involved in the formation of such layers/coatings is scarce. Dipping a solid into a surfactant rich solution facilitates the replacement of the solid/gas interface by a solid/liquid interface from which surfactant adsorption occurs. The concentration of the surfactant is higher at solid surface than in the bulk. AFM based studies[161] have suggested that surfactants do not form continuous monolayers or bilayers at the solid liquid interface, instead they form discrete aggregates of different shapes and sizes, (e.g., lamella, , spherical, or cylindrical) depending on different factors such as, surfactant type, concentration, phase behaviour and solid type, and nature. In practice, mixtures of surfactants and emulsions are applied. The interactions between the solid and the surfactants and the formation of the coatings are even more complicated and not well understood[162]. The amount of surfactant needed to provide durable, sufficiently fast wetting may vary depending on the surfactant type, type of polymer base and how the surfactant is coated[153]. According to published literature [31, 153], surfactants should generally constitute about 0.1-3% by weight of the nonwoven fabric to which it is applied. Very high surfactant levels can block pores and are more easily washed away, providing thus little added wettability, while very low levels may not provide sufficient wettability to the nonwoven fabric.

Furthermore, the drying stage of the coating process is important and is expected to influence long term aging of these materials and subsequently long-term product performance. In this field only a few publications are known[162]. It is difficult to define a dry state and in practice no absolute dry surface exist. Drying involves different stages, initiated by the separation of the solid and liquid phase, with associated liquid draining from the solids and the "temporary" immobilisation of the adsorbed surfactants on the solid. As the temperature is increased the liquid evaporates influencing thus the surfactant concentrations on the residual solution. As the volume of the liquid decreases further discrete droplets or clusters are formed resulting in patch wise surface coverage where the dried areas are covered by higher amounts of unabsorbed, weakly bound surfactants compared to "wet" areas in the surrounding. The transition of the solid-liquid to solid-gas interface after drying is believed to be associated by

restructuring of the layer/coating[162]. This is because of the hydrophilic/hydrophobic groups, charge, polarity, residual humidity, and hydration of the surfactant molecules, all of which are believed to influence the mobility and the alignment of the surfactant molecules or aggregates.

2.6   Solubility of Small Molecules in Polyolefins

<u>Solubility parameters – help predict solubility using a semi-empirical model</u>

Polyolefins are used widely in various processing techniques such as composite manufacturing, blending, and foaming. Depending on how polymers are processed, the properties of finished products can vary significantly. These processes may involve chemical reactions and/or mechanical processes to shape raw materials in pellets, granules, films, flakes, or powders, into the desired finished products. Therefore, the finished product may have different morphologies and properties from the raw materials[163]. Many properties of polyolefins such as viscosity, the glass transition temperature, and crystallinity are all affected by the presence of small molecules in the polymer. These molecules can effect solubility, diffusivity, plasticisation behaviour, surface tension, and crystallisation which can be critical parameters for polyolefin applications. Solubility and diffusivity are key parameters to understand and predict these property changes[164].

The literature documents large amount of data on diffusion and solubility of diffusants/solutes in polyolefins, including diffusion constants[165] and solubility parameters[166]. Solubility parameters are estimated using one physical theory that attempts to model solubility. Hildebrand and Scott in 1936 first introduced the Hildebrand solubility parameter as a numerical estimate to the degree of interaction between compounds. However, these predictions with the Hildebrand solubility parameters are made with the absence of any specific interactions, especially hydrogen bonds. The concept was later refined by Hansen[167] with Hansen solubility parameters (HSP), where the Hildebrand value is divided into three components: i) dispersion forces, ii) hydrogen bonding, and iii) polarity. The motivation for HSP was to quantify similarity in solubility and non-solubility patterns between materials. However, predictions with the Hildebrand solubility parameters do not account for the effects of morphology (crystallinity) and cross-linking. In addition, there may be non-ideal changes with changes in temperature and, in many cases, with changes in concentration. Venkatram et al. [168] carried out a critical assessment of the Hildebrand and Hansen solubility parameters by comparing predictions against actual experimental data. They concluded that Hildebrand model had a better solvent prediction accuracy for nonpolar polymers however, the limited number of parameters these models contain make it hard to capture the full complexity of

polymer−solvent interactions. Both models are built based on the concept of "like dissolves like" and identify a liquid as a good solvent for a polymer if the solubility parameters of them both are close to each other e.g., nonpolar polymers such as polyethylene are expected to be soluble in nonpolar solvents.

In combination with the Flory–Huggins (FH) theory[169] the solubility parameter approach[170] is commonly used to measure the thermodynamic compatibility between solvents and polymers. When a pure polymer is mixed with a solvent at a given temperature and pressure, the free energy of mixing will be given by Eqn 1:

$$\Delta G = \Delta H - T\Delta S \qquad \textbf{Eqn 1}$$

where ΔH is the change in enthalpy of mixing, T is the absolute temperature, and ΔS is the change in entropy of mixing. According to Eqn 1 the dissolution will only take place if ΔG is negative. ΔS is usually positive, since in solution, the molecules display a more chaotic arrangement than in the solid state, and on the other hand, the absolute temperature must be also positive. However, ΔH may be either positive or negative. When a polymer solution is formed, ΔS is significantly small. Since ΔS is small, ΔH must be small too. It must be even smaller than $T\Delta S$ to obtain a negative ΔG, and therefore, make the polymer miscible. For nonpolar macromolecules that do not have specific interactions with a solvent, ΔH is positive and has almost the same enthalpy of mixing value to that for small molecules. ΔH is given by the Hildebrand equation:

$$\Delta H = \emptyset_s \emptyset_p \left(\delta_s - \delta_p \right)^2 \qquad \textbf{Eqn 2}$$

Where $\emptyset_s$ and $\emptyset_p$ are the volume fractions of solvent and polymer, respectively, whereas δ_s and δ_p represent the cohesive energy density for solvent and polymer, respectively. This magnitude is a measure of the strength of the intermolecular forces keeping the molecules together in the liquid state, and it is the commonly known solubility parameter. As expected the literature[171] documents numerous tables displaying solubility parameters for both solvents and polymers, an example list is shown in Table 2. 3.

Table 2. 3 Hildebrand solubility parameters of relevant solvents and polymers.

Solvent/Polymer	δ $(cal/cm^3)^{1/2}$	δ (SI) $(MPa)^{1/2}$
n-Hexane	7.24	14.9
n-Heptane	(7.4)	15.3
n-Octane	(7.6)	15.4
Cyclohexane	8.18	16.8
Toluene	8.91	18.3
Isopropanol	11.97	24.9
Water	23.5	48.0
Polyethylene	7.7 - 8.2	15.8 - 16.8
Polypropylene	7.9 - 8.2	16.6 – 18.8

Standard Hildebrand values from Hansen, Journal of Paint Technology Vol. 39, No. 505, Feb 1967

SI Hildebrand values from Barton, Handbook of Solubility Parameters, CRC Press, 1983

Values in parenthesis from Crowley, et al., Journal of Paint Technology Vol. 38, No. 496, May 1966

Characterisation of polymer morphology

The key morphological properties of polyolefins are their:

- Crystallinity
- Amorphous phase
- Constrained amorphous layer

Many non-polar crystalline polymers do not dissolve, except at the temperature near their crystalline melting points. This is because crystallinity decreases as the melting point is approached and the melting point is depressed by the presence of the solvent. Very few polymers achieve 100% crystallinity, and they are commonly categorised as amorphous and semi-crystalline, with the latter morphology being characterised by tangled and disordered regions surrounding crystalline zones as depicted in Figure 2. 21. It is generally believed that the crystalline region of a polymer is not accessible to penetrants. The presence of a crystalline region imposes a constraint on polymer chains in the amorphous domain[172]. The crystalline region may be considered as cross-links which restrict the swelling or sorption of

penetrants in the amorphous domains in the network. Michaels and Hausslein[173, 174] found that the degree of swelling of the non-crystalline regions of polyethylene caused by the solvent is controlled by the tension of the inter-crystalline tie segments. For many polymer / solute combinations research shows that solubility constants are directly proportional to the volume fraction of amorphous phase[175]. However, there are systems where the solubilities have been found to be higher than those expected from the volume fraction of amorphous phase. This behaviour has been attributed to the higher probability of denser regions of amorphous material crystallising preferentially leaving the residual amorphous phase with a lower density and higher concentration of 'holes' available for absorption.
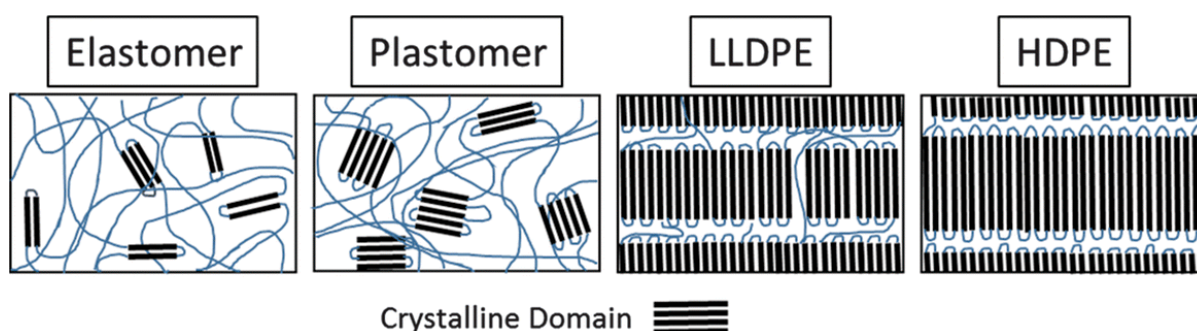
Figure 2. 21 Illustration of polyolefin morphology as a function of crystallinity. LLDPE is linear low-density polyethylene, HDPE is high density polyethylene[176].

There are many experimental methods[43, 177, 178] developed to determine crystallinity, including X-ray diffraction (XRD)[179], and thermal analysis routes such as differential scanning calorimetry (DSC)[180-183] as well as density measurements using pycnometry[182, 184]. Although these methods are widely used, they all have limitations. XRD patterns can be difficult to interpret and depends on subjective determination of the baseline intensity of the pattern due to thermal and air scattering[179]. Additionally, this technique requires a calibration curve build from samples with various known crystallinity percentages, which are difficult to achieve and can affect the results[185]. DSC calculates the crystallinity percentage by measuring the area under the endothermic peak in the heat flow curve which is then divided by specific heat of fusion for a fully crystalline sample[186]. The crystallinity percentage obtained from this method, however, is an average value which is valid for the temperature region around the melting point. In other words, the change of crystallinity that takes place upon heating the sample from room temperature to the melting point is not considered. However, unlike for XRD, it is not necessary to prepare and test calibration samples before examining a sample using DSC. Determination of the crystallinity using densities via pycnometry assumes a knowledge of the densities of 100% amorphous and 100% crystalline reference samples.

Solubility of gases in polyolefins

There has been a vast amount of research carried out on the solubility of gases such as N_2 and CO_2 in polyolefins[187-191]. Most studies involve the solubility of gas molecules in polymer melts, rather than solids, for polymer foaming applications. Plastic foams are widely used in various end-use industries such as building and construction, furniture and bedding, packaging, and automotive[192]. Polymer foaming involves dissolving a gas such as CO_2 or N_2 into a polymer melt under high temperature and pressure. Both pressure and temperature affect the solubility of the gas in the polymer, and thus the final foam product morphology. Morphology plays a major role in the mass transfer process. It is generally accepted that gas sorption and diffusion take place exclusively in the amorphous regions[174, 193]. The crystalline zones can be considered as the excluded volumes for sorption and are impermeable to the permeant[174]. More specifically, Klopffer [194] indicated that these crystalline zones have two effects on gas diffusion: (1) they increase the effective path length of diffusion and (2) they reduce the polymer chain mobility in the amorphous phase because the chain ends are trapped in the neighbouring crystalline lamellae, which leads to a higher activation energy for diffusion. Michaels et al.[174, 193] introduced a "tortuosity factor" and a "chain immobilization factor" to account for these effects.

Koros et al[195] were the first to present the partial immobilization model based on concentration gradient for sorption and permeation processes of gases in polymers. Ohzono et al.[196] measured Henry's constants for a variety of gases including propylene in molten polypropylene. Sato et al.[188] studied the solubility of propylene in samples of polypropylene with varying degrees of crystallinity. Tsuboi et al.[197] reported infinitely dilute partition coefficients for ethylene and propylene in semicrystalline polypropylene. More recently, the solubilities of propylene in high-density polyethylene, low-density polyethylene, and linear low-density polyethylene were studied by Cao et al.[191] They concluded that although LDPE and LLDPE have similar crystallinity, the propylene solubility was higher in the former, suggesting that the propylene solubility in PEs also depends on the chain microstructure. Podivinska et al.[198] investigated polymer swelling by ethylene under different sorption conditions for a broad range of PE densities showing that swelling should not be directly recomputed from the solubility and reaffirms the importance of experimental measurement of swelling in polymers.

Solubility of vapours in polyolefins

In general, processing of polymers changes their morphology by redistributing the crystalline and amorphous regions and changing the available free volume. The conversion of polymer into films, sheets, and containers is typically carried out at elevated temperature to produce a homogeneous melt or by reheating the polymer to a process temperature so that it is soft enough for shaping. The polymer is then subjected to rapid cooling. During this quenching step, many polymers undergo glass transition, which causes their molecular chains to "freeze". The molecular orientation induced may not be uniform, causing anisotropy of barrier properties for the final articles[199]. During vapor sorption, semicrystalline polymers tend to undergo complex changes. Besides gaining in mass, structural changes within the polymer may also occur, such as relaxation of polymer chains, modification of free volume, lowering of glass transition temperature, and manifestation of a viscoelastic behavior[200]. Because of their strong interaction with compatible organic compounds, the sorption behaviour of semicrystalline polymers tends to be both concentration and time dependent. Furthermore, the structural anisotropy that resulted from the conversion process can also affect the sorption behaviour of these polymers.

Sorption experiments are commonly employed to determine the solubility of small penetrant molecules in polymers under different conditions including temperature, pressure, and polymer crystallinity. Existing experimental methods employed to measure the solubility of vapours in polymers can be divided into four main classes: (i) gravimetric methods in which the polymer sample's weight is directly measured during a sorption experiment; (ii) oscillating methods in which the increase in mass is deduced from the resonance characteristics of a vibrating support; (iii) pressure decay methods in which the amount of the sorbed species is evaluated from pressure volume temperature (PVT) measurements; and (iv) flow measurement methods such as inverse gas chromatography.

Although the sorption of gases[187-191] has been extensively studied for PP and PE there appear to be a limited number of published data on the sorption of organic vapours[201] into polyolefins. Hirata et al.[172] studied the sorption characteristics of ester vapors, such as ethyl acetate and ethyl caproate, with low-density polyethylene. They found that solubility of aroma compounds in polyethylene film increased as a function of temperature. Reynier et al.[202] studied stabilisation of aroma compounds through sorption−release by packaging polymers using limonene/low density polyethylene system. In the early stage of contact, the polymer sorbs limonene, and when its concentration in food becomes low, the packaging liberates back limonene into the food. They concluded that this is due to an efficient competition between

sorption/desorption and degradation. Kim at al.[203] investigated correlations between the structure of lamellae geometrically confined in spherulite and the sorption behaviour of small molecules in semicrystalline materials. They found that the amorphous volume fraction was the predominant factor that controlled transport properties for small diffusing molecules like hexane.

Solubility of surfactants in polyolefins

Among all synthetic polymers, olefin polymers such as PP and PE are the most popular thermoplastic polymers which are widely applied in textiles, medical devices, food packaging, automobiles and many other products[204]. A vast amount of research has been done on migration of chemicals such as antioxidants[205] and other additives from plastic packaging into food products which could negatively impact food quality, taste and more importantly safety of food[206]. A number of protocols[207] and guidelines[208, 209] have been published to safeguard the quality and safety of food packaging materials and standardise testing. As a general rule, the mass transfer of chemical migrants from polymer into food stuffs can be described by Fick's second law. It is generally accepted that in semicrystalline polymers such as PE, migration is affected by the presence of the crystalline and amorphous phases[210]. It is commonly understood, from mathematical models[211] and experimental studies, that migration of small molecules occurs mainly through nanocrystalline amorphous region and the migrant movement is restricted by crystals[212]. Alin et al.[213] has shown that the migration of antioxidants from polypropylene-based articles decreases with increasing degree of crystallinity. Apart from the degree of crystallinity, crystalline domains in terms of crystal type, orientation, shape, and dispersion state could affect the diffusion in a complex way[214]. Glatto et al.[215] studied migration of Irganox 1076 from LDPE films with different thicknesses and observed that the diffusion coefficient decreased as a function of film thickness. They explained this behaviour as a result of crystal distribution and size.

The 1983 paper of Roy et al.[216] commented on the growth of interest in the phenomena of diffusion of surfactant molecules through polymeric membranes. Their observations on micellar permeability stated an independence on the surfactant concentration, but a solubility dependence with temperature. They report that the diffusivity of a solute into the polymer is proportional to the ratio of the absolute temperature and viscosity of the transport medium[216]. Furthermore, they found that the viscosity decreases exponentially with elevation of temperature[217] which in turn increased diffusivity of a nonionic surfactant structurally similar to Triton X-100. Around the same time, Needles at al.[159] studied the effect of heat on selected properties of Triton X-100 coated on fabrics. They concluded that the wettability and wicking

properties of surfactant/heat-coated fabrics were improved, and these showed enhanced dye uptake which increased as a function of temperature. Yet, the effect of surfactant/heat-treatment had limited effect on selected physical properties of the fabric including shrinkage, stiffness, wrinkle recovery, and tensile properties. More recent developments reviewed by Lindman et al. [150, 218] highlight the fact that surfactant adsorption increases strongly with increasing temperature and that nonionic surfactants and polymers phase separate at higher temperature. Also, there was some work done on the miscibility of polymers (as copolymers and blends) with polyethylene oxide (PEO)[46, 157, 219, 220] a semi-crystalline synthetic polymer, with general molecular structure $(CH_2CH_2O)_n$. Although, these studies don't directly consider surfactant-polymer interactions in the solid state, one can draw on such findings and be able to indicate attainable miscibility for nonionic polyethylene oxide-based surfactants[143] with polyolefins because they share similar structures and therefore one would expect similar behaviours. The fact that blends of PEO with PE and PP exists is evidence which supports the importance of surfactant–polyolefin solubility.

2.7 Measurement Techniques

A range of experimental techniques have been utilised in this thesis for investigating polymer–surfactant interactions and for understanding the behaviour of polymeric surfaces after modification with surfactants. Often it has been desirable to combine several different methods for a more comprehensive understanding of specific phenomena. The main experimental methods used for this research have been grouped into the following three categories:

1. Surface characterisation techniques
2. Bulk characterisation techniques
3. Network – 3D imaging characterisation methods

The basic operating principles of the main techniques and details of the instruments used in this research are presented in Chapter 3. In the following sections the literature is reviewed on how these different techniques are utilised for studying different materials with a focus on surfactant-polymer systems where available.

2.7.1 Surface Characterisation Techniques

2.7.1.1 X-ray photoelectron spectroscopy (XPS)

The theory and principles of XPS are presented in Chapter 3. This technique provides depth profiling information, quantitative elemental surface composition, surface chemical state identification, empirical formula derivation, electronic state binding energies and densities, elemental mapping (XPS imaging)[221]. It is also non-destructive to the sample and can analyse both conductive and insulating materials with high sensitivity and low detection limits. A typical XPS experiment is conducted under ultrahigh vacuum conditions and this condition could be a disadvantage because some samples cannot be analysed under such conditions. XPS is an expensive technique, data collection can be slow, and data analysis can be complex. A comprehensive review of surface analysis by XPS is published by Watts and Wolstenholme[222]. Cai et al.[153] characterised nonwoven fabrics coated with surfactants using XPS proving the adsorptive presence of surfactants onto the nonwoven fabrics. More recently Tang et al.[223] fabricated polypropylene nonwovens with a grafted surface polymer layer for use as protective materials to remove aromatic gaseous pollutants and particulates from the air. The chemical compositions of original PP nonwoven and functional PP nonwoven were characterised using XPS. Vargha et al.[224] analysed using XPS modified PP nonwoven fabrics after surface oxyfluorination and found the presence of $-CF$, $-CF_2$, $-CHF$ and $-C(O)F$ groups. The $C=O$ groups and the $C=C$ stretching of the formed $-CF=C(OH)-$ groups could also be detected.

2.7.1.2 Atomic force microscopy (AFM)

The theory and principles of AFM are presented in Chapter 3. AFM is considered a useful tool for measurements in polymer science[225-228] and engineering[229, 230]. A recent review by Nguyen-Tri et al.[231] highlights the extensive use of AFM techniques, (sometimes coupled with other methods such as IR) for the nanoscale characterisation of polymeric materials. The surface roughness of the PP nonwoven fabrics exposed to C_2F_6 plasma treatment was measured by Edwards et al.[232] using AFM in contact mode and under ambient conditions. Homola et al[233] used AFM in tapping mode to study the surface changes (surface roughness) of PET films before and after plasma treatment. AFM is used not only for topography images of samples but also to measure force–distance curves which are useful for studying substrate surface properties and material properties, including hardness, surface charge densities, adhesion and Hamaker constants[221]. Other advantages of AFM include, little or no sample preparation, ability to work in vacuum air or in liquids, causing little or no sample damage. Unfortunately, AFM imaging is not a particularly fast technique and is difficult to use for very rough or complex

surface topographies. The data is dependent on the type of the tip being used and it is possible for both the tip and the sample to be damaged during the analysis.

2.7.1.3 Time–of–flight secondary ion mass spectroscopy (ToF–SIMS)

ToF-SIMS is widely used in material science disciplines in studies of materials such as polymers[234], pharmaceuticals, forensics, semi-conductors, and biomedical materials [235]. It has been used to evaluate surface properties of polymers before and after surface modification in similar way to SEM and XPS. Advantages of TOF-SIMS include elemental and chemical mapping on a sub-micron scale, high mass resolution and sensitivity, surface analysis of insulating and conducting samples, depth profiling and non-destructive sample analysis. TOF-SIMS as an elemental analysis technique detects all the elements in the periodic table, including hydrogen. The main limitation of TOF-SIMS relate to difficulty in quantitation of data of samples with complex surface chemistry because of the strong matrix effects on secondary ion yields and lack of relevant standards[236]. Despite its limitations this technique is widely used for polymer analysis. Functionalisation of PP based fibre surfaces conferred by C_2F_6 plasma exposure was explored by means of the semiquantitative ToF-SIMS technique performed by Edwards et al.[232] who examined untreated and treated nonwovens intended for wiping bacterial contamination from frequently touched surfaces. Furthermore, a patent[32] filed by Procter and Gamble details how TOF-SIMS[32] can be used to evaluate the distribution and migration of actives on film or polyolefin based nonwoven surfaces in a semi-quantitative way by providing a mass spectrum and image analysis of surfactant distribution of the outermost 3 nm of the test surface.

2.7.1.4 Contact Angle

The theory and principles of contact angle are presented in Chapter 3. This method is a very common technique used to determine the wettability of a solid surface and is considered the simplest, cheapest, and most rapid method for assessing the surface energy of a polymer substrate. However, it is chemically least informative technique, providing only information about the surface energetics of the material[237]. Also, the accuracy and reproducibility of the measurements can be operator dependant, which can lead to subjectivity and inconsistency on the measurements, especially for non-planar substrates. This issue nowadays is minimised with the advent of automated image capture systems on many contact angle goniometers. Contact angle measurements are most valuable for rapidly detecting the presence – but not the identity – of surface contaminants, and for studying the extent and stability of surface

treatments. Contact angles is very practical for the rapid verification of the efficacy of surface modification procedures which, by the insertion of new chemical groups, usually alter the air/water contact angles[238].

The variety of techniques commonly used to measure contact angles have been discussed by Yuan et al.[239] Various approaches reviewed by Williams[240] and Heng et al.[241] provide methods for measuring contact angles to calculate fibre surface energies. Others have published contact angle studies on natural fibres[242, 243]. Wang et al.[244] investigated the improvement of the hydrophilic properties of the nonwoven surface of polypropylene following plasma treatment. They characterised the samples by contact angle measurements before and after treatment, demonstrating hydrophilic properties after the plasma treatment, evidenced by reduced contact angles. The wettability of nonwoven polymer surfaces can be improved by coating them with surfactants which reduce both the surface tension, and the interfacial tension between the solid and the drop, increasing thus the spreading coefficient[160]. Contact angle has regularly been utilised as the techniques of choice to measure wettability of such materials before and after treatment[30]. The reduction of the surface energy of PP based nonwoven fibres via C_2F_6 plasma exposure was assessed by Edwards et al.[232] using contact angle measurements. They also measured water contact angle on surfaces expected to change due to bacterial contamination and found an increase in contact angle and a decrease in wetting tension as the level of contamination increased. It is known that real solid surfaces like nonwoven fabrics are fundamentally inhomogeneous, and a single value of surface free energy is not necessarily representative of the entire surface. Real solids in fact exhibit a range of lower and higher energy sites on their surfaces due to presence of different types of surface functional groups, surface topographies, surface irregularities or defects. The surface energy measurements are representative of localised areas of the material, where the drops are placed, and it is not easy to map the entire substrate of interest. IGC is instead considered a better technique for surface energy measurements because it measures the surface energy across a much larger sample surface area, giving statistically more meaningful data.

2.7.1.5 Inverse Gas Chromatography IGC

The theory and principles of IGC are presented in Chapter 3. Detailed information about the IGC method and the underlying theory can also be found on many books[245-250] and journals[251-257]. This method is a physio-chemical characterisation technique used for different materials including polymers[258-260], and natural fibres[257, 261, 262]. A detailed application review by S. Mohammadi-Jam et.al.[263] highlights advantages including the high sensitivity, efficiency, and

accuracy of measurements. IGC is the only chromatographic technique in which a solid-state material may be characterised in its native state. Bahners et al.[264] provide a critical analysis comparing the pros and cons of various methods commonly used in textile research summarising that although contact angles can be useful for characterising the effects of fabric finishing's, fibre surface modifications, they are limited, concluding that quantitative discrimination is best achieved via IGC analysis. However, alkanes are not always best suited and for some materials such as polyolefinic materials, they do not work because they absorb into the material limiting the use of IGC in such instances.

2.7.1.6 Brunauer-Emmett-Teller (BET) Gas Adsorption Method

The theory and principles of BET are presented in Chapter 3. The BET theory is based on an simplified model of physisorption,[265] but despite this limitations the BET-nitrogen method is considered a standard procedure for surface area determination for porous solids. Common applications in which knowledge of the surface area is critical include studies of polymers, coatings and paints, catalysts, pharmaceuticals, absorbents, fuel cell technology among a variety of other applications. Aguirre et al.[266] measured specific surface area of the modified PP membranes obtained using UV radiation induced graft copolymerisation utilising N_2 BET analysis.

2.7.2 Bulk Characterisation Techniques
2.7.2.1 Density: Helium Pycnometry

The theory and principles of density measurements by helium pycnometry are presented in Chapter 3. Helium pycnometry is generally the method of choice for density measurements for porous materials due to its simplicity, non-destructive nature, well-established accuracy, and existing measurement guidelines[267]. However, data interpretation could be difficult for samples that require drying or which are mechanically unstable. Measuring the apparent volume is important for many adsorption-based applications relevant to many industries, such as industrial, personal care, construction, and pharmaceutical. Commonly, density measurements of materials including fibres are conducted for quality control purposes. Dudie et al.[268] have used density measurements, (and DSC) to study recrystallisation processes of isotactic PP during accelerated aging. More recently, Nguyen et al.[182] provided methodologies for understanding material characteristics through signature traits from helium pycnometry.

2.7.2.2 Differential scanning calorimetry (DSC)

The theory and principles of DSC are presented in Chapter 3. DSC is used in many industries[269] including, polymers, pharmaceuticals, cosmetics, food, semiconductors, and electronics. Munaro et al. [269] employed DSC and density measurements to quantify the crystallinity and crystallite dimensions of specific grades of LDPE/HDPE blends. However, it is well documented in the literature[180] that DSC, although widely used, does not always provide data on polymer % crystallinity comparable to those obtained by density measurements or other techniques. DSC defines the degree of crystallinity close to melting point rather than at room temperature and this difference could be one of the reasons for the discrepancy between DSC data and data from other analytical techniques such as density, NMR and SAXS[270] which measure crystallinity at ambient temperatures. Regardless, DSC is still widely used as it provides an easy to use means of characterising the important thermal properties associated with polymer materials as reported by Vargha et al.[224] who studied oxyfluorination modified PP nonwoven fabrics.

2.7.2.3 Ellipsometry

The theory and principles of Ellipsometry are provided in Chapter 3. This method is an ideal technique for studying thin films with thicknesses in the nanometre range, up to about 1000nm. Other applications of ellipsometry include, thin film thickness mapping, sample composition analysis, optical constant determination as well as sample crystallinity assessment[271]. Among the various experimental methods suitable for studying thin polymer films, ellipsometry plays a special role[272, 273]. A recent review by Erber et al.[274] concerning the determination of the glass transition of polymers in nanoscopic films pointed out the unique role of ellipsometry as a non-destructive and very sensitive optical technique. Ellipsometry has also been used by Higuchi et al. [275] to characterise molecular nonwoven fabrics in the form of ultrathin helical polymer films by measuring the growth of the helical monolayers. Ellipsometry can be combined with other instrumentations such as a DVS to study properties of a thin polymer film providing thus complimentary information about the diffusion mechanisms of small molecules into polymers and their effects on swelling.

2.7.2.4 Dynamic Vapor Sorption (DVS)

The theory and principles of DVS are presented in Chapter 3. It can be used to study different materials such as those used for personal care products [276], pharmaceuticals [277], food and

packaging[278]. The vapor sorption behaviour of surfactant coated nonwoven fibres (used to manufacture nappies), for example can be studied using a DVS under "real world" conditions covering a range of temperatures, humidities and vapours, (water and organic)[279, 280]. The pharmaceutical industry uses DVS to determine the performance of drug formulations, excipients, and packing films. Any moisture-induced phase changes of these products can have an adverse effect on the chemical properties, altering the dosage, yield and bioavailability calculations. The packaging industry uses DVS to ensure products are performing efficiently by measuring the moisture and diffusion properties of food packaging ensuring thus the food has the longest shelf life possible. A review by Sheokand et al. [281] discusses the use of DVS for quantification of amorphous content in predominantly crystalline materials. Bley et al.[282] evaluate the moisture-protective ability of different polymeric coatings using DVS and DSC. The improved surface properties of nonwoven fabrics of PE and PET coated with several kinds of surfactants, were studied using DVS by Cai et al[59] who showed that the specific surface resistance of the nonwoven decreased substantially after the adsorption of surfactants.

2.7.3 Network – 3D imaging characterisation methods

2.7.3.1 Scanning Electron Microscope (SEM)

The theory and principles of SEM are presented in Chapter 3. SEMs have found use in a variety of applications[283] in a number of scientific and industry-related fields. In addition to topographical, morphological, and compositional information, SEM[284] can detect and analyse surface fractures, provide information in microstructures, examine surface contaminations, reveal variations in chemical compositions when combined with EDX, and identify crystalline structures[221]. Cai et al.[153] characterised nonwoven fabrics coated with surfactants using SEM proving that adsorption of surfactants onto the nonwoven fabrics really occurs. Vargha et al.[224] analysed using SEM modified PP nonwoven fabrics after surface oxyfluorination and showed slight roughening of the oxyfluorinated surfaces. SEM was employed by Edwards et al.[232] to image plasma treated PP based fabric samples before and after wiping tests which removed bacterial contamination. Furthermore, Ghassemieh et al.[285] used SEM to study microstructural changes in nonwoven fabrics. More recently, Cheema et al.[286] used SEM to characterise specially developed nonwovens for apparel applications. Although, SEM provides high quality images of the fibre surfaces it cannot see details within the fibre network or within individual fibres. It is, therefore, insufficient for quantitatively analysing complex 3D porous polymer media due to the inability to image in-side/through the fibre network, because of complex light scattering from these samples, and inability to sensor inside individual fibres.

2.7.3.2 Optical Profilometry

The theory and principles of optical profilometry are presented in Chapter 3. Back in 2001 Fairbrass and Williams [287] applied laser surface profilometry as a non-destructive technique that required little or no sample preparation for studying samples of poly(vinyl chloride) artificially aged by exposure to UV light at ambient conditions. More recently, Jaglarz et al.[288] used optical profilometry to study thin transparent polymer films. Their investigation enabled them to find many interesting features concerning surfaces over a much larger area than with AFM and SEM techniques while successfully determining parameters such as the surface roughness. However, the technique is insufficient for analysing complex 3D porous polymer media due to the inability to image in-side/through the fibre network, because of complex light scattering from these samples, and inability to sense inside individual fibres. Some typical applications of optical profilometry include measuring surface roughness, step heights and critical dimensions analysis as well as film thickness which is useful in many industries[289-291].

2.7.3.3 Confocal Laser Scanning Microscopy (CLSM)

The theory and principles of CLSM are presented in Chapter 3. Although CLSM is routinely used in the biomedical sciences there are a few studies which have utilised CLSM for studying polymer-based materials too. Choong et al.[292] used CLSM for quantitative characterization of both the morphology and topology of the pore space of electrospun nonwoven fibre mats. CLSM was also used successfully by Charcosset et al.[293] to characterize microfiltration membranes and reconstruct 3D images which helped delineate the morphology of the microporous membranes. Equally, CLSM was used to study the surface morphology of polymer blends as a function of blend preparation conditions by Li et al.[294]. Overall, several studies[295, 296] have demonstrated the suitability of CLSM for 3D structural analysis of polymer fibre-based materials. Recently, Lin et al.[297] used CLSM for high-resolution 3D imaging of electrospun fibres fouled by oil presenting a new method for evaluating development of fouling within microfiltration membranes.

2.8   Research Gap Analysis

Chapter 2 discusses research involved in polymer surfactant interactions, with the focus on polyolefin-based nonwovens. Although such materials are commonly used in vast numbers of applications, they are hydrophobic due to the hydrocarbon nature of the base polymers. This limitation necessitates surface modifications to make polymeric based nonwovens suitable for

different functions. Therefore, they are routinely coated with surfactants, which converts them into hydrophilic materials that are wettable and allows water to pass through them. This Chapter examines different modifications techniques, and it has highlighted that most polymer surface modifications are not permanent. It is a common industrial experience that the surface hydrophilicity of nonwoven coated materials is time dependent and significant losses in surface concentrations of surfactants are documented. It is therefore important to understand how the surfactants interact with the polymer and their fugitive nature to improve performance of product manufactured using surfactant coated polymeric nonwovens.

The research gap in this field is emphasised in the literature review which identifies key areas which are poorly understood and need exploring. One example is the limited understanding of the mechanism of interaction between surfactant and the polymeric nonwoven fibres. The location of the surfactant in these fibre networks is not known. There is a lack of literature documenting how surfactants are distributed in time or space following the coating process. Once the nonwovens are coated with surfactants it is unclear how the surfactant and the polymer interact, what are the thermodynamics, kinetics, or molecular factors at work. Nor it is known how their interactions develop over time and/or under different environmental conditions. The analysis of the literature shows that to date, there have been numerous studies on surfactant-polymer interactions, however a limited number of studies[32] have looked at surfactant-polymer interactions in solid state including specifically the migration of surfactants coated onto nonwovens. Therefore, a clear understanding of how surfactants behave in solid state polymers is lacking.

This thesis plans to fill this gap by developing a novel method for visualising and quantifying surfactant distributions on polymeric nonwoven fabrics in 3D. The main motivation for such studies are to improve performance of hygiene products manufactured using surfactant coated nonwovens which lose hydrophilicity properties during storage as a result of the fugitive nature of the surfactants. However, there are plenty of other applications for these nonwoven materials, and these experimental methods in materials science and biological materials where, for example, traditional liquid staining methods are not practical.

2.9 Aims and Objectives

The overarching aim of this theses was to increase the fundamental scientific understanding of the physiochemical relationships of surfactants with complex 3D polyolefinic fibre networks. This was a multifaceted project requiring a mixture of experimental approaches to investigate

different surfaces and polymer materials, perform aging studies and develop practical solutions.

The first objective was to develop a method to visualise and map, both qualitatively and quantitatively in 3D, the surfactant distribution/heterogeneity in space and time across polyolefin-based nonwoven fabrics. This method was an important first step confirming the problem of surfactant migration from material surfaces ahead of the development of a fundamental understanding of the science governing surfactant loss process(es). The second objective was to characterise the surface properties of these classes of materials and to establish critical thermodynamics, kinetics or molecular properties that define the surfactants behaviour in these systems. The third objective was to investigate the significance of surfactant solubility and diffusion into polyolefins as a critical factor to explain the fugitive nature of surfactants and establish the key polymer properties relevant to the understanding of the surfactant loss process(es). Finally, the last objective was to explore ways to model the surfactant loss mechanism so that one can manipulate and control it under real world conditions. In the long term such knowledge is invaluable as it can be used to solve problems concerning different industries and products which have as base material a nonwoven polymer coated with surfactant(s), such as sanitary products, medical sorbent-based products, green house membranes[298], de-misting filters, and porous polymers used for moisture harvesting amongst many others.

3 Experimental Methods and Materials

3.1 Techniques Introduction – Imaging Methods

3.1.1 Confocal Laser Scanning Microscopy (CLSM) – Theory

An explanation of fluorescence is necessary before discussing the confocal laser scanning microscopy (CLSM). Generation of luminescence through excitation of a molecule by ultraviolet or visible light is termed photoluminescence, which is subdivided into phosphorescence and fluorescence, depending upon the electronic configuration of the excited state and the emission pathway. Fluorescence and phosphorescence are best explained with the help of the Jablonski diagram depicted in Figure 3. 1. When a fluorophore absorbs light it causes the transition of an electron into a higher electronic excited state, e.g., from S0 to S2. Once excited, the molecule uses several different pathways to lose the absorbed energy and return to the ground state. Fluorescence emission is one-way fluorophores in an excited state can lose energy. Another pathway of energy loss occurs after intersystem crossing by means of a forbidden transition to the triplet state[299]. Molecules in the triplet state reach the ground state causing light emission termed phosphorescence. This latter process is slow, microseconds, relative to fluorescence, nanoseconds[299-301].
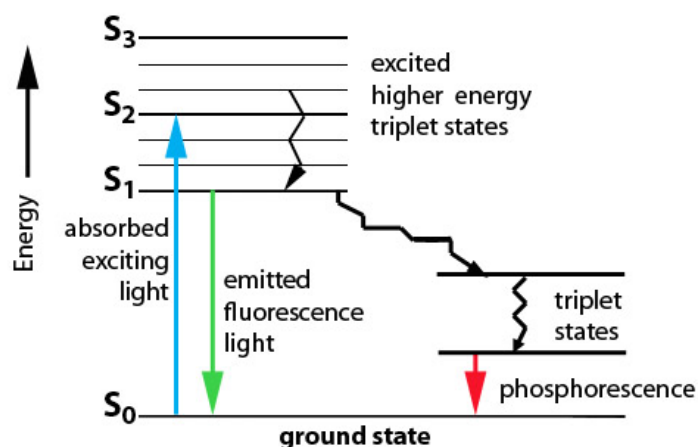
Figure 3. 1 Jablonski's Energy Diagram[302].

Invented by Marvin Minsky[303] in 1955, confocal scanning microscopy is a well-established technique in the biology, biomedical, as well as materials sciences[294, 295, 304-312]. The first commercial confocal microscope was developed in 1987[313]. Since then a range of confocal microscopy techniques have been developed including spinning disk, dual spinning disk, confocal laser scanning microscope and programmable array microscope[314]. The laser scanning microscopes use a laser to scan over the sample, meaning that the image of each

section is built up by adding information from regions that are sampled in sequence[315]. CLSM uses a laser as the light source and used dichromatic mirrors to reflect the light and scan it across the sample. Photomultiplier tube detectors (PMTs) collect the photons emitted by the sample via a computerised acquisition, processing, analysis and display of images. Its confocal exclusivity comes from the utilisation of optical pinholes which eliminate out of focus light that occur at points above and below the focal plane thus producing extremely high-quality images with excellent z direction resolution. Auto fluorescent samples or samples treated with a fluorophores can be analysed using CLSM and 3D images of the sample can be created using a series of optical sections obtained by combining a series of x-y scans taken along the z axis[316]. The confocal light pathway is depicted in Figure 3. 2.
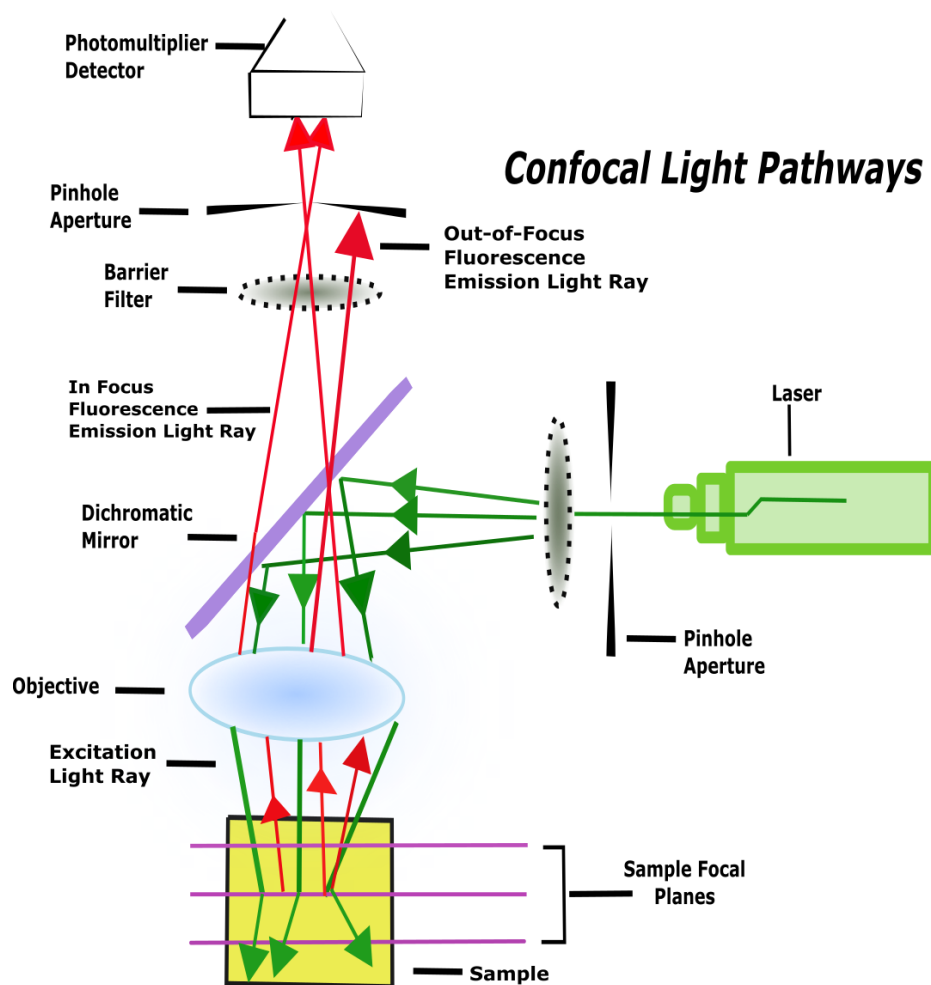
Figure 3. 2 Schematic diagram of the optical pathway and principal components in a laser scanning confocal microscope[317].

The light emitted by the laser system, the excitation source, passes through a pinhole aperture positioned in front of the laser to a right-angle mirror via a barrier filter. As the laser is reflected by the dichromatic mirror and scanned across the sample in a defined focal plane, fluorescence

emitted from points on the sample within the same focal plane, pass back through the dichromatic mirror and is focused as a confocal point at the detector pinhole aperture. Because only a small fraction of the autofocus fluorescence emission is delivered through the pinhole aperture, which eliminates out-of-focus light in samples whose thickness exceeds the immediate plane of focus, extremely high-quality images are produced. The focal volume in the sample is controlled by the numerical aperture (NA) of the system's objective lens and the wavelength of the light source used (λ). These parameters are directly related to the system's resolution. The lateral (x-y) resolution of depends on the wavelength (λ) of light and on the NA of the objective lens[318]. Assuming a complete and uniform illumination, the maximum lateral and axial resolution of a confocal microscope can be defined using Eqn 3 and Eqn 4 respectively:

$$R_{xy} = \frac{0.37\lambda}{NA} \qquad\qquad \textbf{Eqn 3}$$

$$R_z = \frac{1.4\,\lambda\eta}{NA^2} \qquad\qquad \textbf{Eqn 4}$$

where η corresponds to the refractive index of the immersion medium. Rayleigh's criterion is a rule of thumb for estimating the smallest features that can be resolved laterally[319].

Confocal microscopy offers several advantages. It produces high resolution images because of its ability to control depth of field[317] and capability to reduce the background information. It can collect serial optical sections of thick samples facilitating thus reconstruction of 3D images[306] relatively easy in a non-destructive way under STP. Among its many advantages the technique has some short comings too. Confocal imaging in some cases requires a compromise between resolution, scan time, and photo destruction of the sample. The higher the resolution, the more time required for the scan, and the longer the fluorophore is exposed to the laser[310]. Photobleaching is the most significant problem with confocal microscopy. There is a tendency to oversample both spatially and temporally in xy and z direction because of the belief that increasing the laser intensity will increase the signal intensity. The extra light leads to quenching of the fluorophores, heating of the sample, photobleaching and damage of the sample. Although the CLSM facilitates optical sectioning of thick samples, the depth of imaging is limited by optical penetration of incident light and the signal-to-noise ratio. Confocal microscopes can be very expensive[320] too relative to conventional microscopes.

3.1.2 Confocal Laser Scanning Microscopy (CLSM) – Instrumentation

A confocal laser scanning microscope (Leica TCS SP8) with a tunable white light laser (470-670 nm) combined with multiband spectral detector, acousto-optical beam splitter (AOBS) and super-sensitive Leica HyD hybrid detectors was used to analyze all the nonwoven samples. Lasers and detectors were stabilized for 30 minutes before images were taken. The 10x water immersion lens (HC APO LU-V-I 10x water NA 0.3) operating at 530nm (20% laser power and 50% laser intensity) and a 540nm-690nm filter was utilised. A mechanical grid see Figure 3. 3, was used to facilitate sample area identification, though that limited the working distance making it difficult to use lenses with large magnifications. However, a large field of view was beneficial to understand the scale of the heterogeneity in the samples, and hence the choice of lens. An Airy pinhole of 1.0AU was selected as was a scan resolution of 1024 x 1024 pixels and a 1mm^2 x-y scan area. The z dimension scans ranged from 100-500μm with each step-in height set to 4, 5 or 10μm, depending on the overall z stack height. The x scan was bidirectional, with a frequency of 600Hz. Each confocal image was obtained using three different imaging channels; fluorescence, reflected light and bright field. The microscope can be used to image in various scanning modes which include a planar section (xy), a vertical section (xz), and time-dependent imaging modes. Each xyz-scan data set shown represents an average of six scans.
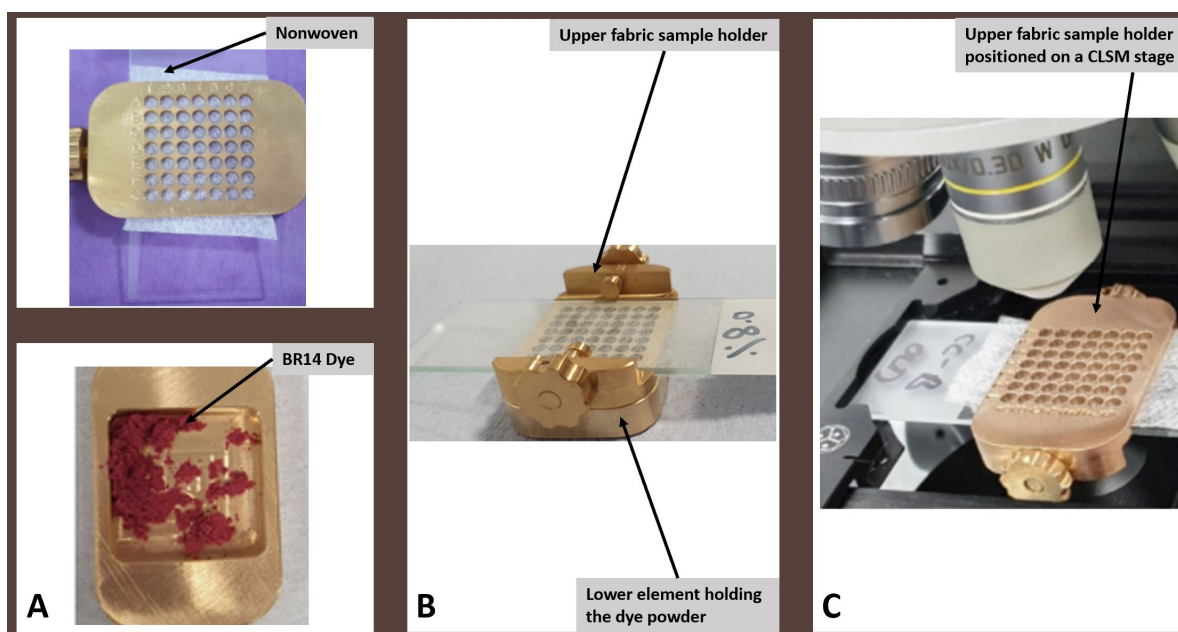
Figure 3. 3 Customised sample preparation unit which consists of A) the upper fabric sample holder and the lower element which contains the dye powder. The unit parts are assembled as shown in B and the fabric sample holder fits in the CLSM stage as shown in C.

Image processing and analysis was performed using Fiji[321]/ImageJ, (https://imagej.net/Fiji) and Comstat2.1[322] (www.comstat.dk/). The Leica LAS X software was used for image reconstruction. The

CLSM raw data files are LIF formats and are converted into ome.tiff files for subsequent analysis with Comstat (http://www.comstat.dk/). The Comstat feature "surface area" was measured in this study because this parameter is the fundamental physical metric of our problem; the surface area of the fabric layers coated by surfactants. In Comstat I applied a light intensity threshold to every pixel of imaged data via the popular Otsu[323] automatic image thresholding technique. Comstat then generates a .txt file representing the total number of pixels in each image which exceed the selected threshold. For both the fluorescence and reflectance image, this relates to total number of pixels which fluoresce and the total number of pixels in which fibre surface area is detected, respectively. Of course, a pixel cannot be fluorescent unless it is also on the fibre surface. These pixel numbers are then averaged for the typically 100 layers which constitute the full 3D confocal image. These results are then normalised using the fluorescence and reflectance pixel numbers to account for sample voids present and random fibre orientations. This way the percentage area of fluorescence (which is associated with locations rich with surfactants) occupied in each layer per unit fiber is measured.

A custom sample preparation unit was fabricated consisting of an upper fabric sample holder and lower element which contains the BR14 fluorescent dye – see Figure 3. 3. The solid-state water-soluble dye, at elevated temperatures, has a high enough vapor pressure to transfer via the gas phase and dissolve in the surfactant domains on the nonwovens. The vapor phase fluorophore dissolves selectively in hydrophilic regions preferentially to hydrophobic areas of the nonwoven because it has higher dissolution affinity for polar solvents (see Chapter 5) as well as surfactant materials. The workflow protocol is presented Chapter 5 and it involves 1) sample preparation/staining with BR14 dye at elevated temperatures, 2) microscopy and image acquisition using CLSM and 3) data processing with Fiji/ImageJ and/or Leica LAS X. Details of image processing and analysis method are presented in Chapter 5.

3.1.3 Scanning Electron Microscopy (SEM) – Theory

The Scanning Electron Microscope (SEM) works on the principle of scattering of electrons from the surface of a sample. It uses a high-energy electron beam, (typically 10-30 keV) to scan across an electrically conducting surface in a raster scan pattern way[324]. Electrons interact with the sample in different ways; some are absorbed, others are back scattered, and some electrons are ejected from the sample as secondary electrons. The dislodged electrons are attracted and collected by a detector, and then translated into a signal. Signals are then amplified, analysed, and translated into images of the topography being inspected. Backscattered electrons are reflected after elastic interactions between the beam and deep

regions of the sample whereas secondary electrons are a result of inelastic interaction between the electron beam and the sample surface. They each provide different types of information, backscattered electrons images show high sensitivity to differences in atomic number whereas, secondary electrons imaging can provide more detailed surface information[324]. If the number of electrons that strike the sample is not equal to the number of electrons that leave the sample, then the sample will build up a charge. This is called charging which negatively affects the quality of the resulting image. Therefore, measurement of nonconducting samples is difficult. To prevent charging many SEM samples are coated, via vapour deposition, with a thin layer of a metal e.g., gold. Most SEM images are produced by collecting secondary electrons which are detected by attracting them onto a phosphor screen which subsequently glows. The intensity of the light is then measured with a photomultiplier[325].

The main parts of a SEM instrument, shown in Figure 3. 4, are the electron gun, lenses, vacuum chamber, sample chamber and the stage, detectors and a computer as the processor and controller. Many electron microscopes have both secondary and backscatter electron detectors. Vacuum of <10^{-5} torr) is required because otherwise the electrons used for imaging will scatter off gas molecules which interfere with the electron beam focusing on the sample.
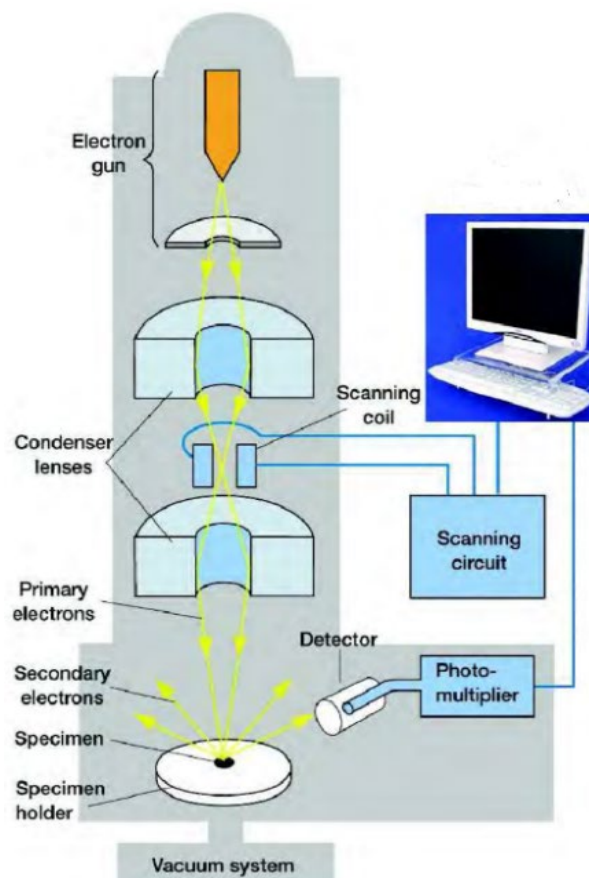
Figure 3. 4 Schematic diagram of an SEM system[326]

SEMs can visualise sample surfaces with high depth of field ~30mm and lateral resolutions 1-20nm thus producing images which are a good representation of the 3D sample, as well as analysing the physical and chemical state of the substrate[324]. The instrument works relatively quickly once sample preparation has been completed and is easy to use. The introduction of environmental SEM in 1980s has made possible the study of wet samples too[283]. Disadvantages of SEMs include high costs, the need for sample preparation, exposure of the sample to high vacuum, requirements for a vacuum and cooling system, vibration-free space housing in isolated areas from ambient magnetic and electric fields.

3.1.4   Scanning Electron Microscopy (SEM) – Instrumentation

A LEO Gemini 1525 Field Emission SEM, (Carl Zeiss NTS GmBH), operated at 5 kV was used to record images of all the samples and document their surface morphology. Prior to analysis all samples were mounted on specimen holders and sputter coated with chromium, (sputtered for 4min at 50mA) to inhibit charging during examination. The detection modes are indicated in the bottom-right corner of each image.

3.1.5   Optical Profilometry – Theory

Optical microscopy, also referred to as scanning white light interferometry, is classic non-contact surface profile measuring technique. It utilises a light source to scan the sample surface, a beam splitter, a mirror to collect the reflected light, and a detector; a schematic depicted in Figure 3. 5. The light beam is split into two paths by the beam splitter. One path directs the light onto the surface of the test material which is passed through the focal plane of a microscope objective, and the other path directs the light to a reference mirror. Reflections from the two surfaces are recombined and projected onto an array detector resulting on an interference pattern based on the phase difference of the arriving signals and their sums. Since the reference mirror is of a known flatness, and as close to perfect flatness as possible, the optical path differences are due to height variances in the test surface. The optical profiler scans the material vertically and the intensity at each pixel is monitored. The maximum of the interferogram, (the interference image), determines where each pixel came into focus and the software stores the z-position. A surface map is constructed by plotting each individual pixel's xyz coordinate position.
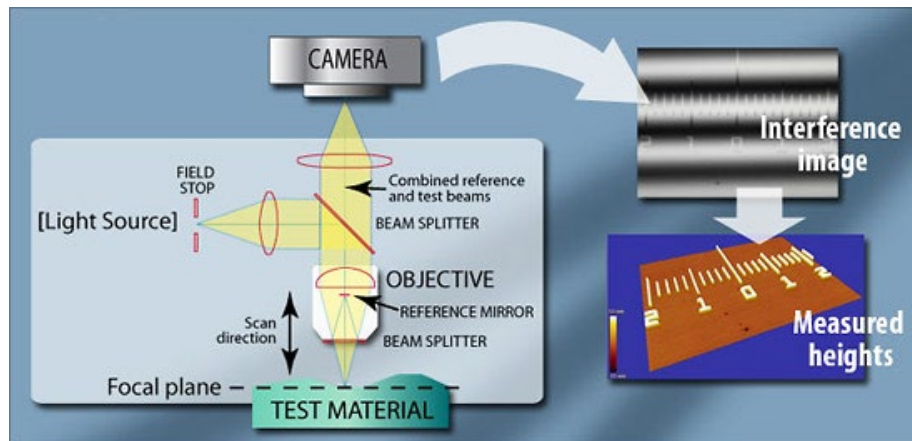
Figure 3. 5 Schematic of an optical profilometer[327].

Advantages of the technique include its non-destructive nature, rapid data acquisition capabilities and high field of view. It also measures samples under ambient conditions and without the need for sample preparation. Limitations of the technique include a similar lateral resolution to that of an optical microscope. Scans in z direction are also limited. If there is a film present on the sample surface it must be thicker than 1μm to resolve the interference pattern reflected from the film and surface, respectively.

3.1.6 Optical Profilometry – Instrumentation

Nexview™ NX2 3D non-contact optical profiler from Zygo was used to measure optical surface roughness and polymer film thickness as well as image nonwoven fibres utilising white light interferometry. All the data was processed using Mx software.

3.2 Techniques Introduction - Surface Characterisation Methods
3.2.1 Inverse Gas Chromatography (IGC) – Theory

Inverse gas chromatography (IGC) is a gas phase sorption technique. It has links to the origins of chromatography pioneered by Tswett in 1903 and principles established in the 1950s for analytical gas chromatography[328, 329]. As a molecular probe method, IGC uses a vapour phase species with known properties to investigate surface and bulk properties of solids. Surface energy is the most commonly measured property determined by IGC. With this information it is possible to predict material properties such as adhesion, cohesion, wetting, spreading, and liquid penetration, all directly related to how a material functions, how it behaves and how it can be used in commercial products. Instruments such as SMS's iGC-SEA allow for experimentation to be carried out at different temperatures and at different humidity's which

means materials can be studied under real world conditions. The instrumentation contains a glass column, in which the material of interest is packed into, which is housed into a temperature-controlled oven. The IGC also contains vapour probe reservoirs, a detector, mass flow controllers and a computer as the processor and controller. The elution time of known vapour molecules, "probes", injected into the carrier gas helium that passes through the packed column of fibres or particles at a known flow rate, determines the strength of solid-vapour interaction. The probes passing through the column and eluted at the end of the column are detected via a flame ionisation detector (FID). A schematic of a typical IGC instrument is shown in Figure 3. 6.
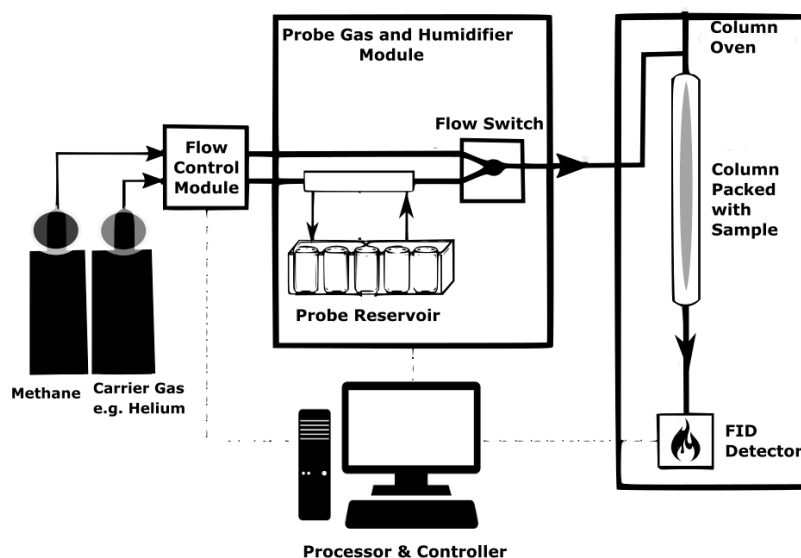
Figure 3. 6 Schematic diagram of a typical IGC.

The retention volume of the probe molecules, the time required for a solvent to pass through the column multiplied by the carrier gas flow rate, is the raw data obtained by IGC. This may be visualised by a chromatogram, an example of which is depicted in Figure 3. 7. The dead-volume of the system, the volume swept through the through the system without any interaction, is measured using methane, a non-interacting probe which is run under the same experimental conditions as the vapour injected under study. This measurement allows the nett retention volume V_N and then the partitioning coefficient for the solid-vapor to be determined. The shape and the retention volume of the chromatographic peak reflect the magnitude and the type of interactions between the solute and the material being studied, and it can be used to measure surface energy, acid base functionality of surfaces, diffusion kinetics, solubility, surface heterogeneity and phase transitions[246, 330].
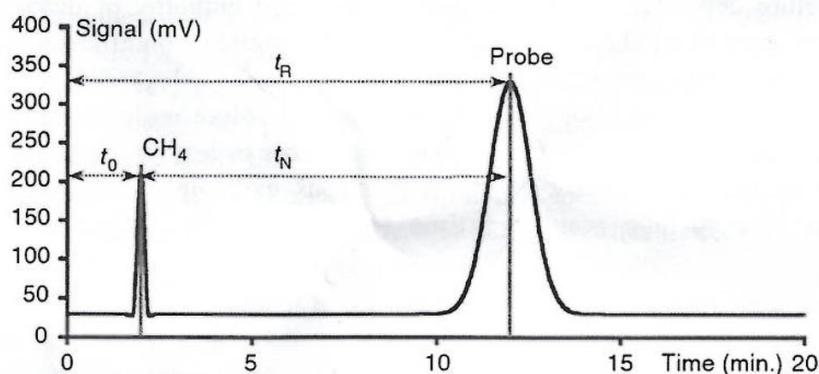
Figure 3. 7 Typical IGC chromatogram[331].

IGC runs in either infinite or finite dilution modes. The former, involves injecting a small amount, (less than 3%) of adsorbate, covering only the high surface energy sites of the stationary phase under investigation. The solute molecules behave independently, and retention behaviour follows Henry's Law, where the number of molecules absorbed is proportional to the adsorbate concentration injected, and the chromatograms are normally Gaussian in shape. The later approach involves injecting higher amounts of solvents covering larger fractions of the solid sample's surface. The solute-solute interactions are significant in the finite dilution mode, probe injections are above Henry's law region, and the chromatographic peaks can be non-Gaussian. For example, skewed chromatograms can exhibit tailing, indicate strong interactions between the adsorbent and the adsorbate[332], corresponding to the type II and type IV isotherms of IUPAC classification[333, 334], depicted in Figure 3. 14.

The retention time, (t_R), is normally estimated from the maximum intensity of the peak. However, for non-Gaussian chromatograms, the retention time (t_R) is estimated using the centre of mass of the chromatogram. The retention volume (V_N) can be calculated using Eqn 5[245].

$$V_N = jt_R F \left(\frac{T}{273.15}\right) - jt_0 F \left(\frac{T}{273.15}\right) \qquad \textbf{Eqn 5}$$

where j stands for the James–Martin pressure drop correction factor, allowing for the pressure drops along the column, F is the carrier gas flow rate, usually given in standard cubic centimeters per minute (sccm). The t_R stands for the retention time of the interacting probe and t_0 stands for the dead time determined via methane injections. Finally, T corresponds to the experiment's temperature and 273.15 K is the reference temperature.

According to Fowkes[335] the surface energy of a solid is composed of a dispersive component, (resulting from the physical long-range interactions) and an acid-base component, (resulting from chemical short-range interactions), as represented by Eqn 6;

$$\gamma_s = \gamma_s^d + \gamma_s^{ab} \qquad\qquad \textbf{Eqn 6}$$

where γ_s^d stands for the dispersive component, (London interactions) and γ_s^{ab} stands for acid-base component, (H-bonding, polar and acid-base interactions).

So, the free energy changes of adsorption will be the results of polar and non-polar interactions depending on the nature of the injected probes. Generally, a series of alkanes are used to measure the dispersive surface energy, while polar probes are used to measure the acid-base interactions of the solid particles and determine the specific surface energy. Two well-established methods are used for the calculation of surface dispersive free energy, Schultz method[336], and the Dorris and Gray method[337, 338]. The fundamentals of these are graphically depicted in Figure 3. 8. The Lewis acid–base surface energy can be calculated from the specific parts of free enthalpy changes of adsorption of a pair of monofunctional acidic & basic probe molecules such as ethyl acetate and dichloromethane, using the van Oss–Good–Chaudhury approach[339].
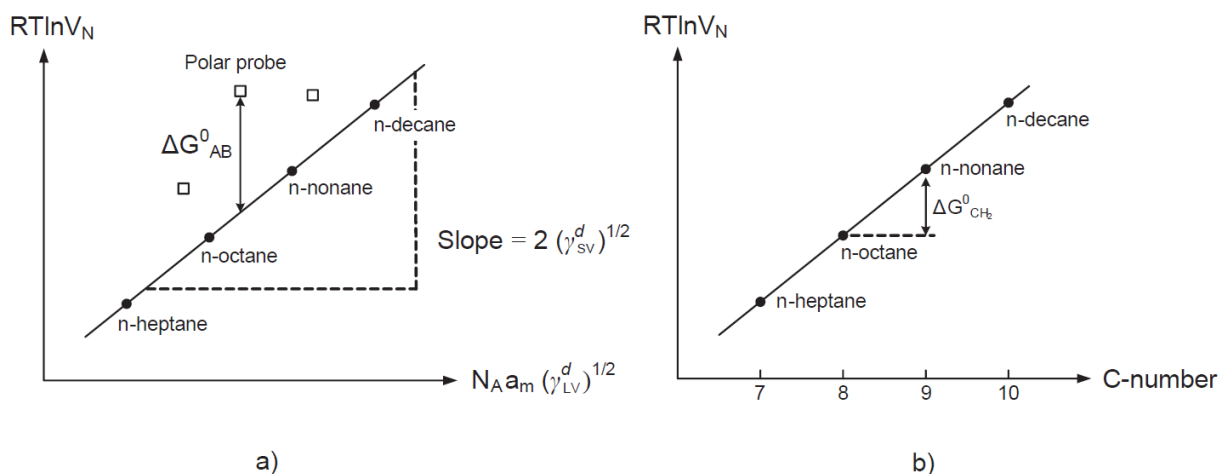
Figure 3. 8 Schematic representation of a) the Schultz method and B) the Dorris and Gray method for the determination of surface energy via IGC[328].

The Schultz method is based on the injections of the series of n-alkanes and these non-polar probes are expected to interact with the solid phase via dispersive forces. Eqn 7 can be used to measure the dispersive surface energy of the solid phase via this method:

$$\gamma_s^d = \frac{1}{4 \cdot \gamma_l^d} \left(\frac{RT \ln V_N}{N \cdot a} \right)^2 \qquad \textbf{Eqn 7}$$

where γ_s^d stands for the dispersive surface energy of the solid, γ_l^d stands for the surface tension of the liquid, R is the universal gas constant and T is the experimental measuring temperature. N is the Avogadro`s number and a is the cross-sectional area of the probe molecule. The Schultz plot can be used also for the calculation of the acid-base component of the surface energy, via the retention volumes of polar probes[332].

The basic principle of Dorris and Gray method is based on the concept that the adsorption of one methylene group can be calculated from the slope of the line achieved when plotting the adsorption free energy of the normal alkanes versus the carbon number. Then the van der Waals component of the surface energy can be calculated according to Eqn 8:

$$\gamma_s^d = \frac{1}{4\gamma_{CH_2}} \left(\frac{-\Delta G^{CH_2}}{N \cdot a_{CH_2}} \right)^2 = \frac{1}{4\gamma_{CH_2}} \left(\frac{RT \cdot \ln\left(\frac{V_{N,n+1}}{V_{N,n}}\right)}{N \cdot a_{CH_2}} \right)^2 \qquad \textbf{Eqn 8}$$

where N is the Avogadro's constant, α_{CH2} is the surface area of a methylene group, γ_{CH2} is the surface tension of the methylene group, $V_{N,n}$ is the retention volume of n alkane and R and T have the same meaning as in the ideal gas equation. The Dorris and Gray method is not as extensively used as the Schultz approach. However, it could be the preferred method to use when working at elevated temperatures because of the assumed temperature independency for the dispersive surface energy of liquid alkanes.

The van Oss, Chaudury and Good approach is generally used to determine the specific surface energy component. This approach is based on the specific free energy of two monopolar probes (one acidic and one basic probe – e.g., ethyl-acetate and dichloromethane). The base parameter (γ_S^-) and the acid parameter (γ_S^+) can be calculated using Eqn 9:

$$\Delta G^{sp} = N_A a \cdot 2\left(\sqrt{\gamma_l^+ \gamma_s^-} + \sqrt{\gamma_l^- \gamma_s^+} \right) \qquad \textbf{Eqn 9}$$

The specific surface energy can then be calculated from the acid and base parameter using Eqn 10.

$$\gamma_s^{sp} = 2\sqrt{\gamma_s^- \gamma_s^+} \qquad \textbf{Eqn 10}$$

3.2.2 Inverse Gas Chromatography (IGC) – Instrumentation

All IGC experiments were conducted with an IGC SEA instrument from Surface Measurement Systems (London, UK) equipped with a flame ionisation detector (FID). This commercial equipment is set-up for pulse chromatography, i.e., a precise amount of adsorbate is transported by the carrier gas through the column containing the sample. Adsorption followed by desorption occur at the sample surface and an elution peak is the result. For the normal experiments, a column temperature of 293K, a flow rate of 10 sccm and 0% RH were used. However, for method development studies experiments were conducted at different temperatures and flow rates as described elsewhere in this thesis. Various solvents and injection amounts were used to develop the methods to determine specific surface area and measure surface energy and its different components. Standard pre-silanised columns (300 mm × 4 mm ID) were packed with ca. 0.3–1.5 g of sample and then plugged with silanised glass wool at either end to avoid contamination of the injection system. Helium was used as the carrier gas and methane as the reference gas to determine the dead time. The retention time was determined as the time of the maximum FID signal. The SEA Analysis software, Advanced Version 1.4.2.0 (SMS, UK) was used for data analysis.

3.2.3 Contact Angle – Theory

Contact angle is a very common technique used to determine the wettability of a solid surface. Wettability, how a liquid spreads on a solid substrate, is measured by quantifying the contact angle formed between a liquid drop and a solid surface. This method measures the angle formed at the three-phase interface between the solid, liquid and gas when a liquid drop is placed onto a solid. A water drop with a contact angle > 90°, depicted in Figure 3. 9, represents a hydrophobic surface which indicates a non-wettable surface. A water droplet with a small contact angle, < 90°, represents a more hydrophilic solid surface indicating some wettability.
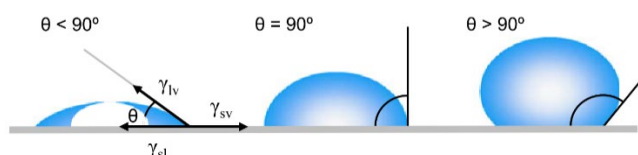
Figure 3. 9 Schematic diagram of contact angles formed by liquid drop and interfacial tensions of the three surfaces at the three-phase boundary[239].

The thermodynamic properties of both the solid surface and the liquid droplet determine the contact angle measured. Specifically, it is the balance of the attractive and repulsive forces at the three-phase boundary between gas, liquid and solid which determine the contact angle. A large contact angle implies that cohesive forces are stronger than adhesive forces, and the liquid molecules prefer to interact more with each other than with the solid molecules. Surface wettability is low and spreading of the drop is minimal. However, a small contact angle implies that cohesive forces are weaker than adhesive forces, and molecules of the liquid interact more with the solid molecules than with themselves. Surface wettability is high and spreading of the drop is great. The principles of this technique have been formulated in 1805 by Thomas Young [340] and the Young's contact angle, θ_y, is used to describe the wetting processess. This is described using Eqn 11:

$$\gamma_{sv} = \gamma_{sl} + \gamma_{lv} \cos \theta_y \qquad \textbf{Eqn 11}$$

where γ_{lv}, γ_{sv} and γ_{sl} represent the liquid-vapor, solid-vapor, and solid-liquid interfacial tensions (surface free energy), respectively. Eqn 11 is usually referred to as Young's equation and it connects the contact angles and surface tension based on the thermodynamic energy balance at a fluid/solid/fluid interface. From Young's Equation we can estimate the work of adhesion $\underline{W}_{sl}$:

$$W_{sl} = \gamma_{lv}\left(1 + \cos \theta_y\right) \qquad \textbf{Eqn 12}$$

which allow the surface energy of the substate to be determined.

There are different methods that can be used for analysing contact angle data to determine the substrate surface energy, with the most common semi-empirical models being the Fowkes[341], the extended Fowkes (Owens & Wendt) and the Van Oss et al.[339] model. Contact angle measurements of different solvents, with known properties, are then used to calculate the surface energy of a solid, including the polar and dispersive components as well the Lewis acid and base components via these semi-empirical models.

There are also different experimental methods used to measure the contact angle. The Wilhelmy plate and sessile drop, depicted in Figure 3. 10, are the two most used methods and hence are described here:
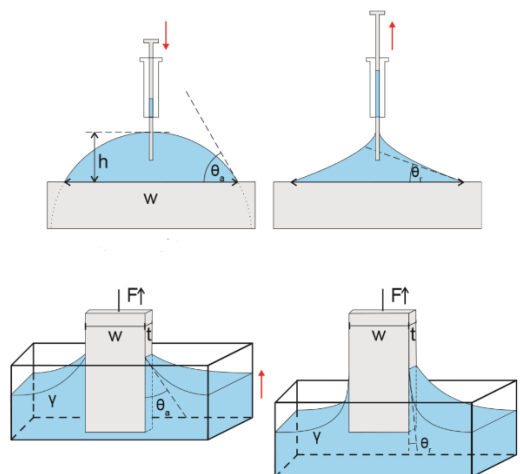
Figure 3. 10 Schematic diagram of the sessile drop (top) and Wilhelmy plate (bottom) contact angle methods[342].

The most common method is the sessile drop technique where a contact angle goniometer[239] is employed, with an optical subsystem, to capture the profile of a pure liquid droplet on a solid substrate[343]. If the size of the drop (e.g., drop volume) is not altered during the measurement then this approach is described as a 'static' measurement. Alternatively, the drop volume can be increased and or decreased in size with an advancing and receding contact angle being determined[343]. Normal experimental practise is to measure the advancing contact angle by increasing the droplet volume. The highest possible angle measured is regarded as the advancing and the lowest possible measured angle is regarded as the receding contact angle, and hysteresis representing any differences between the advancing the receding angle and the receding angles. It is generally accepted that hysteresis rises from surface roughness and/or surface chemical heterogeneity[239] of the substrate. This direct method is advantageous because it is simple and only small amounts of liquid, (a few microliters) and small surface substrates, (a few square millimeters) are required[343].

In the Wilhelmy plate method the substrate is perpendicularly immersed into and withdrawn from the test liquid with a known rate. The weight change of the substrate is measured due to the wetting force. Knowing the liquid's surface tension and the wetting perimeter of the substrate, the contact angle at each position can be calculated [237]. This approach is a dynamic technique and the advancing and receding angles are measured similarly to the sessile drop. One advantage of this method is that several wetting/immersion cycles can be recorded over relatively large distances, (centimetres), thus changes in the different regions of the substrates can be studied [237]. However, a drawback is that only substrates with regular cross-sectional shapes can be accurately measured, typically fibres, rods and thin plates [237]. Contact angles measurements are also affected by the surface topography of the material, and hence, for

chemically well characterised surfaces, one can also infer a roughness factor as a measure of the topography[221]. In the case of nonwovens, which by nature are characterised by a rough surface created from randomly orientated fibrous webs composed of voids, crests and troughs, contact angle measurements are not straightforward because roughness affects the contact angles measured. For coated nonwovens this measurement is further complicated as the surface may be chemically inhomogeneous or soluble components may diffuse from the solid surface into the wetting liquid – and could increase or decrease artificially the contact angle measured. The angles that a drop of liquid makes with a solid are directly dependent on the macroscopic geometry of the solid and for very rough surface contact angle values measured could be unreliable. This challenge is illustrated in Figure 3. 11.
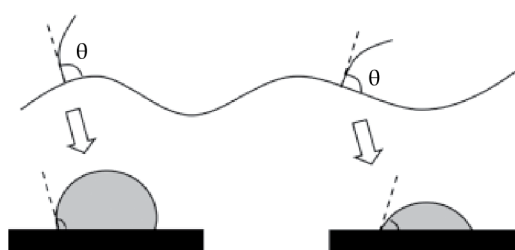
Figure 3. 11 Illustration of the different apparent θ values that may be measured on rough surfaces[160].

There are three possible models which describe how a wetting liquid droplet interacts when deposited onto a rough surface; the Wenzel[344] model, the Cassie–Baxter[345] model, and the metastable Cassie–Baxter[346] model. In the Wenzel model, a liquid completely fills the grooves of a rough surface, whereas a liquid sits on top of the solid protuberances of a rough surface in the Cassie–Baxter model. On a metastable Cassie–Baxter surface, a liquid initially sits on top of the surface and with time is sucked into contact with the rough surface. The drop time depends on the surface tension and volume of the liquid and the surface tension and morphology of the solid surface.

3.2.4 Contact Angle – Instrumentation

The surface wettability of nowoven and woven fabrics was characterised by contact angle (CA) measurements of sessile droplets measured using a Kruss DSA25 Drop Shape Analyser equipped with ADVANCE software. A ca. 75x25mm section of sample was mounted on a microscope slide using double sided tape to fix the sample in place and keep it flat to ease analysis. In house ultrapure deionised water (Millipore, resistivity 18 MΩ·cm) and

diiodomethane with 99% purity and copper stabiliser ordered from Sigma-Aldrich were used for contact angle measurements.

3.2.5 X-ray Photoelectron Spectroscopy (XPS) – Theory

X-ray photoelectron spectroscopy (XPS) is surface sensitive analysis technique that measures the elemental composition and chemical state of a material[347]. Although X-rays may penetrate the bulk sample, the ejected photoelectrons cannot escape except from within a few nanometres (<5nm) of the material surface, and because of this escape depth, XPS is commonly used for surface chemical analysis of surfaces. XPS involves the removal of core electrons when the sample surface is irradiated with X-rays of known energy, hv, which is greater than the binding energy, E_b, of the electrons. The ejected electrons have a kinetic energy, E_k, which can be measured in the spectrometer, and can be calculated using Eqn 13:

$$E_k = hv - E_b - \phi_{sp} \qquad \textbf{Eqn 13}$$

where ϕ_{sp} is a spectrometer work function and this term can be eliminated since it is compensated for electronically, giving Eqn 14:

$$E_k = hv - E_b \qquad \textbf{Eqn 14}$$

Thus, by measuring the E_k of the photoelectrons and using Eqn 15 one can translate this energy into the binding energy, of the electrons:

$$E_b = hv - E_k \qquad \textbf{Eqn 15}$$

An XPS spectrum is generated by plotting the measured photoelectron intensity (current) as a function of E_b. For every element, there is a characteristic binding energy associated with each core atomic orbital and therefore any given element produces a characteristic peak 'fingerprint' in the photoelectron spectrum e.g. C_{1s} [221]. Peak intensities can be related to the surface concentration of the given element allowing XPS to provide a quantitative analysis of surface composition. Changes in oxidation state or chemical bonding environment give rise to small variations in binding energy which in turn leads to small changes in peak position. These shifts are known as chemical shifts. The ability to discriminate between different oxidation states and chemical environments is a major advantage of the XPS technique. XPS is not sensitive to hydrogen or helium but can detect all other elements[222]. Utilising reference materials, substantial databanks have been developed summarising the binding energy corresponding to a wide range of functionalities. These databanks can be used to accurately deconvolute, via optimisation, the relative abundance of different functional groups and elemental species.

The main parts of an XPS instrument are the vacuum sample introduction chamber, an ultra-high vacuum measurement chamber, the sample stage to hold the sample, the electron beam, the energy analyser, the detection system, and a computer as the processor and controller, as depicted in Figure 3. 12. Materials suitable for XPS analysis include; polymers, paper, textiles, metal and steel, glass, biomaterials, catalysts, and electronics [222, 348].
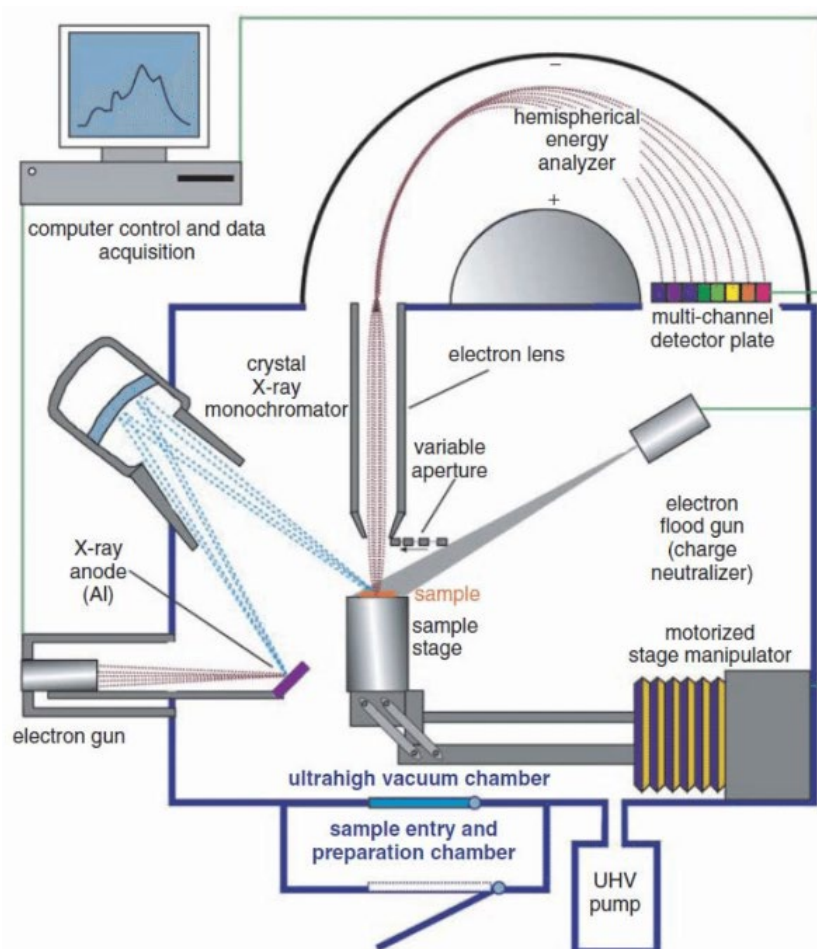
Figure 3. 12 Simplified schematic diagram of an XPS system[349].

3.2.6 X-ray Photoelectron Spectroscopy (XPS) – Instrumentation

The surface chemistry of nonwovens were characterised using high-resolution XPS. The spectra were recorded on a Thermo Scientific KAlpha+ X-ray photoelectron spectrometer operating at 2×10^9mbar base pressure. The system incorporated a monochromated, microfocused Al Kα X-ray source (hv= 1486.6 eV) and a 180° double focusing hemispherical analyser with a 2D detector. The X-ray source was operated at 6mA emission current and 12kV anode bias providing an X-ray spot size of 400 μm^2. Survey spectra were recorded at 200eV pass energy, 20eV pass energy for core level, and 15eV pass energy for valence band

spectra. A flood gun was used to minimise the sample charging that occurs when exposing an insulated sample to an x-ray beam. Charge neutralisation was deemed to have been achieved by monitoring the C1s signal of the adventitious carbon. All XPS spectra were recorded using the Avantage Data System software and quantification analysis was performed using the Avantage software.

3.2.7 Atomic force microscopy (AFM) – Theory

The AFM was invented in 1986 by Gerd Binning et al.[350] based on the scanning tunnelling microscope (STM). Unlike STM, AFM measures both conductive and non-conductive samples. A typical AFM consists of a cantilever with a small tip (probe) at the free end, a laser, a position sensitive photo detector, a piezoelectric scanner, and a feedback mechanism, as depicted in Figure 3. 13.
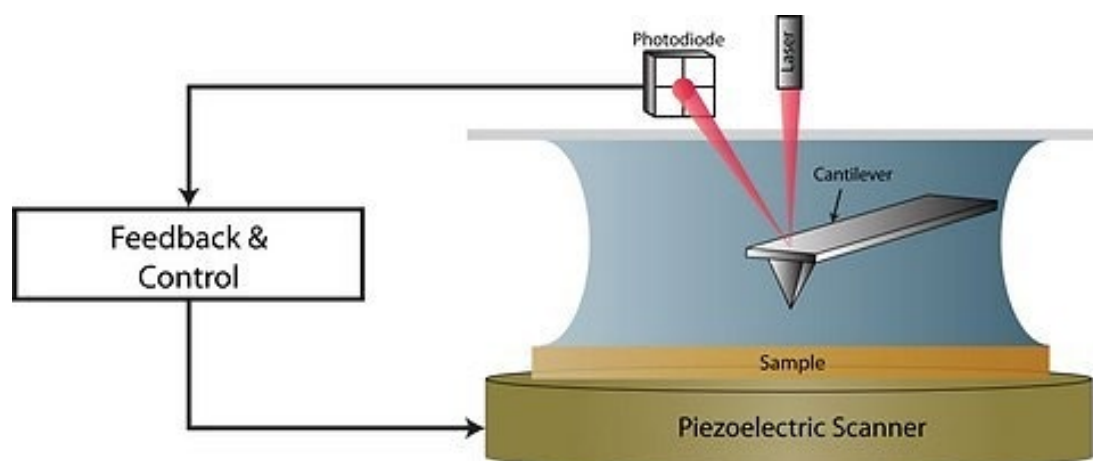
Figure 3. 13 Simplified schematic diagram of an AFM[351].

AFM uses a cantilever with a very sharp tip to raster scan across the sample surface. As the tip approaches the surface the close-range attractive force between the surface and the tip causes the cantilever to deflect towards the surface. However, as the cantilever is brought closer to the surface of the substrate, the tip contacts the surface and repulsive forces dominate causing the cantilever to deflect away from the surface. The interaction between the tip and sample can be measured by monitoring the deflection of the cantilever using a laser beam. Any cantilever deflection causes changes in the direction of the reflected beam from the back of the tip on to a position sensitive photodiode[352]. The raised and lowered features on the sample surface influence the deflection of the cantilever which is monitored by the photodiode using a feedback loop initiated by piezoelectric input[221]. The cantilever can be thought of as a spring. The quantity of the generated force between the tip and the surface

depends on the spring constant (stiffness) of the cantilever and the distance between the tip and the surface. This force can be characterised with Hooke's Law, Eqn 16.

$$F_s = -kx \qquad \textbf{Eqn 16}$$

where F_s is the spring force, k is the spring constant, and x is the cantilever deflection.

As the tip is rastered across the sample, it deflects up and down according to the surface interactions sensed, such as electrostatic, magnetic, capillary, Van der Waals forces[230, 353, 354], between the tip and the sample. These cantilever deflections are measured by the detector and then plotted to reconstruct a 3D topological representation of the surface at sub-nanometer resolution[76]. In these plots, the cantilever deflections may be reported directly, or more commonly they are converted into attractive forces or substrate topography. Surface roughness is often measured by AFM[231] and can be expressed in many ways but is most commonly stated in terms of area average roughness (R_a) and area root-mean-square roughness (R_{ms}) defined by Eqn 17 and Eqn 18 respectively:

$$R_a = \frac{1}{N} \sum_{i=1}^{N} |Z_i - \bar{Z}| \qquad \textbf{Eqn 17}$$

$$R_{ms} = \sqrt{\frac{1}{N} \sum_{i=1}^{N} (Z_i - \bar{Z})^2} \qquad \textbf{Eqn 18}$$

where N is the total number of data obtained, ($Z_i - \bar{Z}$) is the height (z-value) difference between each data point and the average z-value of all data points.

There are three basic AFM imaging modes [230, 355]; contact mode, non-contact mode and tapping mode. In contact mode, the tip is in physical contact with the surface, analogous to feeling a surface's texture by running fingers over it. The cantilever tip can move above the surface maintaining a constant deflection (force) and both the tip and sample can be subject to deformation. The overall force is repulsive, with both long- and short-range forces contributing to the imaging signal. This mode gives good results with hard materials, e.g. SiO_2 films[228] but is unsuitable for electrospun polymers as it causes damage to the sample due to lateral (frictional) forces and cannot maintain contact for these complex substrate geometries. In non-contact mode the tip does not touch the sample. Instead, the cantilever is vibrated at its resonance frequency, so it oscillates above the surface interrogating the attractive surface force nearby. It uses a feedback loop to monitor changes in the amplitude due to attractive

Van der Waals forces as the raster scan occurs. This method has the advantage of causing minimal structural damage to the sample but it is not commonly used for imaging fibres again due their non-planar sample geometry[231]. The AFM mode most often used for studying polymers is tapping mode. In tapping mode, the tip of the probe touches the sample, and moves completely away from the sample in each oscillation cycle. Tapping mode generates smaller forces than contact modes, therefore it is less destructive[356] and hence more commonly used than the other two for most applications[357].

3.2.8 Atomic force microscopy (AFM) – Instrumentation

AFM (Nanowizard 4, JPK Instruments, now Brucker) was used to image the structure of film surfaces down to nanometer resolution. The samples were scanned with a silicon tip (PPP-NCHAuD from APEX Probes) on 50µm × 50µm area with a resolution of 512×512 pixel in Quantitative Imaging[TM] mode. The images were normally levelled, filtered using a median filter, analysed for curvature and roughness and visualised with JPKSPM data processing software (JPK instruments)

3.2.9 Nitrogen Gas Adsorption and BET – Theory

Physical characteristics such as surface area and porosity are two important properties that can affect performance of materials including polymers. Brunauer-Emmett-Teller (BET) [358] proposed a model in 1938 which is routinely used method to determine the surface areas and pore size distributions using N_2 as the adsorbate. This model was an extension of the Langmuir theory, developed in 1916 which related the monolayer adsorption of gas molecules, called adsorbates, onto a solid surface. BET theory extended the Langmuir theory to include multiple layers of gas molecules. Gas molecules such as nitrogen adsorb on the surface of solid substrates due to van der Waals attractive forces at nitrogen liquification temperatures, 77K. These forces lead to the reversible physisorption of gas molecules on material surface in multiple layers. The BET method is used to analyse nitrogen isotherms at 77K, which are then used to calculate their BET surface areas[359]. The BET equation is expressed as:

$$\frac{P}{V_a(P_0-P)} = \frac{1}{V_m C} + \frac{(C_{BET}-1)}{V_m C_{BET}}\left(\frac{P}{P_0}\right) \qquad \textbf{Eqn 19}$$

where, P is the partial vapour pressure of adsorbate gas, P_0 is the saturated pressure of adsorbate gas, V_a is the volume of gas adsorbed STP 273.15 K, V_m is the volume of gas adsorbed at STP to produce monolayer, and C is a constant, related to enthalpy of adsorption

of the adsorbate gas. For the BET method to be an applicable tool for analysis, the equation must provide a linear plot usually in the approximate relative pressure range P/P_0 of 0.05 to 0.3. From the value of V_m the specific surface area, S ($m^2 \cdot g^{-1}$) can then be calculated using Eqn 20:

$$S = \frac{V_m N a}{m \times 22400}$$ **Eqn 20**

Where N is the Avogadro's constant (6.022×10^{23} mol^{-1}), a is the effective cross-sectional area of one adsorbate molecule, m is the mass of powder (g) and 22400 corresponds to the volume occupied by 1 mole of the adsorbate gas at STP (ml).

The shape of gas adsorption isotherms are grouped into six types as depicted in Figure 3. 14. The BET method is applicable only to adsorption isotherms of type II (disperse, nonporous or macroporous solids) and type IV (mesoporous solids, pore diameter between 2 nm and 50 nm)[333]. According to ISO 9277:2010(E) standard, at least 4 data points within the relative pressure range for which the BET is (typically 0.05 to 0.3) should be measured at equilibrium.
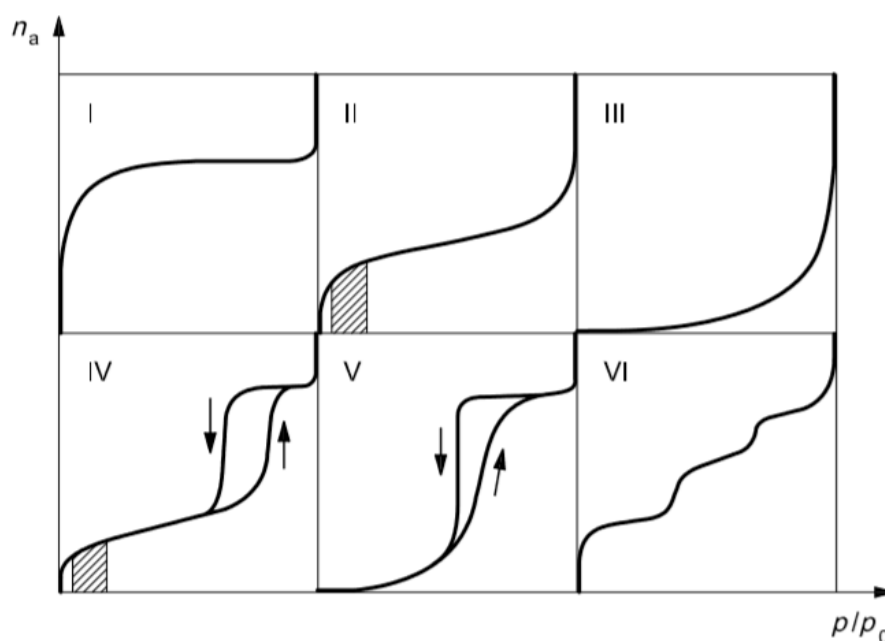
Figure 3. 14 IUPAC classification of adsorption isotherms (typical BET range is indicated in type II and IV by the hatched area) [333, 334].

The main BET instrumentation parts are depicted in Figure 3. 15.
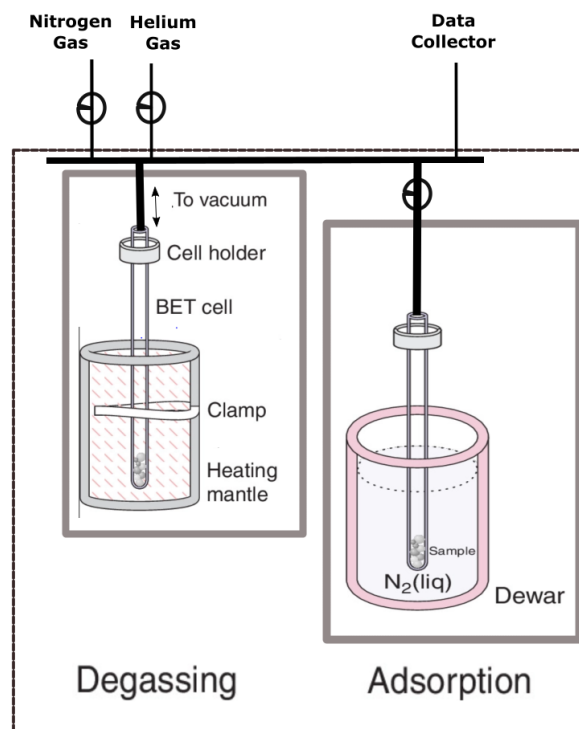
Figure 3. 15 Schematic diagram of BET Nitrogen method.

The two major components of the N_2 physisorption analyser are the degassing and adsorption stations. The glass tube sample holders are filled with the sample and then degassed under high vacuum and temperature. Degassing the sample is to remove physically adsorbed water and volatiles that accumulated during storage. For thermally sensitive solids, mild degassing temperatures are used, and for mechanically fragile porous materials, a stream of inert gas is introduced instead of vacuum. After degassing, the cell is transferred to the adsorption station and evacuated under vacuum. The adsorption cycle is performed by incremental pressure increases in nitrogen via gas lines. During measurements, the sample holder is maintained at the liquid nitrogen boiling point using a Dewar flask filled with liquid nitrogen. A computer is also used which acts as the processor, controller, and data collector for the system.

Although the BET method is used routinely, it is not without limitations. There are assumptions associated with the BET theory such as that the surface is homogenous, multilayer adsorption occurs, the van der Waals forces on the surface are stronger than the van der Waals forces between the probe molecules and that at equilibrium the rate of adsorption is equal to the rate of desorption. It also assumes that all sites on the surface have equally energetic sites and that the gas molecules physically adsorb on a solid in layers and different adsorption layers do not interact. It is not always the case that these assumptions stand true[360]. Other limitations of the technique are linked with how fast equilibrium is achieved and the length of time required for sample preparations pre-analysis due to degassing requirements. Nitrogen is used

because it is easily available and does not chemically interact with most materials. However, nitrogen is not a spherical molecule and it possesses a quadrupole moment so it could adsorb and form site-specific interactions with certain solid surfaces resulting in a different surface area coverage for some surfaces[265]. For low surfaces areas solids, <1m^2/g, nitrogen BET methods have low accuracy and repeatability. Other gases such as argon and krypton can also be used although these are more expensive.

3.2.10 Nitrogen Sorption BET – Instrumentation

BET surface area of all nonwoven and woven samples was determined from isotherms obtained using a nitrogen adsorption at 77 K with a fully automated surface area analyser, Micromeritics ASAP 3Flex Physisorption Analyser (Micromeritics, Norcross, USA). The nitrogen adsorption was used as a reference technique to compare with surface area measurements obtained using IGC. The nonwoven and woven samples had to be cut into short sections before being packed inside the BET analysis glass tubes using a column packing rod. All samples were pre-conditioned with helium purge at 60°C for at least 4 hrs prior to measurement to ensure removal of unwanted absorbed species that may influence surface area measurements. The BET surface areas were calculated from the adsorption isotherm at relative pressure of P/P$_0$ range between 0.01 - 0.99. A standard isotherm was measured with 84 data points. Data analysis was performed using the 3Flex Software (Micromeritics, Norcross, USA) using data in the 0.05 - 0.35 P/P$_0$ range.

3.3   Techniques Introduction – Bulk Characterisation Methods

3.3.1   Ellipsometry – Theory

Ellipsometry is an optical characterisation technique that measures the change in polarised light after it has been reflected (or transmitted) by a sample, typically a thin film[271]. It was developed in the early 1970s and it is now used for determining optical properties and the thickness of thin films with Angstrom resolution. The key components of an ellipsometer are a light source, a polariser, an analyser, and a detector, as depicted Figure 3. 16.
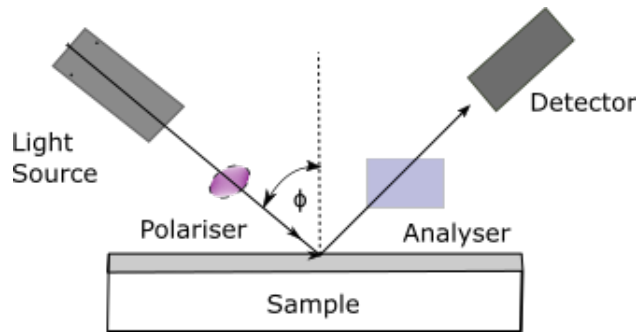
Figure 3. 16 Simplified schematic diagram of an ellipsometer[1].

Ellipsometry measures two values Ψ (Psi) and Δ (Delta)[361]. These represent the magnitude of the reflectivity ratio Ψ and phase difference Δ between reflected p- and s-polarised light waves which are measured as a function of the wavelength of light. In general, measurements are carried out in the UV/vis region, but the infrared region has also been utilised. The principle of ellipsometry is that p-polarized and s-polarized light are reflected differently from the sample. The intensity of the s and p component, after reflection, are represented by R_s and R_p. Ellipsometry measures their *ratio* in the reflected light, which is typically defined by Eqn 21:

$$\rho = \tan \Psi e^{i\Delta} = \frac{R_p}{R_s} \qquad \textbf{Eqn 21}$$

In this equation, ρ (rho) is the complex ratio of the total reflection coefficients, (R_p and R_s) for p- and s- polarised light, which characterise both the magnitude Ψ and phase Δ of the reflected beams. These are properties of the incident light beam. The information about the sample is contained in the total reflection coefficients, and hence in ρ, which then must undergo optical model analysis to infer the material properties. Values for Ψ and Δ are therefore always correct, but the material property accuracy depends on the model employed. The ellipsometric raw data parameters, Ψ and Δ are measured and then fitted and optimised using an optical model to return the sample properties. The procedure used to deduce material properties from ellipsometry measurements follows the work flow chart in Figure 3. 17.

---

[1] Φ is the angle of incidence/reflection.
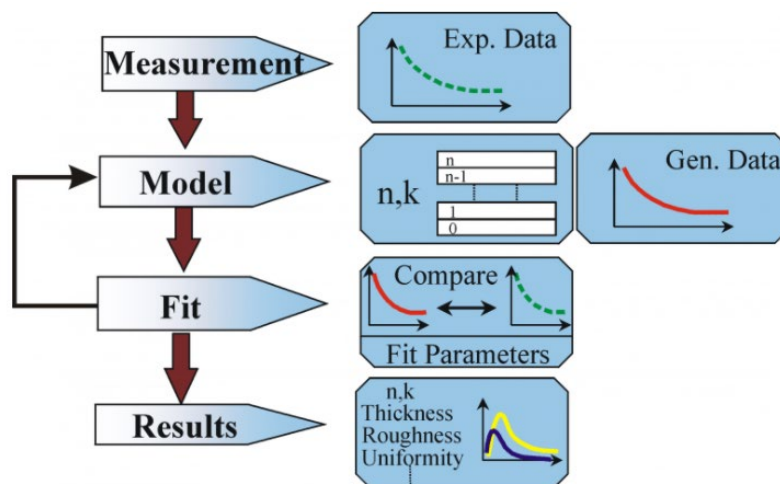
Figure 3. 17 Ellipsometry data analysis work flow chart[362].

Once a sample is measured, an optical model needs to be constructed to describe the sample behaviour optically. The model is used to calculate the predicted response from Fresnel's equations which describe each layer in the material under examination with thickness and optical constants[271]. If these values are not known, an estimate is given for the purpose of the preliminary calculation. The calculated values are compared to experimental data. Any unknown material properties can then be varied to improve the match between experiment and calculation.

Ellipsometry is a non-contact, label-free optical method which requires no sample preparation. It is fast and non-destructive and can be performed in a wide range of environments and is capable of studying single and multilayer samples in solid and liquid form. A unique advantage of ellipsometry is that the measured parameters are independent of light beam intensity because it measures a ratio. This advantage can be very valuable in situations where maintaining constant beam intensity is difficult, such as *in situ* measurements, or long-term measurements requiring high stability. The main drawback of the ellipsometry is the necessity for a reliable optical model, making the data analysis process complicated.

3.3.2 Ellipsometry - Data Modelling

For *in-situ* ellipsometry studies, the samples are in general thin polymer films on top of supporting substrates. When light enters such a sample it reflects and transmits at each of the interfaces. The rays leaving the sample interfere with each other and produce spectral oscillations in the ψ and Δ. In the spectroscopic ellipsometry the measurement generates a pair of ψ and Δ for each employed wavelength. The ellipsometer used in this research used

four wavelengths of 465, 525, 595 and 635 nm. This allows for the characterisation of complex samples, where light absorption, optical anisotropy, density gradients, roughness, and other features of the probed layers can be determined in addition to basic film thicknesses and refractive indexes. Typically, the instrumental standard deviations in ψ and Δ are on the order of 0.01-0.02°. For an optically uniform and transparent polymer film on a polished silicon wafer, this translates into precision in thickness determination on the order of 0.1nm[363]. In certain cases, the ψ and Δ can be directly used to calculate the properties of simple samples, (n and k) from the reflection at the sample/ambient interface. For more complex samples, multilayers, absorbing, anisotropic, a simple deconvolution of the sample properties from the measured ψ and Δ is difficult and therefore optical models are utilised.

Primarily, ellipsometry data analysis is completed when the ψ and Δ for a particular sample on a known substrate are measured, and then the film thickness and dispersion need to be determined. This analysis is done using a layered optical model, which ideally, includes all the pieces of information that are known about the sample, before the measurement is done. Most importantly, the substrate type must be known. In some cases, also an approximate layer thickness or refractive index of the film material are known. The polymeric materials used in this study were simple, transparent layers, therefore, their optical dispersion was modelled according to the Cauchy formula:

$$n_{Cauchy}(\lambda) = A_n + \frac{B_n}{\lambda^2} + \frac{C_n}{\lambda^4} \qquad \textbf{Eqn 22}$$

where A, B and C can serve as adjustable fitting parameters. Generally, a two-term Cauchy function is sufficient to describe a transparent layer, as is the case in the FS-1 software:

$$A_n = n_{633\,nm} - n_{slope} \times \left(\frac{1000}{633}\right)^2, B_n = n_{slope}, C_n = 0 \qquad \textbf{Eqn 23}$$

which gives the re-parameterised 2-term Cauchy formula where the wavelength is in nanometres:

$$n(\lambda) = n_{633\,nm} + n_{slope} \times \left(\left(\frac{1000}{\lambda}\right)^2 - \left(\frac{1000}{633}\right)^2\right) \qquad \textbf{Eqn 24}$$

The extinction coefficient, k, for the polymer thin films is assumed to be zero in this case, as the material is transparent (i.e., non-absorbing) in the visible wavelength range. The fit

difference (fit diff.) between the experimental and the Cauchy model data is minimised using the least squares, non-linear regression "Marquardt-Levenberg" algorithm:

$$Fit\ diff. = \sqrt{\frac{1}{4\cdot3}\sum_{i=1}^{4}\left[\left(N_i^{mod} - N_i^{exp}\right)^2 + \left(C_i^{mod} + C_i^{exp}\right)^2 + \left(S_i^{mod} - S_i^{exp}\right)^2\right]} \qquad \textbf{Eqn 25}$$

where N, C and S are the ellipsometric parameters from the model (superscript *mod*) and experimental (superscript *exp*) data, defined as:

$$N = \cos(2\Psi) \quad C = \sin(2\Psi)\cos(\Delta) \quad S = \sin(2\Psi)\sin(\Delta) \qquad \textbf{Eqn 26}$$

Figure 3. 18 shows the most utilised optical models that represent sample systems. After the model is constructed, the corresponding ψ and Δ data are generated and model parameters, such as film thickness and/or refractive index, are fitted numerically to match the experimental ψ and Δ data[364].
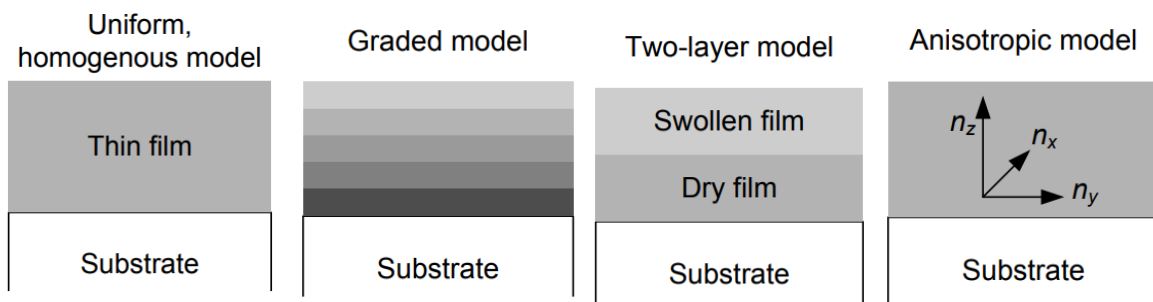
Figure 3. 18 Optical models used typically *in-situ* ellipsometry measurements of swollen polymer films[363].

By far the most used substrate for ellipsometry studies is a silicon wafer with a native oxide thickness of about 1.5 – 2 nm. The optical dispersion of this substrate, and its temperature dependence, are very well known[365] and do not change in most experimental ambient conditions. In addition, the surface roughness of a silicon wafer is very small. Therefore, it is considered an ideal substrate for *in-situ* ellipsometry. In some cases, thicker, thermally grown, oxide layers are utilised. This change is done predominantly to improve the accuracy of the measurements, in particular when layers below 50 nm are studied.

When ellipsometry measurements are coupled or complemented with other techniques such as a DVS, a single experiment allows multiple and simultaneous measurements on the same sample type, using identical humidity (or partial vapour pressure) and temperature. The

bespoke DVS-Ellipsometry system used for this study allows for real-time analysis of both the solute dissolution process and the behaviour of each component within the system, e.g., simultaneous measurements of film thickness and film mass to be achieved.

3.3.3 Ellipsometry – Instrumentation

All the thin film measurements were carried out using a FS-1 multi-wavelength Ellipsometer (Film Sense, USA) with automated mapping. The ellipsometer was housed inside a DVS Resolution acting as an environmental chamber facilitating thus *in-situ* measurement of vapour sorption and ellipsometry measurements, simultaneously.

3.3.4 Dynamic Vapour Sorption (DVS) – Theory

Dynamic vapour sorption (DVS) is a gravimetric technique used to measure how much and how quickly an adsorbate vapour is adsorbed and desorbed by a solid-state sample. It does this by exposing the sample under test to known vapour concentrations while measuring how the sample mass changes over time under typically isothermal conditions. The technique has developed significantly since it was created over 25 years ago by Professor Daryl Williams with the first commercial instrument, (the DVS 1) releasing in 1994 by Surface Measurement Systems (London, UK) [366]. The DVS instrumentation depicted in Figure 3. 19, consists of a temperature-controlled incubator which houses all the other system elements, such as the reference and the sample chambers, the temperature/humidity probes used to measure sample temperature and humidity, and the mass flow controllers used to regulate the relative humidity inside the chambers, and most importantly the microbalance. The DVS includes a capacitance sensor for measuring humidity within the DVS, the actual/measured RH, and the target RH, which is set by the user. The mass flow RH is the theoretical RH calculated from the ratio of the wet and dry air flows using Eqn 27:

$$RH = \frac{wet\ flow}{wet\ flow + dry\ flow} \times 100 \qquad \textbf{Eqn 27}$$

The core of the DVS instrument is an ultra-sensitive microbalance, which records changes in sample mass, (lower than 1 part per million), over time as it adsorbs/desorbs solvent vapours. Only a small sample sizes is needed, (~10mg) for the analysis and thus the experimental time is reduced from weeks or months to hours or days [367], with operating times of a few minutes for the study of surface adsorption phenomena and several hours for the study of bulk sorption.

Sample and reference pans are glass or quartz pan because of their chemical inertness, and ease of sample visualisation.
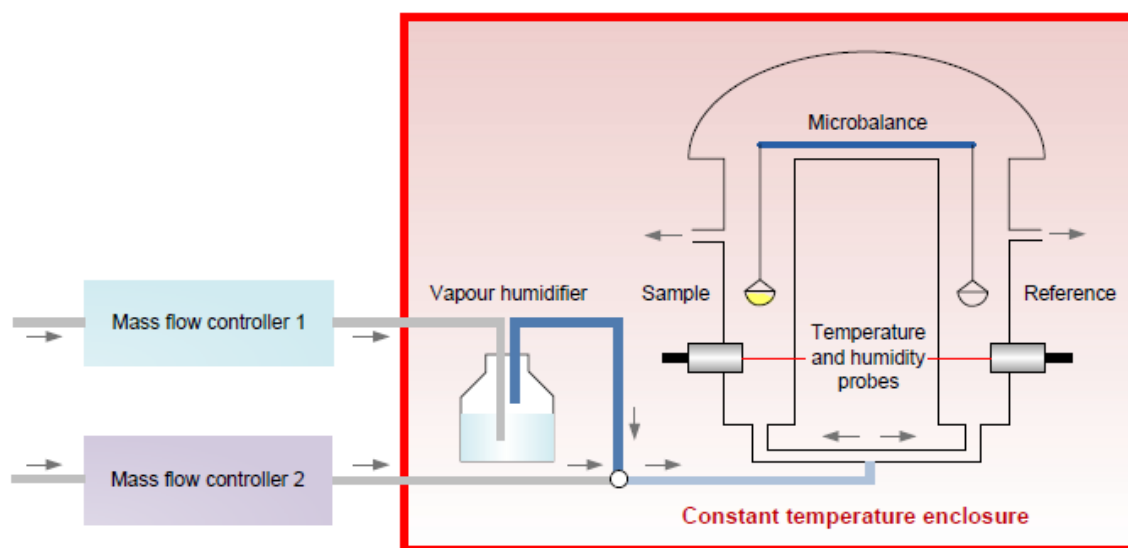
Figure 3. 19 Schematic diagram of a DVS system[280].

A sorption isotherm which represents the quantity of adsorbate on the adsorbent as a function of its concentration at a constant temperature is generated from a DVS. The isotherm indicates the relationship between the amount of sorbed vapor on the solid, and the concentration of vapor species present. As the isotherm is generated, both the sorption constant and vapor diffusion coefficients can be determined, which are both important properties of the material. Adsorption [368] at the solid surfaces strongly depends on the vapor pressure, temperature, and the adsorption energies between solid and vapour. Information about the sample porosity and sorption mechanism can also be obtained if a feature called hysteresis is present in the isotherms. The difference between the adsorption and desorption portions of an isotherm is known as hysteresis, and this can be caused by pore filling, adsorbate dissolution, and or swelling. The vapors used are typically water vapor, but any volatile solvents such as ethanol or cyclohexane can be used. The relative vapor concentration is given as the ratio of adsorbate vapor pressure (p)/saturated vapor pressure (p_0) for any adsorbate; it may be expressed as a fraction or as a percentage.

There are several advantages of DVS over the traditional saturated salt slurry method for water isotherm determinations [369]. The equilibration time is about 10 to 100 times faster than the standard method. The instruments are fully automated and capable of maintaining the desired relative humidity and temperature conditions throughout the duration of the experiment. DVS can be combined with other techniques e.g., near infrared spectroscopy, video imaging,

Raman spectroscopy and ellipsometry to gain a more detailed understanding of materials behaviour[370-372]. It can give the sorption-desorption isotherms for water or organic vapours, solving the problems about the sorption mechanisms, kinetics, and also aid in determining crystalline content and phase transition through modelling and hysteresis phenomenon [373].

3.3.5 Dynamic Vapour Sorption (DVS) – Instrumentation

The sorption profiles of nonwovens and different polymer films using different solvents were determined using the DVS Endeavour and Resolution (Surface Measurement Systems, London, UK). Samples, ranging from a mass between 500mg - 1g, were directly hung on the instruments hang-down hook, and the sample pan was removed. On the DVS Resolution, counterweights were used for the higher mass samples. Most samples were folded into smaller units to keep them compact in size and be able to hang them on the sample hook. A series of experiments were carried out using either fixed times for each experimental humidity setpoint or using % dm/dt threshold mode. The % dm/dt mode uses a percentage change of mass with time dm/dt measured and compares it to a reference value to determine the time when the sample has reached equilibrium at a given RH step. The % dm/dt threshold was set to 0.0005 % for all experiments to ensure the sample had reached a necessary degree of equilibrium before moving on to next step. When the sample percentage change in mass is equal to or below this threshold for a given stability duration (10 min), the step stage is then ended and moved onto the next programmed RH% step. Methods were run in (0 - 90% RH) cycles with increments of 10% RH steps. The drying step at 0% RH was also set to the same % dm/dt threshold value. A flow rate of 200mL/min was used for all experiments and the temperature on DVS was set to 25°C. The carrier gas for these experiments was nitrogen in all cases. The raw data was exported into Microsoft Excel and analysis was done using the DVS Macro Standard Analysis Suite v7.0.13 (Surface Measurement Systems, London, UK).

3.3.6 Differential Scanning Calorimetry (DSC) – Theory

Differential scanning calorimetry (DSC) [374] is a thermal analysis technique used to determine how physical/chemical properties of a sample change, as a function of temperature. The basic principle involves the measurement of the heat flow into or out of the sample of known mass against that of a reference material during a constant or dynamic thermal ramping experiment. A range of physical/chemical changes may take place within the sample, melting, vaporisation, sublimation, glass transition, freezing, condensing, transitioning from amorphous to crystalline, can be quantitatively measured thermodynamically. Because of this flexibility, DSC is used in

many industries[269] including, polymers, pharmaceuticals, cosmetics, food, semiconductors, and electronics as most materials exhibit some sort of transitions. Most of these thermal transitions will either be exothermic, (release of heat) or endothermic, (absorbs heat).

Figure 3. 20 depicts a basic DSC system that comprises of two pans, one for the sample and other for reference material. In the sample pan, the sample (e.g., polymer) is placed while the reference pan is kept empty. Each pan has a heater underneath. These are controlled by a computer. The difference in heat required for the sample pan to keep a zero-temperature difference between the sample and reference pans is measured versus sample temperature. The heat flow from the empty reference pan is compared and subtracted from the heat flow from the sample pan. DSC experiment measures the extra heat by plotting the differential variation in heat flow (y-axis in mW) against that of time/temperature (x-axis in seconds, minutes or °C). A sample may react with air and oxidise or burn and to overcome such problems inert gases like nitrogen, helium, and argon can be used.
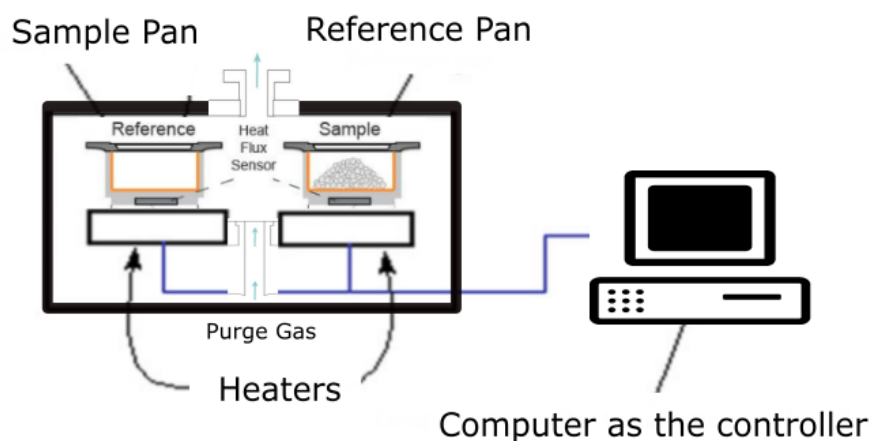
Figure 3. 20 Schematic representation of a basic DSC instrument.

The major advantage of DSC is the ease and speed with which it can be used to observe and quantify thermal and state transitions in materials. Different types of samples can be analysed without any sample preparation and only a small amount of sample is required the analysis; typically, 5mg. There are some limitations[375] associated with DSC such as the difficulty with data interpretation for certain thermal events and its sensitivity to contamination. Additionally, the test analyses the bulk properties of the material of a very small sample size, therefore the sampling region may not be representative of the entire part. Further this technique has difficulty differentiating between materials with similar transitions. For example, Nylon 6 and polybutylene terephthalate cannot be easily distinguished with this method due to their similar melting points.

3.3.7 Differential Scanning Calorimetry (DSC) – Instrumentation

In this thesis, DSC was used for the determination of % crystallinity of polymers and to characterise Basic Red 14 dye. A small portion of the sample was loaded into hermetically sealed pans (part number 900825.902 TA Instruments, Elstree, UK) which were then tested on Q2000 Standard DSC (TA Instruments, Surrey, UK) against an empty pan as reference. The program used involved a heating ramp rate at 10°C/min up to 200°C followed by an isothermal step for 2 min at 200°C and then a cooling step down to 30°C at a rate of 10°C/min. Helium was used as the purge gas at 40 mL min $^{-1}$. Refrigerator cooling accessory (RCS-90 cooler unit) was responsible for heating/cooling rates application. Instrument calibration was conducted using indium and zinc reference materials. TA Universal Analysis 2000 software was used for data analysis.

3.3.8 Density: Helium Pycnometry – Theory

Most of us think of density as the mass of a material divided by its volume. However, there are many definitions of density; ASTM provides over 40 different ones and BSI includes 14 types of densities. Defining the mass of a material is simple but defining the volume of a material can be difficult. The volume of a material cannot be covered by a single definition and it depends on what void spaces are included, e.g., interparticle voids, external voids, open and closed pores, and the volume of solid material[182]. Helium pycnometry measures the apparent (also known as skeletal) particle volume which includes the volume of the solid material and the volume of the closed pores. Helium gas is used because it easily diffuses into all the small accessible open pore spaces while assumed to be nonadsorbing, providing thus the best approximation of the apparent volume of the sample. The method works by measuring the pressure change associated with two volumes: the unknown sample volume and a known reference volume. The instrumentation is simple, and it includes a sample holder of a known volume placed inside a sample chamber, and an empty reference chamber as depicted in Figure 3. 21.
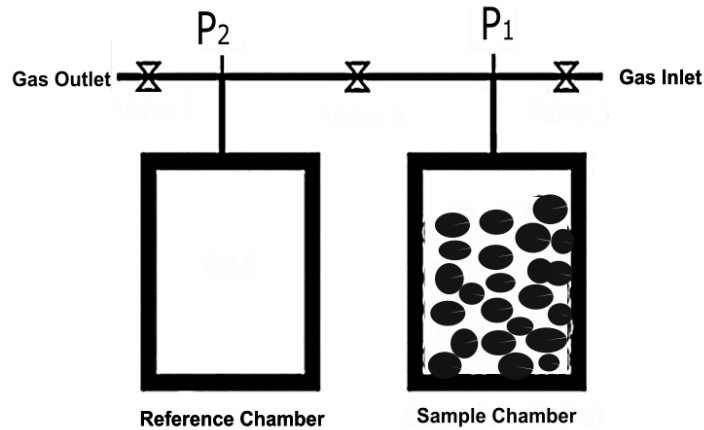
Figure 3. 21 Schematic representation of a Pycnometer instrument.

A sample of known mass is placed in one of the chambers, maintained at a constant temperature, before helium is added to the system under pressure, typically at 5 bar. The difference between the volume of helium of empty sample chamber and filled sample chamber provides the sample solid phase volume. The gas pressure in the sample chamber is measured and then this gas is released to the empty chamber, the pressure of which is measured too. These pressure measurements are used to calculate sample volume using Equation 28. Knowing the volume and having measured the mass of the sample, the density of the material can then be calculated using Eqn 29.

$$V_{sample} = V_{sample\ chamber} - \frac{V_{reference\ chamber}}{\frac{P_1}{P_2}-1} \qquad \textbf{Eqn 28}$$

Where P_1 and P_2 represent the gas pressure in the sample and the reference chambers respectively and V represents the volume.

$$Density_{sample} = \frac{Mass}{Volume} \qquad \textbf{Eqn 29}$$

3.3.9   Density: Helium Pycnometry – Instrumentation

The density of polymer samples was measured via pycnometry using an Accupyc II 1340 (Micromeritics, USA), with Helium gas as the probe molecule. All density measurements were carried out at room temperatures, 25 °C using 1cm^3 sample holder.

3.4   Nonwoven Materials

All the nonwoven samples, both surfactant coated and uncoated, used in this research were donated by Procter and Gamble. These were 25gsm polypropylene based nonwovens and 50/50 polypropylene/polyethylene-based nonwovens. Surfactants are normally applied to nonwoven fabric via industry standard processes such as "kiss roller" coating by the manufacturer. Therefore, all the surfactant coated nonwovens received were precoated with either Stantex S6327/ S6887 from Pulcra Chemicals, (nonionic surfactant mixture), or Silastol PHP-26, (cationic surfactant mixture). Typically, in industry, these are applied to nonwovens in the range of 0.1-3% wt/wt[130, 31, 153]. Some materials were received freshly coated and others were aged for different periods of time.

3.5   Polymers

All polyethylene samples used in this work were ordered from Sigma-Aldrich (Poole, UK) and all the polypropylene samples were ordered from Sp^2 Scientific Polymer Products Inc. (NY, USA). They are all listed together with their properties in Table 3. 1.

Table 3. 1 Properties of polymers.

Material	iPP	aPP	LDPE	MDPE	HDPE
Physical Form	pellets	waxy solid	pellets	powder	pellets
Approx. Mw	12,000	10 000	30 000	60 000	200 000
Density [g/m^3]	0.90	0.84	0.92	0.92	0.94
T_m and T_g [°C]	170/-6	70/-14	100/-120	125/-120	130/-130
Refractive Index [nD]	1.49	1.47	1.51	1.52	1.54
Solvent Soluble in	decalin	toluene	decalin	decalin	decalin

3.6 Laboratory Reagents

All the reagents used in this work were ordered with a minimum of 99% purity from Sigma-Aldrich (Poole, UK) and VWR, UK. All reagents were used without further purification. The di-water (DI) used for all the experiments was ultra-pure Milli-Q grade.

3.7 Surface Modification of D-mannitol – Methylation

Modified D-mannitol powder was used for IGC method development studies. Modified D-mannitol is used as a reference material because its properties and surface energetics have been extensively studied and well characterised using the IGC. In fact, modified D-mannitol is used as a reference material by Surface Measurement Systems, manufactures of the iGC-SEA instrument, for system validation tests and calibration studies. Surface modification of D-mannitol was carried out following the method by Ho et al.[376]. D-mannitol powder, (PEARLITOL® 160C, Roquette Pharma, Lestrem, France) was sieved using a set of ASTM test sieves (Endecotts Ltd., London, UK). D-mannitol sample, comprising of <63µm particle sizes only were methylated by mixing the respective samples in separate solutions of 5% v/v dichlorodimethylsilane (≥99.5% Aldrich, Poole, U.K.) in trichloroethylene (≥99.5% Sigma-Aldrich, Poole, U.K.) at 80 °C for 3 h under constant reflux, resulting on silanisation of the surface as shown Figure 3.48. The mixtures were stirred continuously during the reaction process to ensure good dispersion and methylation of surface hydroxyl groups. The liquid was decanted off after reaction and the samples were dried in a vacuum oven at 80 °C for 3 h. This treatment ensured that a large portion of the surface hydroxyl groups were methylated and that all the solvent was evaporated. Materials were stored at 4 °C before characterisation.
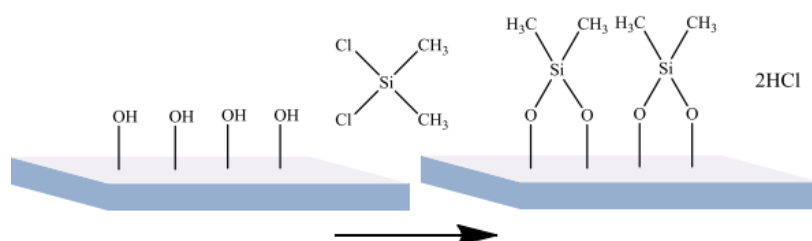
Figure 3. 22 Mannitol silanisation mechanism with hydrophilic surface hydroxyl groups modified to hydrophobic methylsiloxyl groups [377].

3.7.1   Fabrication of Thin Polymer Films

The procedure for the fabrication of thin spin coated polymer films was adopted from Lock et al. [378] with some modifications. The process involved the following stages.

3.7.1.1 Si wafer cleaning

Exposure of Si wafers to air introduces the deposition of contaminating dust particles on the surface even when the processing is done in clean room and therefore all the silicon wafers were cleaned before used as follows:

- 5 mins sonication in 1% (v/v) Hellmanex III aqueous solution
- 2x fast rinse in hot DI water
- 5 mins sonication in IPA
- 2x fast rinse in deionised water
- ozone clean 30min (UV/Ozone ProCleaner™ Plus from BioForce Nanosciences)

3.7.1.2 Polymer solution preparation

Due to the crystalline composition of polyethylene and polypropylene, a range of solvents and solvent mixtures were investigated for the polymer dissolution at room temperature without success, apart from amorphous PP which dissolved in Toluene, Decahydronaphthalene (decalin) was the only solvent which dissolved all the polymers, including a nonwoven, in a reasonable timeframe. To ensure fast polymer dissolving, decalin, anhydrous 99% purity (Sigma Aldrich, mixture of cis and trans) was used as the solvent because it has a high boiling point. Solutions of polyethylene and polypropylene in tetrahydrofuran and toluene are possible but require elevated temperatures and more than 8 hours to be obtained. When decalin was used as a solvent and the temperature was ≥ 160 °C, complete polymer dissolution for both PE and PP cases were obtained in less than 3 hours. A 0.5-6% w/v solution range was investigated. Above 2% w/v the polymer solvent solutions were very viscous and therefore the obtained cast films were highly non uniform. The lower solution concentration range (0.5 and 1%) also did not produce effective surface wetting of the wafer. The best thin films were produced with 2% w/v solution for both polyethylene and polypropylene. To ensure dissolving of polymer pellets in solvent, the solution was heated above the polymer melting temperature. These are 120-130°C for polyethylene and 160-165°C for isotactic polypropylene. Atactic polypropylene was dissolved without heating, at room temperature. The glass pipette used to

transport the solution to the wafer and the tweezers used to transport the silicon wafers were heated to temperature above 100 °C to ensure uniform surface wetting by the polymer solution.

3.7.1.3 Spin coating

Spin coating is a well-established method for preparing smooth polymeric coatings on flat substrates. In this thesis pre-oxidised and pre-diced Ossilla silicon oxide wafers with a 400nm oxide layer, 20mmx15mm, with no photoresist coating, were used as substrates. Spin coating involved a deposited a polymer solution droplet onto a spinning substrate to produce a thin film of solid material. An Ossila spin coater was used and the procedure was as follows:

- the preheated wafer substrate was positioned on the chuck
- a few drops of polymer solution were deposited on the wafer, so that the latter was covered
- the wafer was spun for 2 min at 2000 rpm

As a rule of thumb, increasing of the spin rate causes a decrease of the film thickness. The process of polymer - surfactant films fabrication on silicon oxide substrates, is depicted in Figure 3. 23
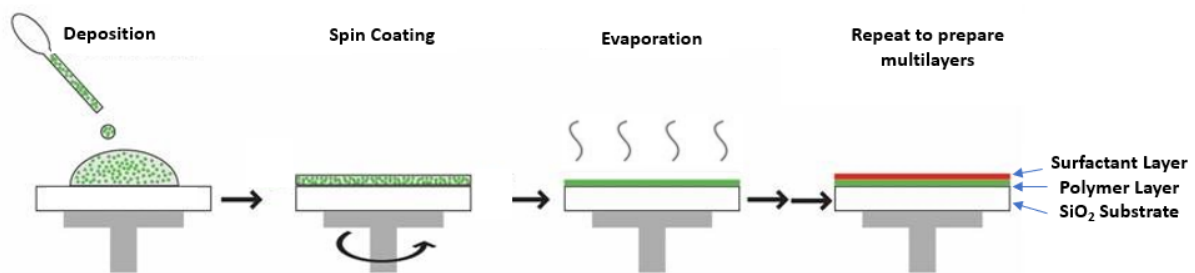
Figure 3. 23 Schematic of the spin-coating process. Adapted from Nikniazi et al.[379].

3.7.1.4 After treatment

The method of drying of silicon wafers needed to be considered. It was found that best way to remove solvent from the surface was by heating the wafer on a hot plate up to 60-70 °C (the heating temperature should be lower than the glass transition temperature of the polymer) so that the residual solvent evaporates.

3.7.1.5 Thin film fabrication on aluminium foil for sorption studies

Thin film fabrication details are included on Chapter 6.

4 Surface Characterisation of Nonwovens

4.1 Introduction

As discussed in Chapter 2, research on the interactions between surfactants and polymeric nonwoven fibres is extremely important because these materials are commonly used in many important sectors, including the personal care industry. When a nonwoven fabric is formed from a hydrophobic polymer like PP and PE, its surface is often modified using surfactants, to transform it into a hydrophilic fabric which can then more easily wet and distribute aqueous fluids. Baby and adult disposable nappies, sanitary towels, and various wipes are examples of products made from nonwovens coated with surfactants. It is a common industrial experience that the surface hydrophilicity of these modified nonwoven materials is time dependent, and this could affect product performance. Understanding the mechanisms of the interactions between polymer and the surfactant in these complex materials systems, could help improve processes used for developing hydrophilic nonwovens, leading to improved products as well as reduced manufacturing costs and waste.

To understand the interaction between surfactants and polyolefins, several chemical properties and physicochemical descriptors of these materials were investigated including wettability, specific surface area, surface energy, sorption kinetics, and their elemental composition. The thermodynamic interactions between surfactant molecules and the polyolefin substrate can be described by a range of physiochemical parameters, including the dispersive and specific component of surface energy, the specific free energy, as well as the enthalpy and entropy of adsorption for molecule's interaction with the substrate of interest. In this Chapter, the focus is on characterising the surface properties of polyolefin-based nonwovens coated with surfactants, such as those manufactured via standard high speed, low-cost coating processes used for production of disposable baby nappies. According to published literature[31, 130, 153] surfactants generally constitute about 0.1-3% by weight of the nonwoven fabric to which it is applied. The industrial coated nonwoven samples used in this research comprise of similar surfactant loadings unless otherwise stated.

4.2 Specific Surface Area BET Measurements of Polymeric Nonwovens

The specific surface area of solid materials is determined by physical adsorption of a gas or a vapour on the surface of the solid, and by calculating the amount of adsorbate gas corresponding to a monomolecular layer on the surface. Traditionally, such adsorption isotherm measurements are carried out at the boiling point of nitrogen (-196°C) using N_2 as the adsorbate and using a volumetric apparatus. This method forms the basis of ASTM D6556[380] and ISO 9277:2010[381] which are the standard approaches for determining the surface area of porous solids which typically have surface areas between 100 and 2000m^2/g. At this temperature, the nitrogen gas is below the critical temperature and so condenses on the surface of the particles. Brunauer-Emmett-Teller (BET) proposed a model which is routinely used to determine the surface areas using N_2 adsorption isotherm data for porous solids[358]. Before the specific surface area of the sample can be determined with this method, it is necessary to remove unwanted gases/vapours adsorbed onto the surface during manufacturing, handling and storage, whilst avoiding irreversible changes to the surface. Without this outgassing step the specific surface area may be reduced or may be erroneously determined because an intermediate area of the surface is covered with contaminant molecules.

The influence of outgassing on the BET values obtained via volumetric N_2 method for a typical nonwoven is depicted in Figure 4. 1. Experimental results reported here show that degassing for at least 3 hours at 80°C under vacuum is necessary for a typical commercially manufactured nonwoven fabric; a PP based core cover sample. Outgassing conditions are critical for obtaining precise and accurate measurements especially for industrial samples of nonwoven which are characterised by generally low specific surface area values. Such materials manufactured at mass scale are prone to contaminants because they are not produced under controlled laboratory conditions. So, in conclusion, it can be seen here that these results for low surface area materials are dependent on the sample preparation/degassing protocol.
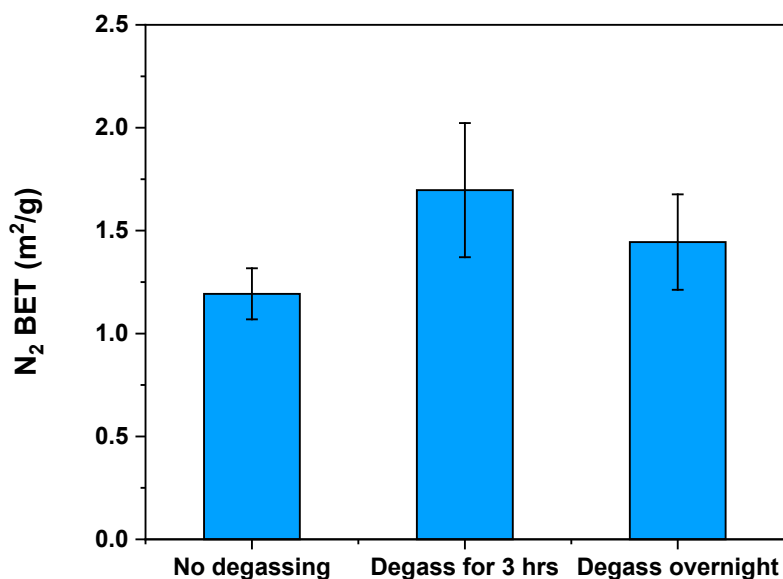
Figure 4. 1 Influence of different outgassing programs on the N$_2$ BET measurements for a typical PP based nonwoven. Results are $\mu \pm \sigma$, n = 3.

Since the BET via the N$_2$ volumetric approach has limitations, including long experimental times, low measurement temperatures and accuracy limitations for surface areas about or below 1.0 m^2/g, alternative approaches, like IGC, were considered. IGC is better suited for analysis of samples with low specific surface area. As highlighted in the literature[262, 265] specific surface area values obtained via IGC for the same samples tend to be lower but more accurate than those obtained via the N$_2$ volumetric method.

IGC determines BET isotherms generally using an alkane such as octane as the adsorbate. However, these organic solvents can potentially dissolve into amorphous polymers including polyolefins. Such bulk sorption is in contrast to the desired surface adsorption processes and will compromise the surface area determination. Therefore, surface area measurements using the standard IGC method with organic solvents can sometimes be problematic. Figure 4. 2 shows the raw chromatographic data, showing the IGC retention peaks for octane (left) and methanol (right) for a PP based nonwoven sample. The retention time for these peaks is a measure of the strength of molecular interactions between the probe and the solid surface of sample packing in the column and is the key measurement parameter in IGC analysis. The data shown in Figure 4. 2 demonstrates a symmetrical Gaussian methanol peak and a wide asymmetric octane peak with strong tailing. Indeed, the octane peak does not come back to baseline even after a 30-minute experiment. This slow tailing is a feature of bulk sorption which can be explained by the alkane probes dissolving into the PP polymer. Octane appears to interact strongly with the substrate and its desorption is very slow and hence the tailing affect. The FID signal intensity for the octane peak is considerably lower than that of the methanol

peak which supports the idea of dissolution of the probe into the substrate. Therefore, it was concluded that alcohols are better suited as test probes for analysis of polyolefin-based materials than alkanes.
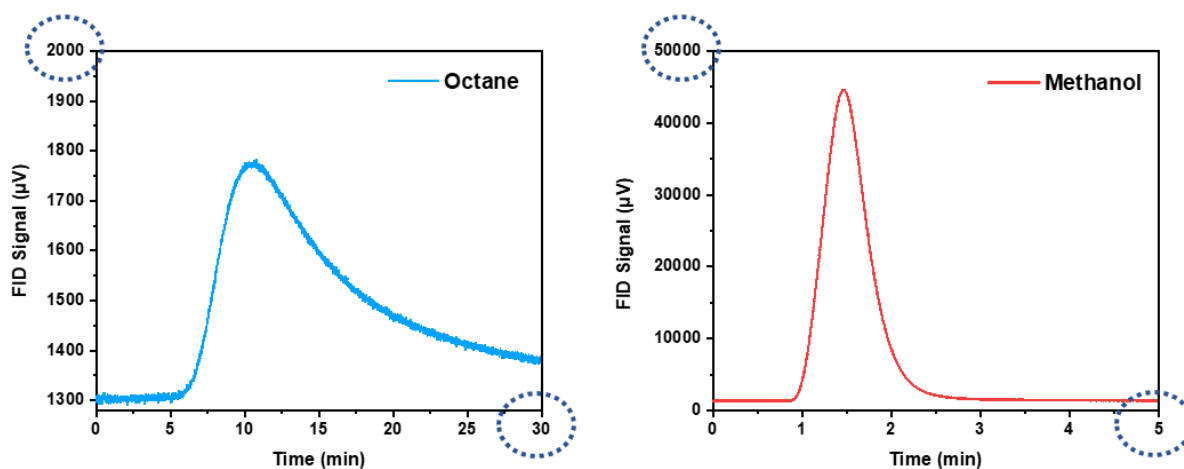
Figure 4. 2 IGC chromatograms of octane (left) and methanol (right) for a PP based nonwoven sample.

Methanol is therefore reported as suitable test probe for determination of the specific surface area of polyolefin nonwovens using IGC. Approximately 1000mg of nonwoven sample, was used for initial BET measurements. All experiments were conducted at 30°C with flow rate of 10 sccm using methanol as the test probe, 180 min conditioning time, and peak maximum method was used for data analysis. Typical methanol adsorption isotherms and the corresponding methanol BET analysis plots for top sheet and core cover nonwovens are presented in Figure 4. 3 and Figure 4. 4, respectively. The adsorption isotherm is the relationship between the amount of adsorbate adsorbed and the equilibrium pressure of the adsorbate at constant temperature. The methanol isotherms show relatively low uptake and strong Type II/IV character indicating a surface-only sorption mechanism, which allows the BET model to be appropriately applied. The BET surface area plots obtained using methanol gave a good straight-line data fit over the partial pressure range of 0.05 to 0.3. The BET surface areas for the PP/PE blended nonwoven was found to be 1.59 m^2/g and for the PP nonwoven was found to be 2.39 m^2/g.
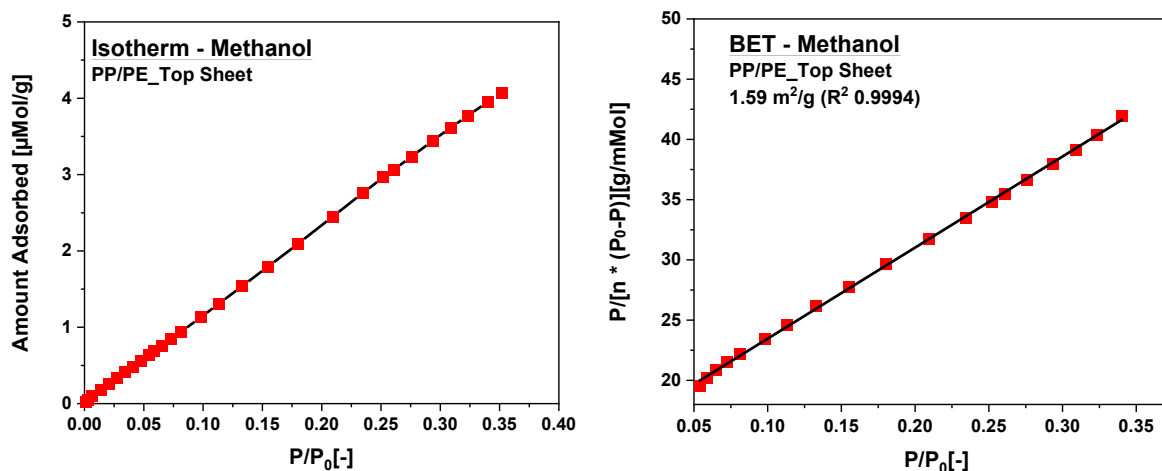
Figure 4. 3 Typical sorption isotherm of methanol on PP/PE based top sheet nonwoven and the BET analysis using methanol.
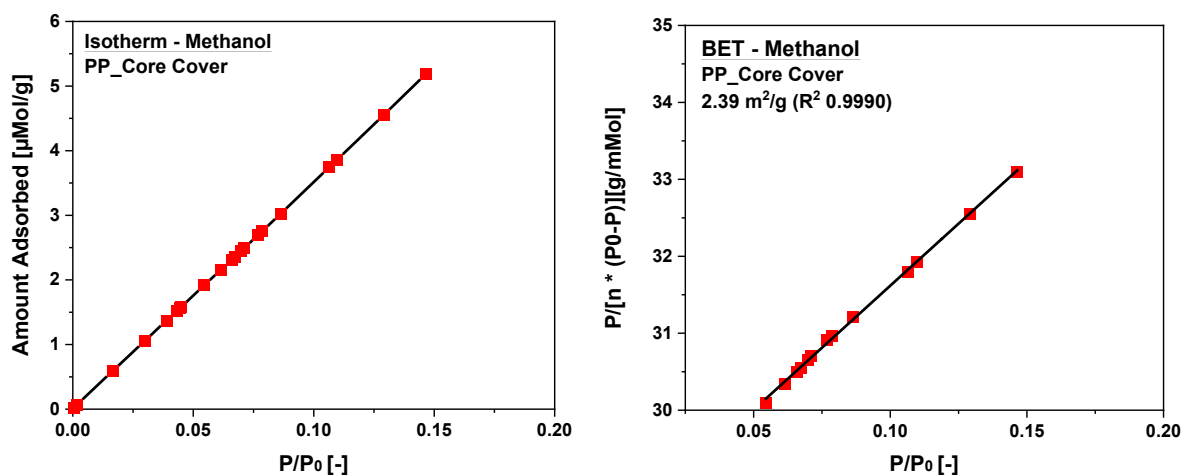
Figure 4. 4 Typical sorption isotherm of methanol on PP based core cover nonwoven and the BET analysis using methanol.

Generally, the P/P_0 range is from 0.05 to 0.35 where there is a linear relationship in the BET equation. However, sometimes the first few points or last few points will not give a linear fit. In these cases, these points could be excluded since they do not fit the BET equation. BET specific surface area measurements for a set of nonwoven samples were obtained with IGC and the N_2 volumetric approach and the results compared as shown in Table 4. 1. Findings from the literature[382] are in line with these results. The relative standard deviation for IGC is less than 5%, indicating the high sensitivity and precision of this method relative to the N_2 volumetric method which features relative standard deviation (RSD) values higher than 10%. The higher RSD's for the nitrogen method could be due to the inherently large dead volumes within the instrument, especially critical for materials with relatively lower surface areas. In comparison, dead volumes are typically less critical for flow systems such as IGC. Another possible reason for the data variability between the two techniques could be due to incomplete sample degassing associated with the nitrogen method. IGC measurements do not require the

sample to be degassed prior analysis in the same way as the nitrogen method. Instead, a sample conditioning process with helium flow is provided by the instrument *in situ*, reducing variation arising from sample preparation thus making the results significantly more reproducible. Furthermore, N_2 BET and IGC BET are determined using different adsorbates. IGC determines BET isotherms generally using either an alkane or an alcohol as test probes. The benefits of using such test probes is that the adsorption isotherms can be measured at room temperature and humidity. Measurements with N_2 BET method can be challenging for some materials because of the unknown effects of exposure to extreme low temperatures, (77 K) on sample integrity[262, 265].

Table 4. 1 BET SSA results of nonwoven fibres measured using the standard N_2 volumetric approach and IGC with methanol as test probe, n = 3.

Nonwoven Samples (Top sheet)	N_2 BET SSA m^2/g / (% RSD)	IGC BET SSA m^2/g / (% RSD)
PP/PE_Surfactant.Coated (fresh)	**1.54 /** (10.1 %)	**1.14 /** (3.4 %)
PP/PE_Uncoated (fresh)	**1.55 /** (15.2 %)	**0.95 /** (0.6 %)
PP/PE_Surfactant.Coated (aged)	**1.36 /** (27.8 %)	**0.72 /** (4.3 %)

%RSD = % Relative Standard Deviation

The batch-to-batch variability for surfactant coated core cover nonwovens using BET measurements via the IGC method, with methanol as test probe is shown in Table 4. 2. Experimental data shows that any variation is within experimental error and that no significant difference is obvious between the three different columns packed with the same nonwoven material.

Table 4. 2 The effect of column-to-column variability on BET measurements using IGC with methanol as test probe for core cover surfactant coated nonwovens. Results are $\mu \pm \sigma$, n = 3.

Nonwoven Samples (Core cover)	IGC BET SSA (m^2/g) $\mu \pm \sigma$
Column 1	**3.57** ± 0.4
Column 2	**3.03** ± 0.1
Column 3	**3.16** ± 0.1

Since IGC columns are packed by the user, two different packing methods were evaluated and the results for three different types of nonwoven samples are shown in Figure 4. 5. In one method the columns were packed with the sample as a whole piece of nonwoven fibre. The other method involved packing the columns with the small pieces, (2x4cm) of the nonwoven cuts. Apart from sample 1 which was significantly different the results for the other two samples, (2 and 3) showed a small variation between the two methods for packing the column which could be within experimental error. An observation was that BET values for the

nonwoven cuts were generally smaller than those obtained for the nonwovens packed as a whole piece. These results are in agreement with findings from Hadjittofis et al.[383] who reported that standardisation of column preparation is important for IGC studies. Therefore, all subsequent IGC experiments were conducted in a consistent way using only columns packed with the nonwoven cut into smaller pieces, which was a more practical method for packing the columns. Another observation was the varied BET values of the three different samples from the same material batch. This variation is not a surprise considering the nature and intrinsic heterogeneity of the structure of these 3D network materials composed of randomly oriented fibres and voids.
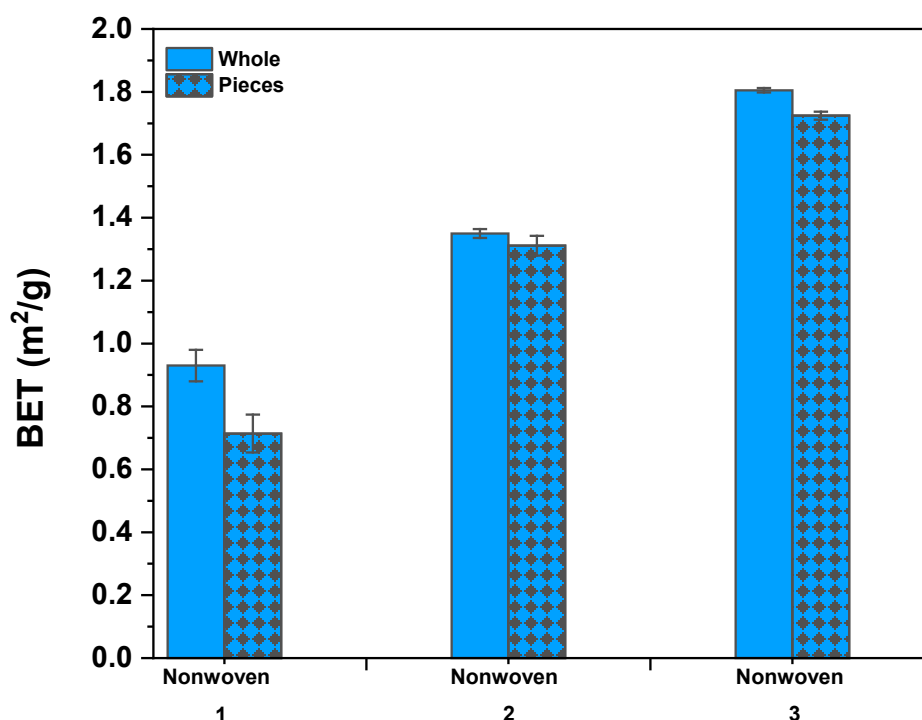
Figure 4. 5 The effect of column packing method on IGC measurements for three different top sheet nonwovens determined using methanol as test probe. Results are $\mu \pm \sigma$, n = 3.

To study the effect of sample aging, two columns packed with approximately 1300mg of industrial nonwoven samples, one surfactant coated and the other uncoated, were repeatedly analysed over the course of six months using methanol as test probe for BET measurements with IGC as a function of time. Each measurement was repeated three times. The results are shown in Figure 4. 6. The data suggests that specific surface area of surfactant coated samples is generally larger, and it changes overtime unlike for uncoated samples. Since both samples are identical apart from the coating, this effect can therefore be attribute to changes caused by the surfactants and their fugitive nature.
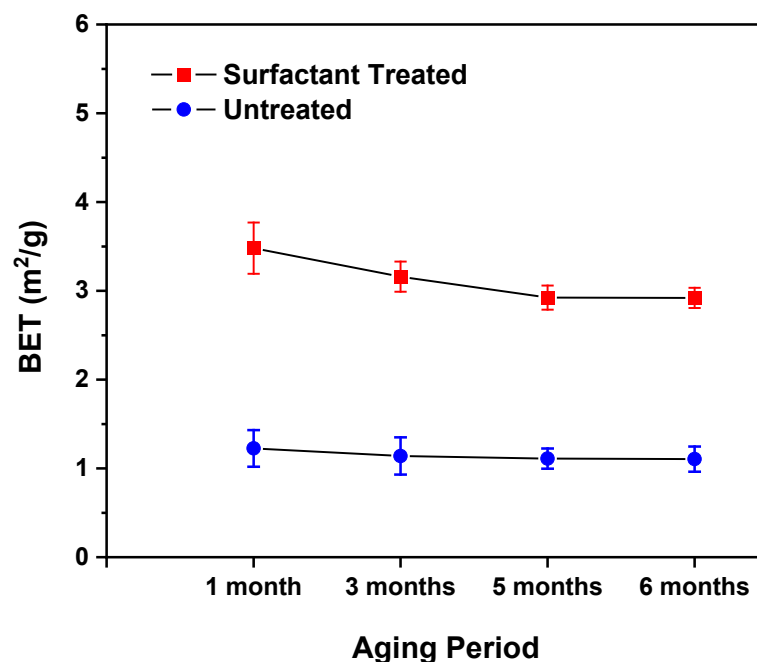
Figure 4. 6 Aging effect on BET measurements with methanol for industrial nonwovens. Results are $\mu \pm \sigma$, n = 3.

4.3   Surface Energy Measurements of Polyolefin Based Nonwovens

Traditionally, surface energy analysis is performed using contact angle measurements which is relatively simple procedure to perform and it works well for flat surfaces. However, polymeric nonwoven fabrics, like most real solid surfaces, are not flat and are fundamentally inhomogeneous. They comprise of voids and fibres randomly interlinked on a horizontal plane. Therefore, contact angle measurements for such materials is complex and the data can have limited use. They cannot be measured using direct sessile drop methods and are usually determined using capillary rise approaches[384, 385]. Furthermore, real solids exhibit a range of lower and higher energy sites on their surfaces due to presence of different types of surface functional groups, surface topographies, surface irregularities and impurities; they exhibit surface heterogeneity. Since contact angle method uses liquid droplets, the corresponding surface energy represents that of localised areas reflecting the droplets' three phase contact line. There is no reliable way of determining the surface energy heterogeneity or such properties for the entire sample of interest for these types of materials with this method.

However, it is possible to observe more generally, the local wetting characteristics of the polymeric nonwoven fabric samples, and such contact angle measurement were performed. In addition, IGC was used since it measures the surface energy across all of the sample

surface area, giving statistically more significant results, as well as allowing the extent of surface energy heterogeneity to be evaluated using a vapour adsorption methodology.

4.3.1 Wettability measurements of nonwoven surfaces using contact angle.

To understand the wetting characteristics of the nonwoven samples coated with surfactants, sessile drop contact angle measurements were performed using a Ramé-Hart goniometer, analytical grade deionised water and diiodomethane (>99%, Sigma-Aldrich, UK), as test probes. The nonwoven samples were fixed onto a microscope slide using double sided tape prior to analysis to help keep samples flat and to facilitate measurements as shown in Figure 4. 7. The sessile drop method for measuring advancing contact angles was used.

Figure 4. 7 Polyolefin based nonwoven, (2x3cm) fixed into a microscope slide using double sided tape.

Contact angle measurements were used to differentiate between surfactant coated and uncoated nonwovens. In general, for the uncoated samples contact angles > 90° were measured for all test locations, whereas for the coated samples a range of contact angles was observed, some of which >90° and some of which were <90° were recorded. All coated samples featured the patch wise wetting heterogeneity as depicted schematically in Figure 4. 8. This characteristic was not observed for the uncoated samples.
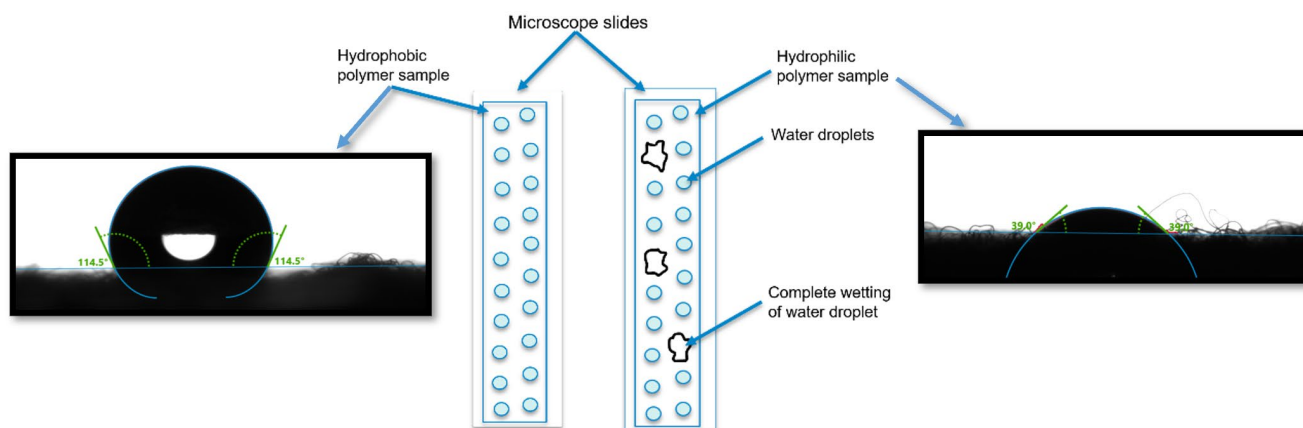
Figure 4. 8 Schematic diagram showing the patch wise heterogeneity effect of coated samples and droplet images of a hydrophobic, (left) and a hydrophilic region, (right) of the nonwoven.

Nine different nonwoven samples were tested, three surfactants coated, three uncoated samples, and three surfactant coated sample which were washed in isopropanol (IPA) for 1hr and dried overnight prior to testing. IPA washing serves to remove the surfactant coating. This population of different samples included "freshly" manufactured, and aged nonwoven samples. An array of 40 water drops per sample has their advancing contact angles determined. It was observed that the contact angle of ~80% of water drops, for 1 week old surfactant coated samples was not possible to be measured as they completely wetted the polymer instantaneously, as shown in Figure 4. 9. This percentage of fully wetted droplets reduced as a function of time. The 2-year-old samples displayed mainly hydrophobic properties confirming its reduced surface hydrophilicity. Also, the data revealed that extraction with IPA of the surfactant from the coated samples changed the characteristics of the hydrophilic samples making them behave more like hydrophobic samples due to the removal of the surfactants.
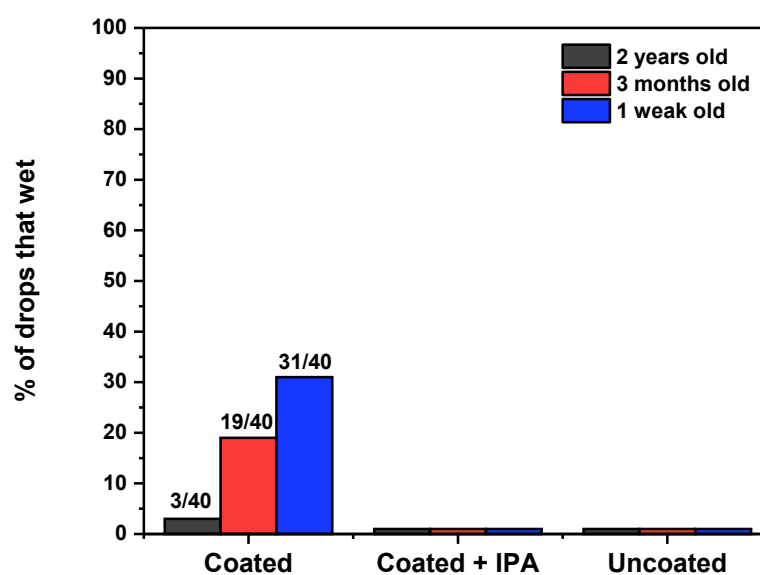
Figure 4. 9 Wetting hydrophilicity results for aged surfactant coated nonwoven samples.

Nonwoven polymeric substrates, like those used for manufacturing disposable baby, feature a "smooth" and a "engraved" surface side, see Figure 4. 10. The engraved side is caused by the presence of a pattern moulded into the fabric during the manufacturing process from one side. This pattern appears to influence the contact angle measurements, see Figure 4. 11. Wenzel [386] and Cassie Baxter[345] provided models that accounted for micro surface roughness. Although these are different models, they both indicate that roughness increases the droplet contact angle and hence effective non-wetting behaviour of a hydrophobic surface, ($\theta > 90°$) but for a hydrophilic surface, ($\theta < 90°$) an increase in surface roughness increases hydrophilicity[387] which is reflected by a decrease in the contact angles. Overall, the surfactant coated surfaces gave slightly lower contact angles. However, all materials displayed contact angles $\theta > 90°$. Therefore, these can be considered hydrophobic in nature. The results show an increased contact angle for the rough samples which would be consistent with the Wenzel[386] and Cassie Baxter[345] theories. However, the larger error bars indicate a wide spread of contact angles, and surface energy heterogeneity which is in line with the patch wise heterogeneity behaviour discussed above.

Figure 4. 10 Photo showing the "smooth" and the "rough" surface sides of a typical nonwoven. Note the 5p is included illustrative purposes to give an idea of the size of these patterns.
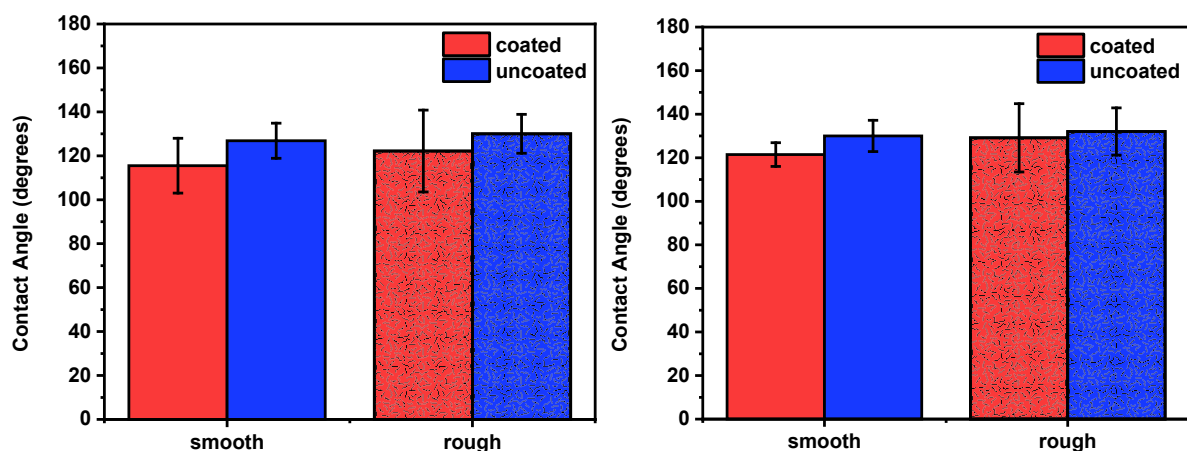
Figure 4. 11 Contact angles of aged PP/PE based top sheet nonwovens on (left) 6 months old and (right) two years old. Results are presented as $\mu \pm \sigma$, n = 8.

The wettability of PP based nonwovens, like those used as core cover for manufacturing baby nappies, were also analysed using water as the probe liquid. A blank uncoated sample, a surfactant coated sample with 0.56% loading, 0.81% loading and 1.07% loading were examined. The results of the study are summarised in Figure 4. 12. The data demonstrate homogeneity for the native hydrophobic nonwovens with small contact angle variations. The results for the coated samples are however nonuniform and are characterised by bimodal distribution of advancing contact angles for water. The nonuniformity of the surfactant distribution is reflected by the wide variation of contact angles observed. The measured variation of contact angle measurements for surfactant coated samples increased as a function of surfactant loading.

The data demonstrated an uneven coating which could be a process dependent feature which is more pronounced for the higher loadings however, it is more likely that this is a material dependent effect. These nonwoven materials are not flat, they comprise of a web of fibres with voids and intersections randomly oriented and as a result the surfactant coating is also randomly distributed to that effect. The coated samples feature patch wise heterogeneity, in agreement with previous findings discussed above, meaning that the surfactant coating does not cover the whole of the sample surface and it is unevenly distributed across the 3D fabric structure network. This work highlights the need for a method which can facilitate quantitative mapping of the surfactant distribution within the complex 3D polyolefinic fiber network.
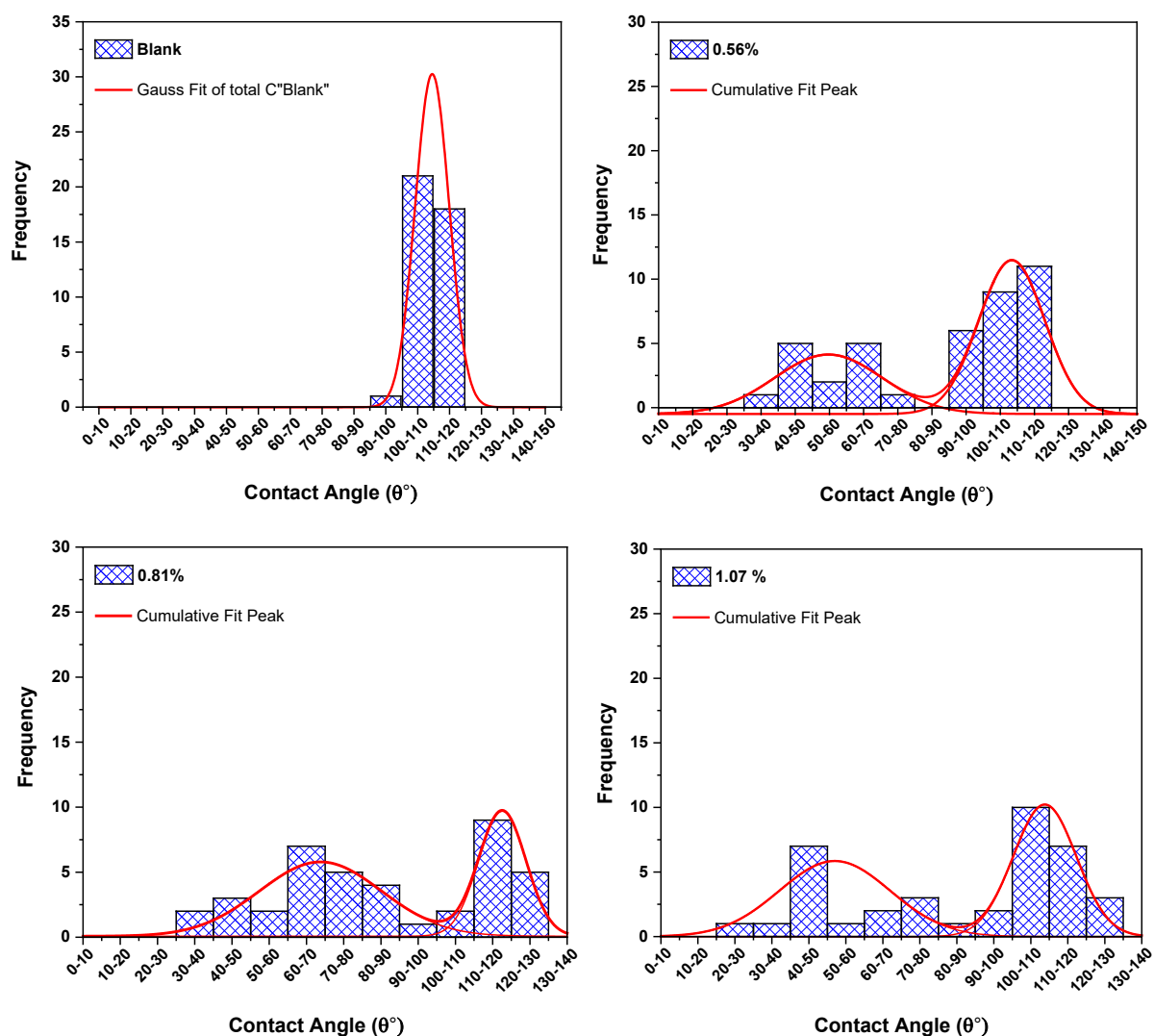
Figure 4. 12 Effect of surfactant loadings, 0.00%, 0.56%, 0.81% and 1.07% on water contact angle measurements on PP based nonwoven, n = 40.

The surface energy of these polymers were determined from measured contact angle values measured with two liquids with known surface energies, water and diiodomethane, using the Fowkes model. The surface tension values of water and diiodomethane used for the calculations are provided in Table 4. 3.

Table 4. 3 Surface tension values of pure water and diiodomethane[388]

Probe	γ_L^P (mJ/m²)	γ_L^D (mJ/m²)	γ_L^T (mJ/m²)
Diiodomethane (DIM)	0.0	50.8	50.8
Di-water	21.8	51.0	72.8

Surface energy of the polymer without surfactants should only contain a dispersion component due to its hydrocarbon base. The expectation was that the presence of the surfactants would

introduce a polar component of surface energy onto the polymer thus reducing the water-polymer interfacial tension and contact angle. Surfactant coated and uncoated nonwovens samples were analysed at room temperature and their surface energy and its components determined as shown in Table 4. 4. The data demonstrated in general higher surface energies for the surfactant coated samples compared with the uncoated samples, which aligns with our expectations.

Table 4. 4 Surface energies determined from measured contact angle values using water and diiodomethane and the Fowkes' analysis. Results are expressed as $\mu \pm \sigma$, n =40.

Nonwoven Samples	θ (DIM) ^{o} $\mu \pm \sigma$	θ (water)^{o} $\mu \pm \sigma$	γ_s^D (mJ/m^2)	γ_s^P (mJ/m^2)	γ_s^T (mJ/m^2)
Core cover (blank)	71 ± 10.1	106 ± 3.4	22.3	0.3	22.7
Core cover (0.56% loading)	61 ± 15.2	100 ± 17.6	27.8	0.6	28.5
Core cover (0.81% loading)	69 ± 23.9	90 ± 29.4	23.7	3.7	27.4
Core cover (1.07% loading)	59 ± 13.2	97 ± 24.6	29.2	0.8	30.0

The relatively high standard deviation values seen in contact angle measurements reflect both the chemical and physical heterogeneities of these samples. As discussed above this technique is a quick and simple method for measuring surface energy, requiring only small amounts of liquid and solid sample, but the method has shortcomings. It measures individual drops and therefore surface energy determinations are for localised and relatively external sample areas only, and there is no comprehensive way of accurately averaging across the entire sample volume. So, though the wetting data has some clearly practical application relevance, it cannot be considered to be a comprehensive description of the sample wetting properties. As already established, for surfaces like nonwoven fabrics which are fundamentally topographically inhomogeneous, a single value of surface free energy is not necessarily representative of the entire surface. Therefore, surface energy data from wettability experiments has limitations. The disadvantages of contact angle approach are well known and documented in the literature[384] a discussion of which is covered in Chapter 2. IGC is a better technique to determine surface energy because it measures the surface energy across a much larger sample surface area, giving statistically more meaningful data.

4.3.2   Surface energy determination using IGC with alcohols.

As previously discussed, a homologues series of n-alkanes are normally used in IGC to determine dispersive surface energy of materials. It is assumed that n-alkanes represent only the dispersive interactions, while the polar solutes exhibit both dispersive and specific interactions. Preliminary BET analysis demonstrated that alkanes are absorbed into the bulk

by the PE/PP nonwoven samples. The effect of temperature and flow rate were investigated to optimise and improve the method with n-alkanes, but without success. The data from these investigations which reflected the bulk sorption of these probes can be found in Appendix A. n-alkanes were not suitable for the IGC determination of dispersive surface energy of polyolefins nonwovens.

Therefore, a homologues series of alcohols have been utilised for the first time here for dispersive surface energy determination of polyolefin nonwovens. Following the basic principle of the Dorris and Gray method when using a series of liquid n-alkanes as probes, here a series of homologous alcohols is characterised in the same way as a homologous series of alkanes. The slope of the alcohol line in the plot of $RTlnV_N$ versus the carbon numbers of the n-alcohol gives γ_s^D as shown by Eqn 30 which is the method originally proposed by Dorris and Gray:

$$\gamma_s^D = \frac{slope^2}{4 \cdot N_A^2 \left(a_{CH_2}\right)^2 \cdot \gamma_{CH_2}} \qquad \textbf{Eqn 30}$$

where N_A is the Avogadro's number, a_{CH_2} is the cross-sectional area of an adsorbed methylene group, $6 \times 10^{-20} m^2$ and γ_{CH_2} is the surface energy of a methylene group in a close packing configuration analogous to that of polyethylene given by Eqn 31.

$$\gamma_{CH_2} = 35.6 - 0.058 \, (T - 20) \, mJm^{-2} \qquad \textbf{Eqn 31}$$

Equation 30 was employed to determine dispersive surface energy, γ_s^D of silanised D-mannitol, an IGC reference material, using both a series of homologues n-alkanes and alcohols. There are two ways of analysing the IGC retention volume data. They are the peak maximum (Peak Max) and the peak centre of mass (COM) methods, and they can be user selected in the SEA-IGC software. The retention time of peak maximum, shown in Figure 4. 13, is the retention time/volume which is associated with the maximum FID signal, and the peak centre of mass (COM) is the first statistical moment of the peak which defines the peaks average position giving the retention time/volume. For a Gausian peak these numbers are identical. The statistical moment theory is a more precise and meaningful way to characterise peaks of any shapes (Gaussian or non-Gaussian peaks) and is in general the preferred method. If the peak is perfectly symmetric, the retention time at peak maximum should equal to that at peak COM. However, for some cases, the peaks are clearly asymmetric with tailing, as in Figure 4. 13. In this case, retention time at peak COM varies from that at peak maximum, generally providing a larger value.
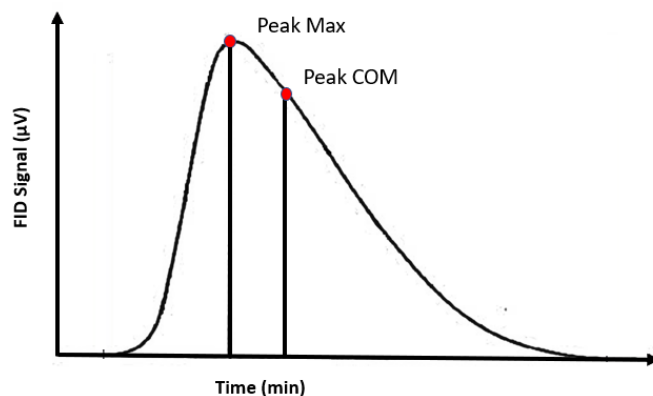
Figure 4. 13 Peak analysis methods for retention time/volume determinations.

Calculations of dispersive surface energy for silanised D-mannitol were performed using both peak analysis methods. The $RT\ln V_N$ values of a series of alcohols and n-alkanes were measured for silanised D-mannitol at 30°C and 10sccm flow rates and the results are tabulated in Table 4. 5 and Table 4. 6 respectively. The variation of $RT\ln V_N$ versus C-number plots are illustrated in Figure 4. 14 and Figure 4. 15, using both centre of mass and peak maximum respectively. The $RT\ln V_N$ values are linearly increased with increasing C-number with excellent correlation. Linear regression analysis using LINEST function on Excel was performed to establish the uncertainties associated with the slope of the linear best fit lines, presented as percentages in Table 4. 5 and Table 4. 6. The uncertainties of the slopes for both alcohols and alkanes are lower than 2%. The slope uncertainty translates into γ_s^D uncertainties as presented in Table 4. 7 and Table 4. 8.

Table 4. 5 RTlnV$_N$ values of alcohols and n-alkanes for silanised D-mannitol using peak COM.

	Fractional Surface Coverage (n/n_m)								
	0.05			**0.10**			**0.20**		
Solutes	RTlnV$_N$	Slope	Slope error (%)	RTlnV$_N$	Slope	Slope error (%)	RTlnV$_N$	Slope	Slope error (%)
Ethanol	-409.6			-626.2			-725.1		
1-Propanol	1964.2	2337.0	0.91	1721.7	2407.6	1.43	1657.2	2454.6	1.70
1-Butanol	4264.3			4188.9			4184.2		
n-Hexane	1021.9			1071.8			1104.6		
n-Heptane	3634.9	2498.1	1.37	3658.6	2488.4	1.21	3693.8	2488.1	1.30
n-Octane	6122.6			6142.5			6184.0		
n-Nonane	8519.7			8538.5			8568.1		

Table 4. 6 RTlnV$_N$ values of alcohols and n-alkanes for silanised D-mannitol using peak maximum.

Fractional Surface Coverage (n/n_m)									
Solutes	**0.05**			**0.10**			**0.20**		
	$RTlnV_N$	Slope	Slope error (%)	$RTlnV_N$	Slope	Slope error (%)	$RTlnV_N$	Slope	Slope error (%)
Ethanol	-1372.9			-1416.8			1372.9		
1-Propanol	1307.6	2576.3	2.34	1277.4	2695.6	0.03	1292.5	2719.7	1.15
1-Butanol	3779.6			3974.4			4066.5		
n-Hexane	988.1			1038.7			1071.8		
n-Heptane	3598.9	2520.7	0.96	3634.9	2517.6	0.81	3676.3	2532.6	0.82
n-Octane	6095.8			6127.0			6199.1		
n-Nonane	8558.0			8599.9			8672.8		
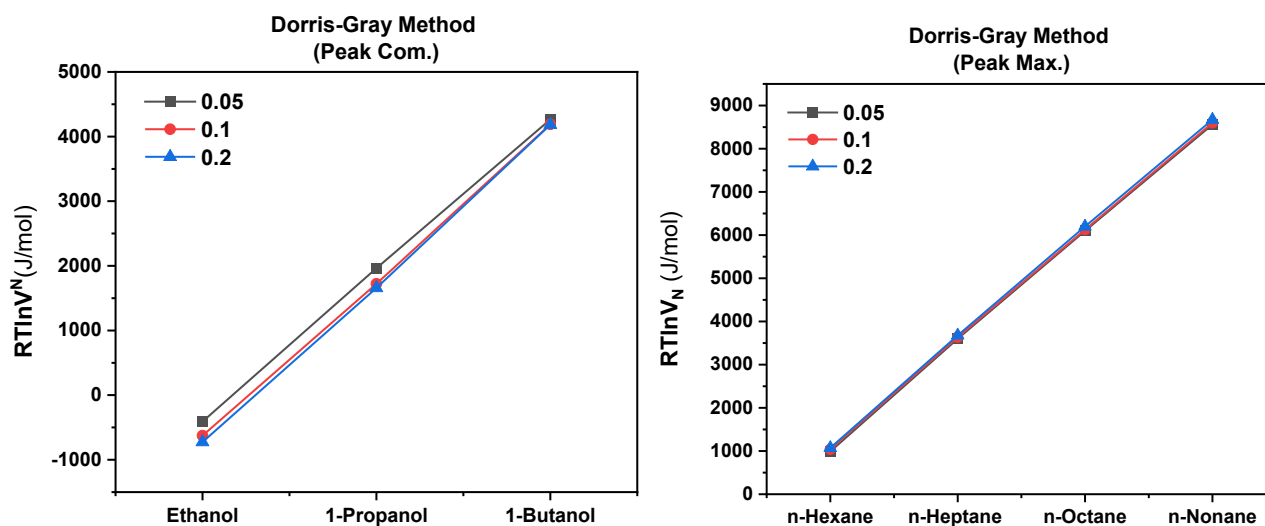
Figure 4. 14 $RTlnV_N$ versus C-number for alcohols and n-alkanes for silanised D-mannitol using Peak COM for three different fractional surface coverages, 0.05, 0.10 and 0.20.
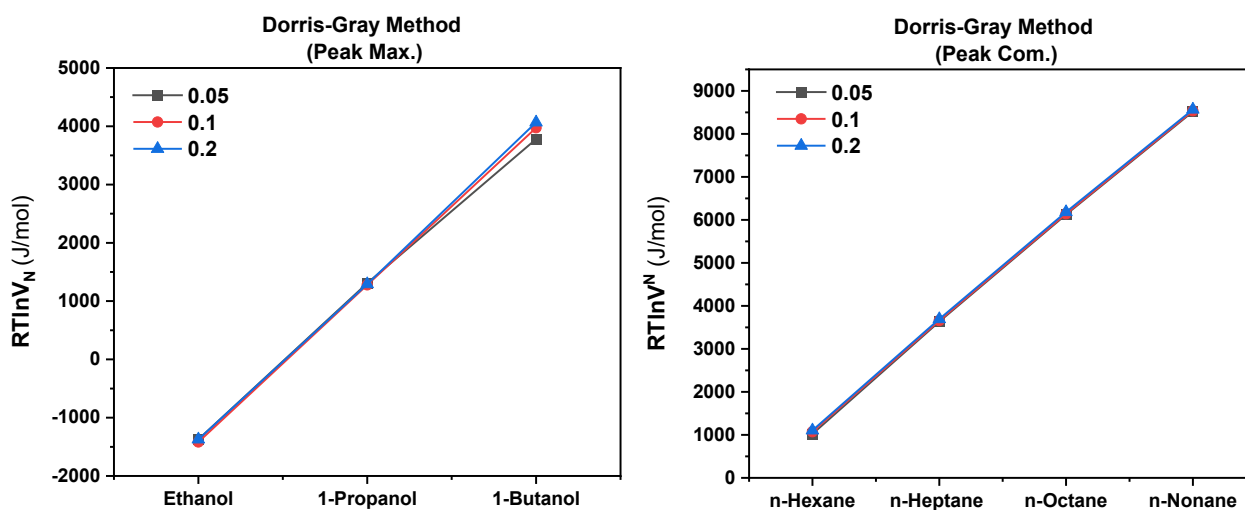
Figure 4. 15 RTlnV$_N$ versus C-number for alcohols and n-alkanes for silanised D-mannitol using peak maximum for three different fractional surface coverages, 0.05, 0.10 and 0.20.

The London dispersive surface free energy, γ_s^D, of silanised D-mannitol was calculated by the Dorris-Gray methods using both n-alkanes and alcohols as test probes and the results are tabulated in Table 4. 7 and Table 4. 8 using both centre of mass and peak maximum respectively. There is good correlation between the data obtained for the different probes suggesting that alcohols are suitable for γ_s^D measurements and can be used as an alternative method in cases where the standard method of using n-alkanes is not suitable.

Table 4. 7 γ_s^D measurements of silanised D-mannitol for three fractional surface coverages obtained for alcohols and n-alkanes using peak COM.

Fractional Surface Coverage (n/n$_m$)	Dispersive Surface Free Energy								Differences in γ_s^D (mJ/m^2)
	n-Alkanes				Alcohols				
	γ_s^D (mJ/m^2)	Slope error (%)	γ_s^D error (%)	γ_s^D error (mJ/m^2)	γ_s^D (mJ/m^2)	Slope error (%)	γ_s^D error (%)	γ_s^D error (mJ/m^2)	
0.05	34.1	1.37	2.74	0.93	29.9	0.91	1.82	0.54	4.2
0.1	33.9	1.21	3.48	0.82	31.7	1.43	2.86	0.91	2.2
0.2	33.9	1.30	2.60	0.98	32.9	1.70	3.40	1.12	1

Table 4. 8 γ_s^D measurements of silanised D-mannitol for three fractional surface coverages obtained for alcohols and n-alkanes using peak maximum.

Fractional Surface Coverage (n/n$_m$)	Dispersive Surface Free Energy								Differences in γ_s^D (mJ/m^2)
	n-Alkanes				Alcohols				
	γ_s^D (mJ/m^2)	Slope error (%)	γ_s^D error (%)	γ_s^D error (mJ/m^2)	γ_s^D (mJ/m^2)	Slope error (%)	γ_s^D error (%)	γ_s^D error (mJ/m^2)	
0.05	34.7	0.96	1.92	0.67	36.3	2.35	4.70	1.70	1.6
0.1	34.7	0.81	1.62	0.56	39.7	0.03	0.06	0.02	5
0.2	35.1	0.82	1.64	0.58	40.4	1.15	2.30	0.93	5.3

γ_s^D uncertainties are twice the slope uncertainties, so typically they in the range of 2-4%. The data in Table 4. 7 suggests that for alcohols and alkanes at the two highest surface coverages the methods are comparable, and γ_s^D are within statistical uncertainties and experimental error for the COM peak analysis – see Figure 4. 16. The peak maximum data in Table 4. 8 the alcohol-based data are constantly higher than the alkane data- see Figure 4. 17. For the lower coverages, the methods appear to be different and this difference is likely due to surface heterogeneity. The hydrocarbons probes will not sense these heterogeneities whereas the retention of polar alcohol molecules will be more likely to be directly affected. So, when alcohols are used to determine γ_s^D it is recommended to select surfaces coverages of 0.2 or higher with the COM peak analysis approach. Figure 4. 15 and Figure 4. 17 present the corresponding γ_s^D profiles. It visualises the better match between the data at higher surface coverages with the alcohols giving slightly lower values overall, for both centre of mass and peak maximum measurements.
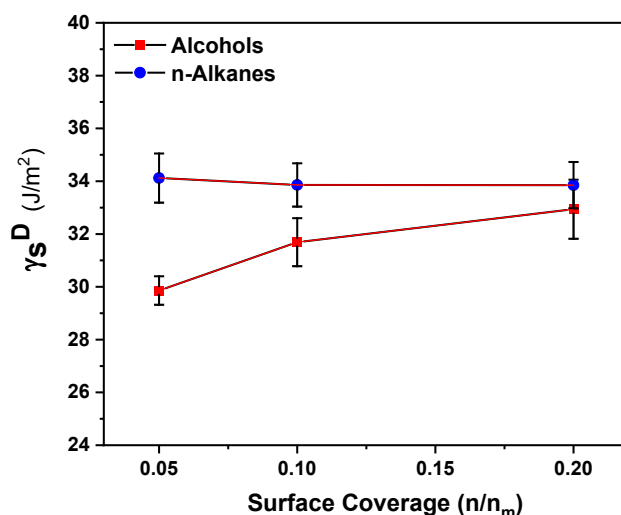
Figure 4. 16 Comparison of γ_s^D profiles for silanised D-mannitol obtained with n-alkanes versus alcohols using peak COM.
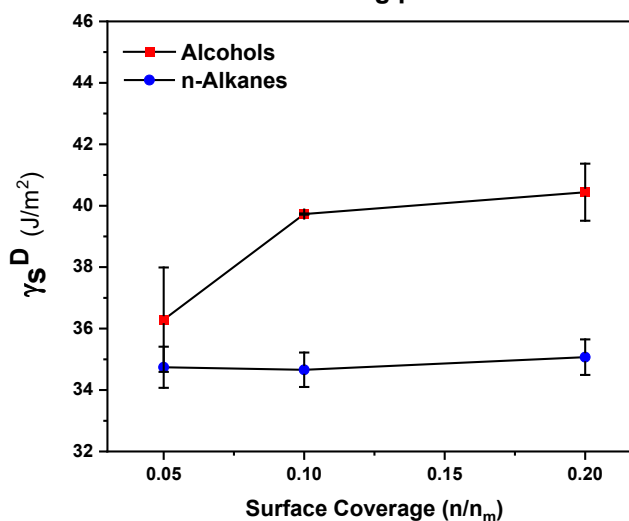
Figure 4. 17 Comparison of γ_s^D profiles for silanised D-mannitol obtained with n-alkanes versus alcohols using peak maximum.

4.3.3 Application of a new method for measuring γ_s^D values using alcohols for characterising nonwoven polymers

Once it was established that alcohols could be used for γ_s^D measurements, the method was tested with different polyolefins, which study using the standard IGC method with alkanes because these tend to absorb into the bulk of the polymer. MDPE, isotactic PP and various polyolefin base nonwovens were tested using a series of homologous alcohols, (ethanol,1-propanol and 1-butanol) at 20°C,10sccm flow rates and approximately ~1gram of polymeric material. The results are depicted in Table 4. 9. The dispersive component of the surface free energy measured using alcohols, varied between 20 and 40 mJ/m^2 for the different materials tested. These results are in line with what the literature documents for γ_s^D values for similar polyolefin-based materials so it was concluded that the new method of using alcohols is suitable for γ_s^D measurements.

Table 4. 9 γ_s^D measurements of different polymer for three different fractional surface coverages measured using alcohols and centre of mass. Results are $\mu \pm \sigma$, n = 3.

Fractional Surface Coverage (n/n_m)	Dispersive Surface Free Energy γ_s^D (mJ/m^2)				
	MDPE (powder)	PP isotactic (pellets)	Nonwoven (1.07% surfactant)	Nonwoven (0.75% surfactant)	Nonwoven (0% surfactant)
0.05	30.3 ±0.1	37.7 ±5.1	32.2 ±1.8	39.0 ±1.3	33.4 ±1.0
0.1	31.3 ±0.1	30.2 ±1.8	19.2 ±2.9	38.6 ±0.8	34.9 ±1.1
0.2	30.5 ±0.2	28.0 ±1.3	33.7 ±2.1	38.7 ±1.4	34.6 ±1.0

4.4 Surface chemical composition analysis using XPS

Surface chemical analysis using XPS was conducted to measure elemental composition of surfactant coated and uncoated nonwoven fibres and confirm differences in surface composition between samples. XPS was not a candidate for routine characterisation of these materials because it required high vacuum conditions which could remove the surfactant coating. The data collection was slow, and data analysis could be complicated therefore, not all the materials were analysed. A set of representative polypropylene based nonwoven fibres, coated and uncoated, were analysed.

XPS spectra for the polypropylene fibres coated PP-A and uncoated PP-B (included in Appendix A) were obtained. The expected carbon (1s) peak at 285 eV and oxygen (1s) peak at 531eV were observed, see Figure 4. 18. After surfactant treatment, the intensity of oxygen-related peak dramatically increased while the intensity of carbon related peak decreased. The

increased oxygen content ratio on the surfactant-coated surfaces, Table 4. 10, indicated the improvement of surface wettability as observed in wetting and IGC experiments. The surface carbon content (C1s) of the uncoated PP fabric was expected to be 100% due to the PP hydrocarbon structure. However, a low oxygen content (O1s) of 2.8% on the uncoated nonwoven was detected which could be due to finishing agents, surface contamination or surface oxidation of the fibres[389, 390]. Degradation/oxidation of polymers during fibre production might also result in the presence of oxygen on the surface[391, 392].

To gain a greater insight into the surface composition of nonwovens coated with surfactants, high-resolution spectra were acquired in the regions of C1s and O1s core levels. As shown in Figure 4. 18 (a), carbon is found at lower binding energy to the standard adventitious carbon (284.8 eV) which could arise from silicon oxycarbide Si-O-C type. Also, Figure 4. 18 (b) shows Si 2p found in its SiO-C (oxycarbide) form at 531.8 eV. Although the composition of the surfactant coating is not fully identified for proprietary reasons, it is known that it is a mixture of fatty acid quaternary ammonia compounds and cationically modified poly-dimethyl siloxanes which is in line with the results shown here.
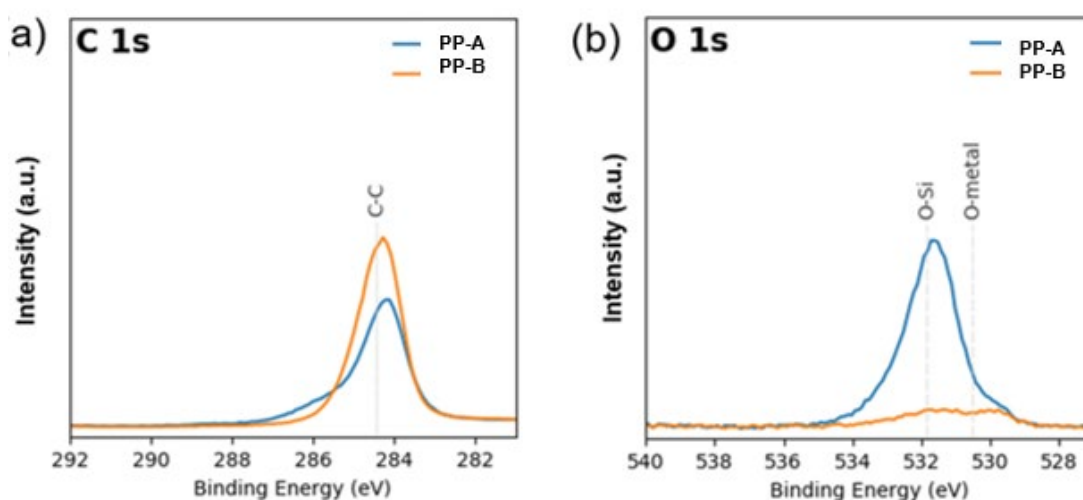
Figure 4. 18 XPS spectra of 3 months old polypropylene PP-A = coated and PP-B = uncoated nonwovens, (a) C1s (b) O1s

The peak fitting and knowledge concerning relative peak positions in the C1s and O1s signals were obtained from literature[393]. The C1s and O1s signal were deconvoluted into Gaussian peak components and by integrating these peaks the quantitative information was reported in Table 4. 10. One-year-old samples of surfactant coated, and uncoated PP based nonwoven fibres were also analysed using XPS to investigate the aging affect. The corresponding survey scan spectra can be found in Appendix A. These showed specific peaks present for the expected carbon (1s) peak at 285 eV for both samples and only a small oxygen (1s) peak at

531 eV, for the surfactant coated sample. These results indicated potential aging of the sample and loss of surface surfactants as a function of time. As with previous samples the carbon peak, shown in Figure 4. 19 is found at lower binding energy to the standard adventitious carbon (284.8 eV) suggesting presence of silicon oxycarbide Si-O-C type bonds. The Si 2p is found in its Si-O-C (oxycarbide) form at 531.8 eV. However, these peaks are present at trace levels and there isn't a noticeable chemical difference between the surface of coated and uncoated one year old nonwoven samples. Therefore, the aging of surfactant coated nonwovens was detectable by XPS.
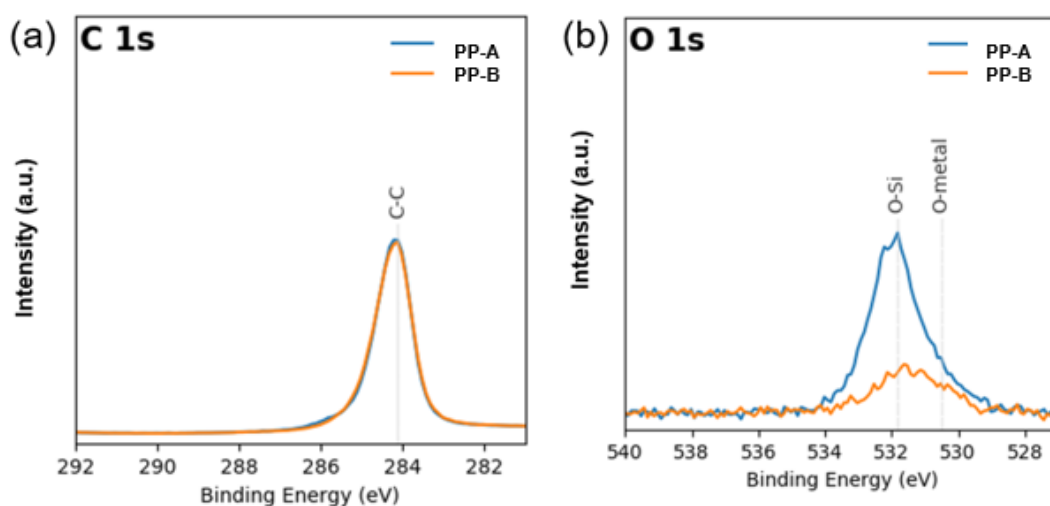
Figure 4. 19 XPS spectra of one year old polypropylene nonwovens, coated = PP-A and uncoated = PP-B (a) C1s (b) O1s.

The relative chemical composition determined by XPS of surfactant coated and uncoated nonwovens are reported as percentages in Table 4. 10. The results for both one year old nonwoven samples and the three-month-old samples are shown in Table 4. 10. The surfactant coated one-year older sample appears to have significantly less oxygen and nitrogen present at its surface than the three months old, coated sample. Again, the aging affect is confirmed and the result support the theory that surfactant surface concentrations are reduced as a function of time. Imaging with XPS is possible but this is a lengthy and expensive process, and it was not explored as part of this thesis.

Table 4. 10 Relative chemical composition determined by XPS for uncoated and surfactant coated PP based nonwovens, three months old.

% Atomic Abundance	Sample Type			
	3 months		1 year	
	Surfactant Coated	Uncoated Control	Surfactant Coated	Uncoated Control
Carbon	72.3 (4)	96.5 (1)	96.1 (3)	98.5 (2)
Oxygen	17.2 (6)	2.7 (8)	3.0 (6)	0.9 (3)
Nitrogen	1.5 (3)	—	0.3 (3)	0.3 (2)
Silicon	7.0 (3)	0.1 (1)	0.4 (8)	0.2 (3)
Iron	0.3 (0)	0.3 (1)	—	—
Zinc	0.0 (9)	0.1 (2)	—	—

Overall, the XPS analysis showed that surfactant treatment of polypropylene fibre surface results in a significant increase in atomic percentage of oxygen species which are responsible for the hydrophilic surface. The intensity of C binding energy levels decreased while oxygen-related binding energy levels increased and expanded for the surfactant coated samples. However, the results from the aged samples showed that the surfactant treatment is not permanent, and the surface concentrations are significantly reduced after one year, rendering the sample hydrophobic. Similar aging effects of hydrophilic nonwovens have been reported in the literature[394, 395].

4.5 Conclusions

This Chapter summarises the different data obtained from studies conducted for the surface characterisation of surfactant coated and uncoated polyolefin nonwoven fibres. Polyolefin based nonwovens have been successfully characterised using various techniques. Specific surface area of different polyolefin-based nonwovens was measured using the traditional N_2 BET method. As literature showed, and my results confirmed, the absolute precision of specific surface area measurements by N_2 BET is not higher than 5% and reproducibility is in the range of 1%[396]. Despite the relative accuracy and simplicity of the BET theory, the approach neglects lateral interactions between adsorbed molecules, minimised by working at low monolayer coverage, and it assumes all adsorption sites are energetically equivalent[397]. Therefore, the specific surface area of nonwovens was carried out using IGC as an improved alternative, the results from which demonstrated that polyolefin nonwovens feature generally low specific surface area in the range 0.1 - 4 m^2/g.

The surface wetting characteristics of polyolefinic fibres effect their processability into finished products. The contact angle measurements representing the wettability of the material under test were utilised to characterise different nonwoven fabrics. The results of this work

demonstrated homogeneous wettability for uncoated nonwovens, whilst surfactant coated nonwovens exhibited patch wise wetting heterogeneity. Surface wettability studies also showed that wettability reduced with sample aging due to potentially surfactant migrations from surface. Contact angle data was also used to calculate surface energy. However, the technique only uses droplets on localised areas and provided general information of the presence or absence of wetting heterogeneity.

Therefore, IGC was used as an alternative and more advanced technique for the characterisation of nonwoven fibres providing information on the surface energy of these materials. Its superiority stems from the fact that its compatible with samples which have porosity surface topographies and surface inhomogeneity, like these nonwoven fabrics. Such measurements can inform whether sample surface changes are associated with chemistry alterations or topographical alterations. IGC was used to determine the dispersive contribution of surface energy across the whole surface area of the sample. Normally alkane probes are used as the standard approach for measuring the dispersive surface energy using IGC. However, alkanes dissolved in the polyolefin nonwoven fibres, so a modified method was developed to determine the dispersive surface energy. Investigations using silanised D-mannitol showed that this novel method using alcohols as probe molecules, (instead of alkanes), can be applied to determine the dispersive contributions of different polyolefin materials including surfactant coated and uncoated nonwovens. The new approach is reliable, and it can easily be used to determine dispersive surface energy of similar polyolefin materials.

Finally, XPS analysis demonstrated the hydrocarbon nature of these materials and some of the polar elements present responsible for the hydrophilic nature when the nonwovens are coated with surfactants. XPS indicated that surfactants introduced a variety of oxidised functional groups onto the surface of the coated polymer. These oxidised functional groups mostly included C-O, and O-C=O, as described above by curve fitting of high-resolution C1s and O1s peaks and are responsible for the changes in the polymer surface properties.

5 Confocal Imaging of Nonwovens in 3D

5.1 Introduction

PP and PE based nonwovens are water repellent and hydrophobic surfaces due to the nonpolar nature of these polymers. However, many nonwoven products including PE and PP materials, most facilitate aqueous liquid transfer and require hydrophilic properties to function. Various surface modification methods can be applied to these nonwoven fabrics to convert them into a hydrophilic, material that wets and allows water to pass through selected materials layers. Nonwovens used in this study were coated with surfactants which is typically done commercially by passing the bonded nonwoven sheet over a roller wetted with the surfactant. The nonwoven sheet is then dried before use. It is a common industrial experience that the surface hydrophilicity of these coated materials is both spatially heterogeneous and time dependent, with significant losses in surface concentrations of surfactants being observed. For example, Lavoie et al[234] have reported on the migration of fluorochemical additives in PP nonwovens. It is therefore important to understand how the surfactants interact with the polymer, as well as their fugitive nature, if improvements in product performance of surfactant treated polymeric nonwovens are to be achieved. Most studies reported on surfactant-polymer interactions published have studied surfactant-polymer adsorption interactions in solution[8, 150, 151, 398]. Few studies have looked at surfactant-polymer interactions in solid state[153, 158] including specifically the migration of surfactants coated onto polymeric nonwovens where the hydrophobic interaction between the alkyl chain of the surfactant and the polyolefinic nonwovens are key.

The amount of surfactant needed to provide durable and fast wetting may vary depending on the surfactant type, type of polymer base and how the surfactant is coated[153]. To understand the surfactant-polymer interactions in a multicomponent solid system, an analytical technique is required that provides two types of information about the surfactants: the 3D spatial distribution of surfactants throughout the polymer fiber network as well as surfactants distributions within the fibers. Table 5. 1 summarises current analytical methods for 2D and 3D imaging of porous networks. The only techniques that can provide true 3D images are x-ray tomography, confocal Raman microscopy, RCM and confocal laser scanning microscopy, CLSM. However, the poor x-ray contrast between polymers and surfactants means that the mapping of surfactant distributions in 3D polymer fiber networks is not routinely feasible using x-ray tomography. Raman spectroscopy is commonly used to characterise chemical composition of various materials[399], including fibers[400] and when combined with a confocal microscope, it can simultaneously map both spectral and spatial features of inhomogeneous

structures. However, mapping on microscopic scale with RCM is challenging due to the resolution of the scanning system being diffraction limited (about 0.2–0.5 micron, depending on the excitation wavelength)[401].

Table 5. 1 Analytical methods for chemical species determinations in 3D material networks.

Method	Spatial Performance			Chemical Species Determinations		
	X-Y-Z Resolution	Z Depth of Field	Imaging	Species Quantification	3D Species Distribution	Comments
SEM [402]	0.01µm	10 mm	2D	No	No	Needs vacuum; conductive sample coating, non-quantitative evidence, can identify elemental species using EDX
FTIR[403]	1µm	2µm	2D	Yes +/-0.1%	No	Needs IR absorbing species; can depth profile a few µm
TOF-SIMS[404]	1 µm	0.01 µm	2D	Yes +/-0.1%	No	Needs vacuum, can image surface in 2D, chemical structural information
X-Ray Tomography[405]	1 µm	10 mm	2D 3D	Maybe	Maybe	Poor x-ray contrast between organic polymers and surfactants
Confocal Raman Microscopy[406]	0.2µm	<1µm	2D 3D	Yes, +/-0.1%	Full 3D image	Requires libraries for chemical composition information and spectra which are sufficiently different which might not be the case when carbon-based surfactant mixtures are applied, e.g., cationic surfactants. CRM also features slow acquisition speed.
Confocal Laser Scanning Microscopy[407]	0.1 µm	1 mm	2D 3D	Yes, +/-0.1%	Full 3D image	The sample must fluoresce, or a fluorescent dye must be used

To differentiate between surfactant coated and noncoated nonwovens from an elemental analysis point of view surface chemical analysis techniques such as XPS[223, 408] and TOF-SIMS[234] can be used. However, these types of techniques are limited in that they cannot provide 3D information of the 3D nonwoven fibre network and can provide 2D images in some applications. It is important to be able to distinguish changes associated not only with chemistry, but also topographical alterations due to coating processes. Several modern imaging techniques such as confocal microscopy[292, 409], AFM[226, 229, 231], SEM[410, 411] and optical profilometry[288, 412] can also be utilised to image nonwoven fibres. Many of these techniques, although extremely powerful in nature, require vacuum conditions and a great deal of sample

preparation is necessary to enable analysis under high vacuum. Others, such as profilometry lack the resolution and sensitivity required to image very small features such as surfactant coatings of low loadings on nonwoven fibres.

Non-destructive 3D profiling of nonwovens is possible with CLSM[294]. Choong et al.[292] used CLSM for the quantitative characterisation of both the morphology and the pore space topology of electrospun nonwoven fiber mats. CLSM was also used successfully by Charcosset et al.[293] to characterise microfiltration membranes and reconstruct 3D images which delineated the morphology of the microporous membranes. CLSM was used to study the surface morphology of polymer blends as a function of blend preparation conditions by Li et al.[294]. Overall, several studies[295, 296] have demonstrated the suitability of CLSM for 3D structural analysis of fiber-based materials. Recently, Lin et al.[297] used CLSM for high-resolution 3D imaging of electrospun fibers fouled by oil. CLSM is reported here for the first time to image the 3D surfactant distributions on polymeric nonwovens.

For CLSM optical contrast is achieved by labelling a critical component with a fluorescent molecule[294] unless the substrate is auto-fluorescent. This species can be a dye, or a fluorescent protein[413] or antibody[414] which binds to the target via a specific chemical reaction or via a non-specific mechanism. A wide range of chemical[415] and physical[416] fluorophores with distinctive spectral characteristics are available and the most common fluorescence labelling method is solution-based staining. Solution methods are incompatible for investigating materials containing surfactants as the solvent would dissolve/displace the surfactants, rendering such methods ineffective. Here an alternative method for introducing a fluorescent dye for nonwoven samples containing surfactants is demonstrated. The method is simple and involves vaporisation, sublimation, of a suitable fluorescent dye at elevated temperatures in the presence of the nonwoven fiber samples, allowing the dye to dissolve into the hydrophilic surfactant layers. Such a dry gas phase approach avoids the problems associated with wet coating methods. This Chapter demonstrates the visualisation and quantification of surfactants coated into nonwoven fibers, including a non-invasive, optical 3D mapping protocol for quantifying surfactant distributions using CLSM.

CLSM was employed in the current study for imaging 3D nonwoven materials because the technique required minimal sample preparation and it could be operated at ambient surroundings, thus allowing samples in their native form to be studied. Therefore, the 3D structure of the nonwoven materials, as well as the surfactant coating, could be visualised under industrially relevant environmental conditions, and the potential effects of invasive sample preparation effecting sample integrity and structure were minimised. CLSM was used to image "thick" (~1mm) nonwovens samples without physical sectioning by collecting serial

optical sections. Each z section thickness was 4 μm and total layer z thickness of 300 μm was used which allowed reconstruction of 3D images[306]. Other advantages of CLSM are linked to its ability to control depth of field[317] and capability to eliminate/reduce background interference, allowing production of high resolution images. Among its many advantages this technique also has some short comings. Confocal imaging requires a compromise between resolution, scan time, and potential photo-destruction of the sample. The higher the resolution, the more time required for the scan, and the longer the fluorophore is exposed to the excitation laser. Sometimes, enhancing resolution does not result in an increase in useful information about the sample[310]. Photobleaching is perhaps the most significant practical problem with confocal microscopy, although fortunately this issue did not affected results of this study, as evidenced by data to follow.

One of the objectives of this thesis was to confirm, quantify and visualise surfactant distributions onto the surface of the nonwoven fabrics like those used to manufacture disposable nappies. To achieve this objective a novel method for visualising in 3D and quantifying surfactant distributions on polymeric nonwoven fibers using CLSM and BR14 dye was developed. The fluorescence properties of water soluble Basic Red 14 (BR14) were exploited for staining surfactants preferentially to the polymeric base nonwoven fabric, on which they were coated. Polymeric base nonwoven fibers of different types coated with different surfactants which were quantitively characterised using this approach. This Chapter presents and discusses the method, the results and the observations of these studies conducted with CLSM for imaging in 3D surfactant distributions onto polymeric based nonwoven fibers in a non-invasive way. The possibility of associating fluorescence microscopy and dye staining for the identification of surfactant coatings on nonwoven fabric using CLSM has been reported with excellent results for the first time here.

5.2   Basic Red 14 Dye Characterisation

BR14 dye is not commonly used for CLSM. Its main analytical use is fingerprint development for forensic purposes[417] where aqueous BR14 fluorescent staining solutions has been applied to of crime scene environments to improve the contrast for development of weak finger-marks. BR14 is not a well characterised dye and there is limited information about it in the literature. Figure 5. 1 shows the chemical structure of the BR14 dye with its highly conjugated multiple π bonding system, which are responsible for its colour, and the ammonium chloride group which is responsible for its polarity and water solubility. The high-water solubility of this dye was the major factor for its selection. The hypothesis was that this polar dye would interact preferentially with the polar surfactant phases, and not with the hydrophobic polymer base

material. Figure 5. 1 shows the measured emission spectrum for BR14 which allowed establishment of optimum optical conditions for fluorescence detection with CLSM; the fluorescence filter region was 540-690nm and laser excitation at 530nm.
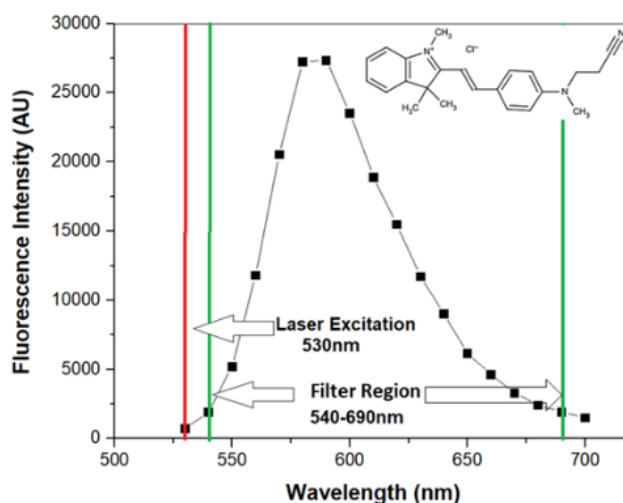
Figure 5. 1 BR14: Chemical structure and fluorescence emission spectrum.

A simple solubility test was conducted using 1mg aliquots of BR14 dye and 1mL of the solvents heptane, decane, pentanol, methanol, water and the two neat surfactants. After each aliquot of BR14 was added to each solvent, the mixture was shaken, and an observation made as to whether the dye had dissolved or precipitated. If dissolved, the procedure continued until the solubility limit was reached. The final vials are shown in Figure 5. 2. In heptane and decane the dye did not dissolve at all, whereas in all other polar liquids the dye was well dissolved. This supports our hypothesis that the dye is solubilising inside the polar surfactant phase and not the hydrocarbon-based polymeric nonwoven fibres.

Solvent	Solubility
Water	0.35 g/mL
Methanol	0.40 g/mL
Pentanol	0.20 g/mL
Heptane	0 g/mL
Decane	0 g/mL
Silastol PHP-26*	0.20 g/mL
Stantex S6327	0.15 g/mL
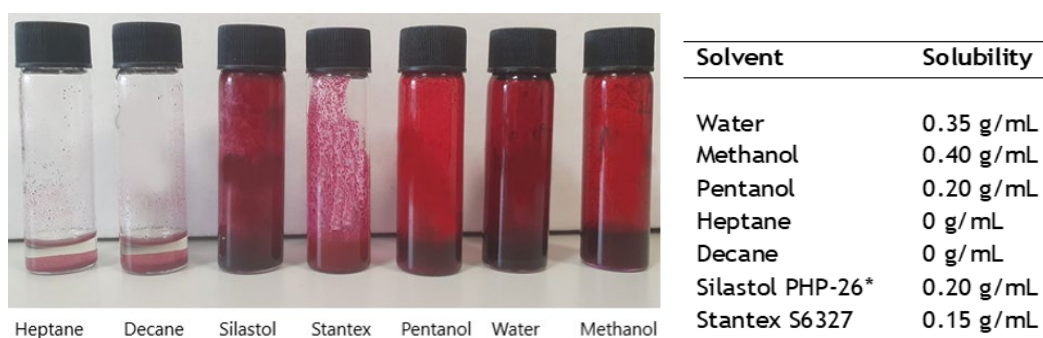
Figure 5. 2 BR14 solubility in a series of solvents and surfactants at 25°C.

A TA Q2000 differential scanning colorimetry was used to measure the melting point of BR14. Figure 5. 3 (left) shows DSC data including four thermal events, two minor events at 60 and 85°C, a major event 145-150°C followed by a melting point at 188°C. The DSC data is consistent with Dynamic Vapor Sorption data which confirms that BR14 is a crystalline hydrate

at room temperature, and that the DSC events at 60 and 85°C are dehydration events. The dye is stable up to 188 °C and can be vaporised for contact with any material which has hydrophilic properties which will allow the dye molecules to dissolve. The vapor pressure for BR14 was measured using a Knudsen effusion method under high vacuum between 45° to 65 °C. This data is shown in Figure 5. 3 (right). The vapor pressure at 100 °C was estimated to be 3.3 Pa based on extrapolation of the data shown in Figure 5. 3 using 17.3mg of BR14.
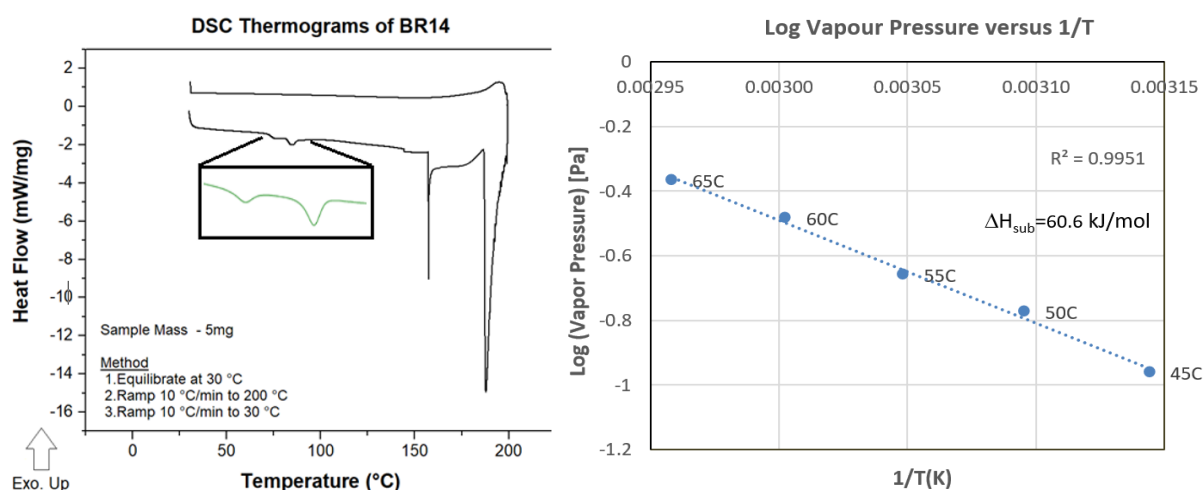
Figure 5. 3 Thermal properties of BR14: (left) DSC trace for 30° - 200 °C and (right) Log (vapor pressure) versus 1/T for 45° - 65 °.

Also, the photostability/photobleaching of BR14 powder was studied as a function of time, 6 min, and laser power;10-100%. Figure 5. 4 shows the mean fluorescence intensity over time for lapsed image stacks measured on a silicon oxide wafer coated with a surfactant which was treated with BR14 via the new sublimation staining method. The data represents intensity measured on the sample, at different locations when irradiated with different laser powers over a period of 6 minutes.

User-defined thresholding is considered the gold standard method for segmenting fluorescence microscopy images[406]. However, manual thresholding is subjective and is prone to inter- and intra-operator variability[418].The inset shows the evaluation of different fluorescence intensity thresholding levels applied when using data collected with the standard experimental condition of 20% laser power. These results demonstrate that BR14 dye is very stable and photobleaching is not of concern and will thus enable the visualisation and quantification of surfactant. A fluorescence intensity thresholding sensitivity test was also conducted. Otsu's thresholding method was compared against a series of manual thresholding using specific values, (10, 50, 100, 101, and 150), see Figure 5. 4 inset. These results demonstrated that the fluorescence intensity observed is relatively independent of thresholding

values chosen, being +/-20 AU, which is within experimental error. Therefore, confirming that the Otsu method is a suitable approach to use for thresholding for the experimental conditions when using 20% laser power.
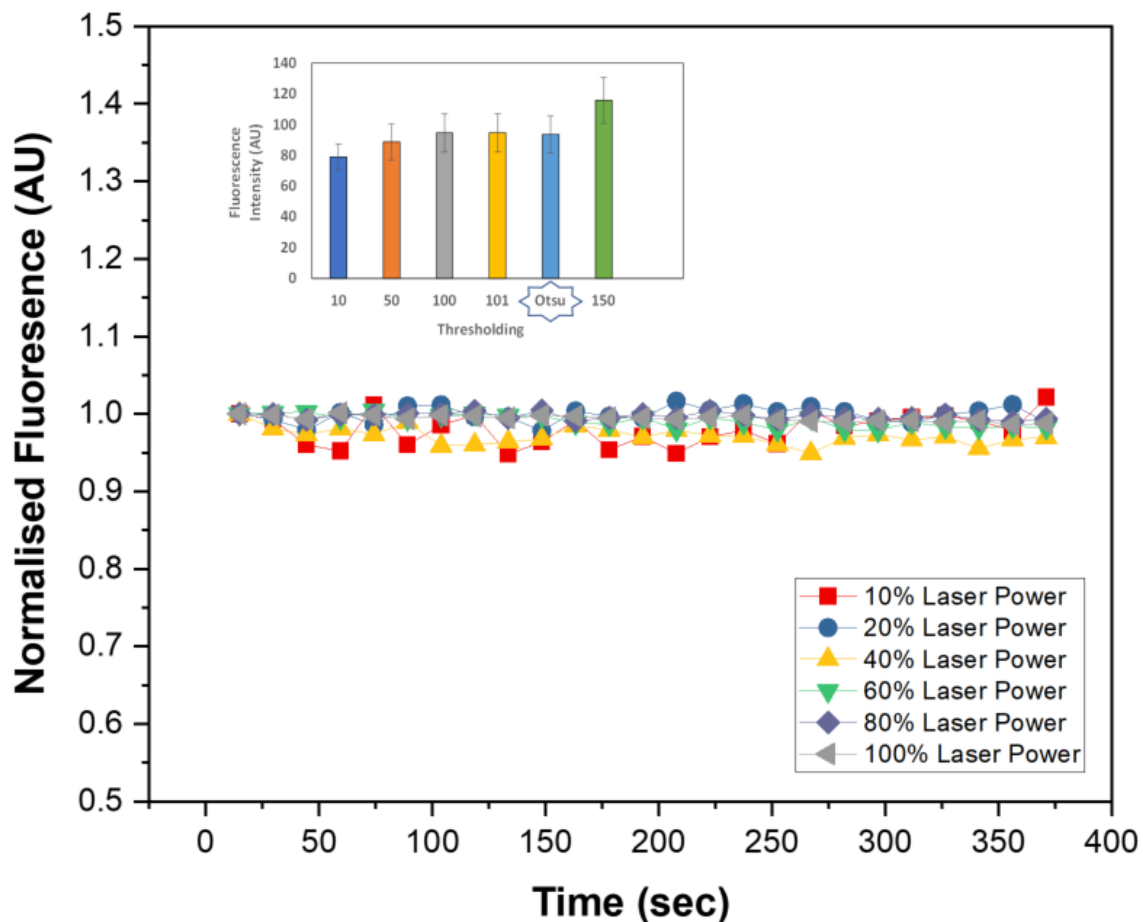
Figure 5. 4 Plot of fluorescence intensity of BR14 dye as a function of time for a range of laser powers demonstrating photostability of BR14. The inset shows evaluation of fluorescence intensity thresholding criteria at different thresholding levels. Each bar on the inset figure corresponds to 3D volume averages $\mu \pm \sigma$, for n = 6

5.3   Method Development

5.3.1   Proof of concept

The qualitative wettability characteristics of nonwovens is obvious if two samples, one surfactant treated and another untreated, are placed into an aqueous solution, as shown in Figure 5. 5. The untreated, hydrophobic sample, floats on top of the solution whereas the treated, hydrophilic, sample immerses into the solution. This phenomenon is easy to see here but difficult to measure quantitatively. In addition, the nondurable, or fugitive, nature of synthetic surfactants coated on polymeric nonwoven fibers is one important topic to be investigated. The amount of surfactant needed to provide durable, sufficiently fast wetting varies depending on the surfactant type, the type of polymer base and how the surfactant is coated.[153] Like most real surfaces, polymeric nonwovens are heterogeneous in nature, highly porous due to the large void zones present, with a complicated non-flat surface structure that varies in different locations along and across the sample. Such variations are of a recurring nature and are very manufacturing process dependent.[3] Therefore, it is essential and advisable to sample different regions of the fabric when making any kind of measurements on these types of materials.
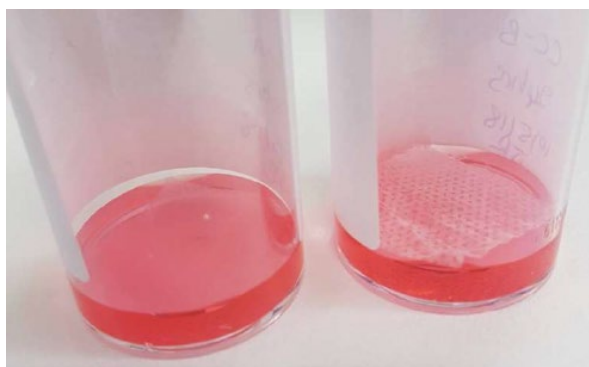
Figure 5. 5 Wetting of nonwoven fibres dipped into aqueous Basic Red 14 solution, (left) surfactant treated sample and (right) surfactant free sample.

To visualise the distributions of surfactants coated onto the nonwoven samples a fluorescent dye labeling method was developed. In fluorescence microscopy techniques, fluorescent labelling and staining methods involve in general preparation of a working solution by dissolving the fluorescent dye into a solvent. Two different fluorescent dyes, Basic Yellow 40 (BY40) which fluoresces under blue light and BR14 which fluoresces under green light, were initially investigated. The dyes were purchased from BVDA and were chosen because they were water soluble and would specifically stain the surfactants preferentially to the nonwoven polymer. Preliminary experiments involved dipping small pieces of the nonwoven fabric, 5cm x 5cm, into the dye solution for a set amount of time, followed by immediate CLSM analysis after removal from the dye solution. Initial data suggested that confocal microscopy was useful in visualising the surfactants on the fibre as shown

in Figure 5. 6 and Figure 5. 7. The yellow-colored sections shown in Figure 5. 6, (left) represent the fluorescent parts of the sample which have been dyed with BY40. It is suggested that these colored locations represent the surfactants because the dye targets hydrophilic areas within the sample. The image on the right shown in Figure 5. 6 corresponds to the untreated, (hydrophobic) nonwoven sample which has also been dyed with BY40, prepared in the same way. As shown, for the control sample there was no fluorescence detected and this implied that there was a lack of surfactants present for the dye to interact with. Similar results were observed with the nonwoven samples dyed with BR14, as shown in Figure 5. 7. The red-colored regions correspond to the fluorescent dyed surfactant regions. Again, such features are missing from the untreated, (hydrophobic) nonwoven sample which underwent the same dyeing process as the treated sample on the right.
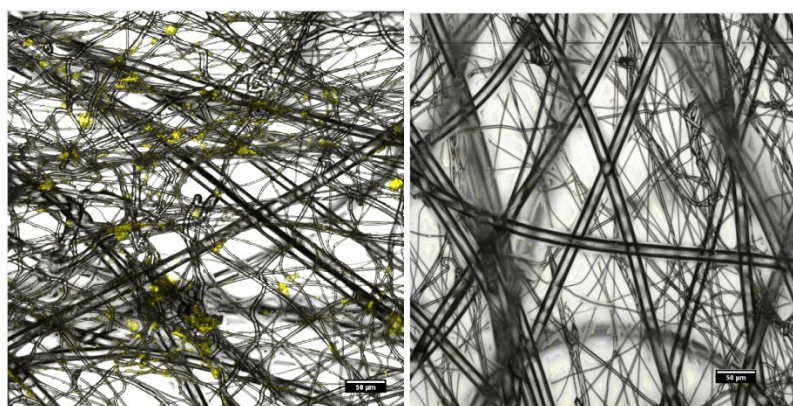
Figure 5. 6 Images taken using a confocal microscope of a treated (left) and untreated (right), core cover sheets of a nonwoven polymer, 2 months old, dyed for 24hr in BY40 aqueous solution.
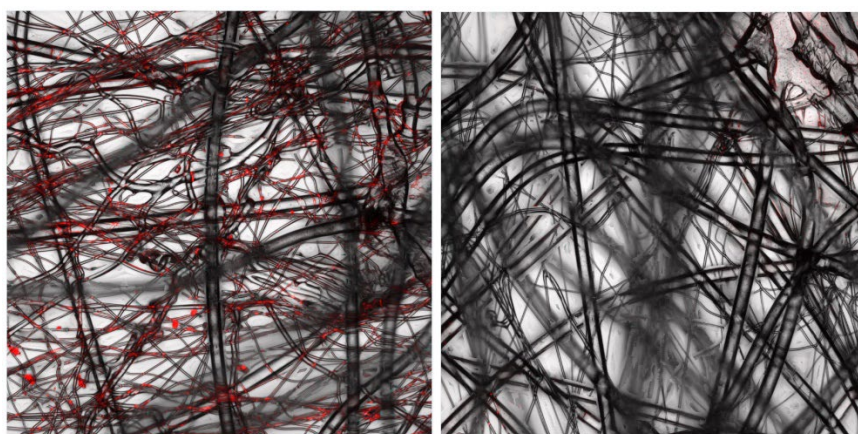
Figure 5. 7 Images taken using a confocal microscope of a treated (left) and untreated (right), core cover sheets of a nonwoven polymer, 2 months old, dyed for 24hr in BR14 aqueous solution.

Regardless of the type of solvent used, this wet method of dyeing the samples, although it works, is incompatible with surfactant containing samples. It is very likely that the solvent would interact and dissolve the surfactants due to their amphiphilic nature, thus fundamentally

perturbing the native surfactant distribution. Thus, the data might not represent the native surfactant distribution. Therefore, an alternative approach of dry dyeing was considered. Only BR14 dye was used hereafter because of its superior vaporisation characteristics in comparison to BY40 dye. The dry dye vapour experiments involved small nonwoven fabric cuts, 8cm x 5cm, placed on top of a small laboratory metallic pan which was holding ~ 50mg of BR14 powder. The pan was contained within a glass petri dish closed with a lid as shown in Figure 5. 8. The petri dish was then placed into a laboratory oven at 100°C and left overnight, CLSM was then used to analyse the sample.
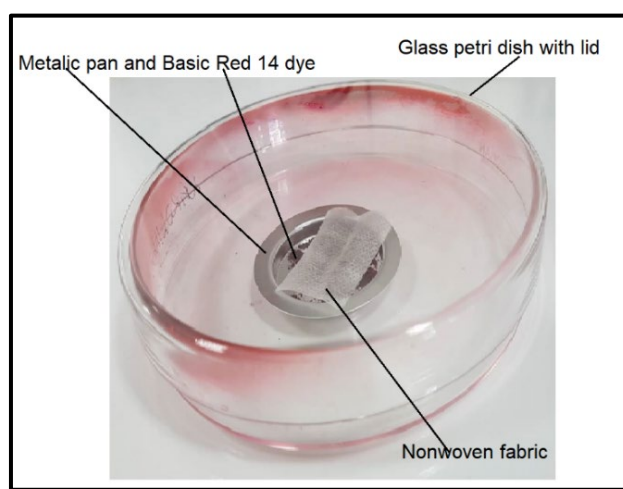
Figure 5. 8 Dye vaporisation experiment set-up.

Preliminary results from the dry state experiment showed that the dye had stained some of the fibres, presented as red coloured fibres in Figure 5. 9, (left). Image on the left represents a surfactant treated sample. The image on the right shown in Figure 5. 9 corresponds to the surfactant free, (hydrophobic) nonwoven sample which has also been dyed with BR14, and there was negligible fluorescence detected for this control sample. This experiment demonstrated that the dye introduced by vapourisation has specificity for the regions surfactant coated in the nonwovens, preferentially to the non-coated regions in the nonwovens.
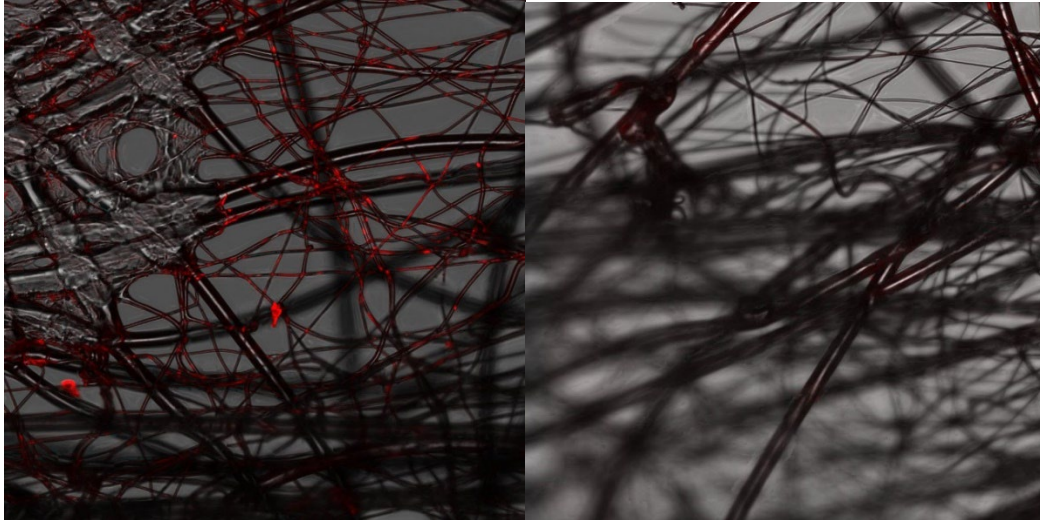
Figure 5. 9 Images taken using a confocal microscope of a treated (left) and untreated (right), core cover sheets of a nonwoven polymer, 2 months old, dyed for 1 week through vaporisation of BR14 powder.

The hypothesis was that the water-soluble dye after it vaporises, it dissolves selectively in hydrophilic regions preferentially to hydrophobic areas of the nonwoven because it has a higher solubility for surfactant treated regions. It is also suspected at elevated temperatures the solid components, the surfactants, start to change their phase from solid to fluid like and thus are more accessible to the dye. Therefore, BR14 preferentially partitions into the surfactant rich areas of the sample. So, fluorescence is associated with the regions rich with surfactants. Figure 5. 10 describes the sample preparation process via dye vaporisation at high temperatures both for a surfactant treated sample and a control, surfactant free nonwoven sample.
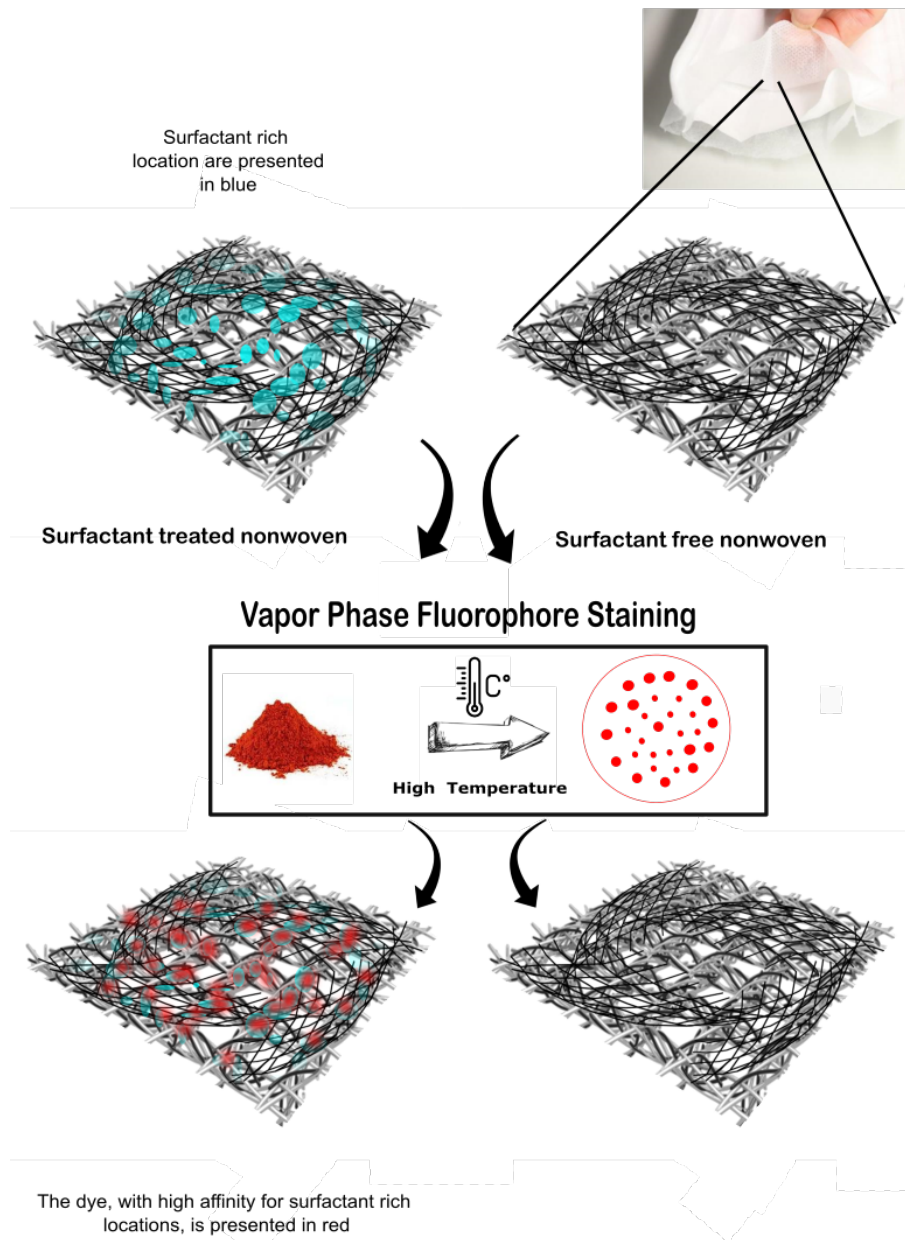
Figure 5. 10 Schematic of the sample preparation process via dye vaporisation at high temperatures, (100°C).

An experiment was conducted to quantify the effect and compare the two different sample preparation approaches: solution versus vapour phase dyeing. Three different nonwoven samples were used, a surfactant free nonwoven (the blank), a nonwoven coated with 0.4% and another coated with 0.8% (v/w) surfactant. Each nonwoven type was confocally analysed on 4 different locations (n=6). Also, for the wet method, two different solution concentrations, 0.01% and 0.001% w/v BR14 of the dye, were tested. The wet samples were prepared via a simple solution-immersion method, for two different time intervals, a) dipping the nonwoven sample in and out of the solution

and b) dipping the sample into the solution for 5 minutes. Figure 5. 11 shows the results of this experiment.
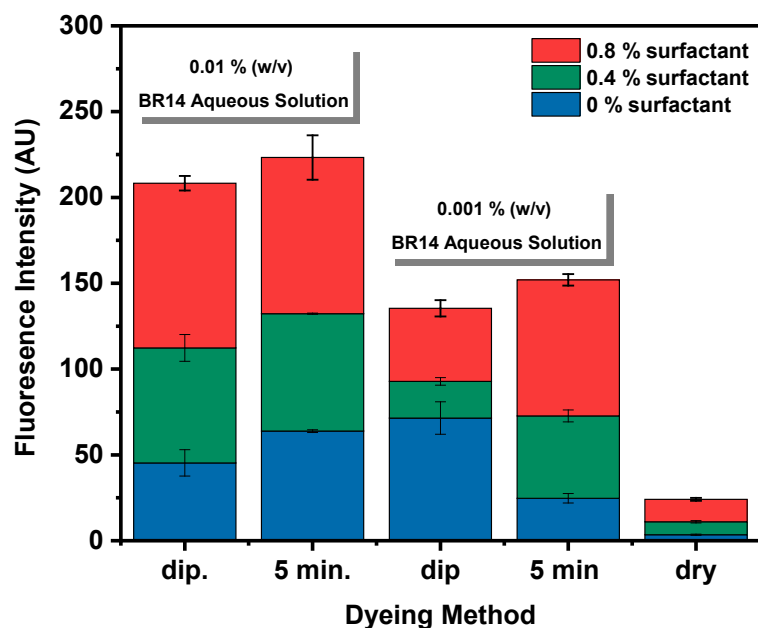
Figure 5. 11 Fluorescence intensity for a series of fabrics with different surfactant loadings stained using a liquid versus a gas phase BR14 staining methods. Results are μ ± σ, n = 6.

The data revealed that the standard dry method of using an oven set at 100°C, (the green bars), produces more specific and precise results than the wet immersion methods, (blue and red bars). The wet dipping methods gave stronger fluorescence intensities, but with high variabilities, for both concentrations of BR14. The 5-minute dipping gave much more reliable data with strong fluorescence intensities, but there were strong intensities even for blank fabrics, for both BR14 concentrations. In addition, liquid based staining can dissolve the surfactant and it could coat other areas of the nonwoven which in the end will lead to a wrong surfactant distribution of the surfactant. Vapour phase dye coating allows the specific staining of surfactant phase at the position where the surfactant is located on the fibre surface. The high blank signal observed for the wet staining method is potentially due to the rearrangement of the surfactant and the interaction of the dye with the liquid. The surfactants could transfer into the water phase and this could be facilitating re-wetting of the hydrophobic nonwoven by the hydrophilic dye solution. The dye vaporisation/sublimation method was therefore selected preferentially because it was effective, simple, and involved introduction of the fluorescent dye under gas phase conditions without any of the drawbacks of the solution-based methods. Vaporisation/sublimation of the dye allowed specific staining of the surfactant phase at the

position where the surfactants were located within the fiber without reducing the amount of surfactants.

5.3.2   Development of CLSM test Protocol

BR14 dye was used for preparing all subsequent fluorescence samples suitable for CLSM analysis. A customised sample preparation unit shown in Figure 5. 12 was fabricated. It consists of an upper fabric sample holder and lower element which contains the powdered dye. The nonwoven fabric sample was mounted between a microscope slide, and the bespoke brass sample holder containing a series of 2.5mm diameter holes forming a 7 x 7 grid, 20 x 20 mm in size. This sample holder was designed for two purposes, a) to fix the fabric sample in place and keep it flat to ease focusing with the microscope on sample surface for analysis and b) to facilitate repeated analysis of the same sample location with confidence for both aging studies and quantification analysis.

For the experiment ~100mg of BR14 powder was loaded into the lower section of the preparation unit and spread-out into a uniform powder layer. The fabric sample, which was fixed the top to holder, was placed on top of the lower section of the holder containing the powder. The distance between the powder and the nonwoven sample was ~ 5mm. The whole unit was then placed in a covered glass petri dish and then placed in an oven. For high temperature treatment of the nonwoven samples with the BR14 dye a Memmert UN30 Universal oven was used. After removal from the oven, the sample was then analysed using CLSM. The idea being that the water-soluble dye, at elevated temperatures, has a high enough vapor pressure to transfer via the gas phase and dissolve in the surfactant domains. The vapor phase fluorophore dissolves selectively in hydrophilic regions

preferentially to hydrophobic areas of the nonwoven because it has higher solubility for the polar surfactant materials.
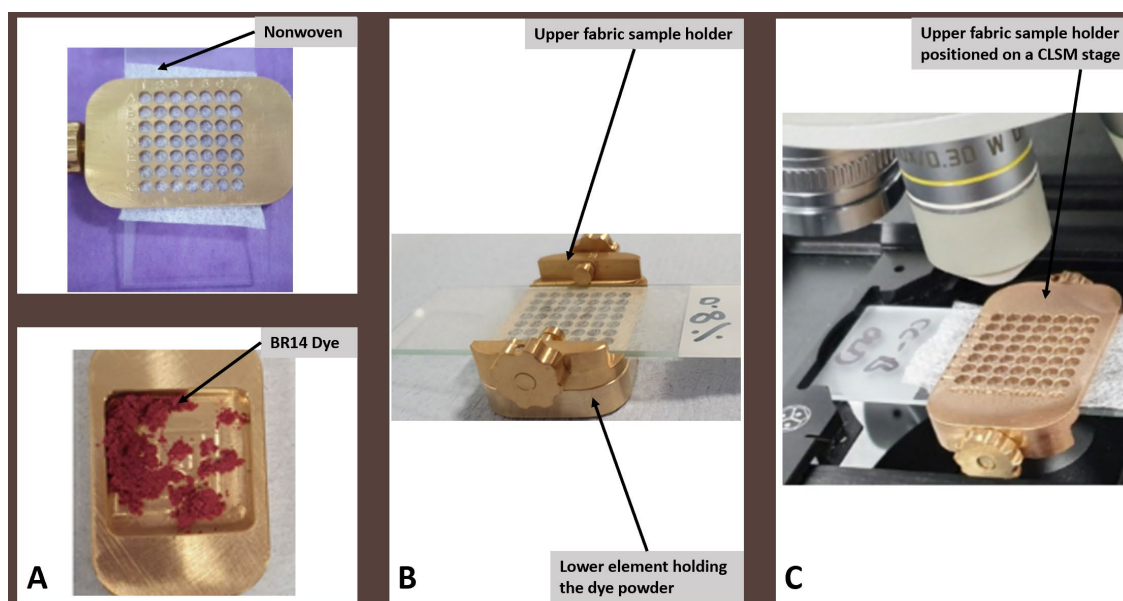
Figure 5. 12 Customised sample preparation unit which consists of A) the upper fabric sample holder and the lower element which contains the dye powder. The unit parts are assembled as shown in B) and the fabric sample holder fits in the CLSM stage as shown in C).

Different heating conditions were evaluated to establish optimum sublimation conditions for the BR14 dye. Four pairs of samples, each comprising of a surfactant treated and a surfactant free nonwoven were tested under different conditions; a) heated at 100°C for 1 hour, b) 5 hours, c) 24 hours, and d) 3 days. The results are shown in Figure 5. 13.
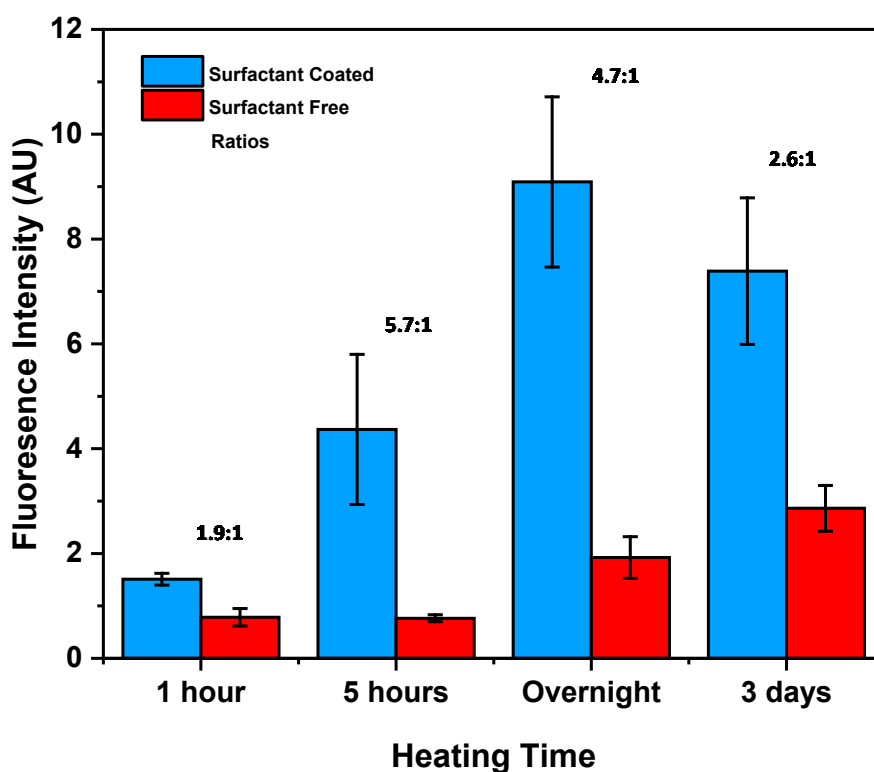
Figure 5. 13 Optimization of BR14 sublimation conditions. Each bar corresponds to 3D volume averages $\mu \pm \sigma$, for n = 3. Included in the graph are also the ratios of surfactant coated/surfactant free for each staining condition.

The results shown in Figure 5. 13 show that heating the samples for 24 hours at 100°C with the dye produced the highest fluorescence intensity for the surfactant treated sample with an acceptably low background fluorescence displayed by the surfactant free sample. However, the highest signal to noise ratio is exhibited by the 5 hours experiment, with the specific dye-surfactant interaction increased after 5 hours. The presence of fluorophores on the surfactant free surfaces is probably due to direct precipitation of BR14 on the fabric surface, rather than the vapour phase partitioning of the BR14 into the hydrophilic surfactant domains on the fabric surface. Therefore, the 5-hour method was selected as it produced the highest signal to noise ratio. Figure 5. 13 also demonstrate degradation of the dye after 24 hours and an increase on non-specific dye interaction, unwanted background fluorescence.

However, it is not always desirable to heat such samples at such high temperatures for the risk of sample damage. Therefore, an alternative heating method using a hot plate was evaluated as a potentially less destructive alternative. The dye was in direct contact with the heat source for this experimental setup, whereas the sample was held at ~ 1cm high from the heat source, reducing thus significantly the temperature the sample is exposed to. Figure 5. 14 shows the results from the evaluation of the effectiveness of using a standard laboratory hot plate for

vaporisation of the dye. The standard oven method, 100°C overnight was compared with results obtained for different heating conditions using a hot plate. Two nonwoven samples, a surfactant free nonwoven, (the blank) and a nonwoven coated with 0.8% (v/w) surfactant, were compared for the different experimental conditions, (1 hour at 80°C, 1 hour at 100°C, overnight at 60°C, 80°C, 100°C and 150°C) and the standard oven method at 100°C overnight.
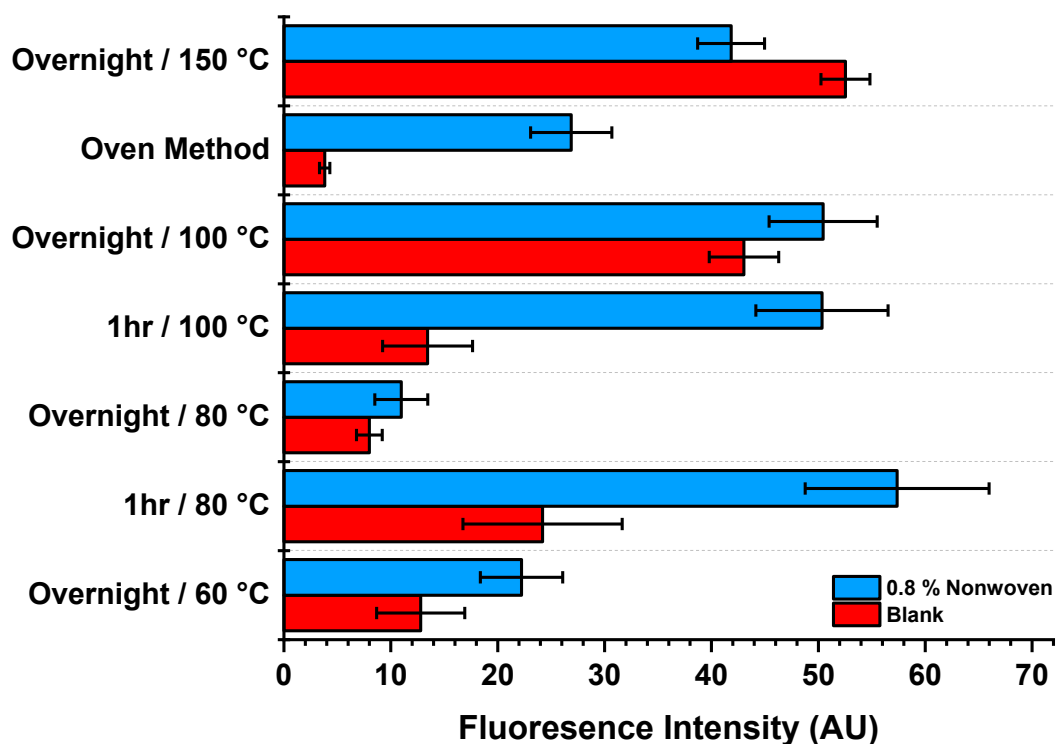
Figure 5. 14 Hot plate test data versus the standard heating in the oven method.

The results show that the hot plate method could be used as an alternative method for dye vaporisation. For example, the 1-hour experiment set at 100°C produces comparable data with the standard oven method. However, the general use laboratory hot plates have relatively poor temperature control mechanism and cannot be always relied upon for an efficient vaporisation process. Based on these results it appears that there are two mechanisms by which the dye reaches the surfactants, a) the dye dissolves into the surfactant at high temperatures through vapour phase dissolution and b) coating by deposition of the whole sample, which needs to be kept to a minimum.

As part of quantification validation studies several samples were initially prepared in the laboratory using surfactant free nonwoven materials and neat Silastol PHP 26 surfactant solution. The neat surfactant solution was diluted with deionised water to make solutions of lower concentrations. A fresh nonwoven sample weighing 6 mg was dipped in each of the surfactant solution for 1 minute and then removed and left to air dry overnight. The samples were then analysed using CLSM. All the samples were then treated with BR14 dye and re-analysed using CLSM. The data in Figure 5. 15 shows % area of fluorescence above threshold measured in a 3D volume. Fluorescence increases as a function of surfactant concentration because the amount of fluorescence is proportional to how much dye dissolves into the surfactants. The results demonstrate the suitability of the method for visualisation and quantification of surfactants coated on nonwovens and proves the concept that we can associate fluorescence with presence of surfactants.
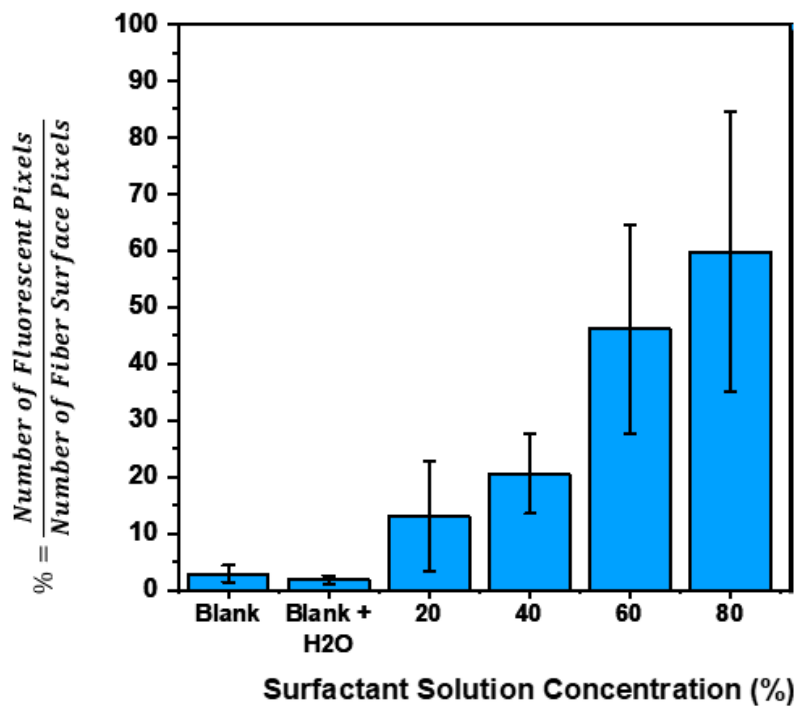
Figure 5. 15 % area of fluorescence above threshold of surfactant, (Silastol PHP 26) treated polymeric nonwoven as a function of concentration, for fluorophore treated fabrics. Results are expressed as $\mu \pm \sigma$.

Industrial samples of polypropylene nonwoven fibers coated with surfactants and surfactant free nonwovens were used to evaluated using this method. Figure 5. 16 demonstrates that the

146

fluorophore BR14 dissolves selectively in the hydrophilic surfactant Silastol PHP 26 regions of the nonwoven compared to the uncoated regions.
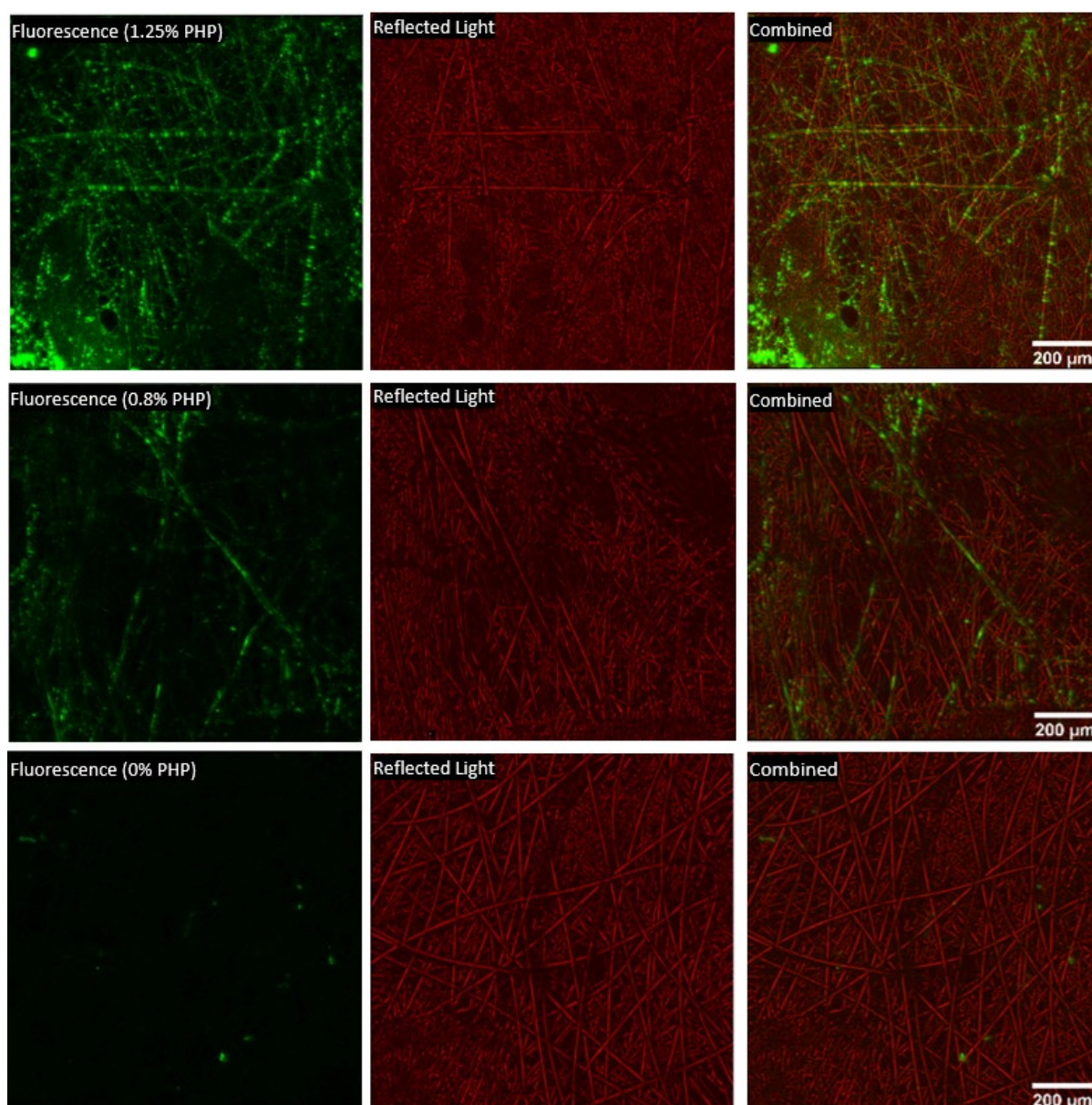
Figure 5. 16 Fluorescence images of surfactant coated, 1.25% (top) and 0.8% (middle) polypropylene based nonwovens and uncoated (bottom) nonwoven treated with BR14. Each sample has been imaged in two channels, fluorescence, and reflected light. An image representing a combination of both channels is also shown.

The interaction of BR14 with polymers such as polypropylene, polyethylene, and polycarbonate was also studied, to help understand the mechanism of the dyeing process. The results confirm that BR14 works by interacting with the surfactant phase and not the polymeric base surfaces. Figure 5. 17 shows typical images which demonstrated that the vapor phase fluorophore dissolved selectively in hydrophilic regions due to the presence of surfactants preferentially to hydrophobic polymeric base

surfaces. The dye did not deposit on the material regardless of whether it was polypropylene, polycarbonate or polyethylene unless there were surfactants present.
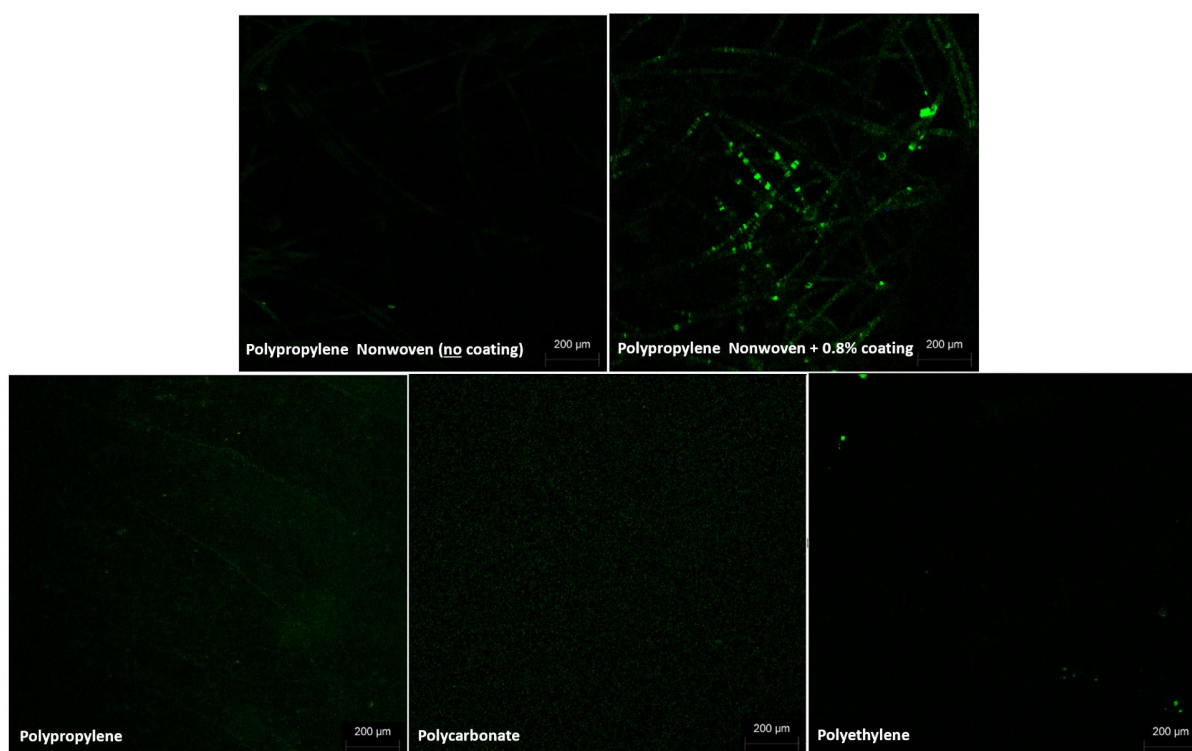
Figure 5. 17 Fluorescence images of uncoated and surfactant coated nonwovens (top images), and polypropylene, polycarbonate, and polyethylene sheets all treated with BR14. All images were generated with ImageJ using the standard coating protocol.

Commercial samples of polymeric nonwoven fibers treated with surfactants had been manufactured by standard industrial processes were used to test the suitability of the method. Figure 5. 18 shows confocal fluorescence images obtained, on the left – the surfactant free nonwoven, and on the right - surfactant, (Stantex® S6327), treated nonwoven both samples prepared in the same way using the dye vaporisation method. In these images the green color represents the fluorescent dye; images A1 and B1. All sample images consist of the three individual channel images, and a merged image of the fluorescence reflectance and bright field channel. Experimental data indicates that the dye vapor dissolving preferentially into the surfactant domains, as distributed on the PP surface, and not the core PP substate.

Overall, nonwovens without surfactants exhibited no or very little fluorescence - see Figure 5. 18 B1. In the case of surfactant coated fabrics, the clear presences of the fluorophores on the fabric surface were revealed by the confocal microscopy - see Figure 5. 18 A1. The presence of the hydrophilic fluorophore BR14 is associated with presence of surfactants, thus inferring their location on the fabric

sample surface. It is observed that most of the surfactant is located on the fiber surface which will be discussed more in detail later.
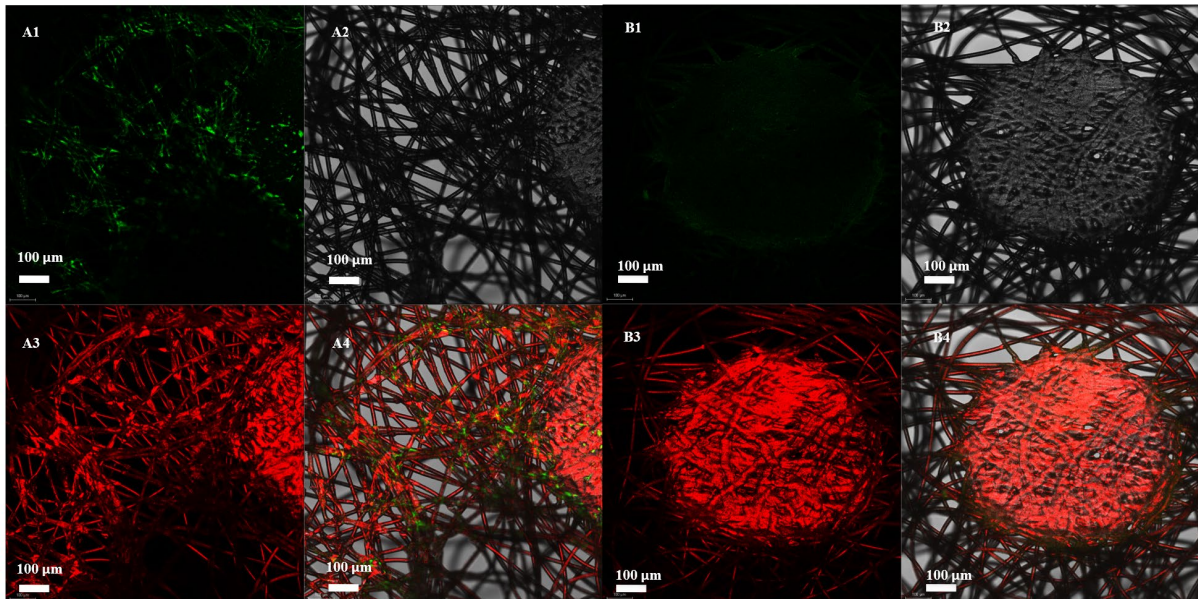
Figure 5. 18 CLSM images of two nonwoven fabrics stained with BR14 dye. A1 - 4 images represent a 1% surfactant, (Stantex® S6327) coated nonwoven sample imaged using 3 different channels, the fluo-rescence channel (green image), the brightfield channel (black and white), the reflected light channel (black and red image) and a combined image of the three channels (A4). B1 – 4 images represent a surfactant free nonwoven sample. The image A1 and B1 show the clear difference in surfactant loading shown by the fluorescence channel, the green images.

A summary of the three-step workflow protocol developed and used in these studies is depicted in Figure 5. 19. This involves, 1) sample preparation/staining with BR14 dye at elevated temperatures, 2) microscopy and image acquisition using CLSM and 3) data processing with Fiji/ImageJ and/or Leica LAS X.
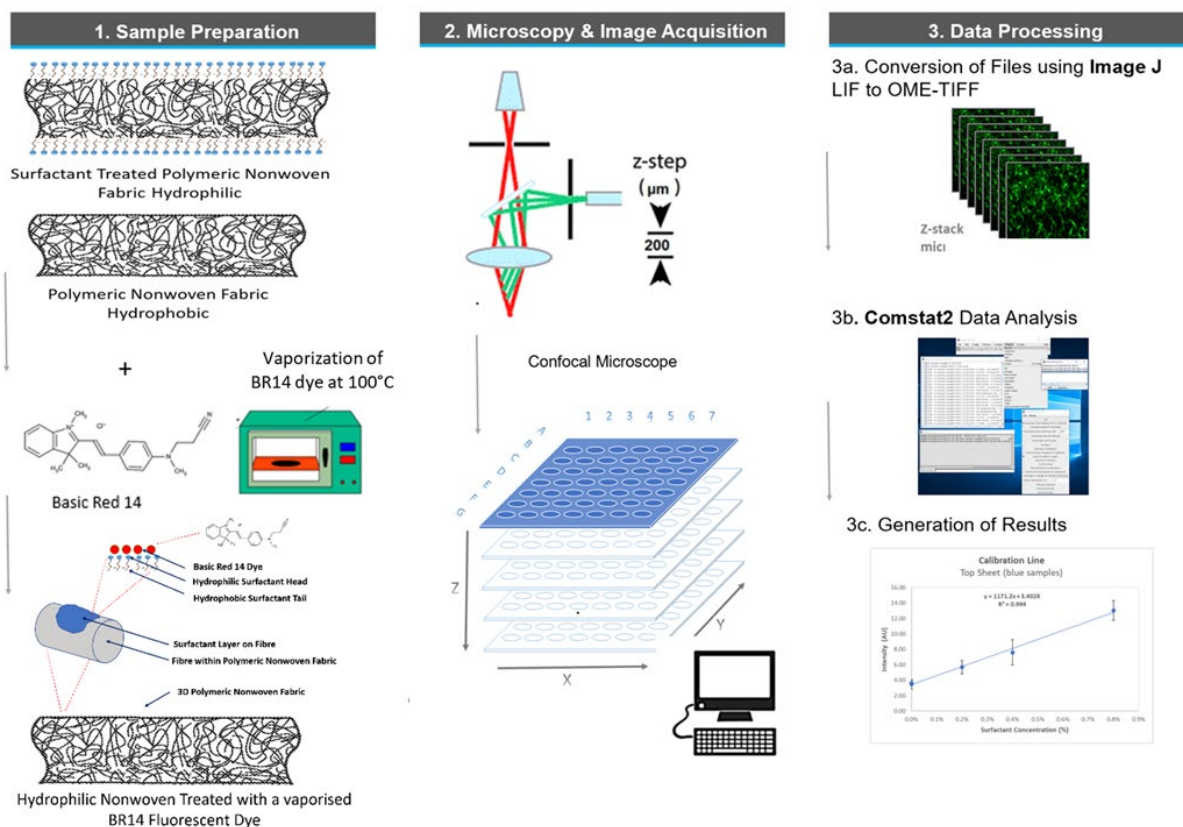
Figure 5. 19 Sample preparation, analysis, and data processing schematic.

5.3.3 Image Processing and Analysis

Image analysis and data processing was done as detailed by the protocol depicted in Figure 5. 20. The raw data files are converted into OMETIFF to be compatible with COMSTATS2. The conversion is done in ImageJ using a plugin. Comstat 2.1 is an image analysis program that is an add-on module to ImageJ. There are many output variables obtained from the software but for this project only "Surface Area" was used. This is the fraction of the area occupied by fluorescence in each image of a stack. The Comstat software works by applying a threshold, which for this project was automatically determined using the Otsu method. Once an image threshold has been applied all pixels with a lower threshold, are assigned a number zero, and those ≥ the threshold are assigned number one. The result is all zeroed data is effectively removed as background, and all data assigned number one, is included in the data analysis. The total number of pixels in each image which exceed the selected threshold are determined using COMSTAT2. For both the fluorescence and reflectance image, this relates to total number of pixels which fluoresce and the total number of pixels in which fibre surface area is detected, respectively. Of course, a pixel cannot be fluorescent unless it is also on the fibre surface. These pixel numbers are then averaged for the typically 100 layers which constitute the full 3D confocal image. These results are then normalised using the fluorescence

and reflectance pixel numbers to account for sample voids present and random fiber orientations, Eqn 32. 2D and 3D image reconstructions are done using both Leica LAS AF software and ImageJ as noted in Figure 5. 20.

$$\frac{AVERAGE\ (Number\ of\ Fluorescent\ Pixels)}{AVERAGE\ (Number\ of\ Reflected\ Pixels)}\ x\ 100 = \% \qquad \textbf{Eqn 32}$$
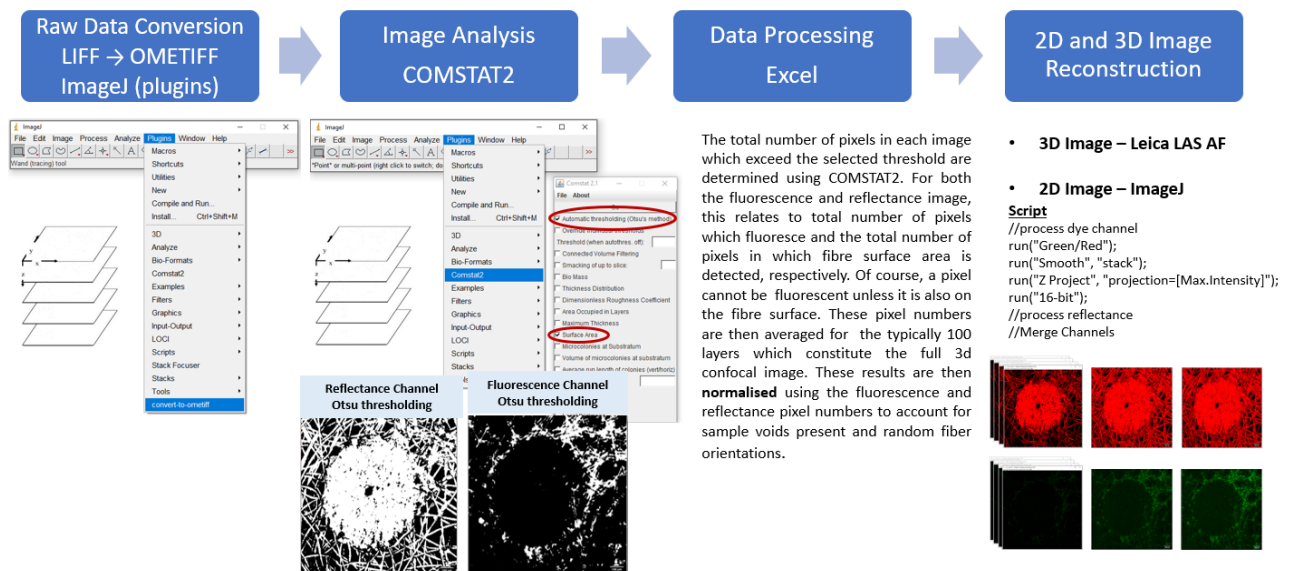
Figure 5. 20 Image analysis and data processing protocol.

5.4 Calibration, 3D Quantification and Imaging

Samples of nonwovens, 100% polypropylene, were coated with different amounts of surfactants, blank, 0.2%, 0.4% and 0.8% surfactant loading, were used to construct a calibration line. The calibration samples were prepared by coating the nonwoven samples with the surfactant solution using a pipette. The amount of surfactant added to the nonwoven was determined gravimetrically by weighing the samples before and after application. The results of this experiment are shown in Figure 5. 21. These results show the fluorescence intensity increasing as a function of surfactant concentration. It is noted that the line does not go through zero and this variation is because of some low-level deposition/precipitation of the fluorophore across the sample surface, producing background fluorescence on the blanks. Such background noise could be subtracted from the raw data sets. These results demonstrate that this technique not only is effective on visualising surfactant rich areas but also can quantitatively distinguish between samples of different surfactant loadings.

151

This is very useful for analysis of aged samples for example to establish the rate of surfactant loss and coating efficiency studies.

Linearity and Sensitivity Results	
Equation	y=3.392+11.812x
R Square	0.997
Standard Error Intercept	0.293
LOD	0.07
LOQ	0.25
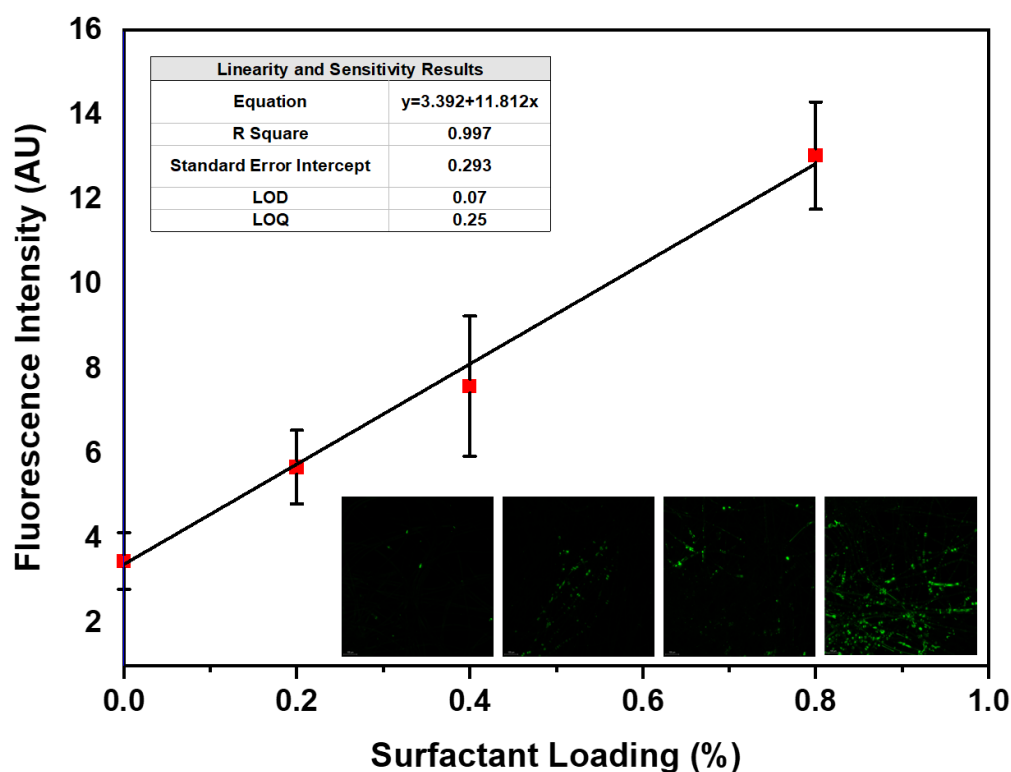
Figure 5. 21 Calibration line for surfactant treated nonwovens with different loadings and representative CLSM fluorescence images of 4 nonwovens treated with BR14 dye via vaporisation, (a) 0.0 % surfactant (b) 0.2 % surfactant (c) 0.4 % surfactant and d) 0.8 % surfactant loading. Results are expressed as $\mu \pm \sigma$, n=3

The 3D image reconstructions were performed using the Leica Las X software provided with the CLSM system. Figure 5. 22 shows an example of a 3D reconstruction of a surfactant coated hydrophilic nonwoven which has been treated with the standard BR14 dye vaporisation method. The images show surfactants adsorbed onto the nonwoven fabric are concentrated at the edge of the circular bonding points. The overall distribution of the surfactants appears to primarily be at the fibre-fibre contact points. This prevalence may relate to the favorable wetting geometry at the fiber junctions. It is also very apparent that the surfactant coating is not homogeneously distributed across the nonwoven fabric, more like a patchwork. This supports the findings from wetting experiments, discussed in Chapter 4. A large portion of surfactants is accumulated on the borders of the bonding points, features created during the manufacturing process of the nonwoven, leaving thus regions such as the middle of the bonding point almost surfactant free, i.e., hydrophobic in nature.

Limitations of the method reported here are the intrinsic limitations faced by all optical microscopic-based methods and relate directly to diffraction, absorption, emission, and scattering behavior of light. A detailed quantum description of the scattering process may be found in R.Loudon[419]. In

general, the potential limiting factors on the penetration depth in fluorescence imaging are the absorption of excitation light by the sample, absorption of fluorescence light by the sample whilst returning to the surface, in addition to scattering of the excitation and fluorescence light beams by the fiber sample. As the fluorescence sampling depth increases, the amount of light that reaches the desired sample region decreases whilst the amount of emitted fluorescence also decreases as it has a larger pathlength to transit. Such factors ultimately limit the performance of all fluorescence based confocal microscopy and influence the quantitative nature of the results obtained using this technique.
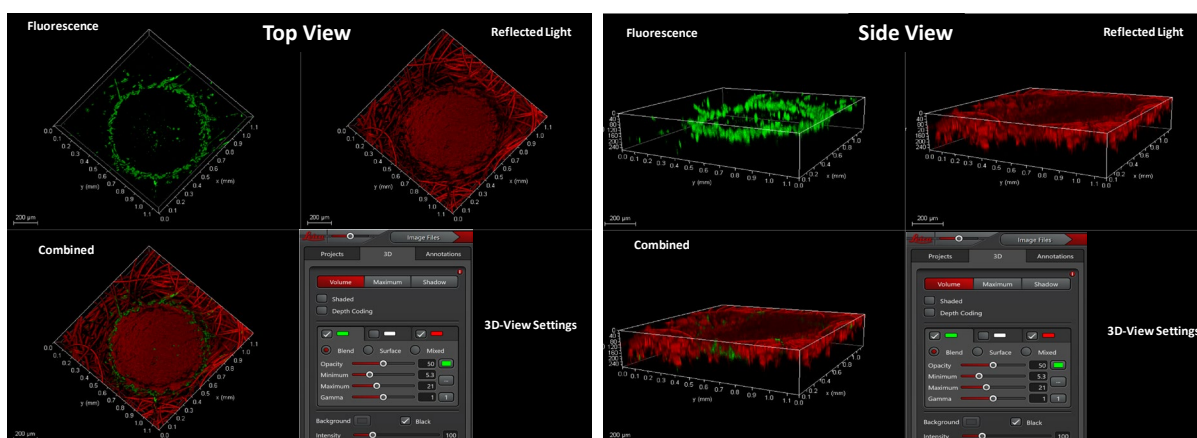
Figure 5. 22 3D image reconstruction of one hydrophilic nonwoven fabric stained with BR14 dye of 25 1x1mm xy sections. LHS images represent – the top view images captured with the fluorescence channel (green image) the reflected light channel (red image) and a combined image. RHS images represent– side view of the same hydrophilic nonwoven fabric sample.

5.5   Conclusions

In this Chapter a novel method was introduced for visualising surfactants coated into nonwoven fabrics using a non-invasive, optical sectioning, 3D mapping protocol. This work utilises a well-established technique, CLSM[294, 420], to investigate for the first-time surfactant-polymer interactions in a 3D nonwoven solid system. To study such complex systems, one needs an approach that provides two types of information, spatial resolution on various length scales within the surface layer and sufficient depth resolution so that the transition from surface to bulk structure in the material can be observed. Surface imaging techniques such as FTIR and TOF-SIMS are unable to provide 3D images of the fibre network, and X-ray tomography, which has the 3D spatial resolution, lacks the contrast to differentiate between fibres and surfactants. However, non-destructive in-depth profiling and high-quality images which showed the relative distributions and the extend of co-localisation of surfactants tagged with fluorophores across the nonwoven fibre surface was achieved with CLSM. Furthermore, confocal microscopy has

153

been used here for the first time to determine the % surfactant loading as well as the extent of co-localisation of surfactants in nonwovens. A range of surfactant loadings, consistent with gravimetric measurements, were quantified this way.

The findings demonstrated that surfactants can be visualised within the 3D fiber network via a newly developed vapor phase fluorophore staining method. Traditional fluorescent labelling and staining methods involving preparation of a working solution by dissolving the fluorescent dye into a liquid phase are incompatible with samples containing surfactants. It is likely that the solvent would interact and dissolve the surfactants due to their amphiphilic nature, thus fundamentally perturbing the native surfactant distribution. The evaporation method developed here is simple and involves introduction of the fluorescent dye under gas phase conditions facilitating thus the study of surfactants coated solid state substrates intact without any solution interferences. Evaporation of the dye allows specific staining of the surfactant phase at the position where the surfactants are located within the fibre without reducing the amount of surfactants. This method is superior to traditional liquid based staining methods because regardless of the solvent used wet methods would likely dissolve the surfactant which could coat other areas of the polymeric fibre leading to a wrong surfactant distribution determination and or quantification due to wash off effects. These issues are all avoided by the vaporisation method introduced here.

Through direct visualisation, the interactions between surfactants and fibres, were observed and compared between polymers with different hydrophilicities. The method was based around the high affinity exhibited by the hydrophilic fluorophore, BR14, for the surfactant coated regions of hydrophobic nonwoven samples compared to the uncoated nonwoven regions. 3D fluorescent images have highlighted significant point to point variability on the extent of surfactants coating. This is consistent with findings from wettability studies, (discussed in Chapter 4) and expected surfactant distribution heterogeneity due to the nature of the nonwovens and the manufacturing process employed for these coatings.

Most importantly, this technique is not limited to the current tested materials. It can also be applied to different nonwoven types with different surfactant coatings, so long as scattering and/or absorption of light is not limiting. Furthermore, this method can be used to study the surfactant nonwoven interaction mechanisms and how these develop with time and under different environmental conditions. Overall, the vapor phase fluorophore staining method has a potential range of applications in materials science and biological materials where traditional liquid staining methods are not practical. Moreover, the method will have application into a number of other important research challenges where imaging droplet/liquid distributions in 3D

networks are important including water harvesting using polymeric fibres[421], wetting of flexible fibre arrays[422], distributions of viral droplets captured by facemask using nonwoven materials[423, 424] as well as oil droplet capture[425] where the efficient process performance requires optimal surface treatments for oil droplet capture and release.

6 Gas Phase Solubility of Small Molecules in Polyolefins

6.1 Introduction

Solubility is defined as the maximum quantity of a solute that can be dissolved in a solvent or substance at equilibrium, which produces a saturated solution. The process of the solute dissolving is termed dissolution. The International Union of Pure and Applied Chemistry (IUPAC) defines solubility as the proportional ratio of a solute in a solvent which is commonly define on a mass basis. Miscibility is when two substances completely mix to form a homogeneous solution. Usually, the term is used to describe liquid mixtures, but it applies to solids and gases, too. The process by which a solute dissolve in a solvent depends on the types of chemical bonds and interactions between the solute and solvent. The chemical interactions between olefinic materials including PP and PE with a range of small molecular species are crucial for the manufacture and industrial use of this important class of polymers. For example, the ability of these polymers to be dissolve into a solvent to become a solution depends on the solvent-polymer interactions. Also, the dissolution of many key polymer additives from dyes to fragrance molecules will directly also depend on their solubility in these polyolefinic materials. So, though it might tend to be thought that polyolefinic materials are very inert and stable materials, and whilst that may be true for small molecules which are polar like water and ethanol, the following literature review will highlight that in the case of more hydrophobic molecules, polyolefinic materials can exhibit significant and strong interactions with these non-polar chemical species.

The systematic study of small molecule transport in polymers has grown exponentially since the classic paper by Graham in 1866 on gas diffusion in polymer membranes.[426] Diffusion can be described as the process where a material is transported by the thermal motion of the molecules in a fluid or a matrix. Solubility and diffusivity act as crucial parameters in many of polymer processing applications. A large amount of information is available in the open literature on the transport of small molecules in polymers, their dissolution in polymers, and the core underpinning solubility and diffusion behaviour. A comprehensive review of this topic would require an amount of space exceeding the confines of the present research, however some key review papers on this area can be found in the following publications:

- Gas solubility in polyolefinic materials[187, 188, 427, 428]
- Solvents and solubility for polyolefinic materials[429]
- Additives for use in polyolefinic materials[430-433]
- Diffusion phenomena for polyolefinic materials[194, 434, 435]

One of the earliest contributors to the study of polymer dissolution was by Ueberreiter[436] who provided a detailed description of the dissolution of polystyrene, a typical amorphous polymer, in organic solvents. Soon after in a series of papers[437-440] Blackadder and his collaborators studied the dissolution of polypropylene in organic solvents describing the effect of temperature, stirring speed, crystallinity, molecular weight, and the nature of the solvent on the rate of dissolution for polypropylene. The dissolution of a polyolefin is considered a slow process dependant on the amorphous structure, the crystallinity, and the molecular weight. Polyolefinic molecules constitute long chains, forming tightly folded coils which are even entangled to each other as well as crystalline domains. Cohesive and attractive both intra and intermolecular forces hold these coils together via long-range van der Waals forces. The lack of polar groups in PP excludes the possibility of chemical interactions such as hydrogen bonding. Due to their molecular size, coiled shape, crystalline domains, and the weak attractive forces which are present, polyolefinic molecules dissolve slower than low molecular weight analogues in organic solvents.

Billmeyer et al [441] demonstrated that there are two stages involved in this dissolution process: firstly the polymer swelling by the solvent, and then the dissolution step itself. When a polymer is added to a specific solvent, attractive forces including mainly dispersion forces effect its segmental behaviour. If the polymer-solvent interactions are stronger than the polymer-polymer attraction forces, the chain segments will start to absorb solvent molecules, increasing the volume of the polymer matrix, and loosening them from their coiled conformations. It is said the segments are now "solvated" instead of "aggregated", as they were in the solid state[34]. The whole "solvation-unfolding-swelling" process can take a long time, therefore, it is desirable to start with fine powdered material, to expose more of their area for polymer-solvent interactions. When crystalline, hydrogen bonded or highly crosslinked substances are involved, and the polymer-polymer interactions are strong, the swelling process stops at this first stage, resulting in a swollen or partially swollen gel. If the polymer-solvent interactions are still strong enough, the "solvation-unfolding-swelling" process will continue until all segments are solvated. Thus, the whole loosen polymer coil dissolves into the solution. The dissolution of the swollen mass can be aided by stirring and heat.

Polyolefinic polymers such as PP and PE are predominantly semi-crystalline polymers consisting of crystalline domains and non-crystalline amorphous domains as depicted in Figure 6. 1. The amount of crystallinity depends on the thermal processing history as well as polymer structure.
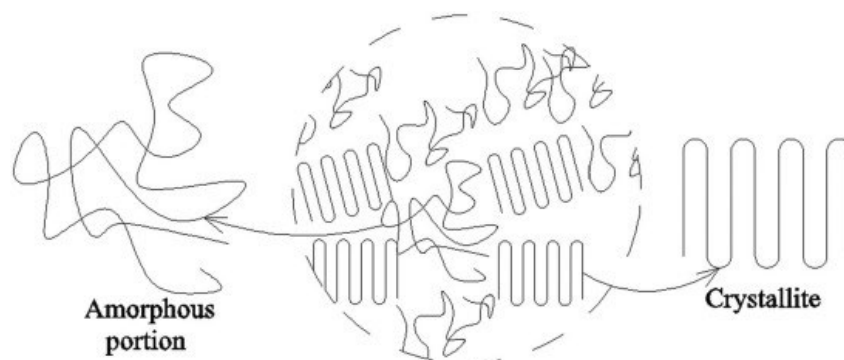
Figure 6. 1 A schematic representation of semi-crystalline "state" of polymeric solids comprising of crystalline domains and non-crystalline amorphous domains[442].

Solubility of small molecules in polyolefins is realised through exchanges of solute molecules in the amorphous phase[174]. Therefore, it is generally accepted[173, 174, 193, 443] that crystalline regions are impermeable to the solute molecules. Solutes will favour mixing in a less dense and already disordered amorphous phase preferentially to the ordered lattice. In practice, this means that the higher the degree of crystallinity the lower the sorption capacity of the polymer and vice versa. According to Qin et al.[444] the sorption of an organic vapor in PP is influenced by the type of processing method which results on changes in surface and bulk morphologies. Maghsoud et al.[205] studied the migration of Irganox 1010, a phenolic antioxidant, from HDPE into a fatty food simulant using samples with different percent crystallinities. They found higher migration in samples with lower crystallinity, and overall, the solute migration decreased linearly with increasing crystallinity. Michaels et al.[174] described the effect of crystallinity on diffusivity. It is understood that in some scenarios there can be the trapping of amorphous regions within the crystalline regions of the polymer, which directly reduces penetrant solubility. Overall, the presence of crystallites restricts molecular mobility by acting as physical crosslinks. The reduction in amorphous phase chain mobility due to crystallites is more pronounced in flexible rubbery polymers such as polyethylene than in glassy polymers, such as PET for example. Penetrant diffusion through rubbery polymers is typically described by the Fickian transport model[445].

Different types of polyolefins are characterised by varying degrees of crystallinity and therefore exhibit very interesting properties such as temperature dependant degree of crystallinity which directly links to varying sorption capacities. PEs can be categorised into three major classes[446]: HDPE, LDPE, and MDPE. The basic difference among the three classes of PEs lies in the degree and regularity of branching. While HDPE has very few branches, LDPE is characterised by larger and irregular branching. MDPE, on the other hand, features intermediate extent and regularity of branching. These structural differences directly reflect the physical properties of

these polymers, such as crystallinity and melting point. As the order of crystallinity is expected to be LDPE < MDPE < HDPE, then the sorption of gases and solutes into these polymers is expected to decrease in the order: LDPE >MDPE>HDPE.

As the degree of crystallinity of a polymer affects its properties, accurately determining this property is important. There are many experimental methods[43, 177, 178] to determine polymer crystallinity. In principle, three primary methods are commonly used based on: 1) thermodynamics, 2) diffraction, and 3) spectroscopy. Among them, thermal analyses to measure thermodynamic properties in determining crystallinity remains the most common method due to its simplicity and speed of the analysis. Techniques such as differential scanning calorimetry (DSC) [180-182] and density measurements using pycnometry[182, 184] have been utilised in this research to determine the degree of crystallinity of polymer samples. The crystal fraction X_c has been used to define the crystalline volume fraction of these semi-crystalline polyolefin samples.

6.2   Characterisation of PP and PE Polyolefins

Characterising polyolefins is important because as discussed in Chapter 2 these materials are widely used for manufacturing a wide range of products. Their versatility makes them suitable for a whole range of applications and comes from the capability of manufacturers to tailor microstructures and therefore properties through control of the processing conditions. In the context of this study, to understand the sorption of a molecule in a polymer, a knowledge of the crystallinity of the polymer sample is important because the mechanical and physicochemical properties of crystalline domains are different from those of amorphous domains for the same polymer. Polymer crystals are much stiffer and stronger than amorphous regions of polymer. An introduction to polymer crystallisation can be found in the texts by Mandelkern[447] and by Sharples[448].

6.2.1   Determination of Crystallinity with DSC

The DSC method is based on thermodynamic principles. The DSC instrument allows analysis of a range of physical or chemical responses taking place within a sample including melting, crystallisation, glass transition, solid-solid transition, enthalpy of fusion or crystallisation, reaction enthalpy, polymerisation, and pyrolysis. The DSC monitors the internal energy changes occurring throughout heating, cooling or isothermal temperature cycles. Most of these transitions will either be exothermic or endothermic in nature. Depending on the equipment

used, the endothermal reaction can either be plotted upward or downward position in the experimental data plots. The general rules are that endothermic reaction are plotted downwards in a heat flux DSC as the heat is absorbed by the sample during enthalpy change. The latter is dependent on the stability of the weight (no gain or loss) and calculated through the integration of the area under the heat versus temperature curve.

DSC measures heat flow, (y-axis in mW), into or out of a material as a function of time or temperature, (x-axis in seconds, minutes or °C). Estimation of % polymer crystallinity by DCS can be determined based on heat of fusion, (melting) data or based on the heat of crystallisation. The results presented here were determined with DSC by quantifying the heat associated with melting of the polymer. This heat has been reported as percent crystallinity by normalising the observed heat of fusion to that of a 100 % crystalline sample of the same polymer. As authentic samples of 100 % crystalline polymer are rare, literature values were used for this value. However, there is general disagreement in the literature on how the crystallinity should be measured using this technique and whether the measured value has any real significance[180, 449]. However, DSC is a commonly used technique both in industry and academia and as such a standard test method for transition temperatures and enthalpies of fusion and crystallisation of polymers by DSC exists, ASTM D3418. It is worth noting however that the % crystallinity determined by DSC differed from % crystallinity determined by density measurements, see Table 6. 6.

Glass transition endotherm, crystallisation exotherm, and fusion endotherm are the main thermal events exhibited by amorphous or crystalline material. The glass transition endotherm is a result of the presence of the amorphous phase, and the crystallisation exotherm results from recrystallisation of the amorphous content. Subsequently, the obtained crystalline state and the pre-existing crystalline content fuse together to form a melting endotherm. The amorphous content of all samples was assessed by their enthalpy of fusion through the following equation:

$$X_c \, (\%) = \frac{\Delta H_m}{\Delta H_0} \times 100\% \qquad \qquad \textbf{Eqn 33}$$

where X_c is the percentage of crystallinity, ΔH_m is the enthalpy of fusion of the sample, (the area under the melting peak when heat flow is plotted against time from a DSC run), and ΔH_0 is the literature value for the same material in 100% crystalline state.

Before making any measurements, it was important to know whether the instrument was calibrated. Indeed, heat flow and temperature need to be measured very accurately as they were utilised in the crystallinity measurements. It is important to calibrate with material samples which span the entire temperature range of the tests been carried out so that interpolation is carried out rather than extrapolation which would be less accurate. In this case Indium (In) and Zinc (Zn) were employed to calibrate the DSC apparatus as these have very well-defined heat flow and melting points as showed in Table 6. 1.

Table 6. 1 Reference materials used for DSC calibration.

Substance	Temperature of Fusion (°C)	Enthalpy of Fusion (J/g)
Indium	156.6	28.5
Zinc	419.6	107.5

The DSC instrument's software used had a built-in calibration function both Indium and Zinc. For Indium 27.85 to 29.05 J/g was the latent heat and 156.3°C to 156.6°C is the melting point of this metal For Zinc 103.7 to 111.3 J/g is the latent heat and 418.9°C to 420.3°C is the melting point of this material.

The DSC experimental parameters used for DSC measurements of the polymer films are shown in Table 6. 2.

Table 6. 2 Parameters used for DSC testing. All samples weight was 5.00 ± 0.05 mg.

Run	Atmosphere	Heat Rate (°C/min)	Temperature Range (°C)
Equilibrate	Helium	0	20
1 (*heating*)	Helium	10	20-220
Isothermal	Helium	0/5min	220
2 (*cooling*)	Helium	10	220-20
3 (*heating*)	Helium	10	20-220
Isothermal	Helium	0/5min	220
4 (*cooling*)	Helium	10	220-20

Estimation of % crystallinity by DSC was based on the heat of fusion (melting) as well as based on heat of crystallisation. The % crystallisation was calculated by integrating the area under the melting endotherm over a wide range of temperatures and are shown in Table 6. 3. The results demostrate that % crystallinity values determined using the heating compared with the cooling cycle are slightly different. Both of these methods compare the unknown sample to a fully crystalline or amorphous sample of the same polymer, and require some reference data

which, if not acurate, (i.e. obtained via the same approach) will affect the results and may cause these variations. Table 6. 3 also documents literature values for the % crystallinity of the samples of interest and they appear to be in the genera range of the calculated values from the DSC measurements from this study. Overall, literature values were slightly at the higher end of the values reported here. Different reference data values exit for the calculations and there is no way to establish which ones are best to use. Also, it was dificult to establish what reference data was used to produce the % crystallinity literature values.

Figure 6. 2 shows the individual DSC curves for each material studied which are similar to those found in the literature[205]. The melting temperature of LDPE was measured as the lowest of all three different PE's studied. The melting temperature measured for MDPE was higher than that of LDPE. HDPE exhibited the highest melting temperature, and the melting peak area of HDPE was also larger than that of MDPE and LDPE peaks. Atactic PP is amorphous and waxy in nature therefore it has no clear melting peak whereas isotactic PP features crystalline and amorphous phases and so a melting and crystallisation peak were recorded. The calculated % crystallinity (X_c) of each polyolefin studied was noted in the individual DSC curves shown in Figure 6. 2.

Table 6. 3 Calculated % crystallinity values for different polymers determined using DSC

Sample	Cycle		Peak Area (mW°C/mg)	Heating Rate (10°C/min)	Heat of Melting/Fusion ΔH_m (J/g)	Theoretical value of the melting enthalpy of 100% crystalline polymer[450, 451]. ΔH_m^0(J/g)	Crystallinity X_c (%)	Literature Crystallinity[181, 178, 184, 224, 452] X_c (%)
LDPE	1	Heat	14.843	0.167	89.058	293	30.4	38 – 40
		Cool	14.577	0.167	87.462	293	29.9	
	2	Heat	14.424	0.167	86.546	293	29.5	
		Cool	14.829	0.167	88.978	n/a	—	
MDPE	1	Heat	20.799	0.167	124.798	293	42.6	45 – 48
		Cool	16.549	0.167	99.291	293	33.9	
	2	Heat	16.511	0.167	99.068	293	33.8	
		Cool	17.469	0.167	104.817	n/a	—	
HDPE	1	Heat	23.308	0.167	139.850	293	47.7	51 – 75
		Cool	25.574	0.167	153.448	n/a	—	
	2	Heat	23.287	0.167	139.719	293	47.7	
		Cool	25.499	0.167	152.995	n/a	—	
iPP	1	Heat	12.289	0.167	73.731	207	45.2	46 – 56
		Cool	12.264	0.167	73.584	163	45.1	
	2	Heat	3.003	0.167	18.021	207	8.6	
		Cool	11.694	0.167	70.162	163	33.6	
aPP	1	Heat	0	0.167	—	n/a	0	n/a
		Cool						
PP Nonwoven	1	Heat	11.753	0.167	70.515	209	33.7	54 – 65
		Cool	13.474	0.167	80.842	n/a	—	
	2	Heat	12.273	0.167	73.635	209	35.2	
		Cool	13.079	0.167	78.471	n/a	—	
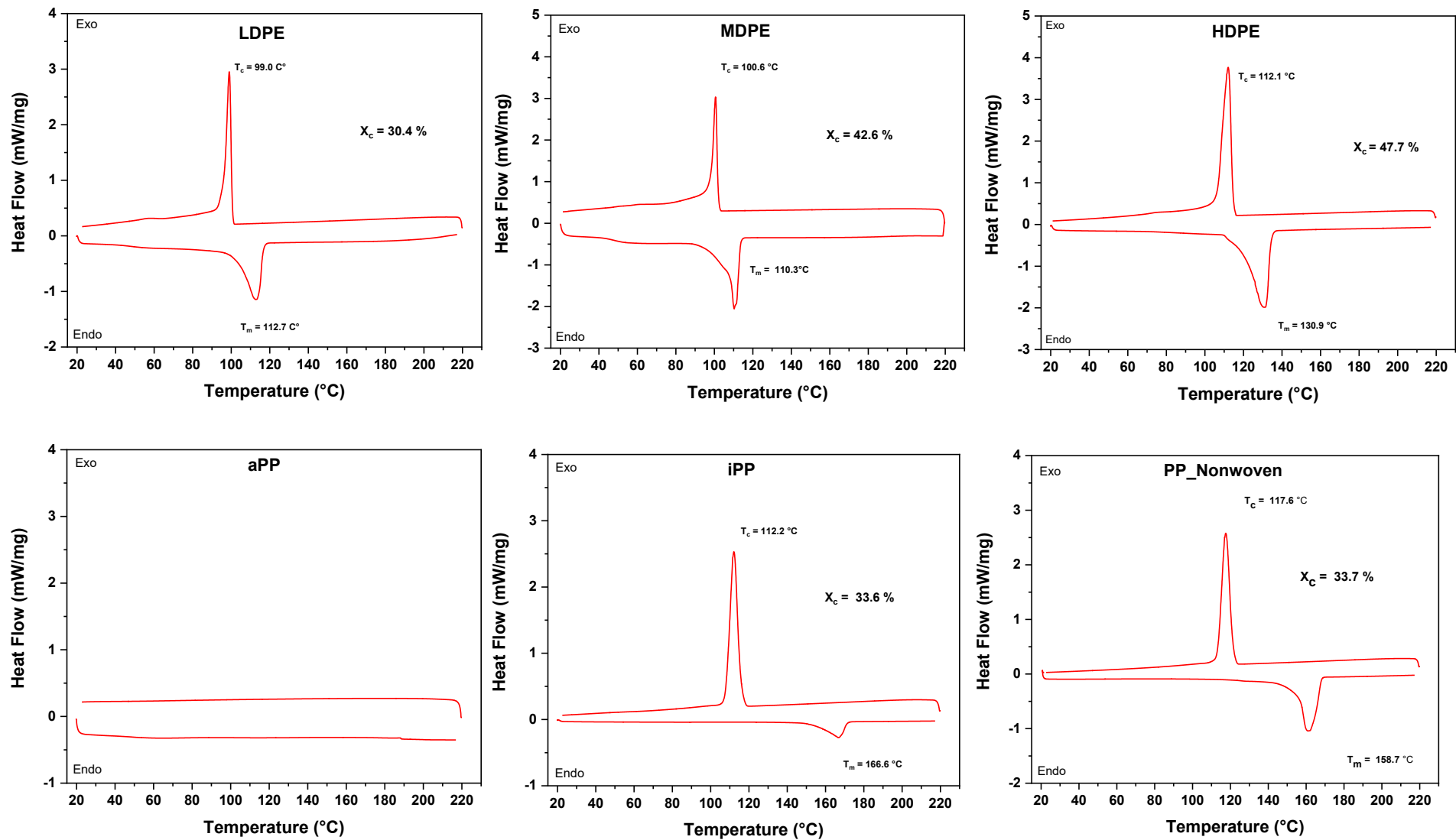
Figure 6. 2 DSC curves for LDPE, MDPE, HDPE, atactic PP, isotactic PP and PP based nonwoven.

6.2.2 Determination of Crystallinity with Pycnometry

Determination of the % crystallinity using densities assumes a knowledge of the densities of 100% amorphous and 100% crystalline polymers. Polymer samples usually are irregular in shape, making it difficult to measure their volume directly. There are different methods for determining the density of a polymer and for this work a method called pycnometry was used. The density is determined by dividing the sample weight by the volume measured by pycnometry. The density is then used to calculate the percent of a polymer that is crystalline. The density measurements via pycnometry were carried out using an Accupyc II 1340 (Micromeritics, USA), instrumentation with helium gas as the probe molecule. All the measurements were carried out at room temperature, T = 15, 25 and 35°C. Operation of pycnometer is based on the Archimedes' principle. The % crystallinity is given by Eqn 34:

$$\% \, Crystallinity^2 \; = \; \frac{\rho_c(\rho_s - \rho_a)}{\rho_s(\rho_c - \rho_a)} \times 100 \qquad \textbf{Eqn 34}$$

where ρ_c is density of the completely crystalline polymer, ρ_a is density of the completely amorphous polymer, and ρ_s density of the sample.

Density measurements of different polyolefins using pycnometry were conducted at different temperatures. The data are shown in Table 6. 4. The results demonstrate predominantly temperature independent density measurements which is reasonable across the small temperature range being studied here.

---

[2] Stoyko Fakirov- Fundamentals of Polymer Science for Engineers

Table 6. 4 Polyolefin density measurements of different polyolefins using pycnometry at different temperatures

Density Measurements (g/cm³) (±0.01)				
Sample	15 °C	25 °C	35 °C	**Literature**[453-456]
LDPE	0.9204	0.9162	0.9109	0.91-0.94
MDPE	0.9179	0.9181	0. 9111	0.92-0.94
HDPE	0.9449	0.9406	0.9397	0.93-0.97
aPP	0.8507	0.8423	0.8404	0.84-0.86
iPP	0.8979	0.8974	0.8970	0.89-0.92
PP Nonwoven	-	0.8825	-	n/a

A summary of % crystallinity calculations determined from density measurements for the different samples are presented in Table 6. 5. As expected, HDPE and iPP have the highest % crystallinity and for amorphous aPP there is no crystallinity measured. The PP based industrial nonwoven sample shows similar % crystallinity to iPP suggesting that this polymer is the major component of this industrial polyolefin. Any variations of the data are considered to be a result of their thermal history. Table 6. 5 also documents literature values for the % crystallinity of the samples of intrest and they appear to be in-line with the calculated values from the density measurments preseneted here. Overall, literature values were slightly at the higher end of experimental data reported. Different reference data values exist for the calculations and adds difficulty when considering what reference data is best to use for the calculations.

Table 6. 5 The % Crystallinity calculations determined from density measurements for different polymers.

Sample	Helium Pycnometry Density (g/cm³)				Crystallinity from Density Measurements[3] 25 °C						
	25 °C	Mean	Std. Dev.	% RDS	ρ_s	ρ_c	ρ_a	$\rho_c (\rho_s - \rho_a)$	$\rho_s (\rho_c - \rho_a)$	Crystallinity X_c (%)	Literature Crystallinity X_c (%)[36, 452, 453, 455]
LDPE	0.9162	0.92	0.00	0.52	0.916	0.999	0.855	0.07	0.14	48.2	45-55
MDPE	0.9181	0.89	0.04	4.98	0.918	0.999	0.855	0.07	0.14	49.5	—
HDPE	0.9406	0.94	0.00	0.30	0.941	0.999	0.855	0.09	0.14	64.2	70-80
iPP	0.8974	0.88	0.03	3.76	0.897	0.950	0.855	0.05	0.09	50.2	70-80
aPP	0.8423	0.84	0.03	3.41	0.842	0	0.855	0.00	-0.72	0.0	—
PP Nonwoven	0.8825	0.88	0.03	0.34	0.912	0.95	0.855	0.06	0.09	35.0	—

---

[3] Crystallinity calculated by density, ρ_a =0.85 g/cm³, ρ_c = 0.999 g/cm³   Ref.457.   Kong, Y.; Hay, J. N., The measurement of the crystallinity of polymers by DSC. *Polymer* **2002**, *43* (14), 3873-3878.

The results comparing % crystallinity obtained with DSC and pycnometry are shown in Table 6. 6. These results show differences between the % crystallinity estimations using DSC and pycnometry measurements. The degree of crystallinity of a polymer is temperature dependent[458] and in comparing its effect on material properties it is vital to carry out these measurements at the same temperature, invariably at ambient temperature and not at the melting point. However, crystallinity percentage obtained from DSC is an average value valid for the temperature region around the melting point and the change of crystallinity that takes place upon heating the sample from room temperature to the melting point is not considered and because of this the degree of crystallinity measured by DSC varies with the values obtained by pycnometry at room temperatures. Furthermore, crystallinity determined using densities, assumes a knowledge of the densities of 100% amorphous and 100% crystalline polymers. Although the results from these two methods of determining crystallinity do not agree completely, it is indicated by the calculations that most probably the samples tested were between 35 and 65% crystalline and these estimations align with similar values reported in the literature for these types of polyolefin materials.

Table 6. 6 The % Crystallinity of different polyolefin samples measured via two different methods, DSC and pycnometry.

Polymer Sample	Crystallinity X_c (%)			
	DSC (±0.05)	Literature [181, 178, 184, 224, 452]	Pycnometry (±0.05)	Literature [36, 452, 453, 455]
LDPE (pellets)	30.4	38 - 40	48.2	45-55
MDPE (fine powder)	42.6	45 - 48	49.5	n/a
HDPE (pellets)	47.7	51 - 75	64.2	70-80
aPP (waxy solid)	0.0	n/a	—	~ 0
iPP (pellets)	45.2	46 - 56	50.2	70-80
PP Nonwoven (fabric)	33.7	54 - 65	35.0	n/a

6.3   Sorption of Small Molecules in PE and PP Polyolefins

In general, the manufacturing processes for polyolefins can change the polymer morphology by redistributing the crystalline and amorphous regions and changing the available free volume. The fabrication of the base polymer into films, for example, is typically carried out at elevated temperature to produce a melt which is then subjected to rapid cooling while solidifying. During this quenching step, many polymers pass through their glass transition state, which causes their molecular chains to "freeze" into a glassy form in the direction of deformation. The molecular orientations induced may not be uniform, causing anisotropy in

the material properties for the final articles made from this polymer[199]. During vapor sorption, semicrystalline polymers tend to undergo complex changes. Besides gaining in mass, structural changes within the polymer may also occur, such as relaxation of polymer chains, changes to polymers free volume, lowering of glass transition temperature, crystallisation of amorphous domains and viscoelastic relaxation behavior[200]. Because of their potentially strong interaction with compatible organic compounds, the sorption behaviour of semicrystalline polymers tends to be both concentration and time dependent. Furthermore, the structural anisotropy that resulted from the manufacturing process can also affect the sorption behaviour of polyolefins. Although the sorption of gases and vapours has been extensively studied for PE and PP[189, 201, 459] there appear to be no systematic investigation of organic vapour sorption into a range of polyolefinic materials. Having establishes the % crystallinity of the different polyolefinic materials under study, the next obvious step is to determine how such characteristics affect the solubility of small molecules into these materials. Solubility was expected to vary in direct proportion to the amorphous fraction of the polymer. Solvent sorption is understood to occur primarily in the amorphous phase therefore, the absence of crystallites enhances the degree of solvent sorption[443].

The dissolution or sorption of organic solvents in PP and PE has been investigated in detail here using a gravimetric sorption analyser. The basic operation principle of a gravimetric sorption analyser, such as DVS, is to measure the change in mass over time of a sample that is kept in an environment of constant temperature and controlled adsorbate vapour pressure. An inert carrier gas, typically dry air, transports the adsorbing organic solute with a known partial pressure over the sample, typically under isothermal conditions. After a change in partial pressure of the vapour phase solute, the sample will either take-up or release the organic adsorbate, and the sample mass is measured by a microbalance at defined time intervals for a few seconds. In the early stage of each sorption/desorption step, the change in weight is relatively significant. Over time, the adsorption process approaches equilibrium, and the change in sample weight is continuously getting smaller. When the sample weight is finally stable, then equilibrium with the surrounding partial pressure of the adsorbate has been established. The measurement is then continued to the next requested partial pressure. Typically, one or more complete sorption/desorption cycles (sorption from low to high partial pressure and desorption from high to low partial pressure in small partial pressure steps which are typically 5% P/Po. The individual equilibrium data points from all partial pressure steps of the sorption/desorption cycles are used to generate the sorption isotherm. The sorption isotherm is the relationship between the adsorbate content of the sample and the partial pressure of the adsorbate at a particular temperature. Measurements are possible over a wide range of temperatures. The present study presents a detailed investigation of sorption

properties of different organic solvents and fragrance molecules on different forms of PP and PE by a gravimetric method between 25 and 55 °C and 0 and 90% P/Po. In terms of polymer type, most polyolefin fibres and textiles are composed of isotactic PP, and/or HDPE. PE, PP and a nonwoven fabric were used for these sorption studies which were coated as thin films.

Materials

All the reagents used, for the generation of vapor isotherms, were ordered from Sigma-Aldrich (Poole, UK) and VWR UK with a minimum of 99% purity. These reagents were used without further purification. The deionised-water (DI) used for all the experiments was ultra-pure Milli-Q grade. All the polyethylene samples used in this work were ordered from Sigma-Aldrich (Poole, UK) and all the polypropylene samples were ordered from Sp^2 Scientific Polymer Products Inc. (NY, USA). Isotactic polypropylene was received as pellets, atactic polypropylene was a waxy solid, low-density polyethylene and high-density polyethylene were pallets and medium-density polyethylene was a fine powder. The commercial nonwoven samples used in this research were donated by *Procter & Gamble.*

Thin film fabrication

Apart from aPP which was dissolved in toluene at room temperature all the other polymers were dissolved in decahydronaphthalene(decalin) at 160 °C to form 2% w/w solutions. The commercial nonwoven sample was pre-cleaned with isopropanol and air dried before dissolving in decahydronaphthalene. All the other polymer samples were used as received. An alumina foil swatch, (diameter 6.5cm) pre-cleaned with deionised-water and isopropanol, then dipped into the polymer solution for 30 seconds and then left to air dry for 30 minutes before being placed in a vacuum oven at 120°C for 3 hours so that the residual solvent evaporates. aPP was dried at 80°C. Each alumina foil was weighted before and after the polymer coating to record the amount of polymer coated on the substrate.

Dynamic vapor sorption measurements

The sorption profiles of polymer films were determined using the DVS Endeavour and Resolution (Surface Measurement Systems, London, UK). Samples had a total mass ranging between 100-140mg, of which typically 10mg was the polymer coating, were directly hung on the instruments hang-down hook, with the sample pan removed. On the DVS Resolution, counterweights were used for the higher mass samples. Most coated foil samples were folded into smaller sizes to keep them compact in size and hang on the sample hook. A series of experiments were carried out using either fixed times for each adsorbate's experimental partial pressure setpoint or % dm/dt threshold. The % dm/dt mode uses a percentage change of mass with time dm/dt measured and compares it to a reference value to determine intelligently the

time when the sample has reached equilibrium at a given partial pressure step. The % dm/dt threshold was set to 0.0005 % for all experiments to ensure the sample had reached a necessary degree of equilibrium before moving on to next step. When the sample percentage change in mass is equal to or below this threshold for a given stability duration (10 min), the step stage is then ended and moved onto the next programmed partial pressure step. Methods were run in (0 - 90% P/Po) cycles with increments of 10% P/Po steps. Organic adsorbate vapour concentrations were generated using liquid solvent bubbling reservoirs and controlled via closed loop use of speed of sound sensors for measuring the adsorbate concentration in real time. Adsorbed quantities were calculated using the change in mass between the ends of the current cycle's adsorption and previous cycle's desorption step. Before the sorption kinetics, the sample was first dried in the DVS chamber to 0% partial pressure at 25 °C (below T_g) for 180 min to establish a dry mass.

After a dry mass was achieved, the sample was exposed at a fixed temperature to the following partial pressure profile: from 0 to 90% and then back to 0 in % partial pressure increments of 5%. A nitrogen flow rate of 200mL/min was used for all experiments and the temperature on DVS was set to 25°C, unless the effect of temperature was being studied where other temperatures were investigated; 35°C, 45°C and 55°C. Between experiments, samples, were dried at 50°C under vacuum for 3 h to remove any residual moisture or other residual adsorbates that may influence adsorption performance. The raw data was exported into Microsoft Excel and analysis was done using the DVS Macro Standard Analysis Suite v7.0.13 (Surface Measurement Systems, London, UK).

6.3.1 Sorption of Small Molecules in PE at 25°C

Solubility of cyclohexane, hexane, heptane, octane, toluene, isopropanol, and water in LDPE, MDPE and HDPE was studied gravimetrically using a DVS. Figure 6. 3 shows an example of a sorption isotherm obtained using a DVS and the corresponding sorption kinetic data for toluene and LDPE at 25°C. This figure is an example of a good isotherm, with no hysteresis which suggests only a single sorption mechanism for toluene. There is relatively fast diffusion of the solvent, dissolving into the amorphous part of the polymer. The kinetic data shows that sorption equilibrium has been reached at each step.

171
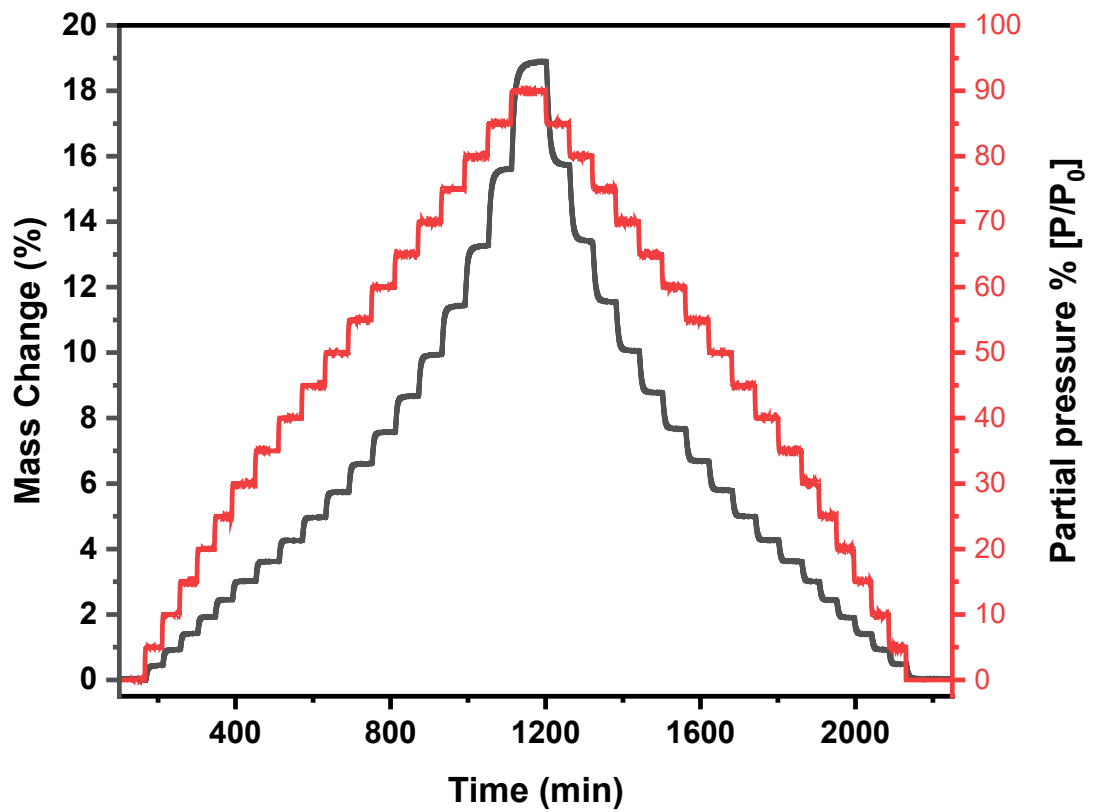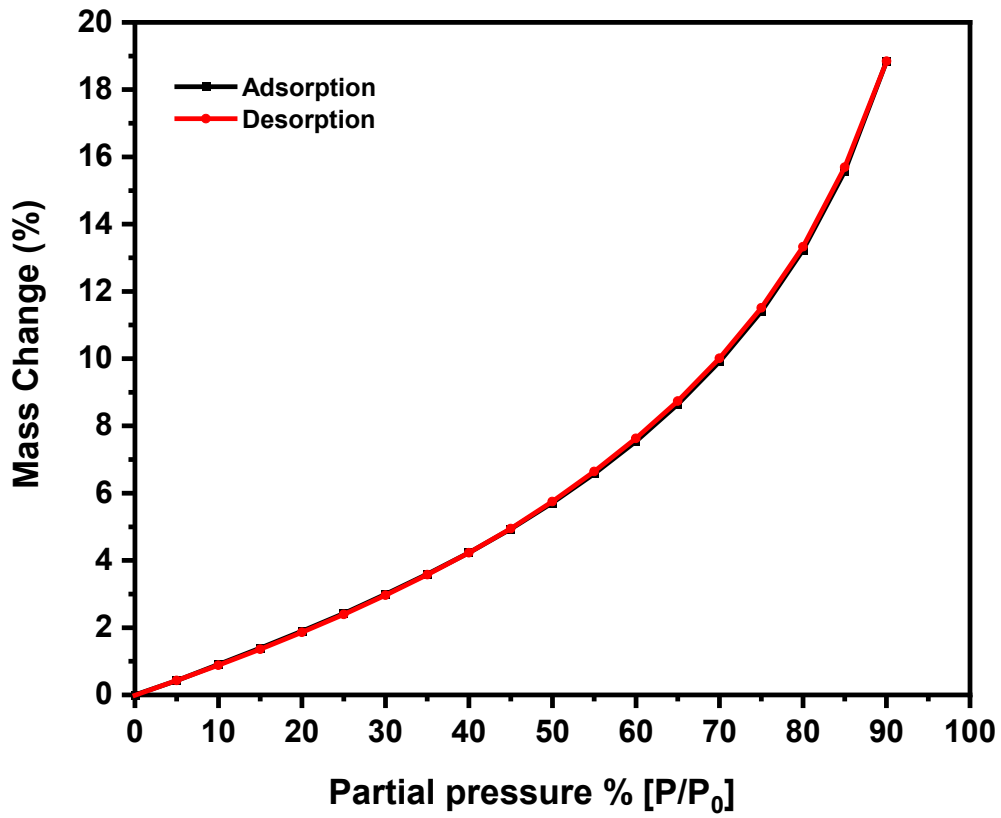
Figure 6. 3 Toluene sorption isotherm (top) and the corresponding sorption kinetic data for LDPE film at 25°C (bottom).

The different forms of PE exhibit varying degrees of branching in their molecular structure. LDPE has the most extensive branching which causes it have a less compact molecular structure which is what makes it less dense; it has a density of 0.91-0.94g/cm³. MDPE has less branching than the LDPE and has a density range of 0.92- 0.94 g/cm³. HDPE has minimal branching of its' polymer chains and as a result it is denser, more rigid, and less permeable than both MDPE and LDPE. HDPE has a density of 0.93-0.97g/cm³. Density measurements using pycnometry confirmed these differences, see Table 6. 4 and were used for the determination of the percent crystallinity of the different polyethylene's, see Table 6. 5. The percent crystallinity increases as a function of density and this influences the solubility of small molecules in the LDPE, MDPE and HDPE, demonstrated by isotherms shown in Figure 6. 4, Figure 6. 5 and Figure 6. 6 respectively.

Since LDPE has the lowest crystallinity and therefore the most amorphous fraction of the three-polyethylenes studied, LDPE exhibited the highest solvent uptake in a polyethylenes for all organic solvents tested. This observation is because the small organic molecules dissolve in the amorphous part of the polymer. On the contrary HDPE has the highest crystallinity and therefore the lowest amorphous fraction out of all the polyethylenes studied which resulted in the lowest uptake for all the different solvents tested. The shape of the organic solvents isotherms for HDPE was different too. The HDPE isotherms are more linear, they have a lower degree of concavity to the x-axis, than the LDPE and MDPE isotherms, suggesting a different sorption mechanism potentially, which could be due to the different flexibility of the molecular chains. The isotherm shape is also affected by T_g which for HDPE is getting closer to room temperature and the material is in a glassy state, instead of rubbery. These results are in line with similar studies documented in the literature[456] for the diffusion and solubility of n-alkanes in polyolefins. Also noticeable from this data is the very low uptake of the polar solvents, like water and IPA, for all the PE samples. HDPE, MDPE and LDPE have no polar functional groups therefore no permanent dipoles. Of course, *organic solvents such as hexane, heptane and octane* interact by non-specific van der Waal forces, while isopropanol is a strong polar compound which contains permanent dipoles. These chemico-physical characteristics explain the very low uptake of polar solvents by HDPE, MDPE and LDPE.
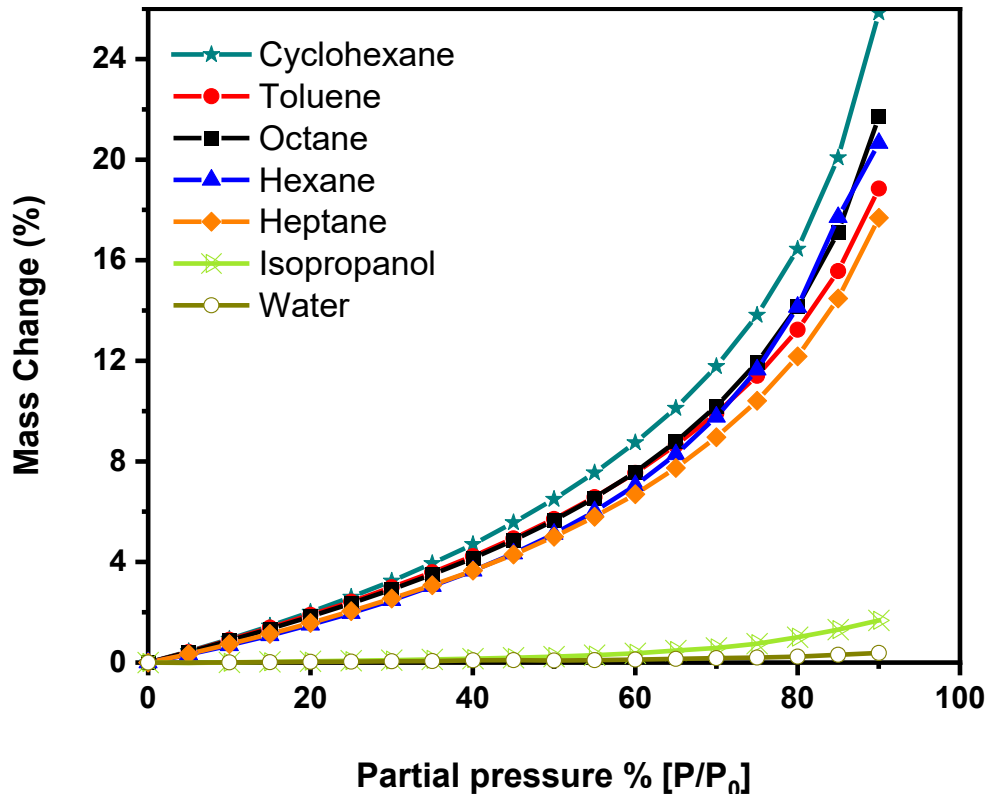
Figure 6. 4 Adsorption isotherms of different small molecules for LDPE. Error bars of 0.1% are smaller than the data symbols.
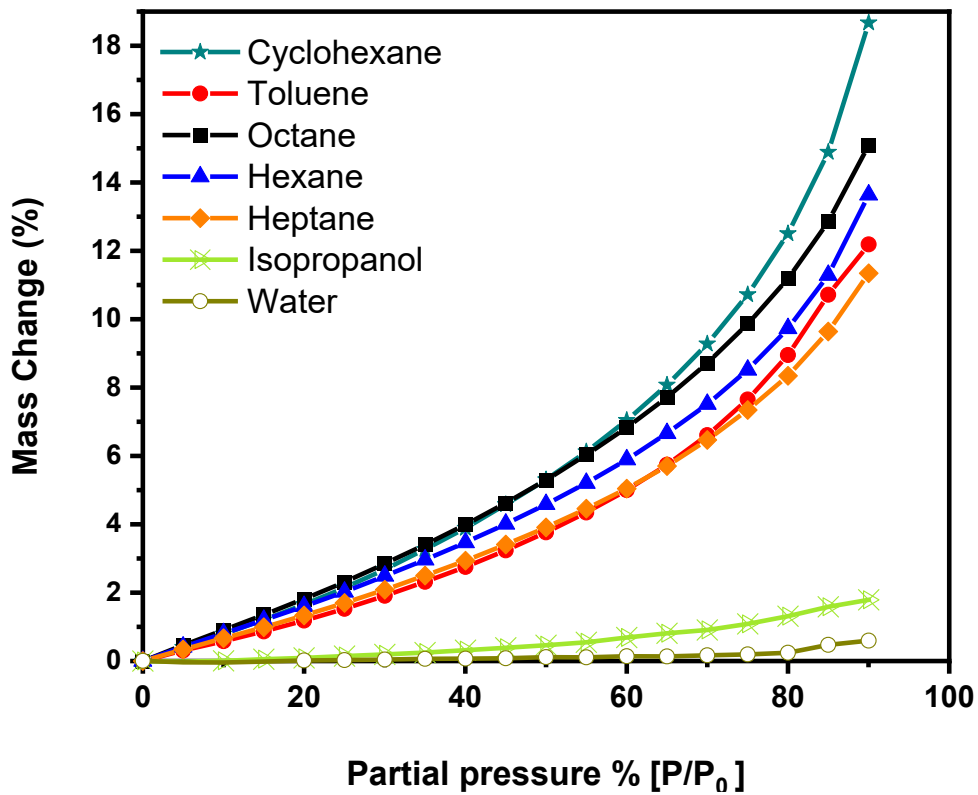
Figure 6. 5 Adsorption isotherms of different small molecules for MDPE. Error bars of 0.1% are smaller than the data symbols.
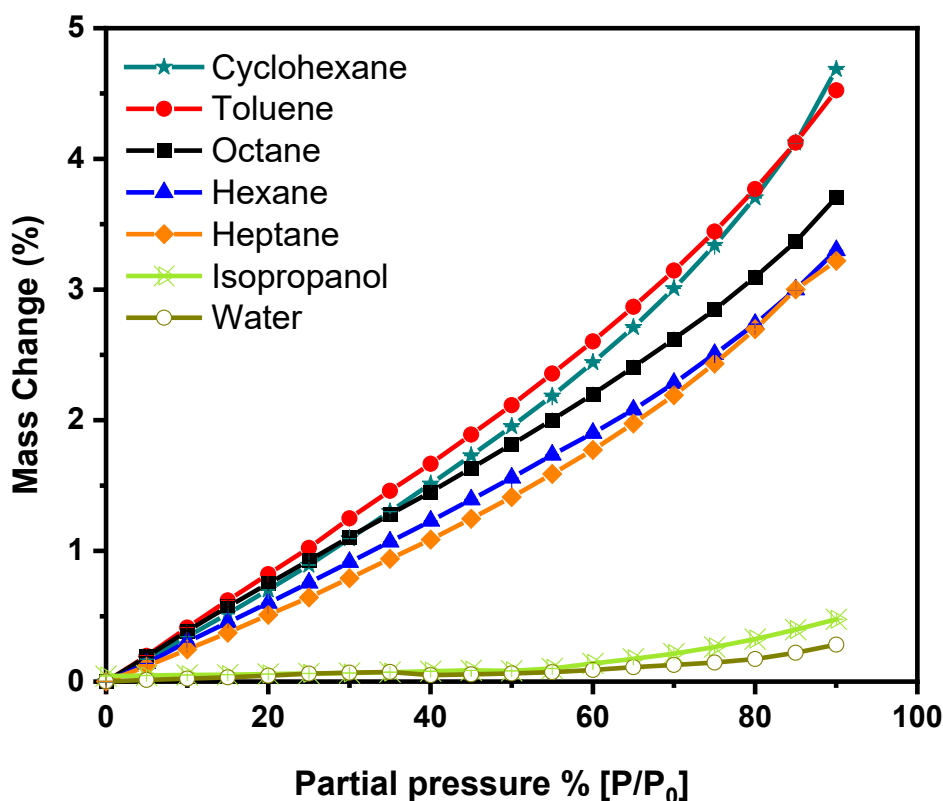
**Figure 6. 6 Adsorption isotherms of different small molecules for HDPE.
Error bars of 0.1% are smaller than the data symbols.**

6.3.2 Sorption of Small Molecules in PP at 25°C

Solubility of cyclohexane, hexane, heptane, octane, toluene, isopropanol, and water in iPP and aPP was studied gravimetrically. Figure 6. 7 shows an example of a sorption isotherm and the corresponding sorption kinetic data for cyclohexane with atactic PP at 25°C. The isotherm shows isotherm hysteresis which could be due to sorption equilibrium not being reached as clear in the kinetics plot. In the case where there is some hysteresis, this might be because the material is getting near to the T_g. Sorption hysteresis in polymers occurs when the material forms a glassy state, and the solute molecules get trapped into the glassy state and as a result the desorption of these molecules slows down. There is relatively slow solvent diffusion in some polymers, and the kinetic data shown in Figure 6. 7 suggests that equilibrium has not been reached at each step, and this hysteresis is more pronounced at higher partial pressures. It appears these experimental steps require more time to reach equilibrium and that would probably improve the isotherm by reducing hysteresis. Atactic PP is 100% amorphous in nature and the high solute uptake is in line with expectations. The extend of cyclohexane sorption of over 100% by mass is a exceptionally high solute content. It is also interesting to note, that despite the high hysteresis, the sample still recovers to its initial mass at the end of the experiment.
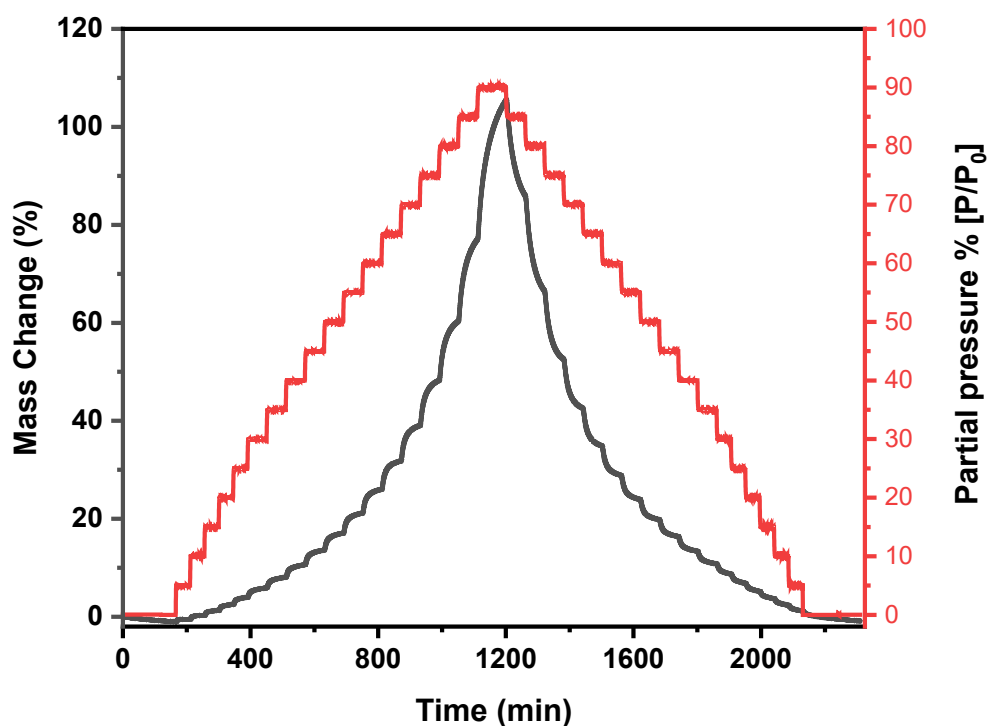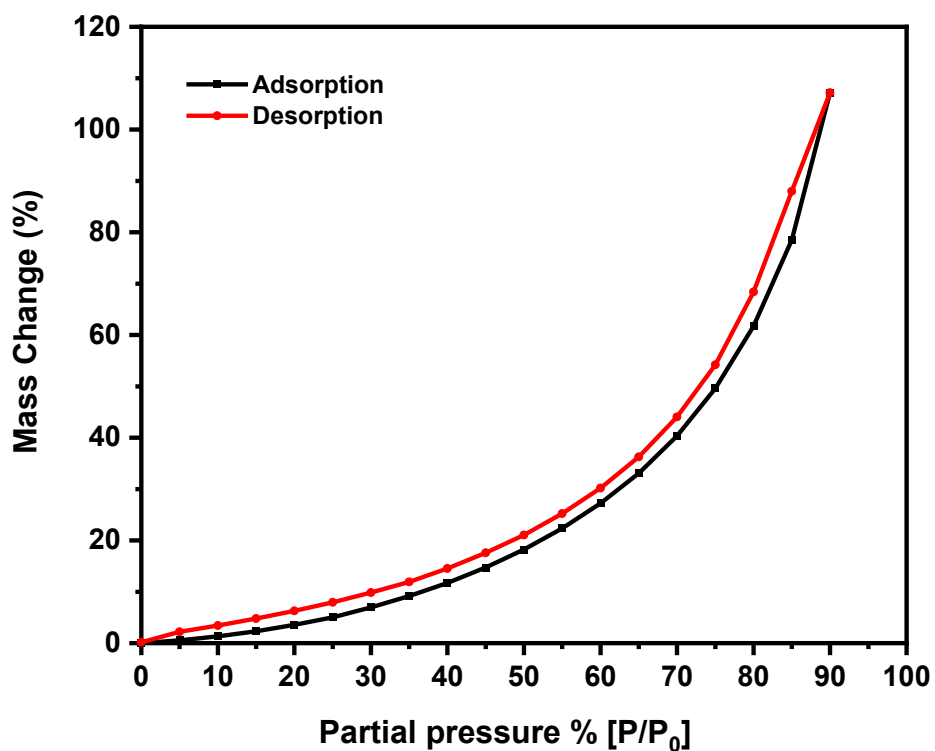
Figure 6. 7 Cyclohexane sorption isotherm (top) and the corresponding sorption kinetic data for atactic PP film at 25°C (bottom).

Overall, polypropylene, though notoriously insoluble in any single solvent at near room temperature sorpted all the different organic solvents with a very preference for cyclohexane.

Hexane and cyclohexane have about the same molecular mass, but have different molecular shapes and their sorption profiles demonstrated that molecular shape affects the solubility of these small molecules into PP. The data suggests that the cyclic ring shape of cyclohexane enhances solubility compared to the aliphatic straight chain shape featured by hexane. Overall, all solvents adsorb significantly more into atactic PP than isotactic PP by ~ 90% as shown in Figure 6. 8 and Figure 6. 9. This difference is in line with our expectations as it is known that diffusion of small molecules in polymers is governed by the mobility of both the penetrant and the polymer chains. It is accepted that transport of small molecules in semicrystalline polymers like isotactic PP takes place only in the non-crystalline regions and this form of PP contains a large impermeable crystalline phase where small molecules cannot penetrate. In the case of atactic PP, the amorphous form of polypropylene, the small molecules penetrate the entire material as it is in a completely amorphous disordered phase.
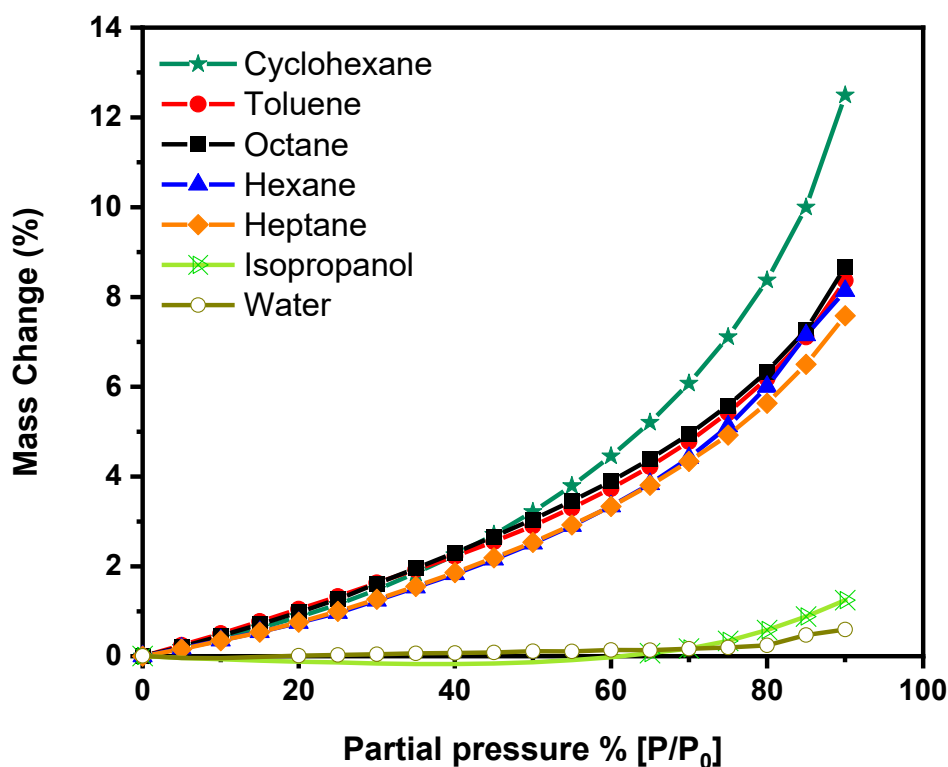
Figure 6. 8 Adsorption isotherms of different small molecules for isotactic PP.
Note substantial differences in Mass Change (%) for these two figures.
Error bars of 0.1% are smaller than the data symbols.
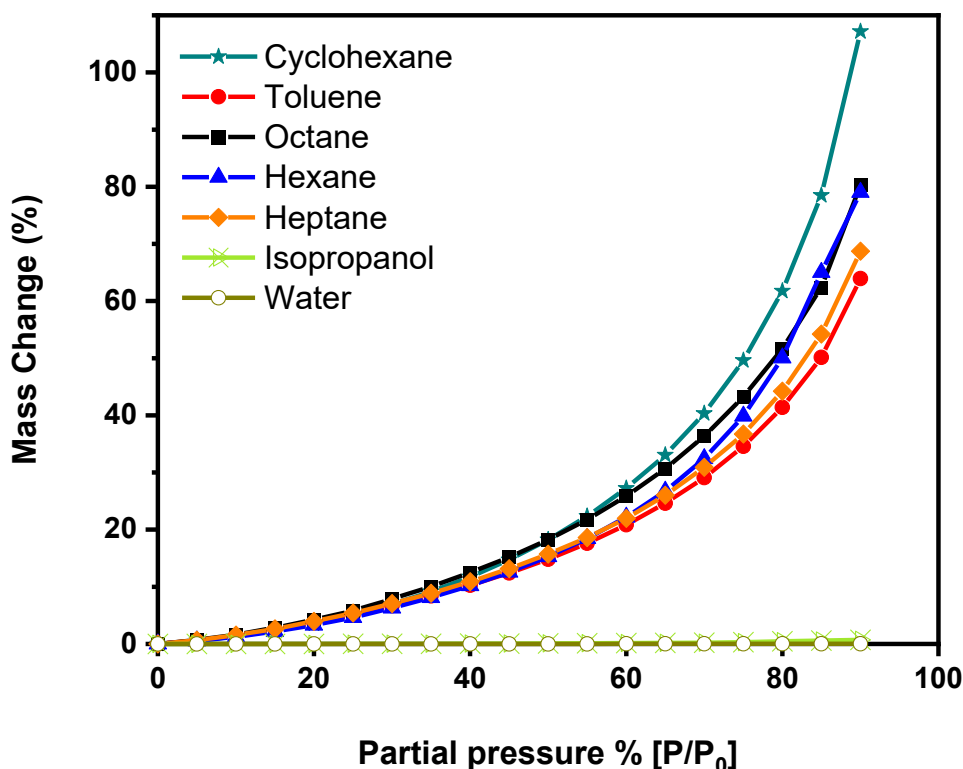
Figure 6. 9 Adsorption isotherms of different small molecules for atactic PP.
Note substantial differences in Mass Change (%) for PP figures.
Error bars of 0.1% are smaller than the data symbols.

It is well accepted that sorption and diffusion take place entirely in the amorphous regions of polymers and that the crystalline areas are impermeable to permeant[174, 193]. The much higher sorption capacity measured here for the amorphous atactic PP (>70%), as compared to the semicrystalline homopolymer, (~7-12%) confirmed that free volume and crystallinity were important contributors for organic sorption in semicrystalline PP. The sorption isotherms at 25°C for the organic solvents display a pronounced curvature shape, i.e., concave upwards when concentration is plotted on the y axis and pressure of solvent vapor on the x axis), indicating a wide deviation from Henry's Law even at moderate adsorbate pressures. It is appropriate at this point to examine the solubility of water and isopropanol in PE and PP from a less empirical point of view. In view of the fact that the amorphous phase of PE and PP is well above its glass transition temperature at 25"C., its molecular architecture should be very nearly that of a liquid aliphatic hydrocarbon. The results show that there is minimal solubility for the polar solvents. Since no such sets of data sets exists in the literature, no comparisons can be drawn.

6.3.3 Sorption of Small Molecules in Industrial Polyolefins

Solubility of cyclohexane, hexane, heptane, octane, toluene, isopropanol, and water in an industrially relevant PP based nonwoven sample was also studied gravimetrically. These results are shown in Figure 6. 10. Compared to the polypropylene studies discussed in Section 6.3.1, these adsorption isotherms more closely resemble isotactic PP than the amorphous atactic PP. The nonwoven PP demonstrated slightly higher uptakes compared with the isotactic PP overall for all the different solvents tested. Since this material is an industrially formulated sample it sorption behaviour could be influenced by various contaminants such as oils from production machinery or whitening chemicals added to the nonwoven for decorative purposes during manufacturing stage. Also, the polyolefin is sometimes fabricated at high temperatures in the presence of atmospheric oxygen, the resulting product may contain oxygenated structures, more polarisable than double bonds in amounts depending upon their thermal history and formulation. Accordingly, measured solubilities higher than those obtained for isotactic PP do not appear unreasonable for a potentially slightly oxidised polymer. It may also be possible that the differences in update maybe due to small changes in the crystalline morphology of this material.

The results in Figure 6. 10 show cyclohexane with the highest solubility, and IPA and water with minimal uptake. The solubility of hexane, heptane and octane increased as a function of carbon chain length. The results show that chemical composition of a polymer has a strong influence on the solubility and diffusion of different vapours. Generally, polymers with polar groups, such as epoxies, have a strong affinity for polar vapour molecules, including water vapour. In contrast, the uptake of polar species is much lower in non-polar polymers[445] which is in line with the data presented here. Overall, the sorption trends for the various solvents at lower vapor activities were different from those observed at higher vapor activities. As expected, the sorption capacity increased as the higher vapor activity increased overall, and for hexane at least the sorption curves flattened toward a maximum at the x-axis as it reached steady state.
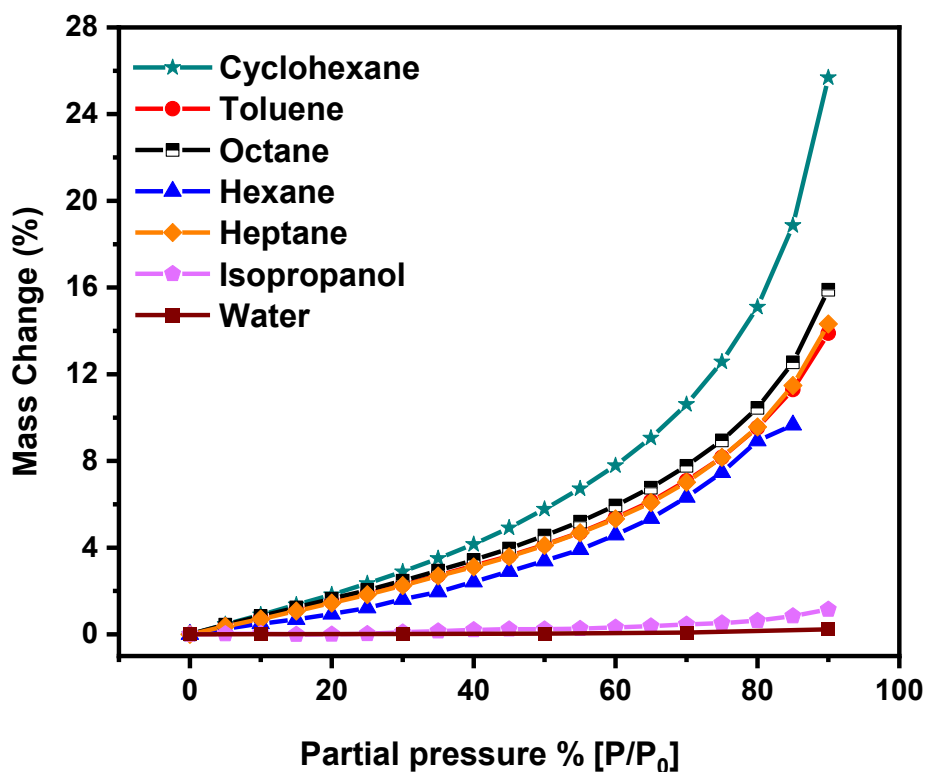
Figure 6. 10 Adsorption isotherms of different small molecules for industrially relevant PP based nonwoven. Error bars of 0.1% are smaller than the data symbols.

6.3.4 Sorption of Heptane and Octane in PP and PE from 25°C to 55°C

The solubility of octane and heptane in PP were also determined as a function of temperature gravimetrically using at 25°C, 35°C, 45°C and 55°C. At higher temperatures, faster equilibrium was expected due to the faster diffusion and interestingly lower uptakes overall were observed. A suggestion is that this behaviour could be due to two competing effects; the desire of the solvent to dissolve in the polymer and its desire to evaporate in the surrounding environment at higher temperatures. The data for octane and heptane are shown in Figure 6. 11 and Figure 6. 12 respectively. These results show clearly that dissolution increased as a function of temperature for both octane and heptane. Out of the two adsorbates, heptane uptake was higher overall and for both heptane and octane the atactic polypropylene, (the amorphous form) exhibited significantly higher solubilities. This behaviour is in line with our expectations as it is known that that transport of small molecules in polymers takes place only in the non-crystalline regions and therefore amorphous PP will have more capacity as it lacks crystalline regions. Overall, temperature tends to increase the rate of solubility for both solutes in PP. The shapes of the different isotherms are concave in shape, type III, like what has been shown by previous results, suggesting similar solubility behaviours. The slopes of the isotherms for both

iPP and aPP curves are similar suggesting that the sorption mechanism is similar, but the amount of dissolution is higher in the aPP, the amorphous PP.
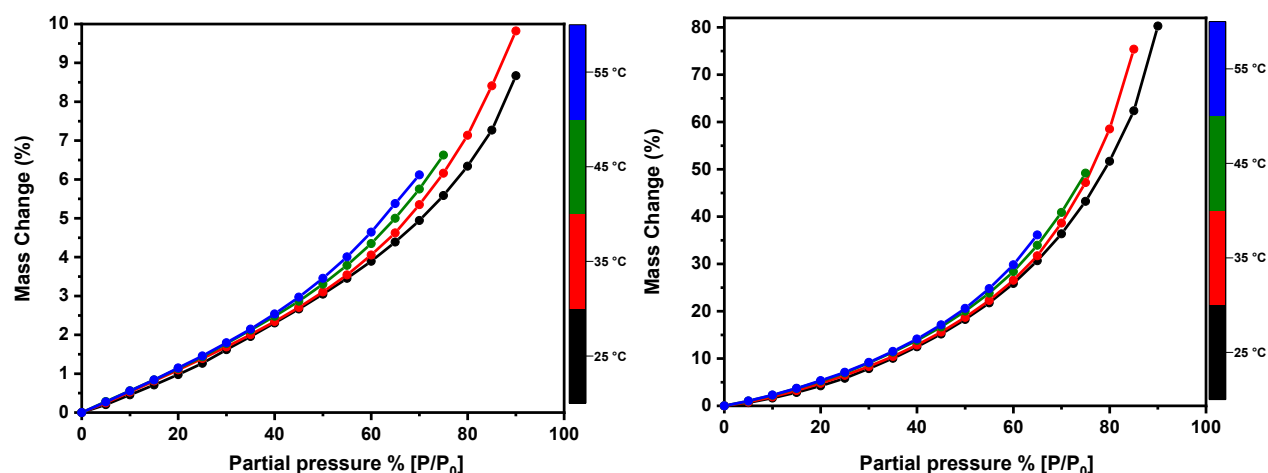
Figure 6. 11 Octane adsorption isotherms at different temperatures for isotactic PP (left) and atactic PP (right). Error bars of 0.1% are smaller than the data symbols.
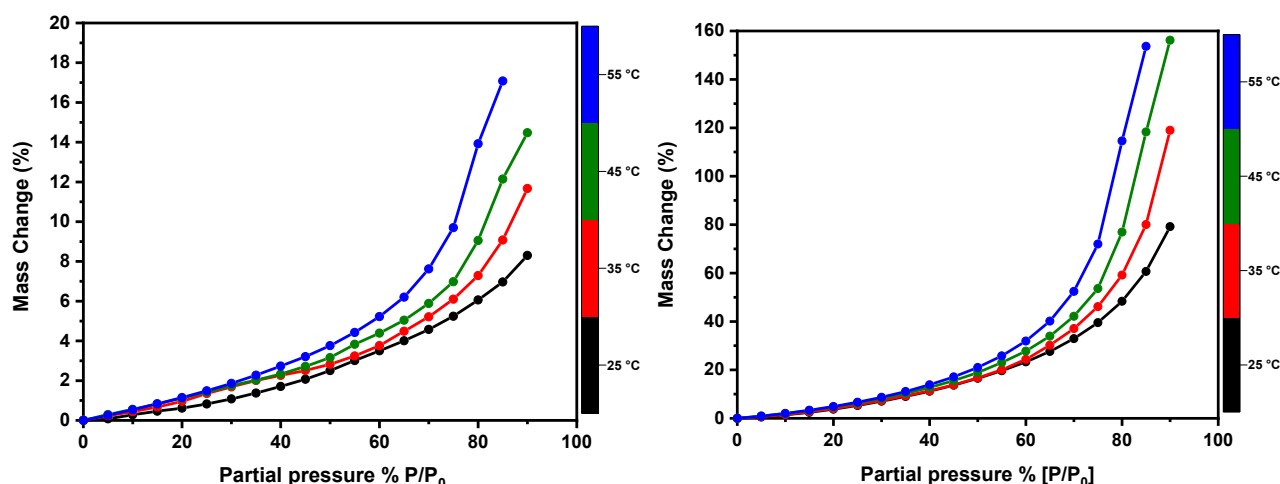
Figure 6. 12 Heptane adsorption isotherms at different temperatures for isotactic PP (left) and atactic PP (right). Error bars of 0.1% are smaller than the data symbols.

The solubility of octane and heptane in PE were also determined as a function of temperature gravimetrically at 25°C, 35°C, 45°C and 55°C. For PE, similar to PP, at higher temperatures, faster equilibrium was expected due to the faster diffusion, leading to higher uptake. Again, the results for octane and heptane as shown in Figure 6. 13 and Figure 6. 14 respectively were surprising demonstrating that dissolution increased as a function of temperature. Out of the two, heptane uptake was higher overall and for both heptane and octane the LDPE, (the least crystalline form) exhibited the highest solubilities and HDPE, (the most crystalline form) exhibited the lowest solubilities. This is in line with our expectations as it is known that that transport of small molecules in polymers takes place only in the non-crystalline regions, in the

amorphous domain and therefore amorphous PP would have more capacity for uptake than semi-crystalline PP. These results confirmed that PP morphology had a major impact on the sorption of organic vapours such as heptane and octane due to the redistribution of free volume and crystalline regions and temperature increased diffusion rates. The expectation was that there would be an increase of the solubility, with increasing carbon number both for hexane, and octane as solvents is a consequence of the growing interaction between alkane and solvent molecule, leading to an increase of the activity however, the data doesn't support this and in fact suggests the opposite is true.
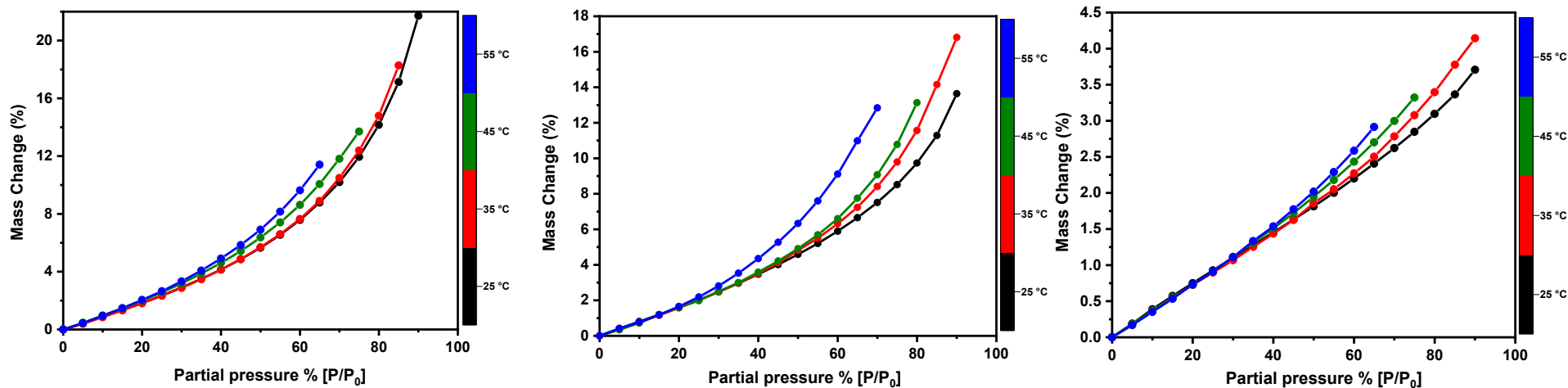
Figure 6. 13 Octane adsorption isotherms at different temperatures for LDPE (left), MDPE (middle) and HDPE (right).
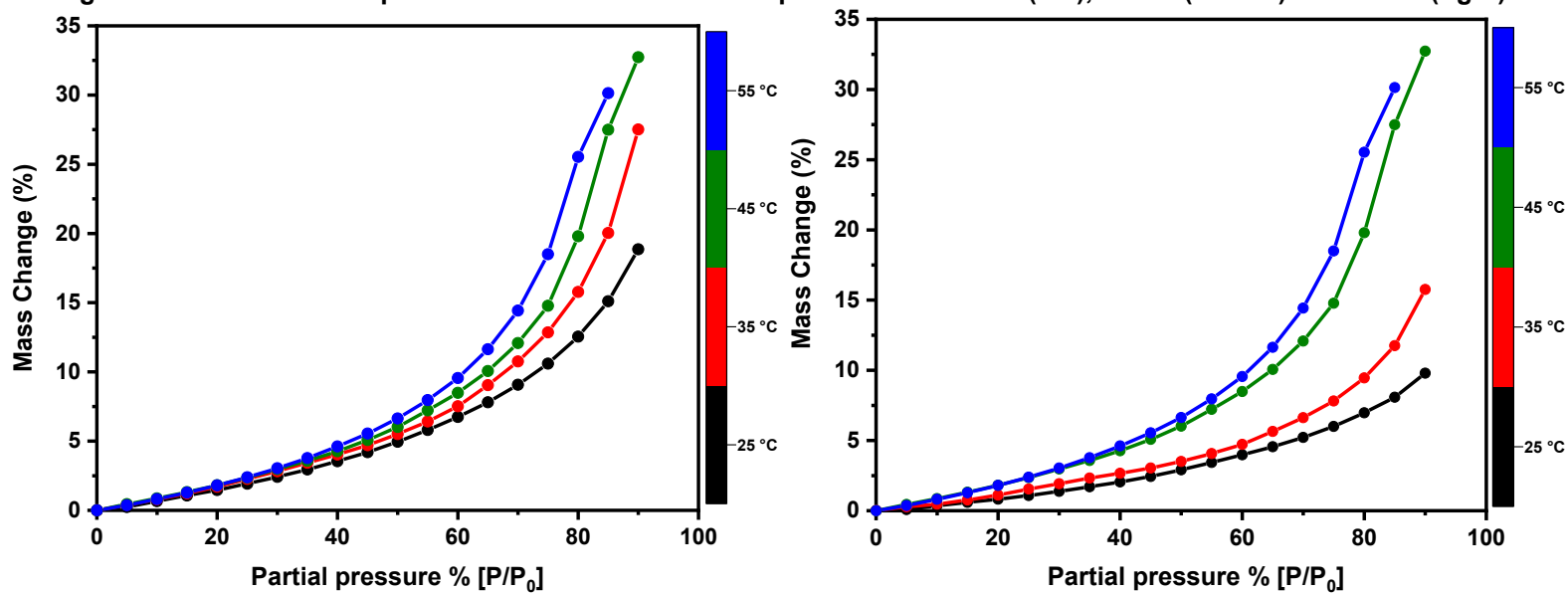
Figure 6. 14 Heptane adsorption isotherms at different temperatures for LDPE (left), and MDPE (right). Error bars of 0.1% are smaller than the data symbols.

6.3.5 Sorption of Limonene and Ethyl Acetate in PP and PE from 25°C to 55°C

Like other hydrocarbon structured adsorbates, select fragrance molecules could be expected to dissolve in the amorphous regions of polyolefins. Limonene and ethyl acetate were studied here as two examples of commonly used fragrance molecules. Their chemical structures are shown in Figure 6. 15. The former is entirely a non-polar hydrocarbon-based molecule, whilst the latter is a polar ester molecule. The name 'limonene' was derived from the name of lemon because limonene has a light, fresh, and sweet citrus scent. Limonene is classified as a cyclic monoterpene and as one of the most common terpenes in nature and is thought to be produced by plants to deter predators and protect them from pests. Limonene finds use in cosmetics, skincare formulations, and as a food additive to improve the scent and taste. Ethyl acetate is a simple carboxylate ester with a sweet, fruity odour widely used as a solvent, for paints, varnishes, lacquers, cleaning mixtures, and perfumes. It also finds use as a flavour enhancer in foods and pharmaceuticals and is also approved for use as an indirect food additive in packaging materials.

Limonene   Ethyl acetate
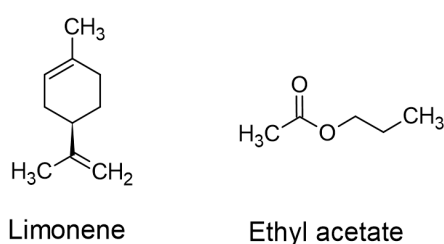
Figure 6. 15 Chemical structures of limonene and ethyl acetate.

The diffusion of these small molecules into, out of, and through polymers is important in many industrial applications. Semi-crystalline polymers are known to be exceptional barrier materials, with their unique morphology resulting in both low diffusivity and low solubility for many vapour molecules, making them popular materials for packaging films. The ease with which fragrance molecule vapours permeate through a macromolecular compound is of importance in applications such as personal care and hygiene as well as packaging industry. Polyolefins like PP and PE are outstanding barriers to moisture but are highly permeable to hydrocarbons. An important property of PP and PE based films when they are used to package certain articles, especially food, is the ability of the film to act as a barrier to moisture, oxygen and aroma species diffusion.

Sorption of limonene and ethyl acetate into different PE and PP morphologies was studied and the data are shown in Figure 6. 16 and Figure 6. 17 respectively. When examining the limonene isotherms the highest uptake is shown by amorphous PP, again because this

polymer has no crystallinity. This uptake is then followed by LDPE which is the semi-crystalline with the second lowest amount of crystalline phase. HDPE showed the least uptake for limonene at 25°C and this is a result of its high crystallinity content. Overall, these results are in line with our expectations based on amorphous contents, and measurements shown in Figure 6. 16.
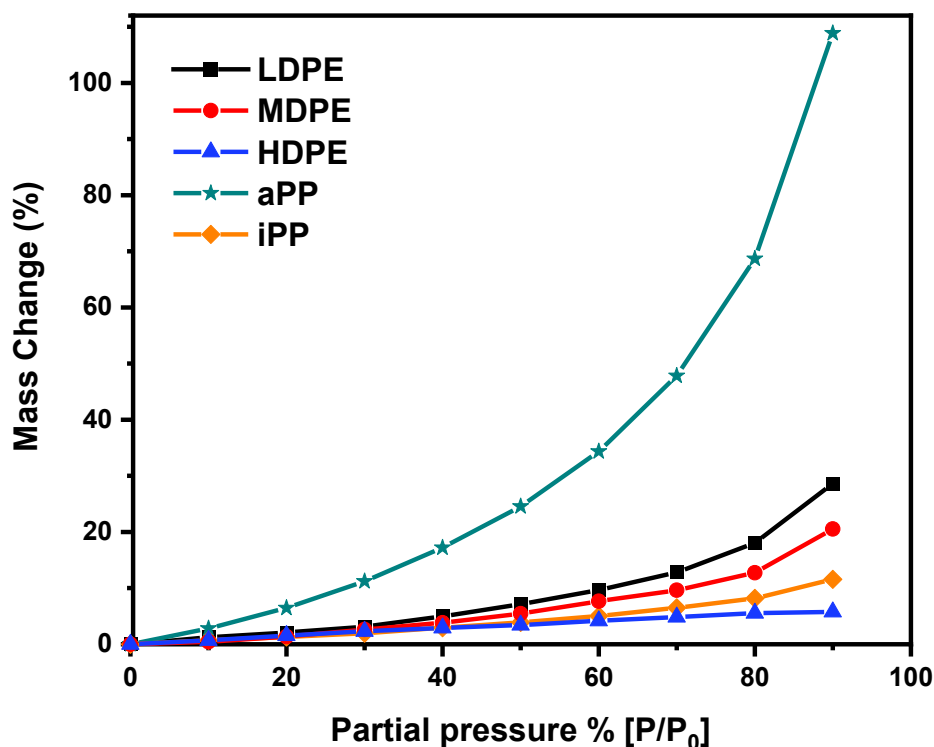
Figure 6. 16 Limonene vapour adsorption isotherms for different PP and PE molecular structures at 25°C. Error bars of 0.1% are smaller than the data symbols.

The effect of temperature on the solubility of fragrance molecules such as ethyl acetate in atactic PP based on sorption data is demonstrated in Figure 6. 17. The results show that temperature increased the extent of solubility for ethyl acetate in aPP increased. The shapes of the different isotherms are concaved, type III, similar to what has been shown by previous results, suggesting similar solubility behaviours at the different temperatures. The slopes of the isotherms are different suggesting that the partitioning constant, the solubility, vary and are higher at higher temperatures. At 55°C the isotherm is becoming more linear suggesting the polymer is getting closer to its T_g.
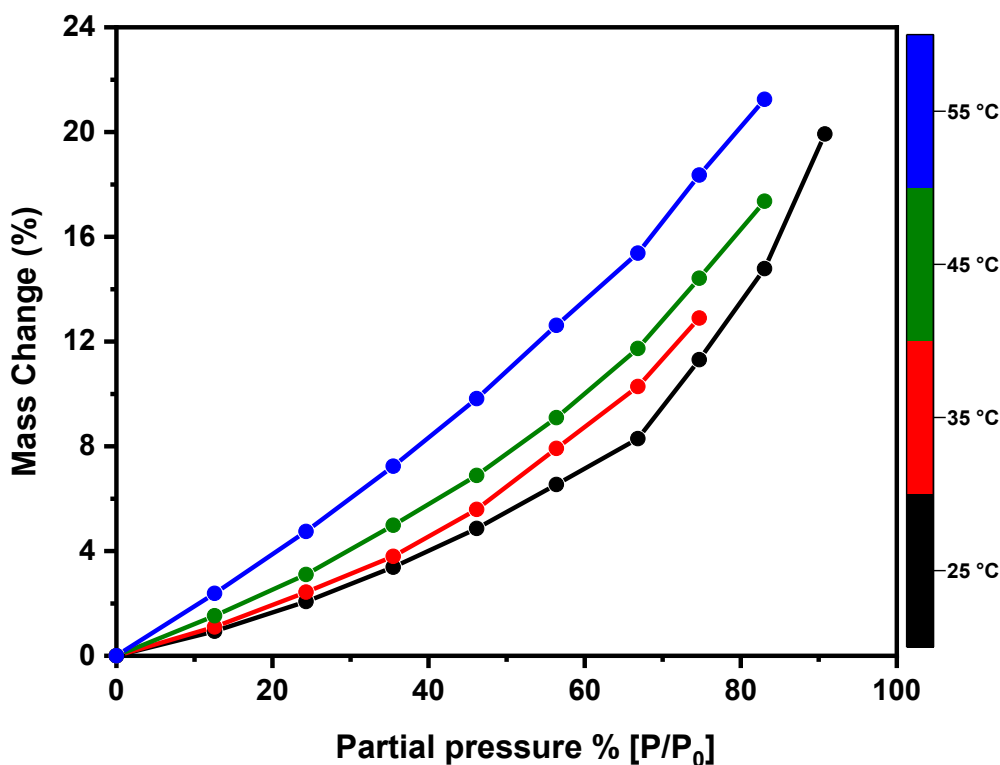
Figure 6. 17 Ethyl acetate adsorption isotherms at different temperatures for atactic PP. Error bars of 0.1% are smaller than the data symbols.

6.3.6 The effect of molecular structure of polymer on solvent uptake based on sorption data

The effect of polymer molecular structure on toluene sorption was studied at 25°C and the shape of the isotherms determined gravimetrically are typical for the sorption of organic vapours in rubbery polymers. Adsorption isotherms for toluene vapor were collected gravimetrically for LDPE, MDPE, HDPE, aPP and iPP. Figure 6. 18 shows the trend in mass change (%) as a function of toluene partial pressure. It is accepted that transport of small molecules in semicrystalline polymers takes place only in the non-crystalline region, assuming impermeable crystalline and permeable disordered regions. The data is in line with expectations and it demonstrated the highest mass uptake, (64%) for aPP which is the amorphous PP followed by LDPE, (19%) which is the PE with the lowest crystallinity out of the three PEs tested. The lowest mass uptake was recorded for HDPE, (4%) followed closely by iPP, (8%) both of which are semi-crystalline polyolefins with high degree of crystallinity, 64% and 50% respectively as determined by pycnometry.
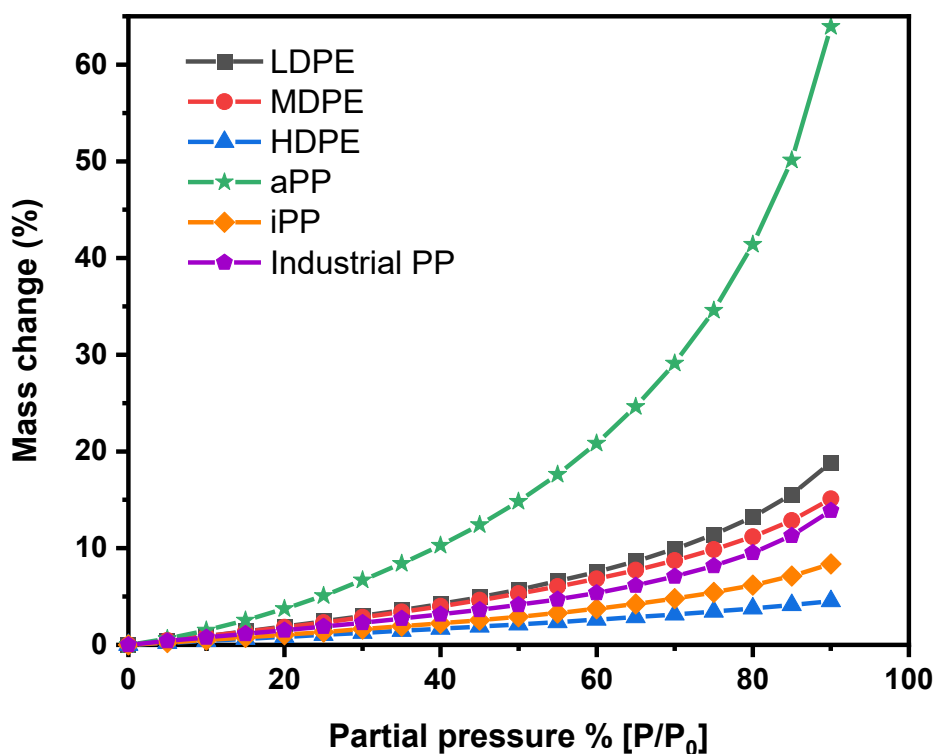
Figure 6. 18 Toluene vapour adsorption isotherms for different molecular structure PP and PE. Error bars of 0.1% are smaller than the data symbols.

6.3.7 The effect of polymer crystallinity on solvent uptake based on sorption data

The effect of polymer crystallinity on the sorption of different polyolefin samples was also studied and the results for two common solvents are shown in Table 6. 7 and Figure 6. 1. The data demonstrates a monotonic relationship where the solvent uptake is approximately scaled with crystallinity in a linear fashion; as crystallinity decreased, the solvent uptake increased. For highly crystalline samples such as HDPE, with ~ 50% crystallinity, there is low solvent uptake. Although there is ~ 50% amorphous content present in HDPE these amorphous materials are unable to sorb significant amounts of solute. As will be introduced in the following Section, for high crystalline content polymers, some of the amorphous material present is tightly constrained by ties with the crystalline domains, which effectively constrained polymer swelling and solute uptake.

Table 6. 7 Calculated % crystallinity values for different polymers determined using DSC and the corresponding % toluene and octane uptake at 90% P/P$_0$ measured using a DVS at 25°C.

Polymer Sample	DSC x$_c$ (%)	Toluene Uptake (90% P/P$_0$)	Octane Uptake (90% P/P$_0$)
aPP	0.00	64.00	80.30
LDPE	30.40	18.85	21.70
Industrial PP	33.74	13.90	15.90
MDPE	42.60	15.10	13.60
iPP	45.20	8.30	8.67
HDPE	47.73	4.52	3.70
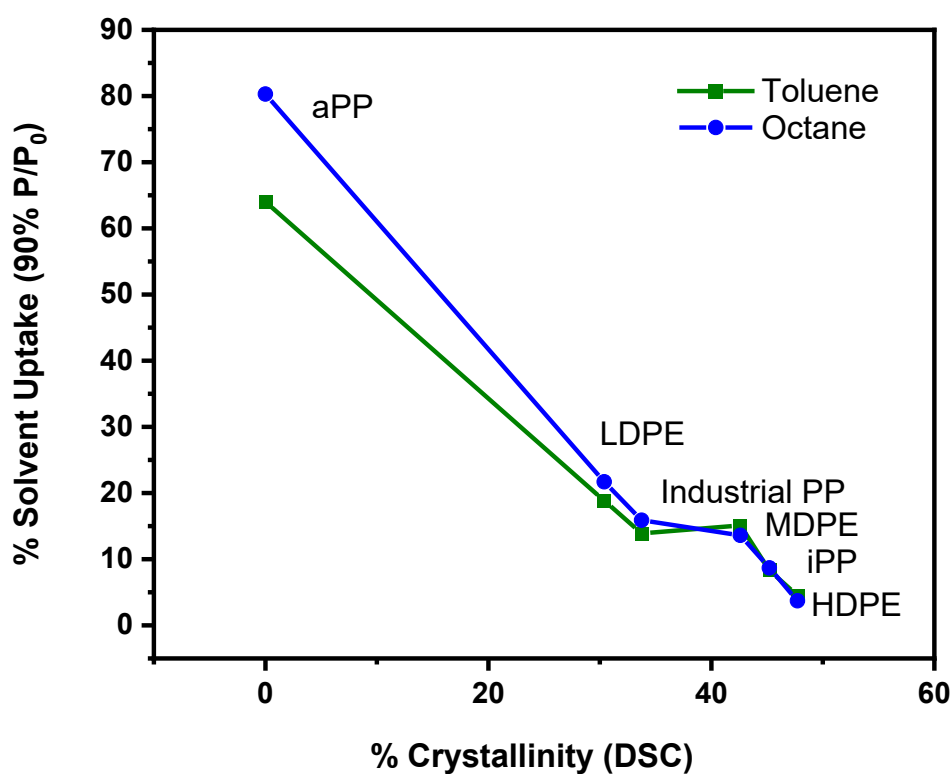
Figure 6. 19 Plot of maximum solute uptake (% w/w at 90 % P/P$_0$) versus % crystallinity of polyolefins measured using DSC.

6.4 Modelling of Small Molecule Sorption in PE and PP

6.4.1 Introduction to Modelling of Small Molecule Sorption in Polymers

Data on the sorption of small molecules in semicrystalline polymers can be obtained by experimental measurements and predicted using computational simulations. Experimental isotherm and adsorption research can be challenging, laborious, time-consuming, and expensive experiments to run. Therefore, prediction models have been developed over the years to describe sorption of small molecules in semicrystalline materials. Modelling of sorption of molecules in polymers is a significant area of research, and though not the focus of this thesis. However, it is important to review the current research status of modelling with relevance to this work. The rapid progress within computation tools, has expedited the progress of mathematical and molecular modelling as a tool which complements experiments. Such models can be categorised into two broad types, and include empirical, semi-empirical and theoretical models:

a) surface adsorption models
b) adsorbate/solute dissolution models

Table 6. 8 lists commonly used surface adsorption theories and polymer solution theories in approximate chronological order. Initial studies on adsorbate adsorption, only considered surface adsorption phenomena. Then work, in the 1940s start to consider bulk adsorbate sorption/dissolution phenomena and were initially based on the classic polymer solution thermodynamics of Flory–Huggins, and as these models developed in the 70s were extended to include dynamics and relaxation phenomena within the 'glassy' state. The more recent modern equations-of-state based approaches such as SAFT, reveal detailed thermodynamic insights into phase behaviour of polymers with solutes/adsrobates. Some of the earlier models are more empirical models include fit parameters and can be considered semi-empirical models as they don't deal with any detail at a molecular level. They ignore molecular shape and intermolecular potentials, when considering processes such as sorption of small molecules into polymers.

Table 6. 8 Common surface adsorption and bulk sorption theories, adapted from Jahn[460]

Theory	Year	Mode	Reference
Freundlich	1906	Surface	Freundlich, H.M.F. J. Phys. Chem. 1906, 57, 385-471
Langmuir	1918	Surface	Langmuir, I. J Am. Chem. Soc. 1918, 40, 1361-1402
Bragg–Williams	1934	Surface	Bragg, W.L.; Williams, E.J. Proc. Roy. Soc. 1934, A145, 699
BET	1938	Surface	Brunauer, S.; Emmett, P.H.; Teller, E. J. Am. Chem. Soc. 1938, 60, 309-319
Flory–Huggins	1942	Bulk	Flory, P.J. J. Chem. Phys. 1942, 10, 51-61
Oswin	1946	Surface	Oswin, C.R. J. Soc. Chem. Ind. 1946, 65, 419-42
Smith	1947	Surface	Smith, S.E. J. Am. Chem. Soc. 1947, 69, 646-651
Henderson	1952	Surface	Henderson, S.M. Agric. Eng. 1952, 33, 29–3
GAB	1966	Surface	Guggenheim, E.A. Application of Statistical Mechanics. Clarendon Press: Oxford, 1966, Vol.1, Ch. 11, pp 186- 207
Caurie	1970		Caurie, M. J., Food. Techn. 1970, 5, 301-307
D'Arcy–Watt	1976		Watt, I.C.; D'Arcy, R.L. J. Polym. Sci. Symp. 1976, 55, 144-166
Sanchez–Lacombe	1978	Bulk	Sanchez, I.C.; Lacombe, R.H. Macromolecules 1978, 11, 1145-1156
Simha–Somcynsky	1980		Jain, R.K.; Simha, R. Macromolecules 1980, 13, 1501- 1508
SAFT	1990	Bulk	Chapman, W.G.; et al. Ind. & Eng. Chem. Res. 1990, 29, 1709-1721
Vrentas–Vrentas	1991	Bulk	Vrentas, J.S.; Vrentas, C.M. Macromolecules 1991, 24(9), 2404-2412
Peleg	1993		Peleg, M. J. Food Proc. Eng. 1993, 16, 21-37
PHSC	1994		Song, Y.; Lambert, S.M.; Prausnitz, J.M. Chem. Eng. Sci. 1994, 49, 2765.
NE-LF	1996	Bulk	Doghieri, F.; Sarti, G.C. Macromolecules 1996, 29, 7885-7896
soft - SAFT	1997	Bulk	Blas, F. J.; Vega, L. F. Mol. Phys. 1997, 92, 135–150
Density functional theory -DFT		Surface	
SAFT-VR Mie EOS	2013	Bulk	Thomas L. J Chem Phys. 2013,139(15)
SAFT-γ Mie	2014	Bulk	Vasileios P. J. Chem. Phys. 140
Monte Carlo	2015	Bulk	Chunlei R, et al., Mathematical Problems in Engineering, 2015
UNIFAC free-volume model	2017	Bulk	Sturm DR, et al, Fluid Phase Equilibria,470, 68-74, 2018
SAFT-γ Mie EoS	2020	Bulk	Andrew J; Alfonso G and co-workers Chem. Eng. Data 2020 65,5862-5890

6.4.2 Modelling of Small Molecule Sorption in Polyolefins using SAFT

The statistical associating fluid theory, (SAFT)[461] appeared in the 1980s and since then it has been adopted and developed over the years into several different versions of the theory, including soft-SAFT[462], SAFT-VR[463], PC-SAFT[464], and more recently, SAFT-VR Mie[465]. The success of this approach derives from its molecular basis which has a firm foundation on statistical mechanics which provides a highly adaptable model. The theoretical development and background to the SAFT-γ Mie EoS has been presented in detail by Papaioannou et al.[466] and summarised by Dufal et al.[467, 468]. Here only a brief introduction to SAFT is provided.

The SAFT-γ Mie model used by Valsecchi, Galindo, and Jackson, our collaborators in the Department, has been used for predicting solute sorption isotherms in PE and PP. This model features a statistical mechanics model of the interlamellar amorphous domains assumed to be in a pseudo-equilibrium state, which determines the swelling of the tie-chains and tie-entanglements as a function of other thermodynamic variables, an idea originally put forward by Michaels and Hausslein in 1965. The model our collaborators have derived is a general model which allows to link the swelling constraint pressures to the morphological properties of the polymer such as the surface density of ties on the lamellae. The model can estimate the aforementioned properties and predict the variation of the lamellar thickness as a function of temperature, a phenomenon known as pre-melting. The solubility of a range of solutes in different samples of PE and PP was then calculated by treating the polymer melts with the SAFT-γ Mie EoS. Comparison with experimental data suggests that in order to accurately predict sorption close to the saturated vapour pressure of the penetrant it is essential to include the "free", unconstrained amorphous domains in the description, resulting in a model with two adjustable parameters which characterise the amorphous morphology of a given semi-crystalline polymer sample. The volume fraction of tied partially constrained, amorphous domains and the volume fractions of totally unconstrained amorphous.

6.4.3 Comparison of Experimental and Modelled Sorption Isotherms in PE and PP

A systematic experimental and modelling study of sorption isotherms of different small molecules in PE and PP was conducted. Figure 6. 20 shows comparison of experimental and SAFT-γ Mie modelled sorption isotherms for n-hexane in different polyethylene samples with varying degree of crystallinity. The computed isotherms are fitted to the experimental isotherms by simultaneously optimising values for the volume fraction ψ of fully amorphous polymer

chains and p_T the volume fraction of tied amorphous domains. These properties directly relate to the polymer system being characterised, its morphology, thermal history and structure.

The symbols represent the experimental data, and the solid lines represent theoretical calculations. Overall, the results in Figure 6. 20 demonstrated that the solubility of small molecules such as hexane in the amorphous domains of PE and PP is overpredicted by the modelling data, if the presence of the amorphous tie constraints is neglected. This observation is true for all the different samples. Hexane amorphous solubility in PE decreased with increasing crystallinity as shown in Figure 6. 20. Furthermore, for the same amount of amorphous phase solubility of hexane varies for the different PEs in the order of HDPE < MDPE < LDPE, suggesting that the amorphous domains of HDPE, MDPE and LDPE are somewhat different in nature. Similar behaviour was observed for other solutes and in other semicrystalline polymers such as polypropylene. The results overall suggested that only a fraction of the amorphous domains are freely available for sorption, resulting in an "effective" crystallinity which is higher than the normally calculated one.

Figure 6. 20 shows that for atactic PP the model predicts the solubility of hexane nearly perfectly. Since atactic polypropylene is fully amorphous, these specific calculations neglect any type of constraint in the amorphous domains; there are no parameters for fit. The agreement between the calculations and the experimental data for aPP confirms that the equation of state is well-suited to describe the PP-penetrant mixtures at ambient temperatures for an 100% amorphous polymer.

For isotactic PP which has amorphous domains (free and tied) and crystalline domains, solubility of hexane is overestimated by SAFT-γ Mie calculations. The isotactic PP and the industrial PP sample demonstrated similar experimental results for hexane solubility.
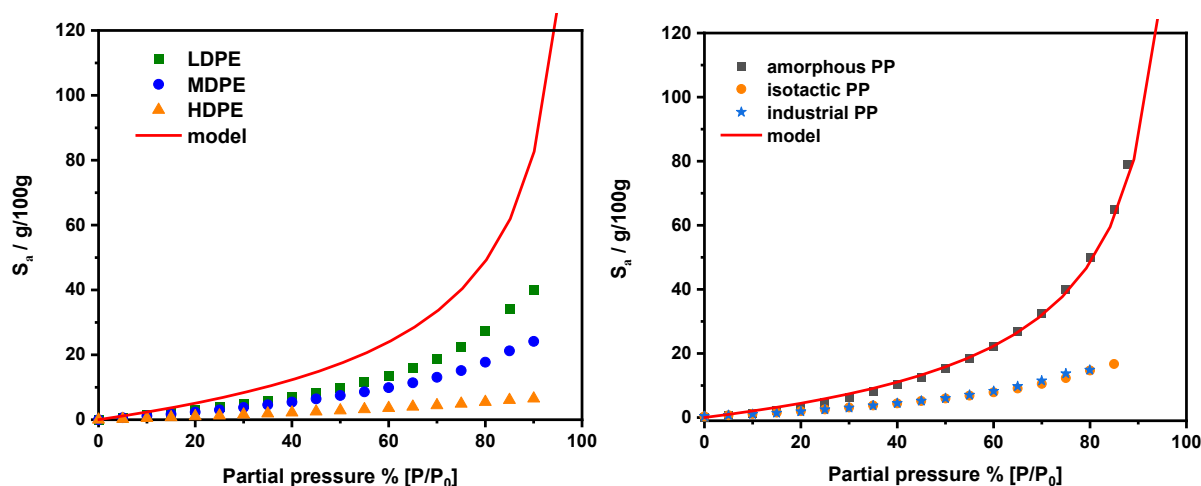
Figure 6. 20 Solubility of n-hexane in the amorphous domains of polyethylene (left) and polypropylene (right) at 25 °C. The solid curves represent SAFT-γ Mie calculations using the model of Papaioannou et al.[466] and the symbols experimental data. This data is included in the following pending publication "The effects of tie-chains and microstructure on the solubility of gases in semi-crystalline polymers" by M. Valsecchi et al.2022.

In Figure 6. 21 and Figure 6. 22 SAFT-γ Mie calculations for cyclohexane, n-hexane, and n-heptane solubility in LDPE and iPP polymer samples respectively were compared to experimental sorption data. The symbols represent the experimental data, and the solid lines represent theoretical calculations assuming that the crystallites are impermeable to the solute with optimised fit of ψ of fully amorphous polymer chains and p_T. Previous data showed that neglecting the presence of constraints, results in a systematic overprediction of the experimental sorption isotherms. However, if all the amorphous mass is subject to constraints – the curvature of the calculated sorption isotherms decreases significantly and the sorption at pressures close to the vapour pressure of the penetrant is better estimated if the low-pressure behaviour is captured. The experimental observation that the free amorphous content decreases with increasing crystallinity is consistent with other studies in the literature[270]. Figure 6. 21 data demonstrated that molecular structure of solutes affects amorphous solubility in LDPE and this characteristic is well predicted by the modelling data. In these plots, as the polymer is identical, the physical properties of the polymer including ψ and p_T are identical for all 3 solutes.

193
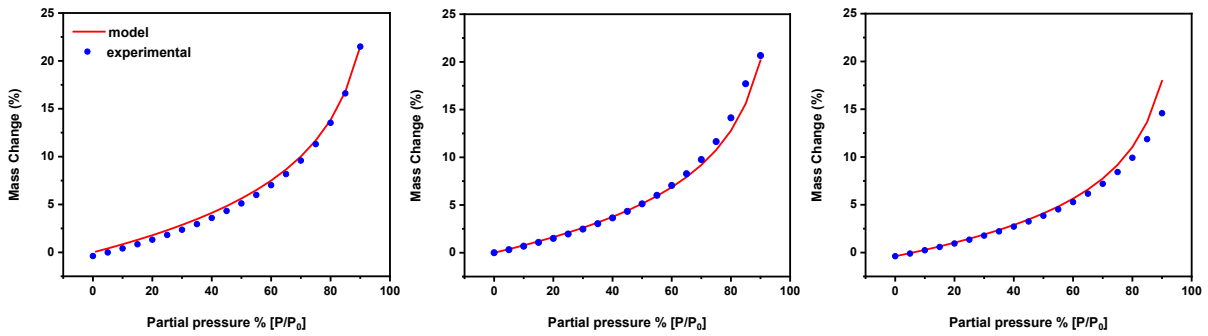
Figure 6. 21 Sorption isotherms of cyclohexane (left), n-hexane (middle), n-heptane (right) in LDPE samples at 25°C. Solid lines represent the model predictions with optimised fit of ψ and p_T. The symbols represent experimental data.
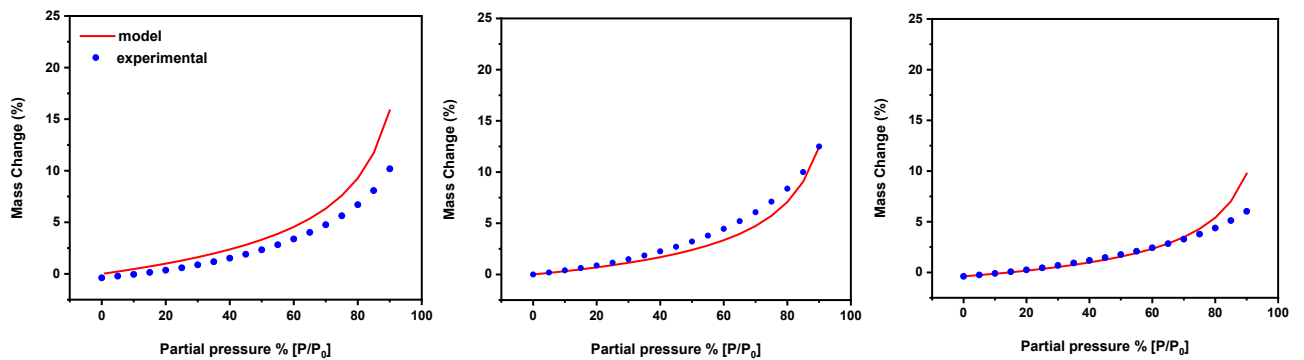
Figure 6. 22 Sorption isotherms of cyclohexane (left), n-hexane (middle), n-heptane (right) in iPP samples at 25°C. Solid lines represent the model predictions with the same values of ψ and p_T being used. The symbols represent experimental data.

The effect of temperature on solubility of small molecules in polyolefin was also studied experimentally and the results were subsequently modelled. Figure 6. 23 shows solubility of heptane in LDPE at 25, 35, 45 and 55°C and the corresponding modelled data. Up to 60% P/Po the model and experimental data agree for all temperatures, however at higher partial pressures and higher temperatures some variations are observed.

194
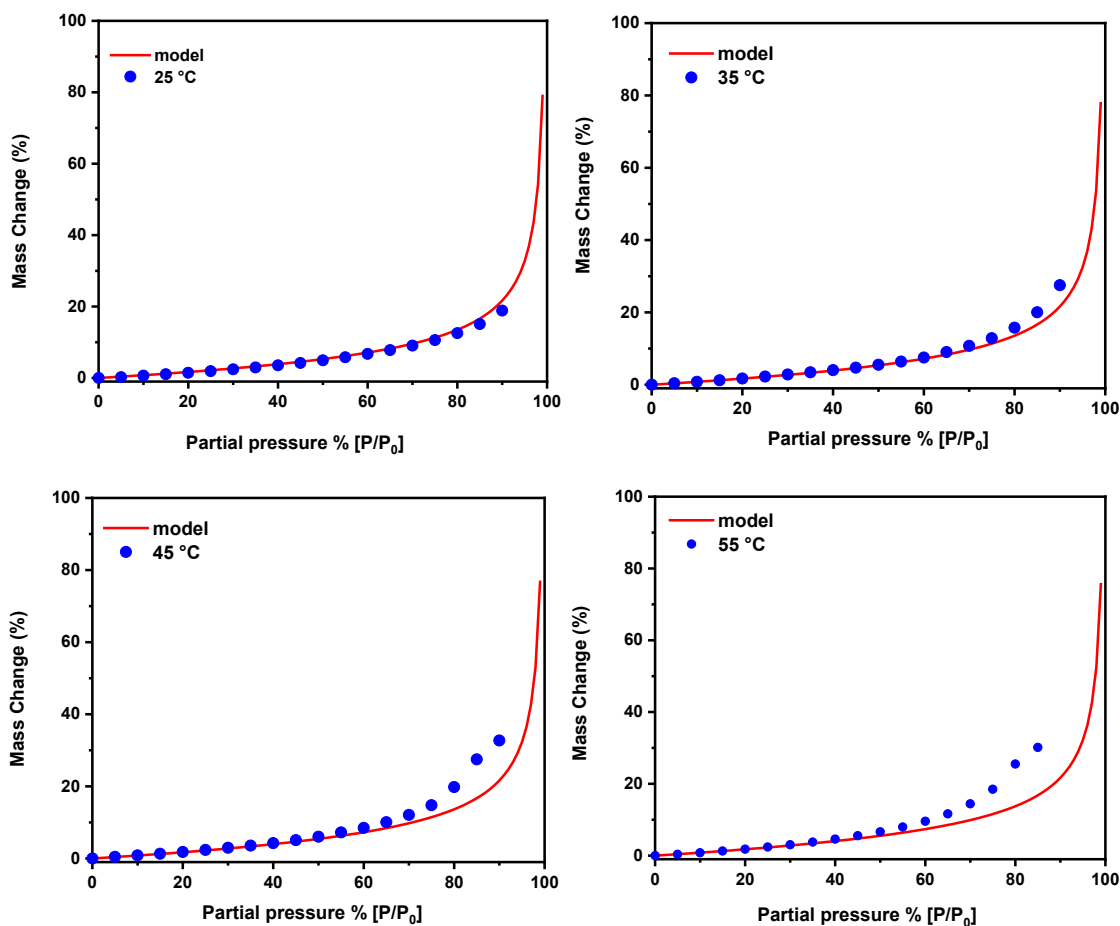
Figure 6. 23 Heptane solubility in LDPE at different temperatures, 25, 35, 45 and 55°C. Solid lines represent the model predictions. The symbols represent experimental data.

Figure 6. 24 shows the temperature dependence of the heptane solubility in iPP, (25, 35, 45 and 55°C) and the corresponding modelled data. The model and experimental data agree well for the different temperatures and across all the partial pressures studied, especially up to 70% P/Po. The experimental expectation was that as temperature increased so would the solubility of small molecules in polyolefins. This behaviour is also well predicted by the model for iPP.
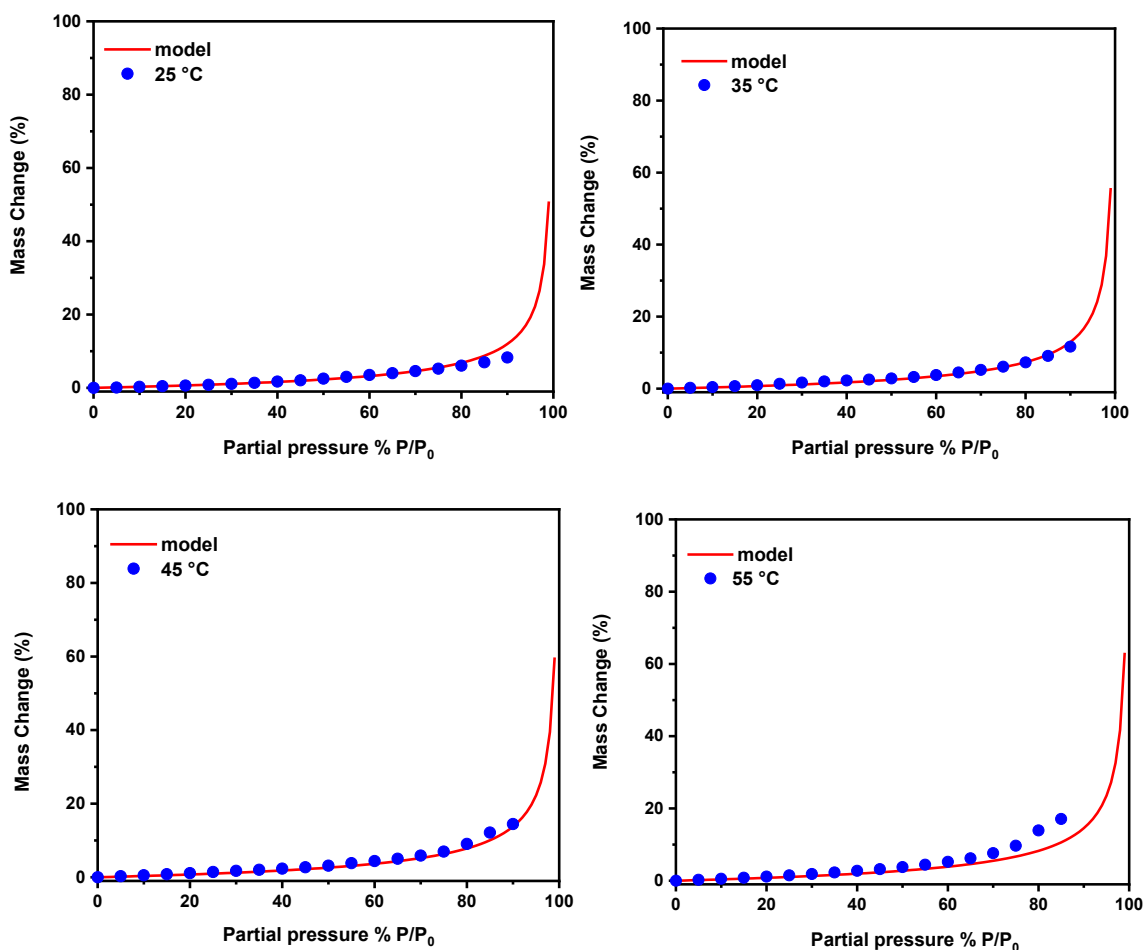
Figure 6. 24 Heptane solubility in iPP at different temperatures, 25, 35, 45 and 55°C. Solid lines represent the model predictions. The symbols represent experimental data.

6.5 Discussions

Generally, the sorption kinetics of organic solutes are slow for polymers and this implies that molecules have some distance to diffusion to achieve an equilibrium location, and therefore it is almost always the case that surface adsorption and bulk sorption is occurring simultaneously. The gravimetric studies presented in this Chapter highlight the dominance of bulk sorption behaviour by confirming the slow sorption kinetics and the large levels of solute uptake. As expected, the presence of crystalline regions decreased the sorption of permeant. The earliest models describing premelting[469, 470] assumed that all the inter-lamellar amorphous domains are composed of non-entangled loops. More recently, Albrecht et al.[471] assumed that these domains are only composed of a network of entangled segments and treated the network junctions (i.e., the entanglement or tie points) as constraints. The presence of a volume fraction of constrained amorphous domains with tie points is important as their presence can explain the observation of different solvent uptakes for polyolefin materials with the same volume fraction of crystallinity.

Temperature normally increase diffusion rates, and this effect was confirmed by the results shown in this Chapter. Furthermore, molecular structure of the solute influences its solubility into the polymer. Increasing molecular size, or rigidity, of the solute appeared to decrease the solubility. For industrially relevant samples impurities in the PE/PP specimens were believed to account for the higher solubilities observed. PE/PP are sometimes fabricated at high temperatures in the presence of atmospheric oxygen, the resulting polymers may contain oxygenated structures, more polarisable than double bonds in amounts depending upon their thermal history and formulation. The measured solubilities for commercial samples do not appear unreasonable for potentially slightly oxidised polymers.

The results included in this Chapter included a brief introduction to a modelling study conducted by our collaborators which demonstrate that DVS sorption data is a very sensitive to the amorphous polymer morphology. Therefore, you want to measure the % volume fraction of the amorphous domains as well as the tie versus free amorphous content in a sample, then DVS studies can be used to measure such properties. Once these properties are measured using a known hydrocarbon solute, then a SAFT model can then be developed to predict the isotherms for any potential solvent for a wide range of temperatures. This development is important because in practice there are sorption experiments that are impractical to do. Providing the correct materials descriptors of the amorphous domains are experimentally established, then these impractical experiments can then be conducted *in silico*.

This collaboration work has led to successful comparisons of my experimental data with model prediction of our collaborators. These new SAFT models appear to be superior to all other models at predicting sorption behaviour of small molecules in polyolefins and they have a sounds physical and thermodynamic basis. The results suggest that these models could be important in the future for modelling the sorption behaviour of all polymeric materials. In this work a thermodynamic model of semicrystalline polymers was studied. Each polymer sample was assumed to contain three distinct materials phase domains, in line with experimental observations. These were the crystalline lamellae, the inter-lamellar amorphous domains and the free amorphous domains. From the modelling perspective, the free amorphous domains were treated as a sub-cooled polymer melt. The lamellar stacks, on the other hand, are assumed to be a sequence of alternating layers of crystalline lamellae and homogeneous inter-lamellar amorphous material with a well-defined boundary with the lamellae. The modelling data has been concluded that the presence of tie-chains and entangled loops causes these domains to be subject to the constraint pressure[472]. This pressure makes the solubility of the penetrant lower in the inter-lamellar amorphous domains compared to the free amorphous

domains and explains the experimental observation that the amorphous solubility in semi-crystalline polymer samples is lower than the one calculated when assuming that all the amorphous domains are sub-cooled polymer melts.

6.6   Conclusions

This Chapter reports of the solubility of small molecules in polyolefins and demonstrates comparisons of experimental data with theoretical model predictions. The measurement of the percent crystallinity by DSC and pycnometry for these different polymers studied have also been reported here too. In semicrystalline polymers, solute diffusion is thought to be confined to the amorphous regions, where the diffusion is primarily classical Fickian in a glassy amorphous matrix. The degree of crystallinity and the morphological organisation have a large impact on the overall diffusion behaviour as well as solute solubility. Since most polyolefins are semicrystalline materials, they have a range of behaviour that can be traced to their morphology and structure. Polyethylene is available in various grades ranging from high-density to very-low density (co-) polymers. The amorphous morphology of polyolefins strongly influences its sorption properties. Most studies are usually concerned only with the crystallinity and non-critically adopt the classical two-component model of polyolefins, which considers a crystalline (rigid) and an amorphous (mobile) phase which is insufficient to explain the solute sorption processes in polyolefinic materials.

The studies presented in this Chapter provide an interesting comparison of experimental and theoretical predictions concerning the dissolution of organic small molecules in amorphous and semicrystalline PP and PE. Under appropriate experimental conditions the different organic solutes studied dissolved at a steady rate, but there were differences between them based on molecular weight, molecular structure, polarity, and temperature. Gravimetric studies using DVS instrumentation proved useful in understanding the sorption behaviour of different organic solvents in PE and PP over a range of temperatures. Factors controlling the sorption behaviour and kinetic have been identified and analysed. Among the factors identified as having a bearing on the extent of solute sorption by these polymers include:

- molecular weight of the solute
- the size of the solute molecules
- the thermodynamics of the polymer and solvent interactions
- the temperature
- the % crystallinity of the polymer
- the % of free amorphous and % of tied amorphous domains.

The dissolution of large range of small organic molecules in PP and PE have now been studied in here in detail.

It is accepted that transport of small molecules in semi-crystalline polymers takes place only in the non-crystalline regions. As reported from Kofinas et al[473], gas molecules are unable to permeate through the polymer crystallites, because they are insoluble into the material. Thus, the gas permeation into semicrystalline polymers is then confined into the amorphous regions. The reduction of crystallite permeability by organic solutes is due to the decrease in available volume of polymer for gas penetration and to a large tortuous path between the crystallites. The reduction in permeability value is proportional to the volume fraction of the crystalline phase.

In connection with the structure of the amorphous portion of polyethylene, it can now be reported that amorphous constraints exist, and these differ for different types of PE. Since the commercial manufacture of polyethylene-based materials is now accomplished by rather complicated production techniques, it is likely that the structure of the amorphous phase could be significantly influenced by the process variables. It is current practice to incorporate additives (i.e., antioxidant, slip and antiblocking agents, and modifiers) into polyethylene to assist in processing. The effect of these materials upon the vapor transport properties of these polymers has been investigated and reported in the experiments discussed in this Chapter.

DVS has been shown to have potential as an alternative polymer characterisation technique when there is a need to quantify the extent of both free and tied amorphous domains present in a semi-crystalline polymer. Indeed, once these descriptors have been estimated from an experimental solute sorption isotherm, then this knowledge of both free and tied amorphous domains will allow sorption behaviour for other solutes to be reliably predicted. Modelling has become important for the estimation of properties and the change in properties of materials when subjected to diffusion and sorption by external solutes. Behaviours of solutes in semicrystalline polymers have been extensively modelled over the years. Predicting the sorption of solutes in polyolefins is important for a vast number of applications including barrier films in the packaging industry, as their transport properties are dependent on the degree of solute dissolution. The new SAFT model developed by our collaborators and used in here to compare with the DVS isotherm data can only be applied if the lamellar structure does not undergo major changes during the experiments. If the temperature is too close to the melting point of the polymer or if the interaction between the penetrant and the polymer causes sudden irreversible changes to the structure, then this will invalidate the model. The model has been demonstrated here to work for polyolefin materials in temperature ranges in which the

amorphous domains of the polymer are rubbery. Although in this work the solute was an external fluid as a gas, the same framework can be applied to studying the sorption isotherms of liquids or super-critical fluids in contact with semi-crystalline polymers eg swelling. The only difference is that at equilibrium the sorption levels of liquids is much higher than that of gases. It is also likely to be easy to extend the current model to calculate the equilibrium sorption of multiple solute components in a given polyolefin.

7   Determination of Surfactant Loss Processes in Polyolefins

7.1   Introduction

Surfactants exist in a variety of forms, but they all contain a hydrophobic and a hydrophilic part. The degree of hydrophobic and hydrophilic character of surfactants is described by the hydrophile-lipophile balance (HLB) number[474, 475] which predicts solubility of surfactant in a solvent. Using this industrial classification system the HLB value can be used to predict the surfactant properties of a molecule[474] and is described in Table 7. 1. More detail about surfactants is provided in Chapter 2.

Table 7. 1 The hydrophilic-lipophilic balance (HLB) scale.

HLB number	Surfactant solution behaviour, solubility in water and application
< 10	Indicates lipid-soluble molecules (water-insoluble)
>10	Indicates water-soluble molecules (lipid-insoluble)
1 to 3	No dispersibility in water / represent anti-foaming agent
3 to 6	Poor dispersibility in water (milky dispersion) / represent water in oil emulsifier
7 to 9	Milky dispersion / represent wetting and spreading agent
13 to 16	Translucent to clear solution/ represent detergents
8 to 16	Represents an oil in water emulsifier
16 to 18	Clear solution/ represent a solubiliser or hydrotrope

The incorporation of surfactants within polymers is usually undertaken to modify the properties of the base polymer. For example, olefinic polymers such as polypropylene and polyethylene are hydrophobic by nature, but they can be made hydrophilic by a coating with surfactants. Wettable polymers are extensively used for designing products for different industries. In most applications, the durability of the wetting effect is desired to be long-lasting. However, the effectiveness of the some surfactant coatings is unfortunately found not to be permanent[298].

In Chapter 5, surfactant distributions and quantification on 3D for nonwoven polyolefinic fibers have been visualised. This information though relevant to the problem being examined here, it provides no insight on the chemical interactions between the polymers and the surfactants. There are known to be significant chemical interactions between non-polar, or weakly polar, organic species with polyolefinic materials, resulting in significant solubility, as have been clearly demonstrated in Chapter 6. The question naturally arises - can surfactants also dissolve in polyolefinic materials is a similar fashion to small organic solvent molecules? Evidence for

this phenomenon in the open literature is very limited, but the loss of surfactants from polyolefinic materials, via a yet as to be understood mechanism, is a well-established industrial observation. In the industrial application a nonwoven polyolefinic fibre network, (fibre diameter~10μm) is coated with a thin surfactant layer, (~100nm). With time the surfactant layer disappears. One hypothesis is that surfactants dissolve into the polymer nonwoven fibre over time. As discussed in Chapter 5, a method was developed to image nonwoven polyolefinic fibres with and without surfactants. However, this method doesn't reveal any information about the process by which surfactants disappear from these polymers.

This Chapter explores the solubility of surfactants in polyolefins and aims to propose reasons behind the surfactant loss processes. Despite its importance, there are limited number of direct studies concerning the migration of surfactants in polyolefins. Here efforts are focussed on answering the fundamental question – are surfactants soluble in PP/PE? Understanding the transport process of surfactants in polymers its important because a number of important practical applications depend wholly or in part on such systems. These applications include coatings (e.g., surfactant coatings, paints, and varnishes), packaging materials for foods and beverages, selective barriers for the separation of gas and liquid mixtures, biomedical devices, as well as the all-important personal hygiene products.

7.2 Thin Film Characterisation using Dynamic Vapor Sorption

Because of the small fibre diameters within the nonwovens, and the low surfactant concentrations in use, the surfactant layers are naturally very thin, and most likely to be 100's of nm thick. Therefore, the use of experimental techniques that can examin thin films of this dimension is logical. Therefore, in this Chapter thin film samples of both polymer films and surfactant layers will be investigated.

7.2.1 Water uptake analysis on a reference sample, a plain aluminium foil.

A cleaned aluminium foil blank sample was tested for water uptake using a typical 0-90-0%RH cycle in a DVS Resolution (Surface Measurement Systems, London, UK). This Al foil is reference data for baseline measurements. The measurements were carried out at atmospheric pressure under dry air flow of 200 ml/min, T = 25°C. Figure 7. 1 shows the kinetic mass profile (left) and the corresponding sorption isotherm (right). The data suggests that a monolayer of water forms on the aluminium foil with an associated 0.04% mass change. These

very low uptake levels correspond to sub-monolayer levels of water adsorption as would be expected for these blank reference samples.
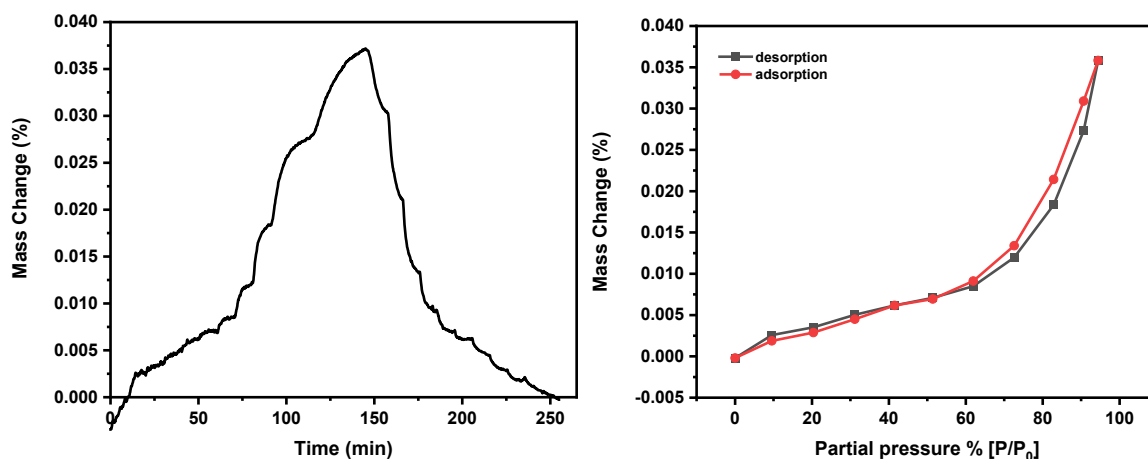
Figure 7. 1 Kinetic mass profile (left) and corresponding sorption isotherm (right) of water vapour interacting with an aluminium foil. Note error bars of 0.01% are smaller than the data symbols.

7.2.2 Water uptake analysis on a reference sample, MDPE film.

A cleaned aluminium foil sample dip coated with MDPE, was tested for water uptake using a typical 0-90-0%RH cycle in a DVS Resolution The measurements were carried out at atmospheric pressure under dry air flow of 200 ml/min, T = 25°C. Figure 7. 2 represents the data for the water sorption experiments for this thin MDPE film. The results are consistent with water monolayer formation, as the mass change is small, less than 1%.
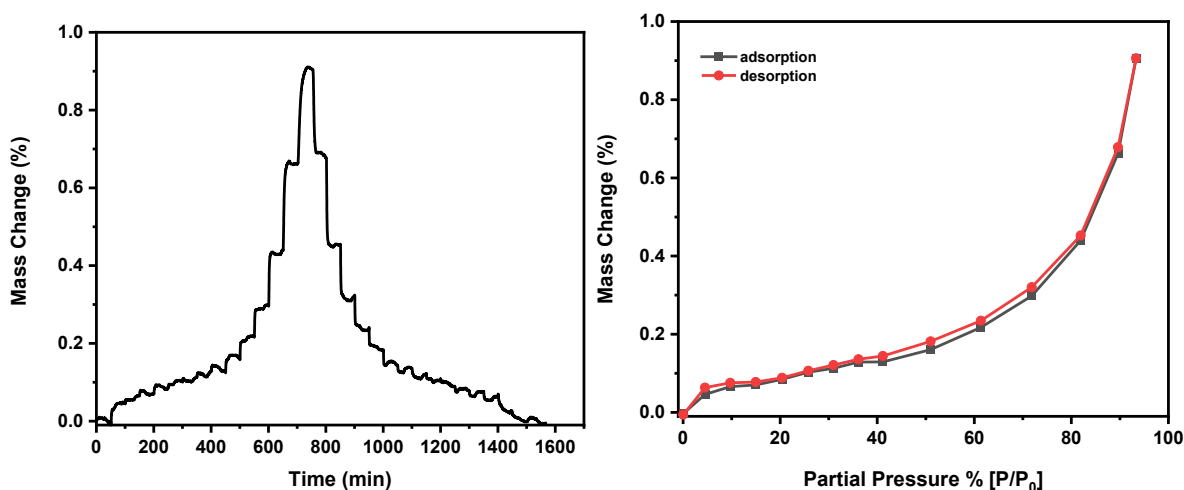
Figure 7. 2 Kinetic mass profile (left) and corresponding sorption isotherm (right) of water vapour interacting with thin polymer, (MDPE), film coated onto an aluminium foil. Note error bars of 0.01% are smaller than the data symbols.

203

7.2.3 Water uptake analysis on a reference sample, surfactant, Silastol PHP-26, film

A cleaned aluminium foil was sample dip-coated with surfactant; 2% PHP w/v in IPA. This foil was tested for water uptake using a typical 0-90-0%RH cycle in a DVS Resolution. The measurements were carried out at atmospheric pressure under dry air flow of 200 ml/min, T = 25°C. Figure 7. 3 shows the kinetic mass profile (left) and the corresponding sorption isotherm (right). The data demonstrate a 50% increase in mass for the foil coated with a film of the surfactant PHP following exposure to 80% RH.
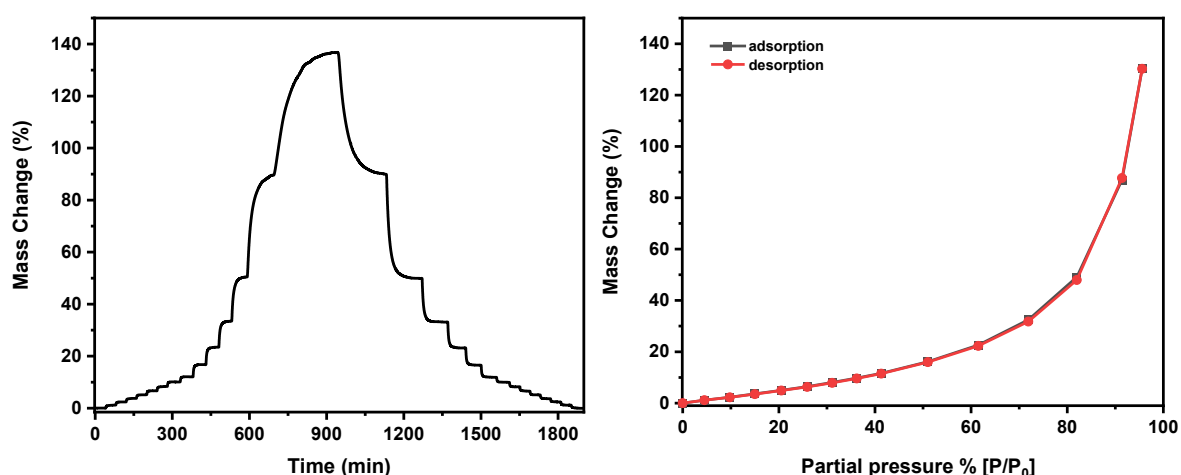
Figure 7. 3 Kinetic mass profile (left) and corresponding sorption isotherm (right) of water vapour interacting with thin surfactant, Silastol PHP-26, film coated onto an aluminium foil at 25°C. Note error bars of 0.01% are smaller than the data symbols.

The experiment was repeated at 50°C and 70°C. Figure 7. 4 shows the sorption isotherms for 25, 50 and 70°C. The data demonstrate a decrease in mass uptake as temperature is increased. This is expected because water is more likely to evaporate as the temperature is increased than stay dissolved into the surfactant film. The data demonstrated the high solubility of water in these thin surfactant layers.
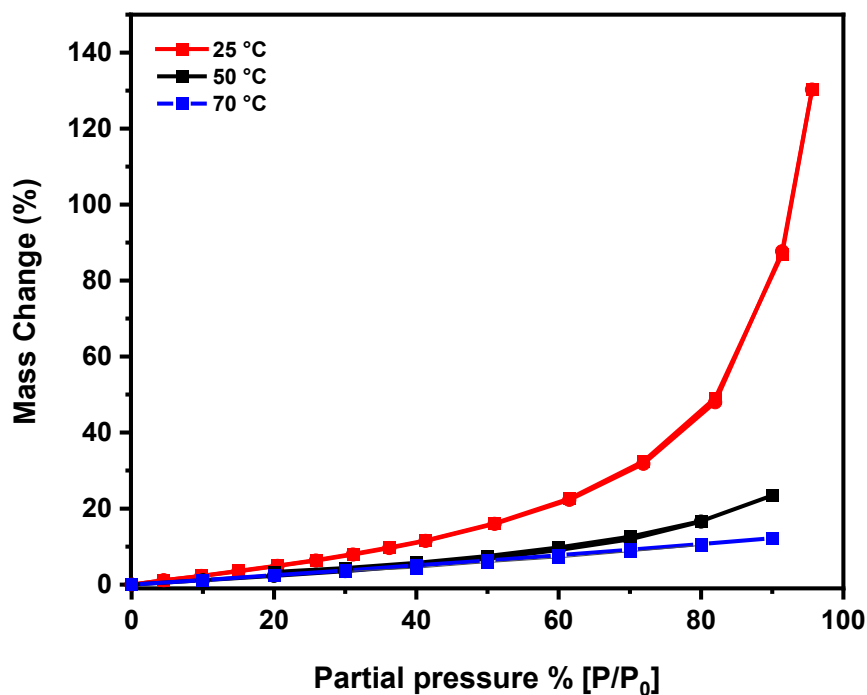
Figure 7. 4 Sorption isotherms of water vapour interacting with thin surfactant, Silastol PHP-26, film coated onto an aluminium foil at 25, 50 and 70°C.

7.3 Aging Studies

7.3.1 Aging of Surfactant Coated Nonwovens

The aging effect of surfactants coated onto polymer based, PP, nonwoven fabric was studied using a DVS Endeavour, (Surface Measurement Systems, London, UK). Five nonwoven fabric samples of about 100mg, were washed in IPA and left to air dry overnight in a fume hood. Three of these were dip coated using Silastol PHP-26, in 0.5, 1 and 2% PHP (w/v in IPA) and left to air dry overnight in a fume hood. Two surfactant free samples of nonwovens were used as blanks. All samples were folded into smaller units to keep them compact in size and hang on the DVS sample hook. All five samples were tested for water uptake simultaneously. A series of experiments were carried out using fixed times for each experimental humidity setpoint. Water adsorbed quantities were calculated using the change in mass between the ends of the current cycle's adsorption and previous cycle's desorption step. Before the sorption kinetics, the sample was first dried in the DVS chamber to 0% RH at 25 °C (below T_g) for 60 min to establish a dry mass. After a dry mass was achieved, the sample was exposed at a fixed temperature, either at 50°C and 70°C to the following RH profile: from 0 to 80% and then back to 0, each cycle took 18 hours.

Figure 7. 5 presents the experimental data for the actual water sorption by material by mass between the 0 and 80 %RH as a function of time for five different PP based nonwoven samples. The differences in these, 0-80% RH water uptake, reflects the different amounts of the hygroscopic surfactant present on the polymer surface. These results shows that there is a difference in the amount of surfactant in each material based on the magnitude of the mass differences between the different samples. This data therefore indicated that the amount of surfactant present is decreasing with time as 0-80% RH water uptake is decreasing for the 3 surfactant coated samples. This indirect measurement method demonstrates that the amount of surfactant, (by a factor of 3) scales approximately with the surfactant coating levels, (by a factor of 4) and that more surfactant is lost when more surfactant is present. The data shows that the mass of the blanks surfactant free samples remained constant during the 10 days of the experiment.
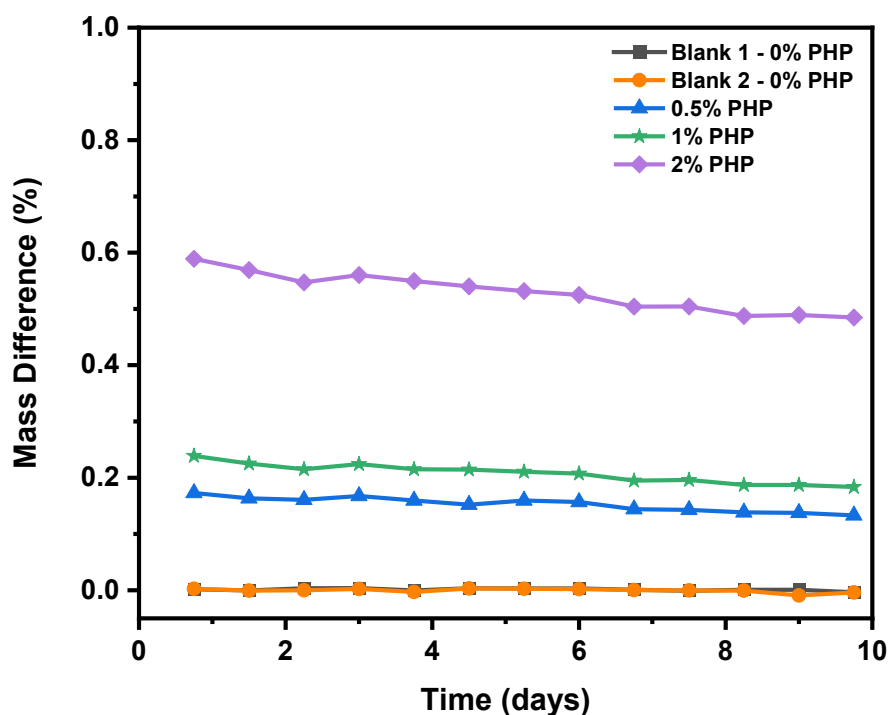
Figure 7. 5 Experimental mass loss difference between 0 and 80% RH as a function of time for PHP solution coated polymeric nonwovens samples studied at 50°C. Note error bars of 0.01% are smaller than the data symbols.

Reference experiments shown in Figure 7. 5 show that at 50°C and between 0-80% RH there is a 17% water uptake for a pure surfactant sample. Since there is a 6:1 ratio between surfactant mass and water uptake mass, actual amounts of surfactant mass loss can be calculated for the different surfactant loaded samples. Figure 7. 6 shows the calculated surfactant mass losses as a function of time. A linear trendline for each data set has been drawn and the slope of the line is indicative of the loss of surfactant. The amount of material

that is being lost as a function of time scales with the amount of surfactant that is present in the sample, the larger the slope, the large the amount of surfactant loss.

This data is important in two ways. Firstly, it shows direct quantification of how much surfactant is present and the scaling is broadly in the order expected. From the lowest to the highest surfactant loading, it should be a factor of 4, and the data confirms that it is approximately by a factor of 4. Also, the order is correct for each different surfactant loading. Secondly, this measurement is an absolute determination of the amount of surfactant present in a sample at a given time and under specific conditions. One thing to note is that there has been no correction for water uptake on the substrate. That has a minimal effect on the results for the 2% PHP sample, but it could have a small effect for the lower concentration sample data.

The plot displays the following fitted equations:

$y_{(2\%)} = -0.07686x + 4.2634$

$y_{(1\%)} = -0.03285x + 1.6374$

$y_{(0.5\%)} = -0.02495x + 1.3354$

$y_{(0\%)} = -0.00119x + 0.2588$

$y_{(0\%)} = -0.00153x + 0.29945$
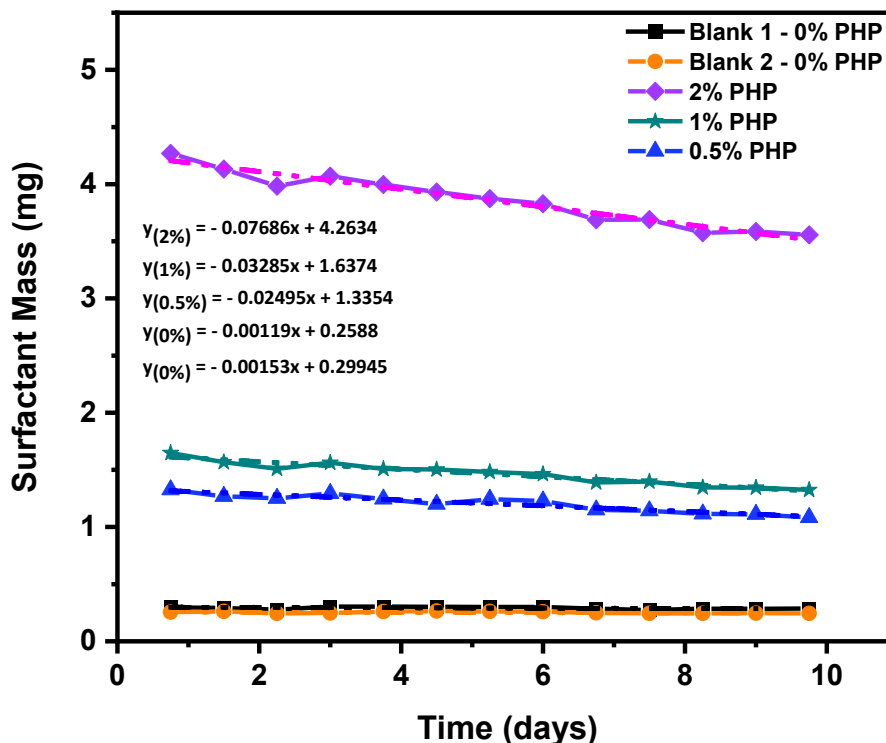
Figure 7. 6 Estimated surfactant, (PHP) mass loss between 0 and 80% RH as a function of time studied at 50°C. Note error bars of 0.01% are smaller than the data symbols.

The aim of these studies was to establish if water uptake decreased as amount of surfactant decreased due to aging affects. Figure 7. 7 results show initial high mass loses. The data suggest that over time surface surfactant concentration of fibres decreases, making the surfactant treated samples more likely to become hydrophobic and this behaviour is why there is a decrease on water uptake over time. Over the first few days, the mass loss appears to be dominated mainly by slow water loss- drying. However, after ~4 days as the water loss is completed and surfactant loss become the dominant mass loss mechanics. So, all the mass loss observed after that initial 4 days period can be attributed to surfactant loses, which are

207

small but clearly evident. As the surfactants are lost presumably to evaporation over long time, the amount of surfactant present decreases and therefore a smaller 0-80%RH water uptake is observed over time and hence reduction in total mass.
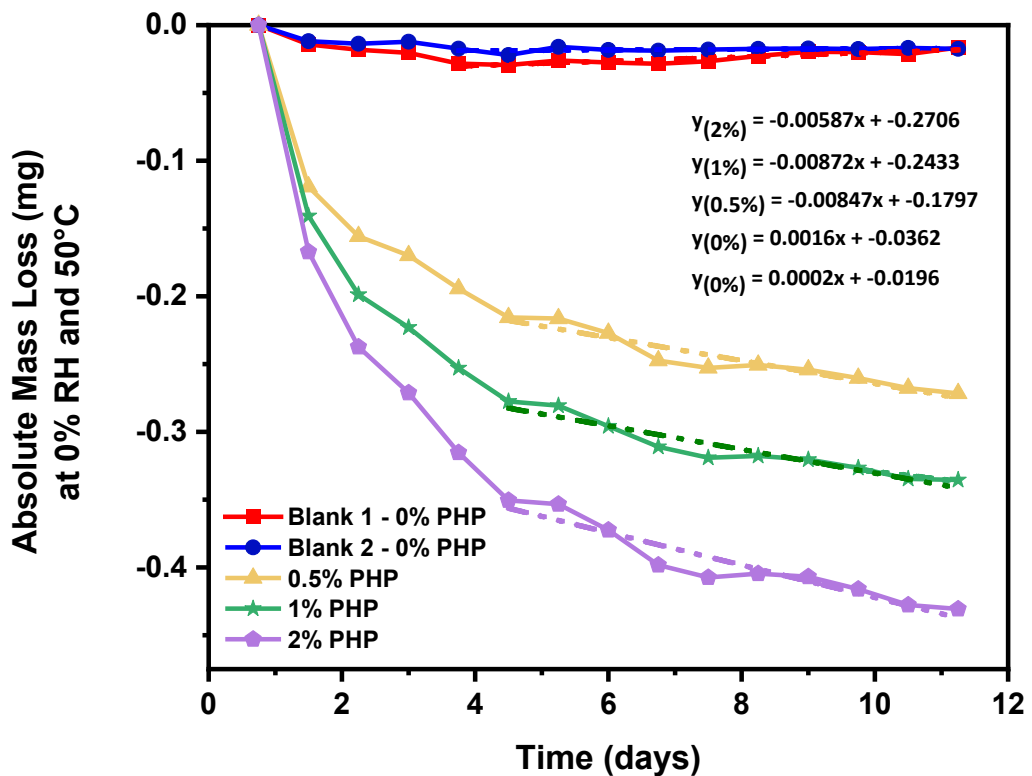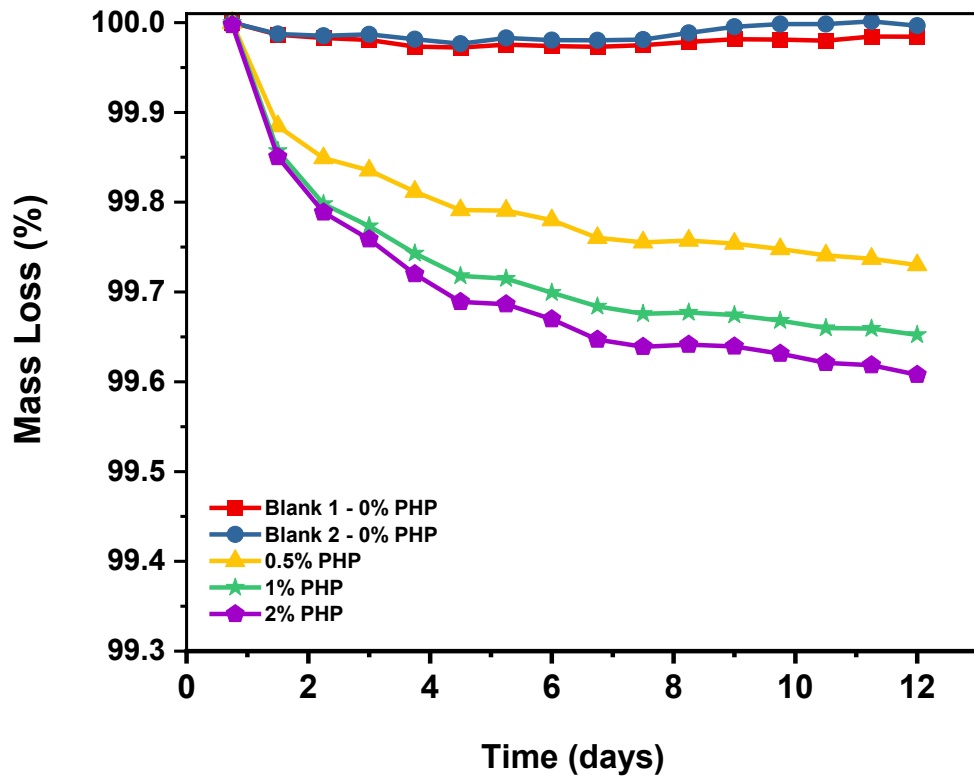
Figure 7. 7 % mass loss (top) and as absolute mass loss (bottom) plotted as a function of time for PHP solution coated polymeric nonwoven samples studied at 50°C and 0% RH. Note error bars of 0.01% are smaller than the data symbols.

The experiment shown in Figure 7. 7 was repeated at 70°C. The data demonstrates that surfactants are lost as a function of time and this depends on temperature i.e., it increases in an Arrhenius fashion. Figure 7.122 data shows that the mass of the blanks remained constant during the experiment even at 70°C. However, the surfactant treated samples reduced in mass over time and at elevated temperatures the loss was greater. This shows that temperature increases the surfactant loss process for PP based nonwovens.
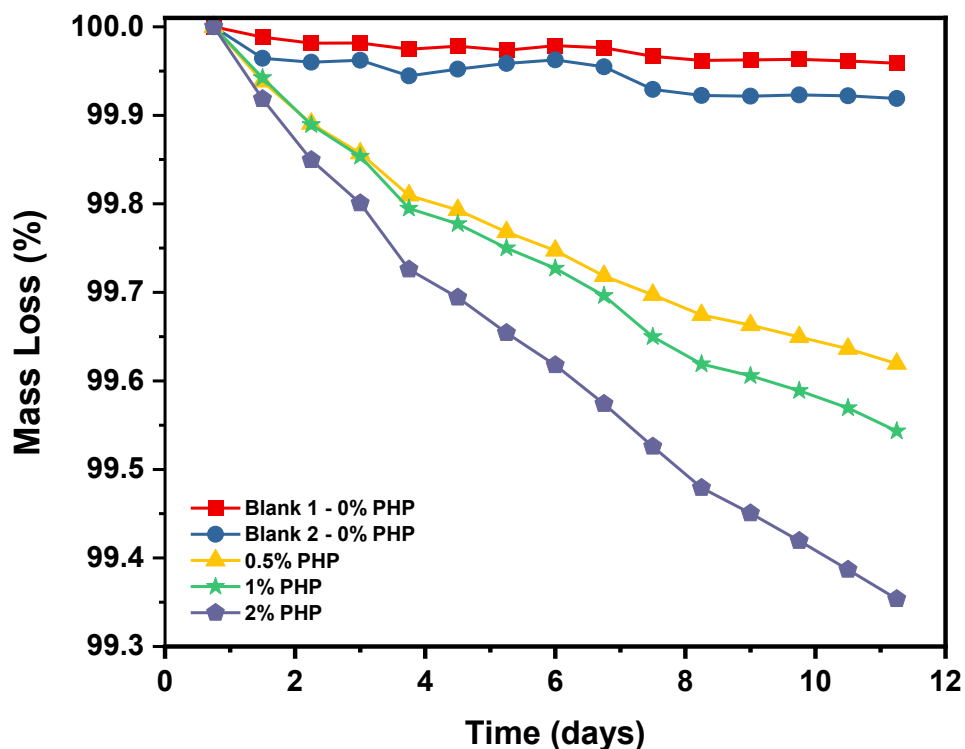
Figure 7. 8 Mass as a function of time for PHP solution coated polymeric nonwovens samples studied at 70°C and at 0% RH. Note error bars of 0.01% are smaller than the data symbols.

Table 7. 2 summarises the calculated rate of loss for surfactants for different loadings on nonwoven samples studied at 50°C. The results compare absolute mass loss rates at 0% RH with mass loss rates based on changes in the 0-80% RH water sorption for the different samples studied. It appears the rate loss for the two different methodologies are not fully comparable but follow the trends observed by the experimental data, i.e., surfactant loses increase as a function of surfactant concentration. This data shows that the physical rate of mass loss is 10 times lower than the rate of surfactant loss predicted based on the 0-80%RH water sorption experiments. The blank sample data sets agree for both methods.

Table 7. 2 Calculated rate of surfactant mass loss for different surfactant loaded nonwoven samples studied at 50°C. Comparison of total mass loss rates with estimated surfactant mass loss rates.

Samples industrial nonwovens (w/v in IPA)	Estimated Rate of Surfactant Mass Loss between <u>0 and 80% RH</u> (mg/day)	Rate of Total Mass Loss at <u>0% RH</u> (mg/day)
Blank 1 – 0% PHP	- 0.00153T* + 0.29945	0.0002T - 0.0196
Blank 2 – 0% PHP	- 0.00119T+ 0.2588	0.0016T - 0.0362
Nonwoven – 0.5% PHP	- 0.02495T + 1.3354	-0.00847T - 0.1797
Nonwoven – 1.0% PHP	- 0.03285T + 1.6374	-0.00872T - 0.2433
Nonwoven – 2.0% PHP	- 0.07686T + 4.2634	-0.00587T - 0.2706

Note: T is time in days

Overall, water sorption for all the surfactant loaded nonwovens goes down with time which suggests that there is less surfactant, and the mass goes down with time which suggests less mass. Therefore, it is reasonable to assume that less mass means less surfactant present. The evaporative losses at 50°C and 70°C appear to be small but they are measurable. The rates of mass loss have been calculated using the Arrhenius Equation. The data for 25°C has been extrapolated. The calculated data are shown in Table 7. 3 and Table 7. 4. These are energy activated processes and therefore temperature dependant and that is why the rate of loss measured varies for the two different temperatures. The results suggests that the 3% surfactant present in the 2% loaded sample should last for 16 years if stored at 25°C based simply on surfactant evaporation. However, this prediction does not agree with industrial experience which indicates that this type of coating lasts for about 6-12 months. The experimental data so far has revealed surfactant losses via evaporation, but this process alone doesn't account for all the losses measured.

Table 7. 3 Calculated evaporation losses at different temperatures and for different surfactant loaded nonwoven samples.

Temperature (°C)	1/T (k^{-1})	Rate of Mass Loss (%/day)			Number of Days to 100% PHP loss
		0.50 %	1.00 %	2.00 %	2.00 %
50 (Experimental)	0.0031	-0.0057	-0.0067	-0.0084	356.1
70 (Experimental)	0.0029	-0.0182	-0.0310	-0.0446	67.3
25 (Predicted)	0.0034	-0.0011	-0.0008	-0.0008	3911.6

Table 7. 4 Calculated activation energy and temperature dependant experimental evaporation rates, using Arrhenius equation, for different surfactant loaded nonwoven samples.

Temperature (°C)	Ln (Drying Rate Constant)		
	0.50%	1%	2%
50	-5.166	-4.999	-4.951
70	-4.006	-3.475	-3.111
Slope	-6.426	-8.440	-10.192
$E_{activation}$(kJ/mol)	-53.40	-70.14	-76.68

Figure 7. 9 demonstrates that the 2% loaded sample requires more energy to evaporate. This suggests that the process is thermally activated which is common with most such processes, the higher the temperature the faster the rate. For evaporation it is expected the reaction rate to change with temperature and this appears to be the case.
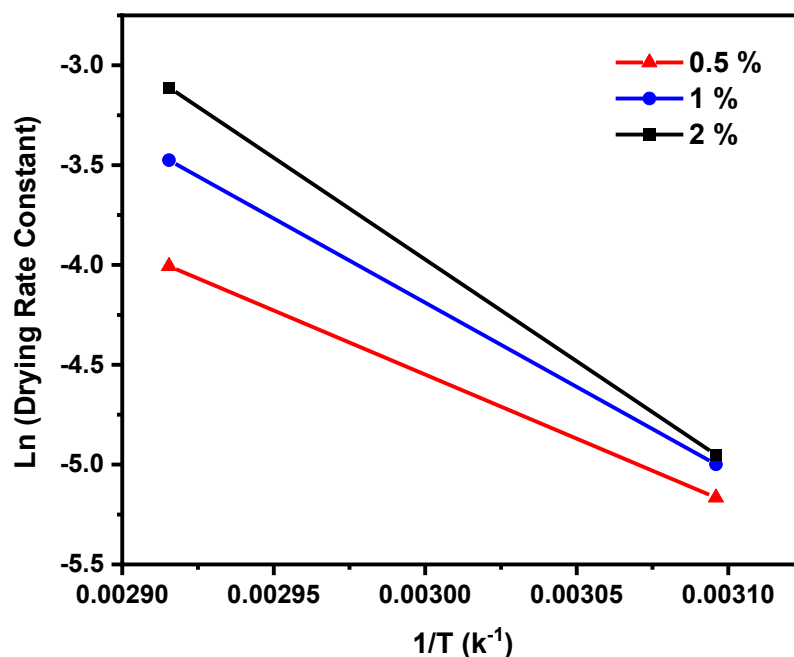
Figure 7. 9 Arrhenius plot for surfactant evaporation for different surfactant loadings.

Overall, the experimental data presented in this Section demonstrated that surfactants are being lost and at different temperatures the rates of loses are consistent. The DVS data confirms that some of the loss is due to very slow evaporation over time. However, simply based on evaporation, the surfactant loss process appears to be much slower than expected based on industrial observations (i.e., it takes years rather than months). Therefore, evaporation doesn't appear to be sufficient to account for all the losses expected; evaporation cannot be the only factor affecting the surfactant loss process. Some mass loss could be attributed to slow drying, residual solvent losses and maybe some small free water losses too, however something more significant is suspected to be responsible for the unaccounted losses observed experimentally.

The working hypothesis which will be explored in the remainder of this Chapter is that surfactant loss in these industrial materials is driven by two processes, evaporation, and dissolution. This current study is the first time that water uptake has been used as a proxy for presence of surfactants. In this way it was found that surfactant loss is more than just surfactant evaporation.

7.3.2   Aging of Surfactant Coated Model Polymer Films

To understand what happens in real industrial samples, model polymer substrates were coated with surfactants for investigated. Experiments were conducted to measure the behaviour of a

213

thin film of surfactant coated onto a thin polymer film on an inert substate. A set of aluminium foils pre-coated with a thin polymer layer of LDPE, HDPE, commercial PP, iPP and aPP were dip coated with a 2% w/v solution mixture of PHP, (Silastol PHP-26) in IPA. These were left to air dry overnight. Consecutive experiments of water vapour measurements were carried out and the sorption profiles of polymer-surfactant films were determined using a DVS Resolution. Samples ranging between 100-140mg in mass, of which typically 100mg of Al foil, ~ 5 - 20mg would be polymer coating and ~ 0.5 - 3mg would be surfactant film, were studied. The list of the different samples studied, and their weights is presented in the Table 7. 5.

A series of vapour sorption experiments were carried out using either fixed times for each adsorbate's experimental partial pressure setpoint or % dm/dt threshold. Methods were run in (0 - 90% P/Po) cycles with increments of 10% P/Po steps. Adsorbed quantities were calculated using the change in mass between the ends of the current cycle's adsorption and previous cycle's desorption step. The measurements were carried out at atmospheric pressure under dry air flow of 200 ml/min, T = 25°C. Measurements for each set of samples were repeated 4 to 5 times sequentially and the amount of water dissolved in the material was monitored and this quantity has been used as a proxy to the amount of surfactant present in the material at a given time.

Table 7. 5 List of polymer-surfactant coated aluminium foil samples studied and their mass.

Polymer Samples	Polymer + Surfactant / Silastol-PHP 26 mg (± 0.0001 mg)	Polymer (± 0.0001 mg)	Surfactant / Silastol-PHP 26 (± 0.0001 mg)
LDPE	25.4298	22.4437	2.9861
MDPE	8.6997	5.8857	2.8140
HDPE	9.4541	7.9919	1.4622
Commercial PP	12.2914	10.5553	1.7361
Atactic PP	21.2333	19.9092	1.3241
Isotactic PP	20.4831	19.9744	0.5087

Figure 7. 10 shows a drying curve for a LDPE-PHP film coated aluminium foil during consecutive experiments of water vapour measurements with a DVS at 25°C. The data shows a very clear initial solvent drying process followed by a long-term mass loss of ~0.434% over 14 days. The long-term mass loss seems to be independent of humidity and therefore the loss cannot be attributed to water molecule loss, drying. The proposal is that the mass loss is due to something else other than water molecules and a reasonable explanation is that this is due

to the loss of surfactant via evaporation, since aluminium foils are inert, and no surfactant solubility is likely. These surfactant losses are very small and don't account for the surfactant losses observed in practice. Initial solvent mass losses were observed for all experiments and it was difficult to establish exactly when the transition between solvent loses and surfactant loses happened. However, day 4 has been chosen as the cut off point for all the experiments to minimise associated uncertainties.
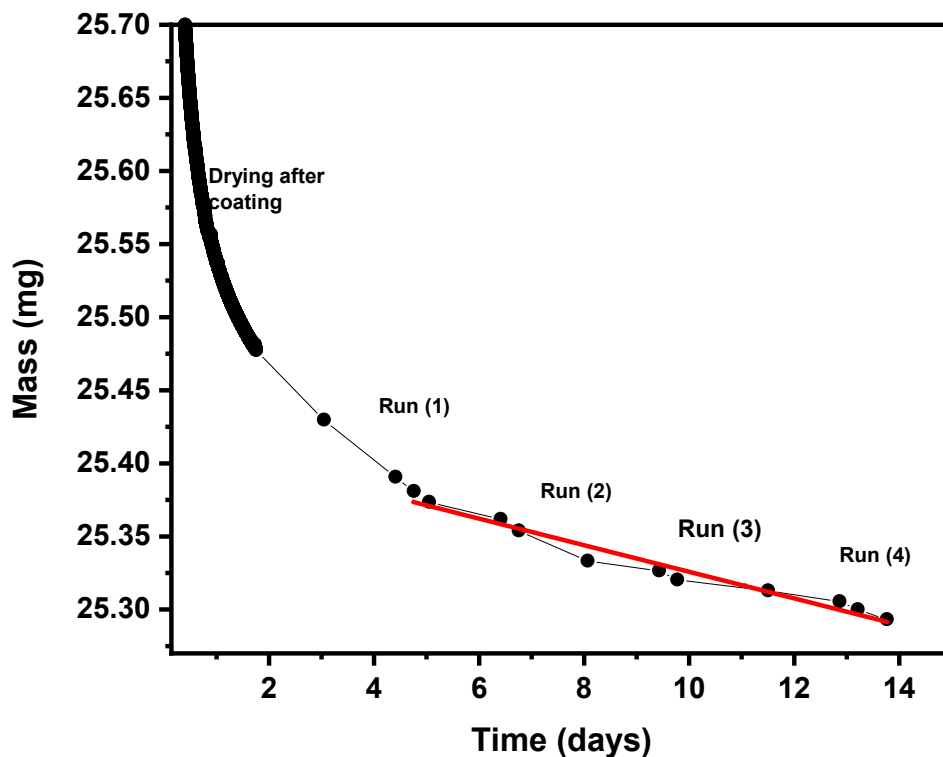
Figure 7. 10 Evolution of mass profile of LDPE-PHP film coated onto an aluminium foil during consecutive experiments of water vapour measurements with DVS. Each experiment cycle is represented by 3 dots, 1st = initial sample mass, 2nd = final sample mass and 3rd = mass of sample after some time once the experiment has finished.

Figure 7. 11 shows a drying curve for a HDPE-PHP film coated aluminium foil during consecutive experiments of water vapour measurements with a DVS at 25°C. The same as for LDPE, this data shows an initial drying process followed by a long-term mass loss, which seems to be independent of humidity. This suggests that the loss cannot be attributed to free water molecules but must be due to something else other than water molecules and the suggestion is that this is due to the loss of surfactant.
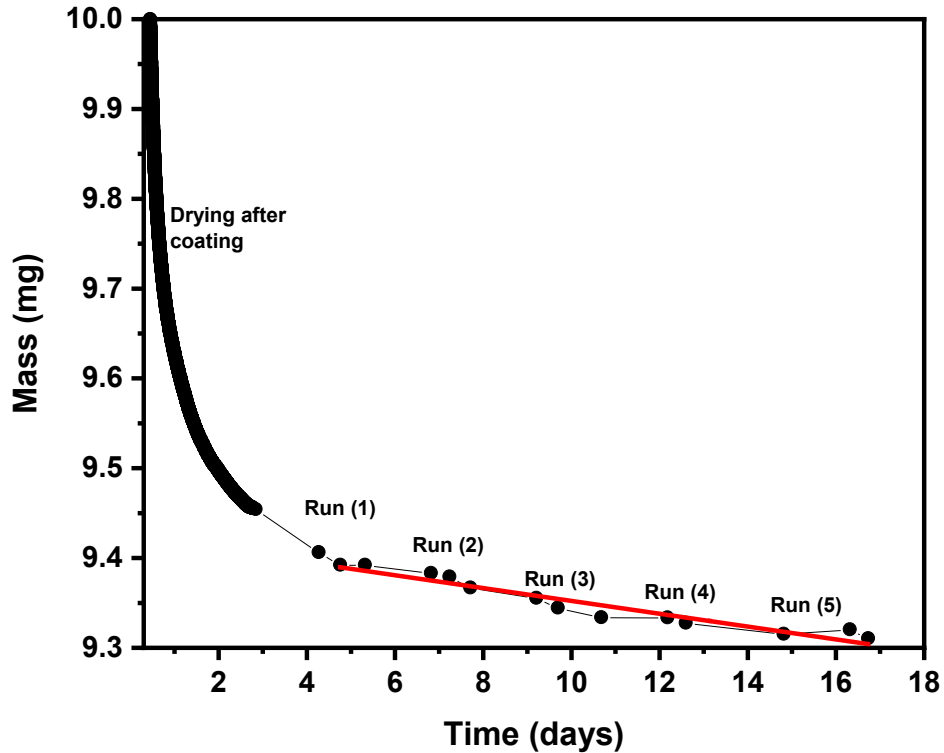
Figure 7. 11 Evolution of mass profile of HDPE-PHP film coated onto an aluminium foil during consecutive experiments of water vapour measurements with DVS. Each experiment cycle is represented by 3 dots, 1st = initial sample mass, 2nd = final sample mass and 3rd = mass of sample after some time once the experiment has finished.

Figure 7. 12 shows a drying curve for a commercial PP-PHP film coated aluminium foil during consecutive experiments of water vapour measurements with a DVS at 25°C. Similarly, to LDPE and HDPE, the data for this sample shows a very clear initial drying process followed by a long-term mass loss, which is independent of humidity and therefore the loss cannot be attributed to free water molecules but must be due to something else other than water molecules and the suggestion is that this is due to the loss of surfactant.
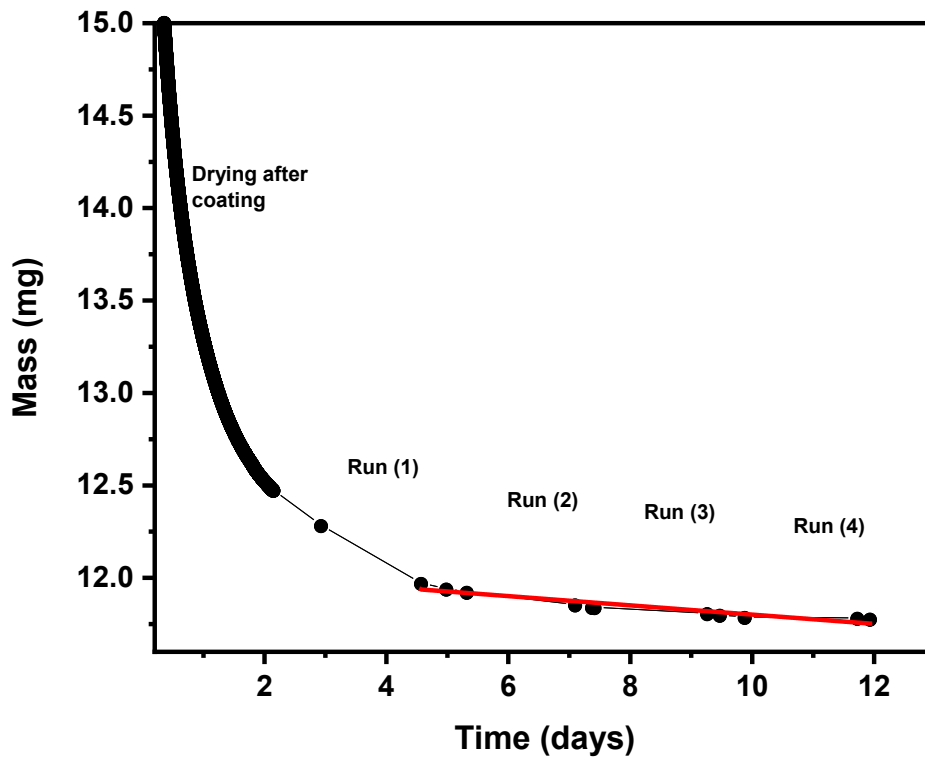
Figure 7. 12 Evolution of mass profile of commercial PP-PHP film coated onto an aluminium foil during consecutive experiments of water vapour measurements with DVS. Each experiment cycle is represented by 3 dots, 1st = initial sample mass, 2nd = final sample mass and 3rd = mass of sample after some time once the experiment has finished.

Figure 7. 13 shows a drying curve for an iPP-PHP film coated aluminium foil during consecutive experiments of water vapour measurements with a DVS at 25°C. The data here, like the previous samples, demonstrates an initial fast drying process followed by a long-term slow mass loss which is suggested to be due to the loss of surfactant.
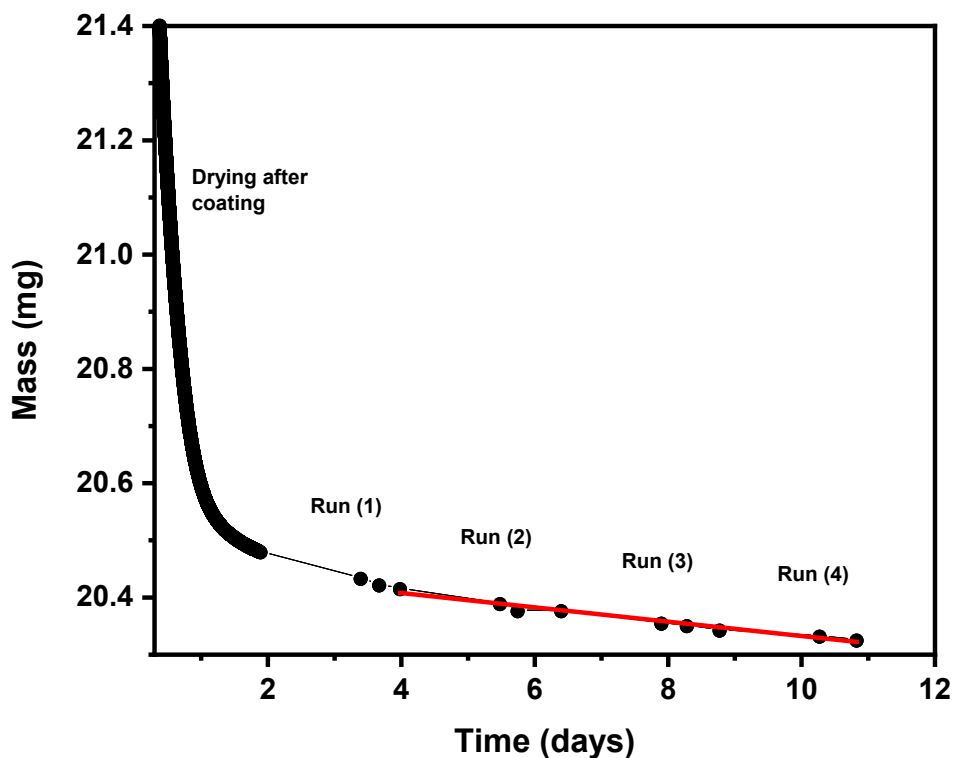
Figure 7. 13 Evolution of mass profile of iPP-PHP film coated onto an aluminium foil during consecutive experiments of water vapour measurements with DVS. Each experiment cycle is represented by 3 dots, 1st = initial sample mass, 2nd = final sample mass and 3rd = mass of sample after some time once the experiment has finished.

Figure 7. 14 shows a drying curve for an aPP-PHP film coated aluminium foil during consecutive experiments of water vapour measurements with a DVS at 25°C. The data here, like all the previous samples, demonstrates an initial fast drying process followed by a long-term slow mass loss which is suggested to be due to the loss of surfactant.
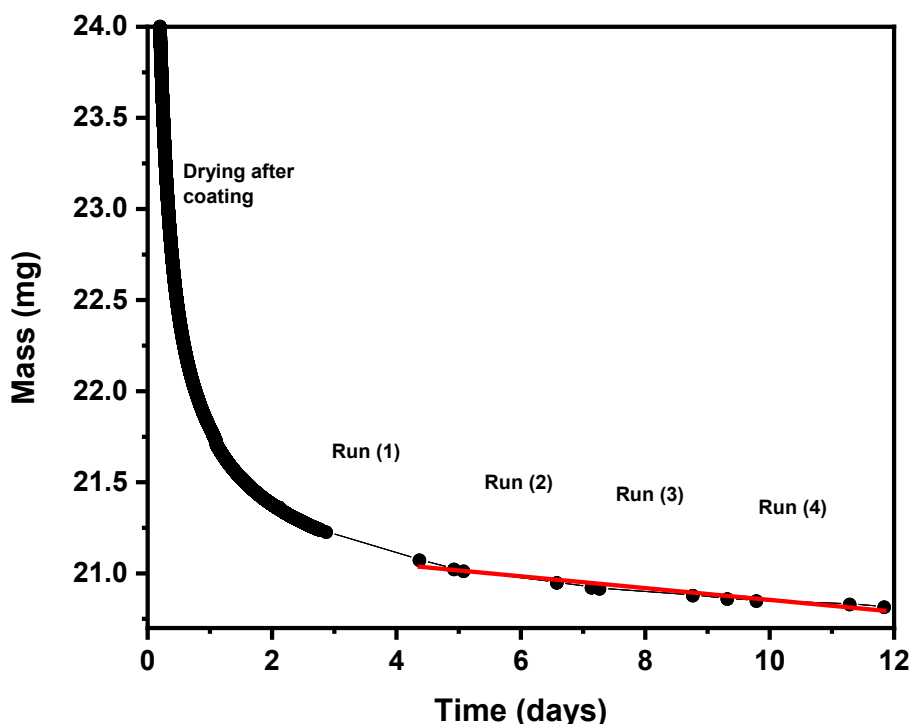
Figure 7. 14 Evolution of mass profile of aPP-PHP film coated onto an aluminium foil during consecutive experiments of water vapour measurements with DVS. Each experiment cycle is represented by 3 dots, 1st = initial sample mass, 2nd = final sample mass and 3rd = mass of sample after some time once the experiment has finished.

A linear trendline for each of the above data set has been drawn. The slope of the line is indicative of the loss of surfactant. This slope has been used to calculated evaporation losses at 25°C for different surfactant loaded aluminium foil polymer coated samples and the results are shown in Table 7. 6.

Table 7. 6 Calculated evaporation losses at 25°C for different surfactant loaded aluminium foil polymer coated samples.

Samples (aluminium foils)	Rate of Mass Loss (mg/day)	X_c (%) Crystallinity Pycnometry (±0.05)
Aluminium Foil Blank	-0.00033 ± 0.00005	-
Aluminium Foil Blank+ PHP	-0.99477 ± 0.17000	-
LDPE + PHP	-0.00909 ± 0.00056	48.2
HDPE+ PHP	-0.00714 ± 0.00059	64.2
Commercial PP+ PHP	-0.02503 ± 0.00288	35.0
Atactic PP + PHP	-0.03235 ± 0.00268	00.0
Isotactic PP+ PHP	-0.01253 ± 0.00083	50.2

Figure 7. 15 shows the calculated rate of mass loss as a function of crystallinity for different surfactant loaded aluminium foil polymer coated samples. There appears to be a positive correlation between the mass loss and crystallinity.
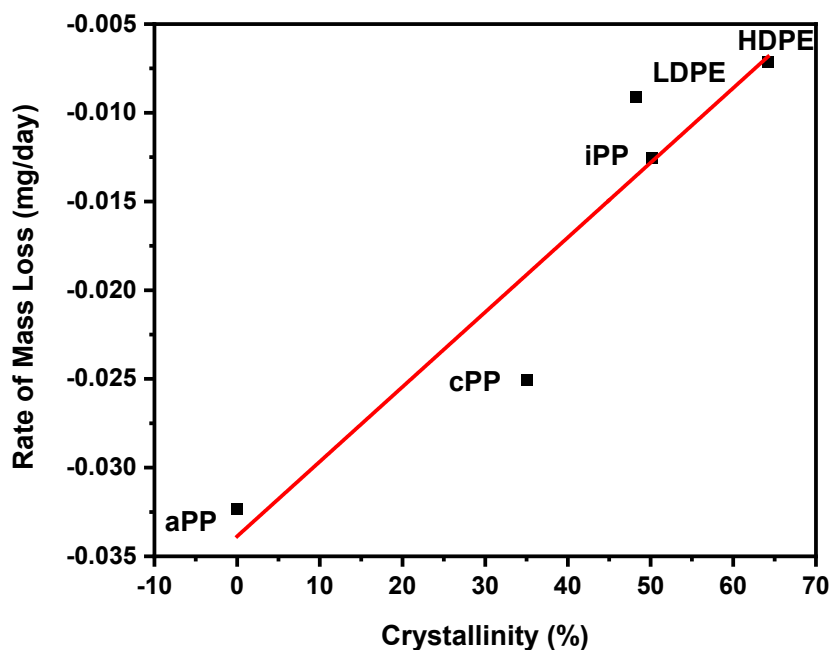
Figure 7. 15 Rate of mass loss as a function of crystallinity plot for different for different surfactant loaded aluminium foil polymer coated samples.

In summary, the experimental data presented in this Section demonstrated that all the samples studied lose weight over time which cannot be ascribed solely to solvent (water) losses, suggesting that surfactants are being lost too. Although the rates of surfactants losses are low, they were observed experimentally. The rate of mass loss scales with surface area and it is very challenging to measure accurately the surface area for all the individual studied substrates, i.e., the nonwovens and the cast films on aluminium foil.

The results showed that the rate of mass loss, which can only be due to surfactant loss, is temperature dependant. This process also appeared to be dependent on the amount of surfactant present. Specifically, the coating level and the tacticity of the material i.e., % crystallinity of the substrate. The surfactant loss process was slow at 25°C but it increased as function of temperature and surfactant concentration. There also appeared to be a trend between the surfactant loss process and polymer crystallinity, as shown in Figure 7. 15. The type of polymer effecting the rate of loss. The largest mass loss was observed on the atactic PP, which is amorphous in nature, and the least mass loss was observed for the HDPE sample, which is the polymer with the highest % crystallinity. The temperature dependence was as expected, if one of the processes of mass loss is evaporation. The dependence on coating level also seems reasonable. However, the dependence on tacticity was less clear. Previous data showed that that surfactant loss was driven by two processes a) evaporation and b) dissolution. Therefore, the dependence of mass loss on polymer tacticity can be seen as

further evidence supporting the hypothesis for the dual processes responsible for surfactant migration.

7.4 Solubility of surfactants into PP/PE analogues low molecular weight polymers

Fundamental measurements using DVS, (as detailed in the previous section), show that surfactants are lost, and that evaporation contributes to these loses. However, the actual surfactant loses observed in practice are much faster and evaporation alone doesn't account for all the loses. The only other explanation is solubility of surfactants into the polymer. To understand the solubility of surfactants, (Silastol PHP-26, Stantex S6327, sodium dodecyl sulfate (SDS), and hexadecyltrimethylammonium bromide (CTAB)) in polymers a study was carried out using paraffin wax, atactic polypropylene and n-Decane as PP/PE low molecular weight analogues. The solubility of the surfactants in the different polymer analogues was estimated in glass vials by adding the surfactant to the polymer analogue in liquid form and observing whether the surfactant was soluble in the liquid or not. The paraffin wax, and the atactic polypropylene were first melted and then the surfactant was added while stirring the mixture with a magnetic stirrer. Solutions of different concentrations, (1, 2, 5, 10, 20 and 50% v/w) were prepared for each polymer analogue. Observations on the solubility and when the surfactant precipitated out of the mixture were noted for two scenarios:

a) observations when the mixture was hot
b) observations after mixture had cooled down to room temperature.

Since n-decane was in liquid form no heating was required for the mixture with the surfactant and therefore observations at ambient conditions were noted only. All the observations were summarised in Table 7. 7. The findings for Silastol PHP-26 solubility into PP/PE analogues low molecular weight polymers were as follows:

- Paraffin Wax (65°C) – 20% soluble
- n-Decane (25°C) – 5% soluble
- Atactic Polypropylene (80°C) - fully soluble

For Stantex S6327 solubility into PP/PE low molecular weight polymers the result were:

- Paraffin Wax (65°C) – fully soluble

- n-Decane (25°C) – 5 % soluble
- Atactic Polypropylene (80°C) - fully soluble
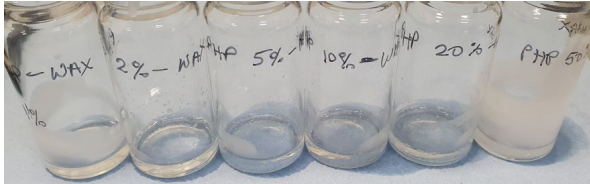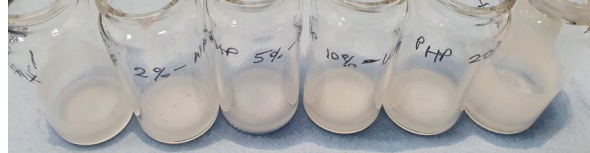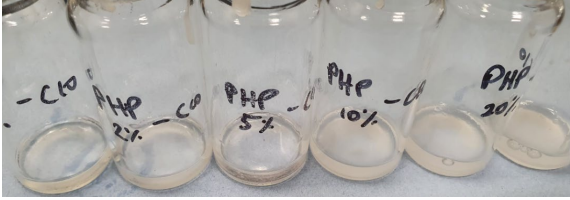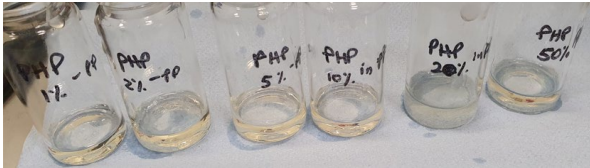
The findings for SDS (anionic) and CTAB (cationic) solubility into PP/PE analogues low molecular weight polymers were as follows. Due to time restrictions SDS and CTAB were not tested with n-decane or atactic PE but the expectation was that they would behave similarly to Silastol PHP-26 and Stantex S6327 because they are similar types of surfactants i.e., both CTAB and Silastol PHP-26 are cationic:
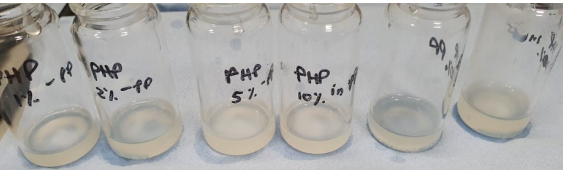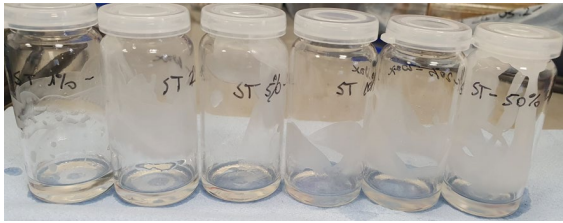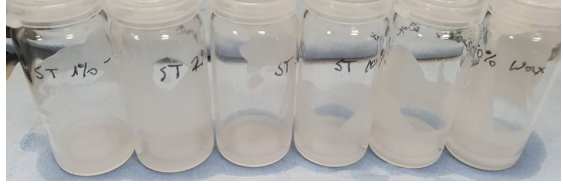
- Paraffin Wax (65°C) – fully soluble
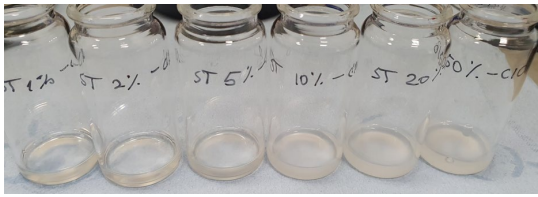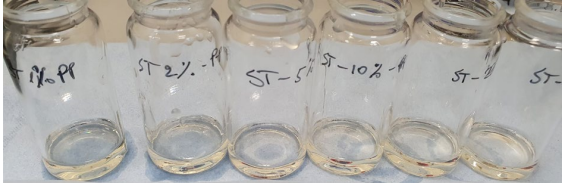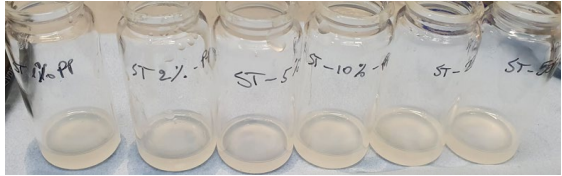
The results showed that as these solution mixtures cooled down, they all solidified into what looked like one homogenous phase. This observation was true for all the different mixtures. The question was, do the surfactant mixtures dissolve into PP/PE analogues? Visually, based on the data presented here, it appeared that the surfactants tested did dissolved. However, visually it is hard to establish if the surfactants fully dissolved at a molecular level. This is because semi-crystalline PP/PE polymers feature crystalline domains and non-crystalline amorphous domains, as discussed in Chapter 6. Morphology and distribution of crystalline and amorphous regions is believed to have an effect on the surfactant solubility into polyolefins.
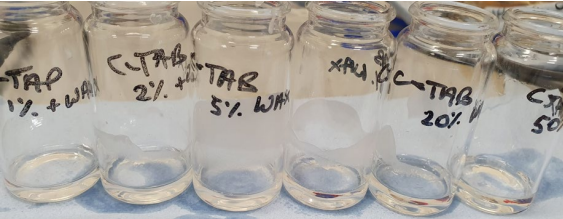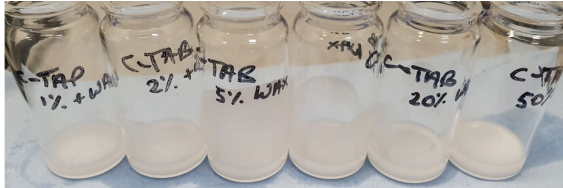
As mentioned above when the mixture cooled down it formed a cloudy solution. It was difficult to ascertain visually whether that was a result of PE/PP-crystalline phase and the PE/PP-amorphous phase with the surfactant dissolved into it or that was formed from droplets of the material dispersed into the polymer. However, the data presented here is sufficient evidence that surfactants dissolve/disperse into PP/PE analogues low molecular weight polymers. Therefore, it can be reasonable proposed that these surfactants are likely to be soluble into the PE and PP. The increase of solubility observed with increasing carbon number is considered a consequence of the growing interactions between surfactant and hydrocarbon fluid molecules.

Table 7. 7 Solubility of surfactant mixtures into PP/PE analogues low molecular weight polymers.

Silastol PHP-26 (cationic)	1% (v/w)	2% (v/w)	5% (v/w)	10% (v/w)	20% (v/w)	50% (v/w)	Comments	Images
Paraffin Wax (65°C)	✓	✓	✓	✓	✓	X	When hot, all mixtures apart form 50% one dissolved fully. As solutions cooled down, mixtures solidified as one homogenous phase.	Hot Cold
n-Decane (25°C)	✓	✓	✓	X	X	X		
Atactic Polypropylene (80°C)	✓	✓	✓	✓	✓	✓	When hot, all mixtures dissolved fully.	Hot

| | | | | | | | As solutions cooled down, mixtures solidified as one homogenous phase. | Cold |

Stantex S6327 (non-ionic)	1% (v/w)	2% (v/w)	5% (v/w)	10% (v/w)	20% (v/w)	50% (v/w)	Comments	Images
Paraffin Wax (65°C)	✓	✓	✓	✓	✓	✓	When hot, all mixtures dissolved (dispersed) fully. As solutions cooled down, mixtures solidified as one homogenous phase.	Hot Cold

	1% (v/w)	2% (v/w)	5% (v/w)	10% (v/w)	20% (v/w)	50% (v/w)	Comments	Images
n- Decane (25°C)	✓	✓	✓	X	X	X	Clear solutions	
Atactic Polypropylene (80°C)	✓	✓	✓	✓	✓	✓	When hot, all mixtures dissolved fully. As solutions cooled down, mixtures solidified as one homogenous phase.	**Hot** **Cold**
SDS (anionic)	**1% (v/w)**	**2% (v/w)**	**5% (v/w)**	**10% (v/w)**	**20% (v/w)**	**50% (v/w)**	**Comments**	**Images**
							When hot, all mixtures dissolved fully.	**Hot**

Paraffin Wax (65°C)	✓	✓	✓	✓	✓	✓	As solutions cooled down, mixtures solidified as one homogenous phase.	Cold
CTAB (cationic)	**1%** (v/w)	**2%** (v/w)	**5%** (v/w)	**10%** (v/w)	**20%** (v/w)	**50%** (v/w)	**Comments**	**Images**
Paraffin Wax (65°C)	✓	✓	✓	✓	✓	✓	When hot, all mixtures dissolved fully. As solutions cooled down, mixtures solidified as one homogenous phase.	Hot Cold

7.5 Solubility of Industrial Surfactant Mixtures in Different Solvents
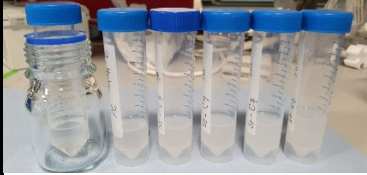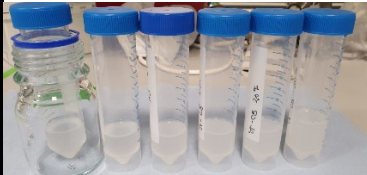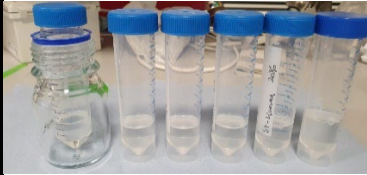
The observed solubility of surfactants in PP/PE low molecular weight analogues directly support the view that surfactants can solubilise in polyolefins. Chapter 6 results shows that both organic and hydrocarbon-based solvents dissolve in polyolefins, so it is interesting to establish if surfactants dissolve in different solvents. The solubility of surfactant, (Silastol PHP-26 and Stantex S6327), in different solvents, (methanol, isopropanol, cyclohexane, hexane, heptane, octane, limonene, ethyl acetate and water) was estimated in glass vials at 22 ± 2°C by adding the surfactant to the solvent and observing whether the surfactant was soluble or not. Solutions of different concentrations, (1, 2, 5, 10, 20 and 50% v/w) were prepared for each solvent-surfactant mixture. After each addition the solution was shaken to form a homogenous mixture. The results of the observations for Stantex S6327 are summarised in Table 7. 8. Silastol PHP-26 yielded similar results. The summary findings for Stantex S6327 solubility in the different solvents are as follows:
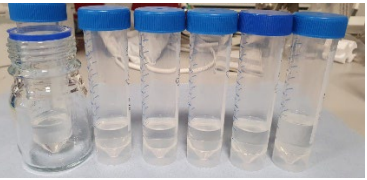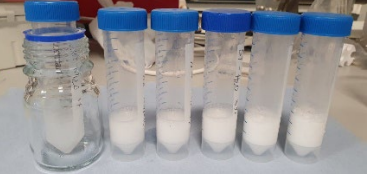
- Methanol – 1%
- Isopropanol – fully soluble
- Cyclohexane – 2%
- Hexane – 2 %
- Heptane – 2%
- Octane – 2%
- Limonene – fully soluble
- Ethyl acetate – fully soluble
- Water - 1%

As demonstrated, Stantex S6327, (a nonionic surfactant) dissolved into hydrocarbon-based solvents and therefore proposing that the surfactants can dissolve into a hydrocarbon polymer is not an unreasonable hypothesis. Overall, these preliminary estimates of surfactant solubilities into different solvents and into PP/PE analogues low molecular weight polymers support the hypothesis that surfactants are likely to be soluble and can dissolve into PE/PP based polymers including nonwovens, especially relevant here are the surfactant behaviours in hydrocarbons.

Table 7. 8 Solubility of industrial surfactant mixtures, (Stantex S6327) into different solvents.

Stantex S6327 (non-ionic)	1% (v/w)	2% (v/w)	5%(v/w)	10% (v/w)	20% (v/w)	50% (v/w)	Comments	Images
Methanol	✓	X	X	X	X	✓	Cloudy solutions	
Isopropanol	✓	✓	✓	✓	✓	✓	Clear solutions	
Cyclohexane	✓	✓	X	X	X	X	Cloudy solutions	

Hexane	✓	✓	X	X	X	X	**Cloudy solutions**	
Heptane	✓	✓	X	X	X	X	**Cloudy solutions**	
Octane	✓	✓	X	X	X	X	**Cloudy solutions**	
D-Limonene	✓	✓	✓	✓	✓	✓	**Clear solutions**	

Ethyl Acetate	✓	✓	✓	✓	✓	✓	Clear solutions	
Water	✓	X	X	X	X	X	Milky solutions (within CMC)	

The experimental data so far has demonstrated that surfactants were being lost from the surface of polymers because of evaporation and dissolution process. The question then is – do surfactants simply dissolve into the polymer and then slowly desorb out to the surface, prior to evaporate over time? If the surfactants were only at the polymer surface, it is hard to understand why they would take so long to disappear. The suggestion is that the rate of surfactant desorption on the surface relates to solubility. The highest surfactant solubility is expected to be in aPP which is 100% amorphous. As the data in Chapter 6 showed that the most amorphous materials have the most solvents dissolved in them. Therefore, more surfactant would desorb from aPP as more can dissolve in this amorphous polymer compared to HDPE, which is semicrystalline in nature, see Figure 7. 15.

7.6 Solubility of Surfactants in PP and PE films Based on Dynamic DVS-Ellipsometry Data

7.6.1 Experimental method (Ellipsometry & DVS)

The theory and basic operation principle of a standalone DVS and an integrated ellipsometer are detailed in Chapter 3. Also, the method for preparation of all polymer solutions and fabrication of polymer films on aluminium foils and silicon wafers discussed in this chapter has been provided in Chapter 3 and 6. For this research a bespoke DVS instrument (Surface Measurement Systems Ltd., UK) coupled with a FS-1 multi-wavelength ellipsometer (Film Sense, USA) was utilised to perform all experimental measurements. The water vapour sorption experiments were carried out in an environmental chamber at a temperature of 25 °C and partial pressure range between 0 and 90%. The partial pressure was maintained using mass-flow controllers operating in open or closed-loop mode using dry air as the carrier gas with a flowrate of 200 ml/min and monitored using a humidity probe. The ellipsometer used four wavelengths (465, 525, 595 and 635 nm) at a chosen optimal angle of incidence between 60° and 70°, whichever produced the highest possible signal intensity. The prepared coated Al foil and thin film coated Si wafer samples were measured in parallel and equilibrated at each relative humidity level in steps of 5-10% to produce kinetics profiles and calculate isotherms. The DVS was used to monitor the change in mass of foil coated samples using a microbalance and the ellipsometer to monitor the change in optical properties of the thin films including film thickness.

7.6.2 Aging of PHP film spin coated on a silicon wafer based on ellipsometry

A reference experiment was conducted to measure the behaviour of a thin PHP spin coated film on a silicon wafer over time. A 2% w/v coating solution of PHP in IPA was used. The measurements were carried out at atmospheric pressure under dry air flow of 200 ml/min, T = 25°C. The PHP film was optically modelled as a Cauchy layer, where the thickness and refractive index were fitted. Every time the optical properties of the PHP film were measured, the same model was used so that the properties could be plotted as a function of time.

The data demonstrates clearly that surfactant materials is lost as a function of time. Figure 7. 16 shows the data representing PHP surfactant film thickness as a function of time. The results demonstrate a ~20% decrease in thickness over 100 days. This surfactant film thinning over time suggests that over time the surfactant is lost but the rate of loss is decreasing from the initial rate. If the first two points of the plot are ignored on the basis that there might have been residual IPA solvent still being lost at this point, then the data shows a ~9% decrease in thickness over 100 days which suggests that a 3.5nm PHP layer takes would take over 1000 days to disappear. Since silicon oxide is an inert oxide accepted from the EU Directive on migration[476], the only way the surfactant can be lost in this scenario is due to vaporisation. The data shows unequivocal evidence of loss of surfactant from an inert surface by evaporation, *a* process which appears to be slow but significant.

$$y = 3E\text{-}10x^2 - 9E\text{-}05x + 37.448$$
$$R^2 = 0.9815$$
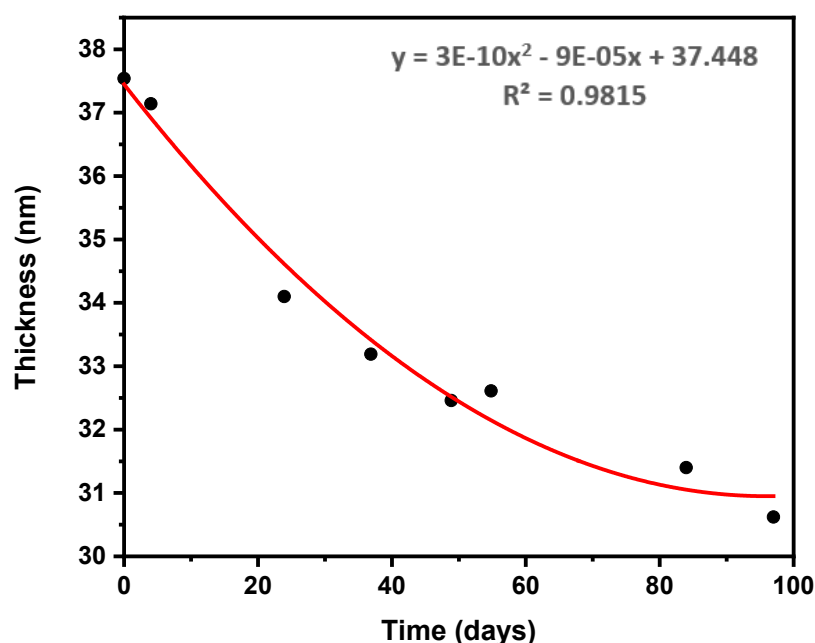
Figure 7. 16 Aging of a surfactant, (Silastol PHP-26) 2% film spin coated onto silicon wafer at 25°C. Note error bars of 0.1% are smaller than the data symbols.

7.6.3   Ellipsometry - DVS Reference Experiments

<u>Aluminium foil and silicon wafer water uptake measurements</u>

A typical cleaned aluminium foil blank sample and an uncoated silicon wafer were tested for water adsorption to generate the reference data for baseline measurements. A layer of water was added to the model of the blank wafer to account for the adsorption of water and fitted across the collected data. Figure 7. 17 shows the data which indicates that as water vapour interacts with the substrates, over time a monolayer of water forms, on both the silicon wafer, (~ 0.25 +/- 0.05 nm thick) and the aluminium foil substrates, 0.04% mass change which equates to ~30μg. These uptake levels correspond to sub-monolayer levels of water adsorption. These very low uptake levels are as would be expected for blank reference samples of this type.
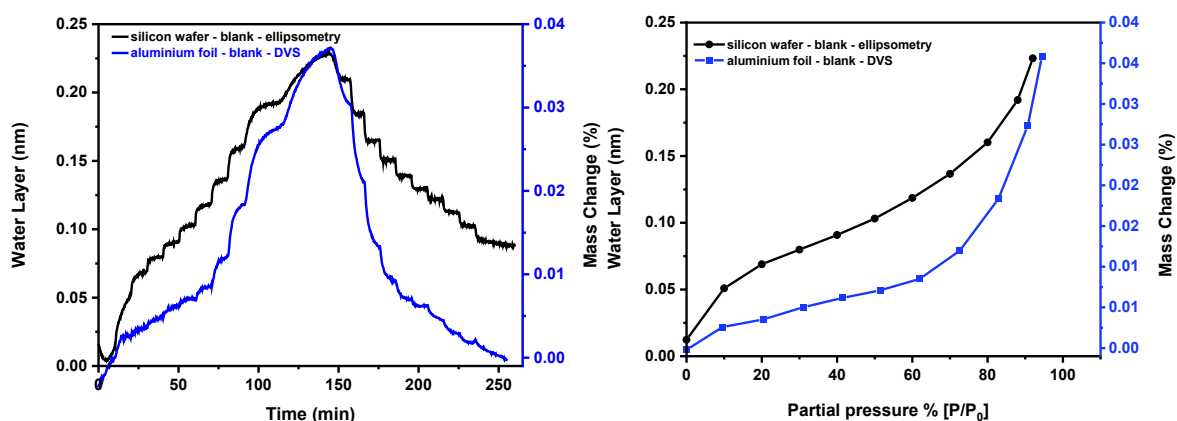
Figure 7. 17 Kinetic mass profile and water layer thickness (left) and corresponding sorption isotherm (right) of water vapour interacting with an aluminium foil and a silicon wafer.

<u>LDPE film water uptake measurements</u>

A cleaned aluminium foil sample dip-coated with LDPE, and a cleaned silicon wafer spin coated with LDPE, were measured simultaneously for water uptake. All the polymers studied were expected to not absorb any water vapour, except for PPa which is amorphous. Hence, for LDPE, a layer of water forming on the surface of the polymer was modelled. Figure 7. 18 presents the results which show the formation of a monolayer of water, (0.20 +/- 0.05 nm thick). The mass change of the aluminium foil dip-coated with LDPE is small, less than 0.35 %. Since LDPE is hydrophobic in nature it is not expected to absorb water, instead water molecules have adsorbed on the polymer surface forming a monolayer of water, similarly to the blank uncoated substrates. The isotherms obtained for these samples are type III, with the linear region representing the water monolayer formation as water is introduced.
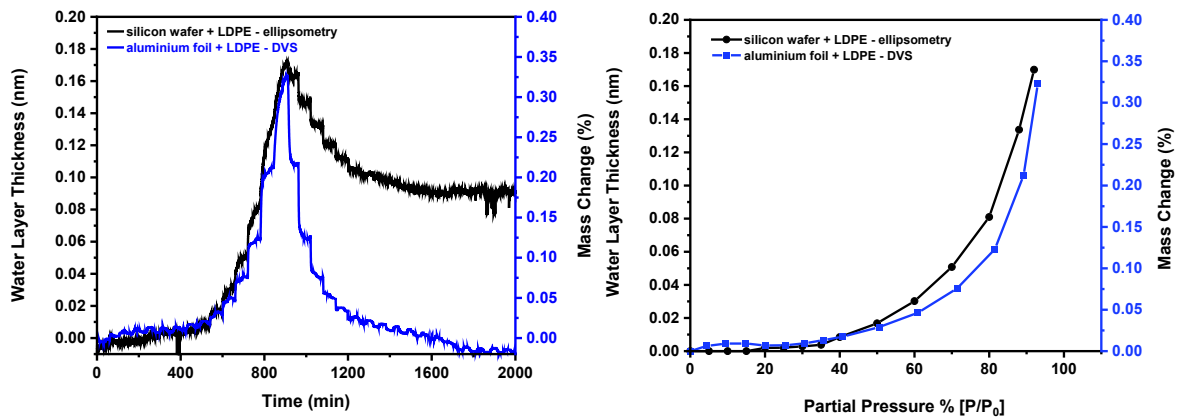
Figure 7. 18 Kinetic mass profile and evolution of water layer thickness (left) and corresponding sorption isotherm (right) of water vapour interacting with thin LDPE films coated onto an aluminium foil and a silicon wafer.

MDPE film water uptake measurements

A cleaned aluminium foil sample dip coated with MDPE, and a cleaned silicon wafer spin coated with MDPE, were measured simultanesly for water uptake. A layer of water forming on the surface of the polymer was modelled. Figure 7. 19 presents the experimental data which show water monolayer formation and transition to multilayer water formation, (2.2 +/- 0.05 nm thick). There appears to be a type 2 and 3 isotherms which could be due to the presence of inhomogeneous films formed differently on the foil versus the wafer. The mass change is small less than 1%.
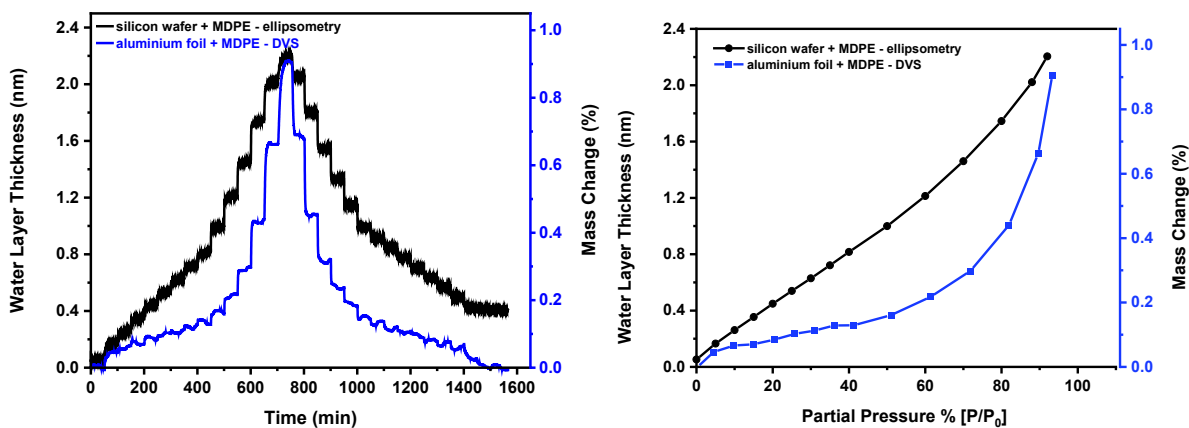
Figure 7. 19 Kinetic mass profile and evolution of water layer thickness (left) and corresponding sorption isotherms (right) of water vapour interacting with thin MDPE films coated onto an aluminium foil and a silicon wafer.

234

HDPE film water uptake measurements

A cleaned aluminium foil sample was dip coated with HDPE, and a cleaned silicon wafer spin coated with HDPE, were measured simultaneously for water uptake. The layer of water forming on the surface of the polymer was modelled for the ellipsometry on the silicon coated sample. Figure 7. 20 represents the data collected simultanesly with a DVS and the ellipsometer. Like the previous blank data these results show little change, apart from the formation of a monolayer of water, (0.35 +/- 0.05 nm thick). Since HDPE is hydrophobic in nature it is not expected to absorb water, instead the water molecules adsorb on the polymer surface as a monolayer.
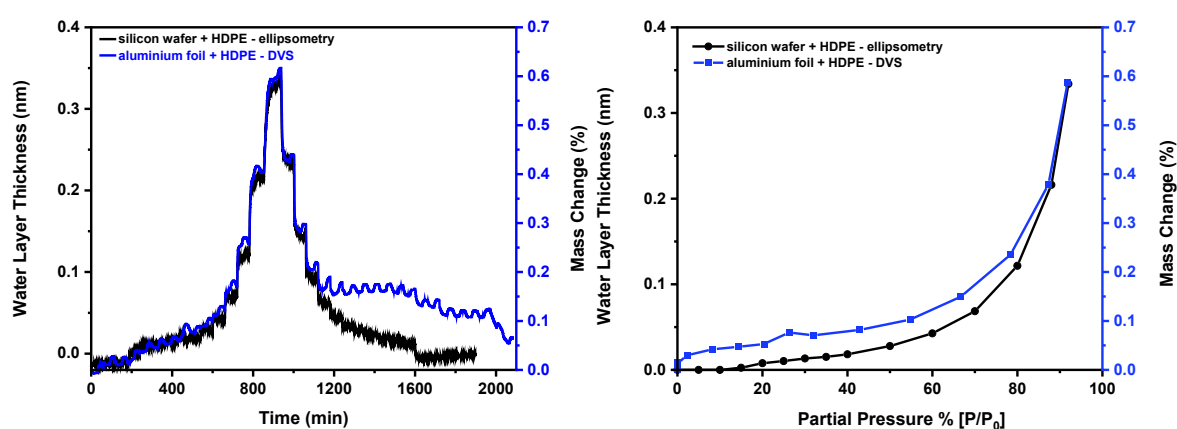
Figure 7. 20 Kinetic mass profile and evolution of water layer thickness (left) and corresponding sorption isotherm (right) of water vapour interacting with thin HDPE films coated onto an aluminium foil and a silicon wafer.

Commercial PP film water uptake measurements

A cleaned aluminium foil sample dip coated with a commercial PP, and a cleaned silicon wafer was also spin coated with commercial PP, and both were tested simultaneously for water uptake. A layer of water forming on the surface of the polymer was modelled. Figure 7. 21 shows the data collected simultanesly with a DVS and ellipsometer for thin commercial PP based films prepared using melted industrially relevant PP based nonwoven. The results show 3x times more uptake for the commercial PP films than the PE films implying a water monolayer formation transitioning to a multilayer water formation, (>1.4nm +/- 0.05 nm thick). The mass change is 1.5%. Since this is a commercial polymer sample impurities and additives could be present and these could be responsible for the different behaviour observed with the commercial PP compared to the other films studied. Also, the commercial PP might be more amorphous in nature than LDPE.
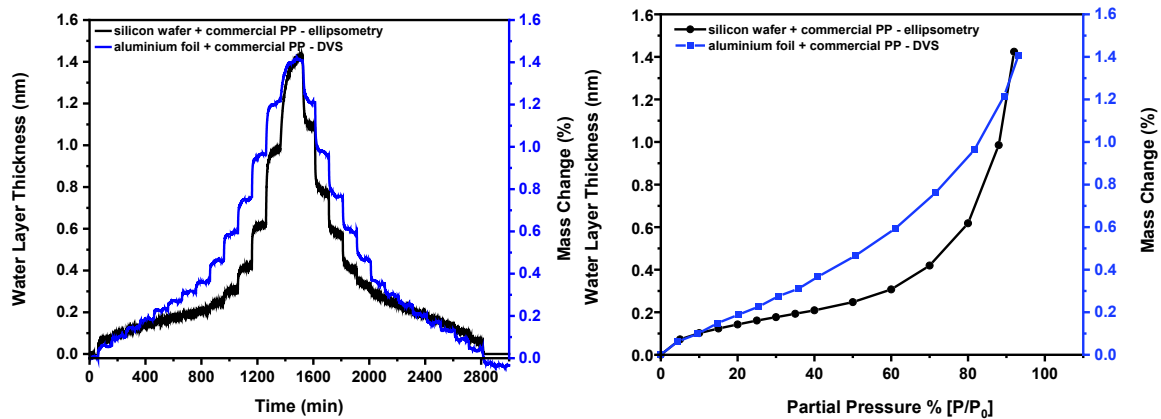
Figure 7. 21 Kinetic mass profile and evolution of water layer thickness (left) and corresponding sorption isotherm (right) of water vapour interacting with thin commercial PP films coated onto an aluminium foil and a silicon wafer.

Isotactic PP film water uptake measurements

A cleaned aluminium foil sample dip coated with iPP, and a cleaned silicon wafer spin coated with iPP, were tested simultaneously for water uptake. A layer of water forming on the surface of the polymer was modelled. Figure 7. 22 presents the data which show minimal change, apart from the formation of a monolayer of water, (0.9 +/- 0.05 nm thick). Like the other polymers studied so far, iPP is hydrophobic in nature it is not expected to absorb water, instead the water molecules adsorb on the polymer surface as a monolayer. The mass change is ~ 0.5%.
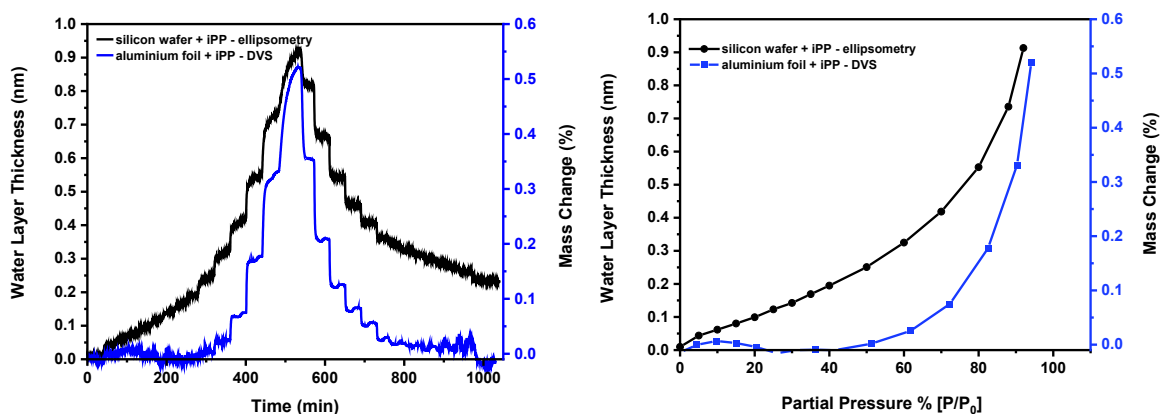
Figure 7. 22 Kinetic mass profile and evolution of thickness (left) and corresponding sorption isotherm (right) of water vapour interacting with thin iPP films coated onto an aluminium foil and a silicon wafer.

Atactic PP film water uptake measurements

A cleaned aluminium foil sample dip coated with aPP, and a cleaned silicon wafer spin coated with aPP, were tested simultaneously for water uptake. Water was assumed to be absorbed

into aPP film and therefore the Bruggeman Effective Medium approximation was used to calculate the water volume fraction. Figure 7. 23 presents the data which show significant uptake, an increased water volume fraction in aPP, (0.7 +/- 0.05 %). Since aPP is amorphous it is expected to absorb some water. The assumption is that the aPP and water are a homogenous mixture, but this might not be true because the polymer might adsorb more at surface then deeper within the film e.g., featuring a graded adsorption mechanism. The mass change is ~ 0.65%.
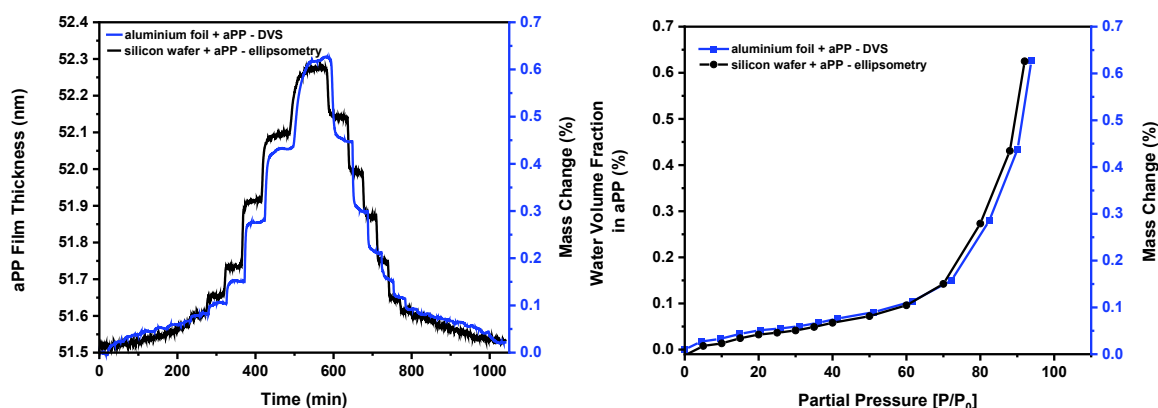
Figure 7. 23 Kinetic mass profile and evolution of thickness (left) and corresponding sorption isotherm (right) of water vapour interacting with thin aPP films coated onto an aluminium foil and a silicon wafer.

7.6.4 Ellipsometry - DVS Thin Film Characterisation (Surfactant – Polymer)

To establish what happens when surfactants are coated into a real industrial material over time, experiments were conducted on model substrates under controlled conditions. Silicon wafers and aluminium foils pre-coated with a thin polymer layer of LDPE, HDPE, commercial PP, iPP and aPP, then a thin layer of surfactant, 2% w/v solution mixture of PHP, (Silastol PHP-26) in IPA was cast. The surfactant-polymer films were measured over time using a DVS coupled with an ellipsometer. Measurements for each set of samples were repeated sequentially 4 to 5 times and the amount of water uptake was monitored. Again, this quantity has been used as a proxy to the amount of surfactant present in the material at a given time.

LDPE-PHP film "in-situ" aging studies

A set of samples, a silicon wafer, and an aluminium foil coated with LDPE-PHP were analysed simultanesly using a typical 0-90-0%RH cycle. The analysis was repeated 4 times without removing the samples from the instrument between each run. The data are presented in

Figure 7. 24, and Table 7. 9. The results shows that the amount of water dissolved in the material decreases as a function of time and this suggested that the amount of surfactant decreased over time and that is why the dissolution of water is reduced. The presence of water has been used in this research for the 1st time as a proxy to the amount of surfactant present on the polymer surface at a given time.
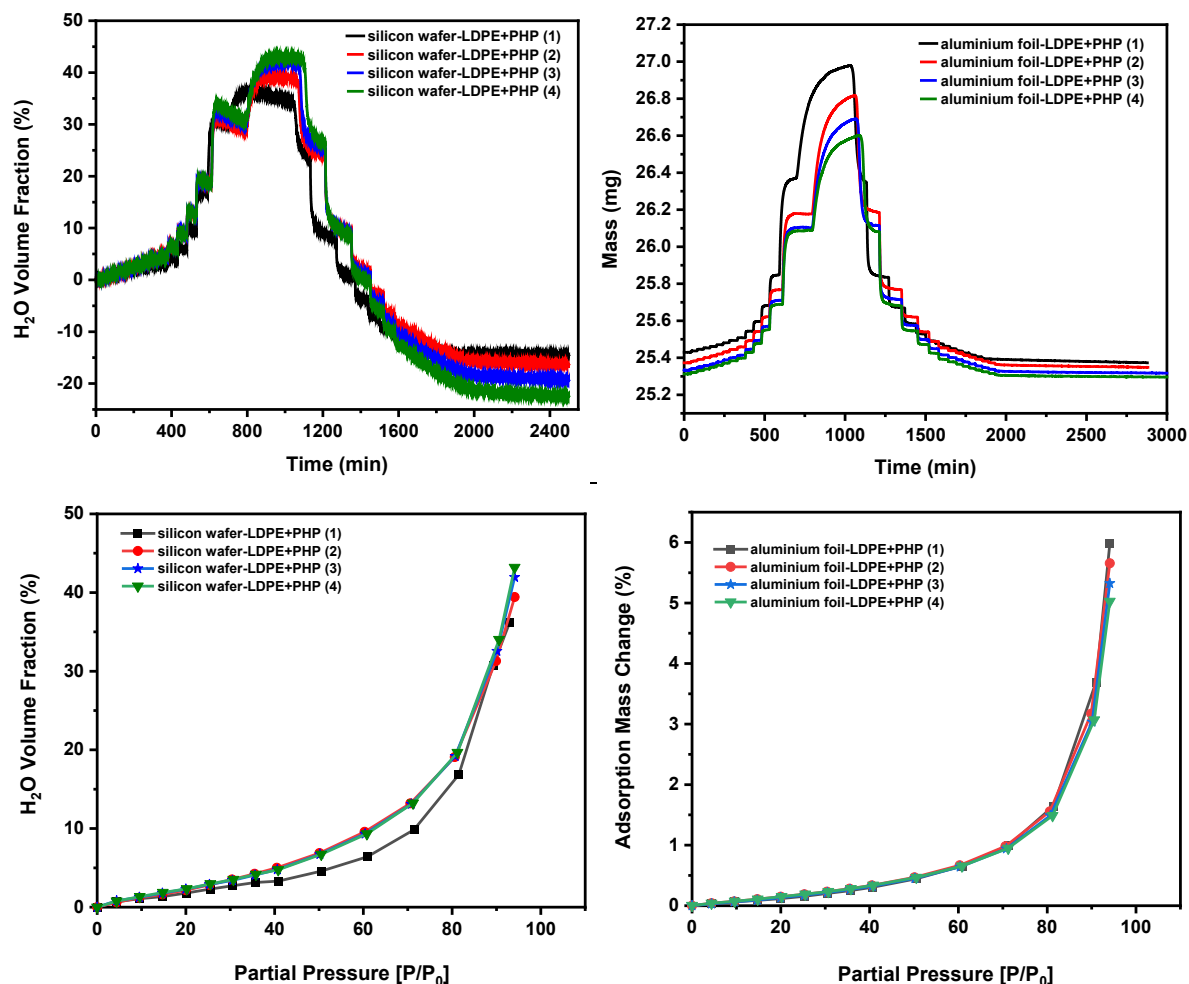
Figure 7. 24 Ellipsometry (left) and DVS (right) data of LDPE+PHP films coated onto silicon wafer and aluminium foil and the and corresponding water vapour sorption isotherms (bottom) for each substrate.

Table 7. 9 DVS Mass losses of LDPE-PHP films for four consecutive DVS experiments.

DVS Run	Initial Mass (mg)	Final Mass (mg)	Mass Difference (μg)	Mass Loss (%)
1	25.4298	25.3729	-56.90	0.2238
2	25.3728	25.3487	-24.10	0.0950
3	25.3329	25.3176	-15.30	0.0604
4	25.3121	25.297	-15.10	0.0597
total			**-132.80**	**0.4388**

HDPE-PHP film "in-situ" aging studies

The same experiment as above was conducted using HDPE-PHP films. The results show similar data to the LDPE-PHP experiment. Please see Appendix B for details.

Commercial PP-PHP film "in-situ aging" studies

The same experiment as above was conducted using commercial PP-PHP films. The results are shown in Figure 7. 25, and Table 7. 10. Again, the data shows that the amount of water dissolved in the material decreases as a function of time and this suggested a decrease of the amount of surfactant in the material over time.
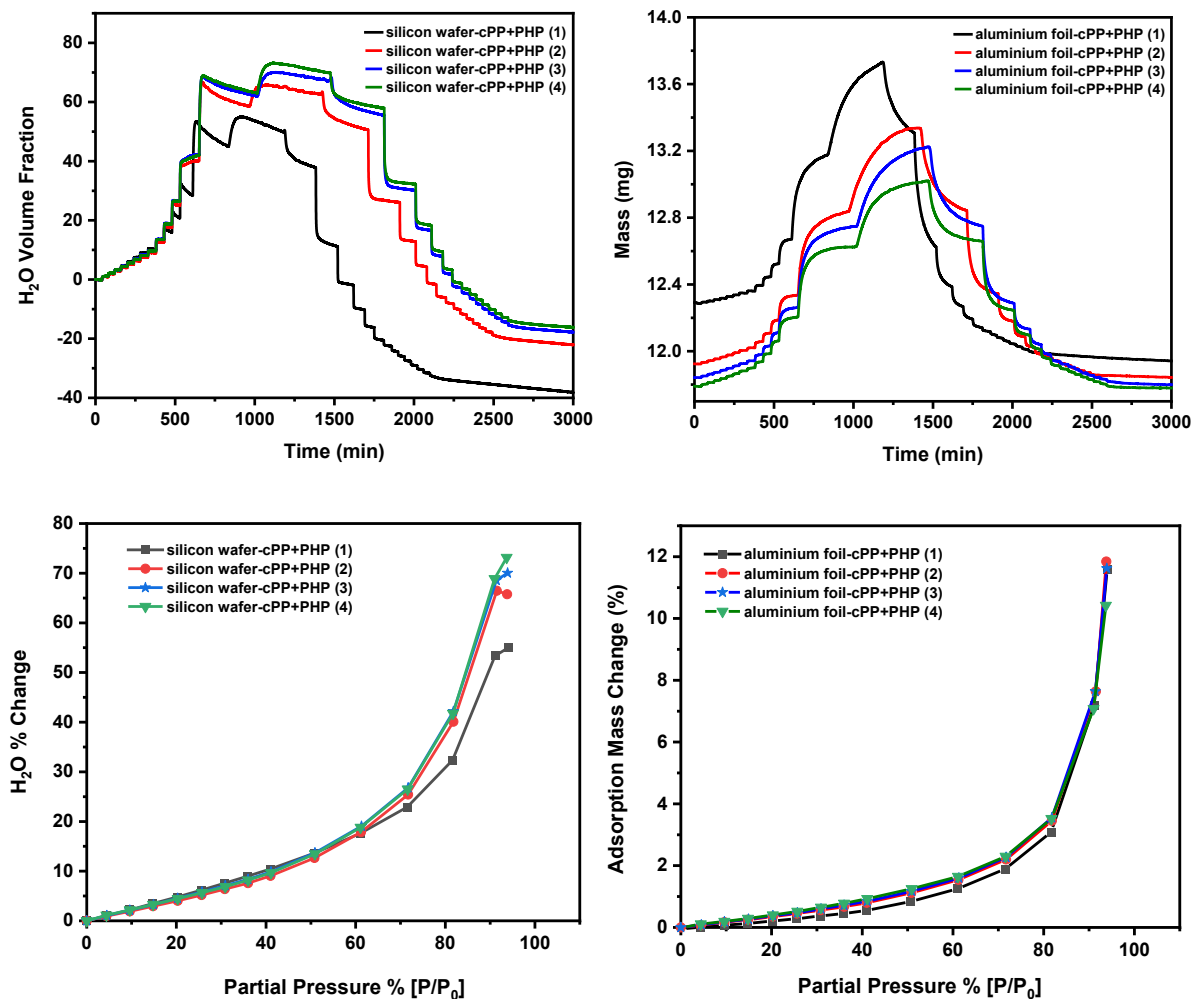
Figure 7. 25 Ellipsometry (left) and DVS (right) data of commercial PP+PHP films coated onto silicon wafer and aluminium foil and the and corresponding water vapour sorption isotherms (bottom) for each substrate.

Table 7. 10 Mass changes of commercial PP-PHP films for consecutive experiments of water vapour measurements with a DVS.

DVS Run	Initial Mass (mg)	Final Mass (mg)	Mass Difference (µg)	Mass Loss (%)
1	12.2914	11.9420	-349.40	2.8430
2	11.9244	11.8423	-82.10	0.6890
3	11.8422	11.7996	-42.60	0.3600
4	11.7904	11.7800	-10.40	0.0880
total			-511.4	3.9790

Aging of iPP-PHP films coated onto a silicon wafer and an aluminium foil

The same experiment as above was conducted using iPP-PHP films. The results show similar data to the commercial PP-PHP experiment. Please see Appendix B details.

Aging of aPP-PHP films coated onto a silicon wafer and an aluminium foil

The same experiment as above was conducted using aPP-PHP films. The results are show Figure 7. 26, and Table 7. 11. The data shows that the amount of water dissolved in the material decreases as a function of time and this suggested a decrease of the amount of surfactant in the material over time. Main learnings from these plots are that samples takes up less water as a function of time, and the sample mass also decreases with time. These loses are attributed to the loss of surfactant.
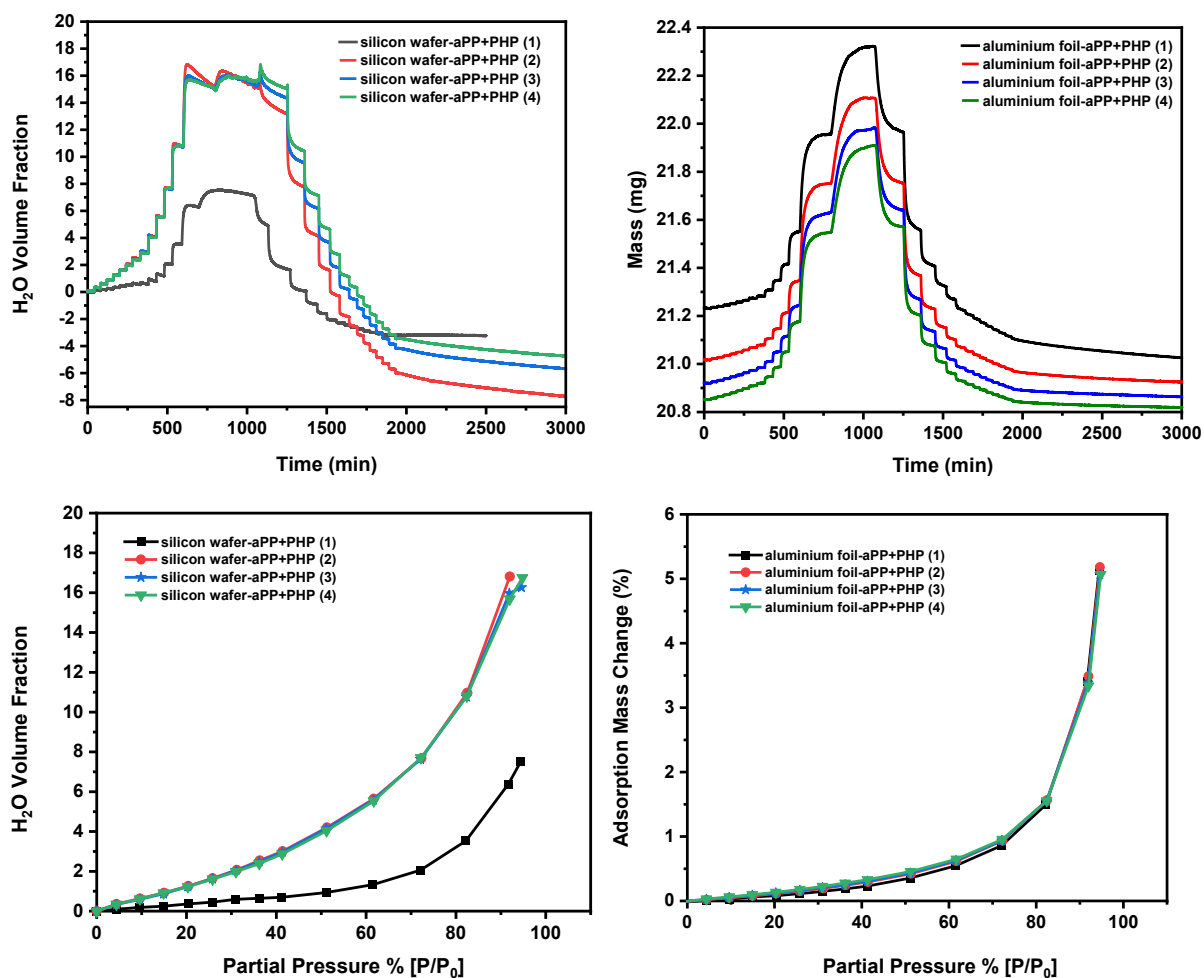
Figure 7. 26 Ellipsometry (left) and DVS (right) data of aPP+PHP films coated onto silicon wafer and aluminium foil and the and corresponding water vapour sorption isotherms (bottom) for each substrate.

Table 7. 11 Mass changes of aPP-PHP films for consecutive experiments of water vapour measurements with a DVS.

DVS Run	Initial Mass (mg)	Final Mass (mg)	Mass Difference (µg)	Mass Loss (%)
1	21.2333	21.0198	-213.50	1.0055
2	21.0180	20.9208	-97.20	0.4625
3	20.9207	20.8607	-60.00	0.2868
4	20.8526	20.8172	-35.40	0.1698
total			**-416.10**	**1.9245**

7.7 Conclusions

From a theoretical point of view, a range of experimental techniques can be utilised for determining surfactant loss processes in polyolefins. The main techniques have been reviewed in Chapter 2 of this thesis. This Chapter shows that a combination of different methods are needed for a more comprehensive understanding of surfactant migration process. In particular, the current studies focused on the migration of Salistol PHP-26, an industrially relevant surfactant, in polymer films of industrially relevant thickness, made of LDPE, MDPE, HDPE, commercial PP, isotactic PP and atactic PP. DVS, ellipsometry and simple solubility studies have been successfully used to determine the surfactant loss process in polyolefins.

Typically, surfactant coating involves a thin layer of a liquid applied to a solid substrate via process such as dip coating. Surfactant is a chemical whose use and advantages have long been established in literature to alter the wettability of many materials. They are commonly used as coating materials to modify surfaces. Polyolefinic nonwovens coated with surfactants are widely used for the manufacturing of many personal care hygiene products. Despite the present knowledge on surfactants, polymers and coatings on their own, important questions regarding complex systems of polyolefins coated with surfactants remain open. For example, the longevity of the surfactant coatings in many products has been questioned. As a general observation from industry is that such coatings are not permanent[298]. In this Chapter we provide a series of systematic experimental results revealing processes responsible for surfactant losses in polyolefins, including surfactant losses from industrially relevant polyolefinic nonwovens.

DVS experiments provide data which shows that over time, polymer coated substrates with a surfactant top layer adsorbs less and less water vapour over time, whilst also continuing to loose mass over time. The amount of water dissolved in the surface layer was monitored this way and this measurement has been used as a proxy to determine the amount of surfactant present here for the first time. The DVS studies show that when surfactants are coated on inert surfaces such as aluminium foil, mass loss is observed over time, potentially due to evaporation effects, which can contribute to the overall loss processes of surfactants. The working hypothesis is that as the surfactant is lost from the surface due to evaporation, less surfactant is present, and therefore over time water uptake by the sample reduces.

Experiments were conducted to test this hypothesis by coating the surfactant onto a polymer and studying gravimetrically the rate of loss of the surfactant using a DVS. The results confirmed mass loses but demonstrated a rate of mass loss which was much higher than the rate of mass loss from the reference experiments, suggesting that there must be two concurrent processes occurring. The mass loses observed experimentally and attributed to surfactant loses changed as a function of temperature and surfactant loading/concentration. The surfactant loss process was slow at 25°C but it increased with temperature and surfactant concentration. These trends are expected when the mass loss process is attributed to evaporation. The highest surfactant loaded sample required more energy to evaporate. This suggested that the process is thermally activated which is common with most such processes, the higher the temperature the faster the evaporation rate. These are energy activated processes and therefore temperature dependant and that is why the rate of surfactant loss measured varied for the different temperatures.

The rate of surfactant loss appears to be dependent on the tacticity of the material too i.e., % crystallinity of the substrate. DVS data showed that the total loss of material on the polymer surface is by mass is much greater than evaporation rate, indicating solubility of the surfactant into the polymer. Therefore, the suggestion is that there are two processes occurring a) evaporation of the surfactants into the surrounding environment and b) dissolution of the surfactants into the polymer. There is direct evidence from DVS data that there is mass loss as a function of time, and that this mass loss is due to surfactant evaporation. But this rate of loss is 10 times too low to fully account for all the overall loss of surfactant. The DVS data confirms that the surfactant loss due to evaporation is very slow over time. However, these evaporative surfactant loss process appears to be much slower, than expected based on industrial observations (i.e., it takes years rather than months). Therefore, evaporation doesn't appear to be sufficient to account for all the losses reported, so surfactant solubility must be also responsible for the most significant component of the surface loses observed.

As discussed in Chapter 6 semi-crystalline PP/PE polymers feature crystalline domains and non-crystalline amorphous domains. Morphology and distribution of crystalline and amorphous regions is believed to influence the surfactant solubility into polyolefins. The solubility of the surfactants in the different polymer analogues was estimated in glass vials by adding the surfactant to the polymer analogue in liquid form and observing whether the surfactant was soluble in the liquid or not. At a molecular level it was hard to establish if the surfactants fully dissolved, i.e., formed one phase with the polymer or were dispersed within the polymer, i.e., formed more than one phase with the polymer during these simple experiments. However, the data presented in this Chapter is sufficient evidence that

surfactants dissolve/disperse into low molecular weight analogues of PP/PE polymers. Therefore, it can be proposed that surfactants are likely to be soluble into the PE and PP. It has been demonstrated that Stantex S6327 also dissolved into hydrocarbon-based solvents and therefore proposing that the surfactants can dissolve into a hydrocarbon polymer is not an unreasonable hypothesis. Overall, these preliminary estimates of surfactant solubilities into different solvents and into PP/PE analogues low molecular weight polymers support the hypothesis that surfactants are likely to be soluble and can dissolve into PE/PP based polymers including nonwovens. This assertion was further supported by the DVS data.

Many of the observations documented in this Chapter have shown that using a DVS it is possible to estimate the amount of surfactant present on different substrates. Actual amounts of surfactant mass loss were calculated for the different surfactant loaded samples using the DVS raw data. Potentially, this information can also be achieved by alternative spectroscopic methods such as ATR but for this one approach needs to make contact with the sample which is difficult for non-woven samples. Another way you can potentially estimate the amount of surfactants in these complex systems is by simple extractions with a solvent. However, the complication is that other chemicals dissolved into the polymer could be extracted this way, including undesirable impurities and hence such measurements will be inaccurate. The approach presented in this Chapter for determining surfactant loading levels using a DVS provides direct measurements which are reproducible and accurate. Therefore, an important milestone is to produce more experimental data to establish if this method can be equally as useful for long term aging studies. In general, efforts in several directions are still required e.g., need to test different types of surfactants and polymers, before this method can be used as standard for studying such complex systems, but this research has shown it DVS is a suitable method that can be used successfully for determining surfactants-polyolefins interactions over time.

A bespoke DVS combined with an ellipsometer was used to study surfactant solubility in thin films of polyolefins. Ellipsometry data shows that over time the rate of surfactant loss from the surface decreases which is characterised by the surfactant film thinning, and the rate of thickness loss is much greater than the rate of mass loss evidenced by DVS data. There is no supporting evidence to suggest that the surfactant is evaporating any faster, so the only explanation is that it is migrating somewhere else i.e., dissolving inside the polymer layer. Some issues remain, and unfortunately, a clear picture cannot emerge because there doesn't always appear to be consistency on the measurement of the data across the different measurement approaches on the exact rates of surfactant loss. However, the important thing is that all the data confirm absolute loss of surfactants over time in a temperature dependant

fashion. When evaporation is concerned then temperature plays a key role. As for the most common commercial polymers like polyolefin, the relative humidity has a considerable effect on permeability and sorption characteristics. DVS data evidence that temperature expedites the migration of surfactants from the material. It is believed that temperature has a greater effect on the surfactant evaporation process than the process of surfactant dissolution into the polymer layer.

In analysing the ellipsometry data, the best fit between experimental and modelling data was obtained when it was assumed that the surfactant dissolved in polymers. That is, the model that fitted best was the one where the surfactant and the polymer were assumed in the same phase. The ellipsometry data for 5 different polymer-based samples coated with PHP confirmed surfactant dissolution into the bulk of the polymer layer. It is accepted[473] that small molecules are unable to permeate through the polymer crystallites, because they are insoluble into these strongly ordered materials. Thus, the small molecule permeation into semicrystalline polymers is confined into the amorphous regions. This finding aligns with the data in Chapter 6 which showed the most amorphous materials have the most solvents dissolved in them. In the same way solubility of surfactants in semicrystalline polymers takes place only in the non-crystalline regions. This observation is supported by the results of this study which demonstrate that the highest surfactant dissolution for the polyolefins occurred for the lowest crystallinity. The highest surfactant solubility was observed for aPP which is 100% amorphous, with aPP demonstrating a rate of mass loss of -0.03235 ± 0.00268 mg/day. In comparison, HDPE featuring ~ 64 % crystallinity had a rate of mass loss of -0.00714 ± 0.00059. The explanation is that more surfactant desorbed from aPP since more can dissolve in this amorphous polymer compared to HDPE, which is semicrystalline in nature, such correlations are shown in Figure 7. 15.

Understanding sorption, solubility, and transport mechanisms of surfactants into polymeric materials is important although challenging area. This is a complex phenomenon and not very well understood. The experimental data presented in this Chapter, via both direct and indirect analysis, have helped determine the fundamental processes responsible for the surfactant losses from polyolefins surfaces. In conclusion it has been established that surfactants were being lost from the surface of polymers due to evaporation as well as transport into the polymer bulk. Based on data from the rates of surfactant loses it can be proposed that surfactants coated onto the polymer surface simply dissolve into the polymer before slowly desorbing out to the surface again. This dissolution is then followed by the very slow evaporation of the surfactants from the surface over time.

8 Conclusions and Future Work

8.1 Summary of Conclusions

The objective of this thesis was to investigate surfactant - polymer interactions in a multicomponent solid system and establish how these interactions develop over time. The unique properties of PP and PE make them excellent candidate base materials for manufacturing nonwoven fibres. Polyolefin based industrial nonwovens are routinely coated with surfactants, which converts them into hydrophilic materials that are wettable and facilitate water movement throughout the fibre networks. This hydrophilicity is an essential attribute which allows these materials to be used for manufacturing disposable hygiene products, like facemasks, wipes, absorbent materials, baby, and adult nappies. It is a common industrial experience that the surface hydrophilicity of these coated materials is time dependent, with significant losses in surface concentrations of surfactants being observed[32]. It is, therefore, important to understand how the surfactants interact with the polymer and their fugitive nature if improvements in products manufactured using surfactant treated polymeric nonwovens are to be achieved.

The work conducted in this Thesis can be roughly divided in four main parts. The first part comprises of Chapters 1 and 2. In these Chapters, the reader is provided with a review of developments in man-made polymers, key attributes of these materials, with a focus on polyolefins, and the different approaches used for engineering their different surface properties for a wide-ranging industrial purpose. Developments in new polymerisation technology and catalysts during the past decade have tremendously influenced the use of polyolefins for many applications, especially in textiles and nonwovens. Polyolefin nonwovens are used in a great variety of applications, such as household air filters, insulating house-wraps, automotives, as well as health care and personal hygiene products. These Chapters review and discuss the nonwoven processing operations as well as the advances in polyolefins suitable for nonwoven application. This review is particularly important because polyolefin-based spunbond and melt blown fabrics are the material of choice for disposable hygiene and medical applications like diapers, incontinence pants, sanitary napkins, and the more current topical products in the Covid era including disposable surgical gowns and face-masks[477].

From a theoretical point of view, a range of experimental techniques can be utilised for investigating polymer–surfactant interactions and for understanding the behaviour of polymeric surfaces after modification with surfactants over time. Many of these techniques

have been reviewed in Chapter 2 and select techniques have been utilised in this research. Overall, this thesis has demonstrated that a combination of several different experimental methods are necessary for understanding the surfactant migration on polymeric substrates in a comprehensive way.

The main experimental methods utilised in this thesis can be grouped into the following three categories:

1. Surface characterisation techniques
2. Network – 3D imaging characterisation methods
3. Bulk characterisation techniques

8.1.1 Surface Characterisation Techniques

The second part of this thesis, covering studies presented in Chapter 4, focused on researching methods for characterising the surface properties of polyolefin-based nonwovens, including those coated with surfactants manufactured via standard high speed, low-cost coating processes used for production of disposable baby nappies. To understand the interaction between surfactants and polyolefins, several chemical properties and physicochemical descriptors of these materials were investigated including wettability, specific surface area, surface energy, sorption kinetics, and their elemental composition.

Specific surface area BET measurements demonstrated that industrial nonwovens are characterised by generally low specific surface area values, in the range 0.1 - 4 m^2/g and that IGC was better suited for the analysis of these materials than the standard N_2 volumetric approach because it exhibited higher sensitivity and precision. IGC was also used for surface energy measurements of surfactant coated and uncoated nonwovens. The thermodynamic interactions between surfactant molecules and the polyolefin substrate has been described by physiochemical parameters, such as the dispersive contribution of surface energy γ_s^D. This property was determined across the whole surface area of the nonwoven sample using IGC. Normally alkane probes are used as the standard approach for measuring the dispersive surface energy of particulate solids using IGC. However, alkanes dissolve in the polyolefin nonwoven fibres, so a new method using alcohols as probe molecules instead of alkanes was developed here for the first time. Various polyolefin base nonwovens were tested, and the γ_s^D measured using alcohols was determined to be between 20 and 40 mJ/m^2. These results were in line with the literature documents for γ_s^D values for similar polyolefin-based materials so it

was concluded that the new method of using alcohols was a suitable alternative for γ_s^D measurements, when the standard method of using alkanes cannot be used.

Contact angle measurements using water as the probe liquid were utilised to differentiate between surfactant coated and uncoated zones for nonwovens. The data demonstrated good surface homogeneity for the native hydrophobic nonwovens. However, the surfactant coated samples were characterised by bimodal distribution of advancing contact angles for water. The nonuniformity of the surfactant distribution reflected by the wide variation of contact angles measured, increased as a function of surfactant loading. This could be a process dependent feature which is more pronounced for the higher loadings but more likely this is a material dependent effect since the nonwovens are not flat but comprise of a web of fibres with voids and intersections. The coated samples featured patch wise wetting heterogeneity, meaning that the surfactant coating did not cover the whole of the sample surface and it was unevenly distributed across the 3D fabric structure network.

To measure the elemental composition of surfactant coated and uncoated nonwoven fibres XPS was utilised. Analysis of freshly coated and aged nonwoven samples confirmed that the surfactant treatment was not permanent, and the surface concentrations were significantly reduced after one year. Similar aging effects of hydrophilic nonwovens have been reported in the literature[394, 395]. XPS analysis demonstrated the hydrocarbon nature of these materials and some of the polar elements present responsible for the hydrophilic nature when the nonwovens were coated with surfactants. XPS indicated that surfactants introduced a variety of oxidised functional groups onto the surface of the coated polymer which were responsible for the changes in the polymer surface properties.

Overall, this Chapter makes a significant contribution towards characterising polyolefinic based nonwovens coated with surfactants. Furthermore, it provides an effective and novel protocol for accurate surface energy measurements using IGC as an important surface characterisation technique for these materials. One of the main advantages of IGC is that it enables measurements in ambient conditions (room temperature and humidity), which means a solid-state material can be characterised in its native state.

8.1.2   Network – 3D Imaging Characterisation Methods

The third part of this thesis, covering studies presented in Chapter 5, focuses on imaging of nonwovens in 3D. One of the objectives of this thesis was to confirm, quantify and visualise

surfactant distributions onto the surface of the nonwoven fabrics like those used to manufacture disposable nappies. To achieve this objective a novel method for visualising in 3D and quantifying surfactant distributions on polymeric nonwoven fibres using CLSM and BR14 dye was developed. Wettability studies, in Chapter 4, revealed the patch wise topographical heterogeneity of the surfactant coated nonwovens. However, this phenomenon is difficult to visualise and quantify in a 3D fibre network.

To understand the surfactant-polymer interactions in a multicomponent solid system, an analytical technique was required that provided two types of information about the surfactants: the 3D spatial distribution of surfactants throughout the polymer fibre network as well as surfactants distributions within the fibres. Techniques such as x-ray tomography, confocal Raman microscopy, and confocal laser scanning microscopy were all considered. However, x-ray tomography produced poor contrast been between the polymers and surfactants. Confocal Raman spectroscopy can simultaneously map both spectral and spatial features of inhomogeneous structures. However, mapping on microscopic scale with RCM was challenging due to the resolution of the scanning system being diffraction limited (about 0.2–0.5 micron, depending on the excitation wavelength). CLSM[314] proved useful for studying materials containing surfactants in an effective way.

CLSM is reported here for the first time to image the 3D surfactant distributions on polymeric nonwovens. A novel method has been developed as part of this thesis for visualising surfactants coated into nonwoven fibers in a non-invasive way. Data presented in Chapter 5 provides information on the 3D spatial distribution of surfactants throughout the polymer fibre network in a quantitative manner. Optical contrast has been achieved simply by introducing a fluorescent dye, via vaporisation at elevated temperatures, which preferentially dissolves into the hydrophilic surfactant regions of the nonwoven sample. The most common fluorescence labelling method is solution-based staining which is incompatible for investigating materials containing surfactants as the solvent would dissolve/displace the surfactants, rendering such methods ineffective. The approach proposed here for introducing a fluorescent dye to nonwoven samples is effective and without the short comings of the liquid based staining approaches. Through direct visualization with CLSM, the interactions between surfactants and fibers, were observed and compared between polymers with different hydrophilicities. The method is based around the high affinity exhibited by the hydrophilic fluorophore, BR14, for the surfactant coated regions of hydrophobic nonwoven samples compared to the uncoated nonwoven regions.

This method will have application into a number of other important research challenges where imaging droplet/liquid distributions in 3D nonwoven materials are important including water/fog harvesting using polymeric fibres[421], wetting of flexible fibre arrays[422], distributions of viral droplets captured by facemask using nonwoven materials[423, 424] as well as oil droplet capture[425] where the efficient process performance requires optimal surface treatments for oil droplet capture and release.

8.1.3 Bulk Characterisation Techniques

The final part of this thesis focuses on understanding the fugitive nature of surfactants in polyolefins. Although the 3D spatial distribution of surfactants throughout the polymer fibre network was visualised utilising CLSM, this provided no insight on the chemical interactions between the polymers and the surfactants. There are known to be significant chemical interactions between non-polar, or weakly polar, organic species with polyolefinic materials, resulting in significant solute solubility. One of the hypotheses considered was the dissolution of the surfactants into the polymer as responsible for the aged, related surfactant loss phenomena noted for industrial nonwovens coated with surfactants.

Chapter 6 and 7 provide comprehensive experimental studies looking into the bulk properties of amorphous and semicrystalline PP and PE, as well as for these polymers in contact with solutes including surfactants. The % crystallinity of a range of PP and PE types of samples were determined and their effect on the sorption of organic solutes was studied. It is accepted in the literature that transport of small molecules in semicrystalline polymers takes place only in the non-crystalline regions, assuming impermeable crystalline and permeable disordered regions. Unsurprisingly, these studies have shown that the presence of crystalline regions decreased the sorption of organic solutes. For example, toluene mass uptake in aPP, (which is entirely amorphous) was 64% compared to 4% for HDPE, which is a semi-crystalline polyolefin with high degree of crystallinity, ($X_c \sim 64\%$). This is because aPP which is 100% amorphous has more solute capacity as it lacks crystalline regions.

DVS was utilised to measure sorption and transport mechanisms of small organic molecules and surfactants in polyolefin films over time. The effect of different molecules on different types of PE and PP were studied over a wide range of temperatures, (25°C, 35°C, 45°C and 55°C) and humidities, mimicking different environmental conditions. It was demonstrated that temperature increased diffusion rates of organic molecules into polyolefins and this behaviour can be explained because at higher temperatures there is faster equilibrium and therefore,

faster diffusion. However, increasing the molecular size, or polarity, of the solute decreased the solubility. Cyclohexane for example demonstrated the highest solubility, whereas IPA and water showed minimal to no uptake. The somewhat high solubilities observed for industrially relevant samples were attributed to impurities. PE/PP based nonwovens are sometimes fabricated at high temperatures in the presence of atmospheric oxygen, the resulting polymers may contain oxygenated structures. The measured solubilities for the commercial samples did not appear unreasonable for the potentially slightly oxidised polymers. Overall, DVS studies have shown that the different organic solutes dissolved at a steady rate, with differences between them based on molecular weight, molecular structure, polarity, and temperature.

Data on the sorption of small molecules in semicrystalline polymers can be obtained by experimental measurements and predicted using computational simulations. Collaboration work during this research has led to successful comparisons of experimental data with model projections from our modelling collaborators. The new SAFT model developed by our collaborators and used in here to compare the DVS isotherm data allowed the solubility of a range of compounds in different samples of PE and PP to be calculated. Predicting solubility of different compounds in semi-crystalline polymers is of critical importance for a vast number of applications, as their mechanical and transport properties are heavily dependent on the amount of solutes that dissolve in the bulk. The findings demonstrate DVS as a potential alternative polymer characterisation technique when there is a need to quantify the extent of both free and tied amorphous domains present in a semi-crystalline polymer. These descriptors can be estimated from an experimental solute sorption isotherm, and this knowledge of both free and tied amorphous domains allows sorption behaviour for other solutes to be reliably predicted. Once these properties are measured for a known hydrocarbon solute, then a SAFT model can then be developed to predict the isotherms for any hydrocarbon solvent or temperature. This development is important because in practice there are sorption experiments that are impractical to do, including high temperatures, high pressure and over very long-time frames. Providing the correct physiochemical descriptors of the amorphous domains are established, then these impractical experiments can then be conducted *in silico*. Predicting the sorption of solutes in polyolefins is important for a vast number of applications as their transport properties are dependent on the degree of solute dissolution.

The thesis has also looked at the determination of surfactant loss processes in polyolefins. As discussed before, the longevity of the surfactant coatings in many products has been questioned and observation from industry is that such coatings are not permanent[298]. The final part of this thesis provides a series of systematic experimental results which reveal the

processes responsible for surfactant losses in polyolefins, including surfactant losses from industrially relevant polyolefinic nonwovens. The amount of water dissolved in the material was used here for the first time as a proxy to the amount of surfactant present on the polymer sample surface. Reference DVS studies confirmed very slow mass losses due to evaporation effects from the coated polymer, which contributed to loss of surfactant from the polymer surface. Additional experimentations using polymers demonstrated a rate of surfactant mass loss from the polymer surface which was much higher than the absolute rate of mass loss, suggesting that there were two processes occurring.

The solubility of the surfactants in the different polymer analogues was estimated with simple solubility studies. At a molecular level it was difficult to establish if the surfactants were fully dissolved. However, the data from preliminary estimates of surfactant solubilities into different solvents and into PP/PE analogues low molecular weight polymers support the hypothesis that surfactants are soluble and can dissolve into PE/PP based polymers including nonwovens. Therefore, based on these findings the proposal here is that there are two processes occurring a) a slow evaporation of the surfactants into the surrounding environment and b) a faster concurrent dissolution of the surfactant into the polymer, which then facilitates slow long term surface evaporation.

Temperature was shown to expedite the migration of surfactants from the material. It is believed that temperature has a greater effect on the surfactant evaporation process than the process of surfactant dissolution into the polymer layer. The mass loses observed experimentally and attributed to surfactant loses changed as a function of temperature and surfactant loading/concentration. These trends were expected when the mass loss process is attributed to evaporation. The highest surfactant loaded samples would require more energy to evaporate because these are energy activated processes and therefore temperature dependant. Therefore, the rate of surfactant loss measured varied for the different temperatures and surfactant concentrations. The rate of surfactant loss appeared to be dependent on the tacticity of the material too, showing that polymer morphology also influenced the surfactant solubility into polyolefins. The highest surfactant dissolution for the polyolefins occurred in the polymer with the lowest crystallinity, aPP which is 100% amorphous demonstrating a rate of mass loss of -0.03235 ± 0.00268 mg/day. In comparison, HDPE featuring ~ 64 % crystallinity had a rate of mass loss of -0.00714 ± 0.00059. This is because more surfactant is desorbed from aPP since more can dissolve in this amorphous polymer compared to HDPE, which is semicrystalline in nature. The finding aligns with the data in Chapter 6 which demonstrated that the most amorphous materials have the most solvents dissolved in them.

This thesis showed that it is possible to estimate the amount of surfactant present in different substrates using a DVS combined with an ellipsometer. Over time the rate of surfactant loss from the surface was found to decrease which was characterised by the surfactant film thinning, and the rate of surface film loss was much greater than the rate of mass loss evidenced by the DVS data. It is not reasonable to suggest that the surfactant was evaporating any faster, so the only plausible explanation was that the surfactant dissolved inside the polymer substrate. Thus, providing further evidence in support of the proposed two-mechanism migration process for the surfactants. Analysis of the ellipsometry data supported the view that the surfactant dissolved into the polymer layer. Specifically, the model that fitted best the ellipsometry data was the one where the surfactant and the polymer were assumed to be in the same phase.

Understanding sorption, solubility, and transport mechanisms of surfactants in polymeric materials is an important, though challenging research area. This thesis offers explanations of the fundamental understanding of the mechanism by which surfactants are lost in these complex systems, and methodologies for visualising surfactant distributions on complex 3D nonwovens. Finally, a more detailed experimental and theoretical understanding of the solubility of small molecules in polyolefins is also presented.

8.2   Overarching Learnings from this Work

This thesis includes a novel protocol for visualising surfactants in nonwoven polymer fibres, which was successfully used to determine the patch wise heterogenic nature of surfactant coatings on complex 3D nonwoven materials. The aging of these coated materials was confirmed and more importantly two processes, evaporation, and dissolution, were establishes as responsible for the fugitive nature of surfactant coatings on polymeric nonwoven samples. As depicted in Figure 8. 1 this research shows that surfactants are lost from the surface of polymer initially because of evaporation and diffusion/dissolution into the bulk polymer. Overtime, diffusion becomes the prominent process, resulting on surfactant film thinning because surfactants coated onto the polymer surface simply dissolve into the polymer. However, there appears to be a drive for the surfactant molecules to slowly desorb out to the surface of the polymer again. The re-surfaced surfactants from the bulk of the polymer, are then very slow evaporated off from the polymer surface resulting on further surfactant film thinning and mass loss until all the surfactants are lost.
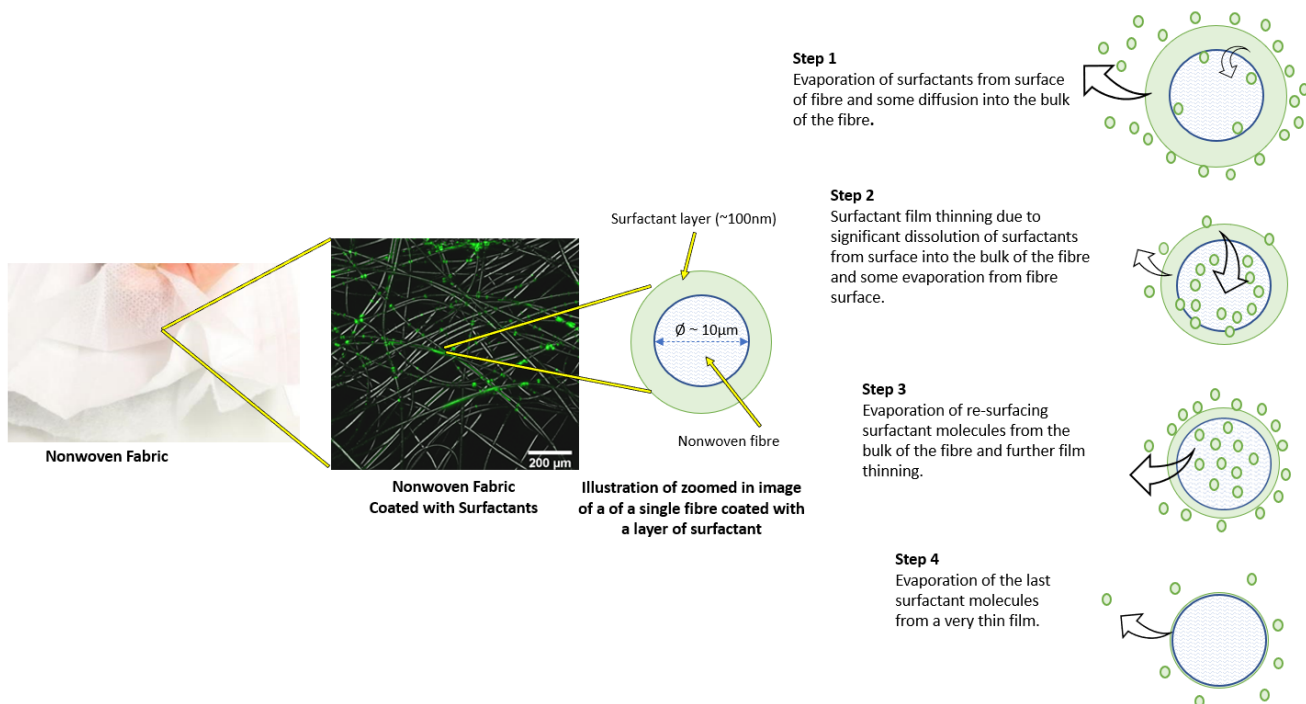
Figure 8. 1 Illustration of processes responsible for the migration of surfactants from coated polyolefin based nonwoven fabric. Not to scale.

8.3 Directions for Future Work

Research in this thesis has opened new areas of studies and in addition to the work presented in this thesis, there remains several key areas for much further exploration that could yield further interesting information.

Future work could address the following:

There remain avenues to pursue in regard to mapping out surfactant distributions for a wider range of materials coated with surfactant, not only nonwovens. In Chapter 5 a novel method was reported for visualising surfactants in nonwovens. It would be beneficial to conduct additional experimental studies to validate this method so that it can be implemented by the industry for use as part of their QA process. The test protocol could be validated for a range of different surfactants. To further this study, increasing the catalogue of surfactants analysed in polymer films would allow better correlation of properties to their behaviour. This could be extremely useful when choosing a surfactant for industrial applications.

Also, the question whether aging is affected by sample history during prolonged time scales and long-term storage, could be further explored. A broader spectrum of conditions could be examined. Additional work and perhaps modelling can be applied in regard to surfactant solubility in polymers and the impact on the overall diffusion behaviour with regards to the degree of crystallinity and the morphological organisation.

The complex nature of the surfactant layers that can form on the surface of the thin polymer films is of significant interest. It appears that the concentration of surfactant and the environmental conditions determines the relationship and how this develops over time, and hence the thickness of the surfactant layer changes. As the maximum concentration of surfactant studied was 2% w/v it would be of interest to increase the concentration of surfactant further and observe the extent to which the thickness of the surfactant layer changes. The stability of multiple surfactant layers on the surface of polymer and their evolution with time would also be of interest, do they continue to thin out? Further ellipsometry studies on the films as they develop with time and perhaps introduction of some frictional force microscopy would help to answer these questions.

The functionalisation of polymer surfaces requires significant effort. Relatively complex methods such as atmospheric pressure plasma jets and chemical grafting have also been used by others. Additional further studies could also look at comparison of these different methods for functionalisation of polymer surfaces mapping their corresponding effects on long term stability on polymer function. Therefore, an important milestone is to produce more experimental data to establish how the aging affects observed in this research compare with aging of polymer surfaces functionalisation by other methods.

In general, efforts in several directions are still required for example establishing methods which could be used to control the process of losing surfactants so that manufactures can minimise such losses and improve their products. Modelling the choice of surfactant(s) in combination with the chemistry of the substrate could also be beneficial and assist with determining a robust and controlled process of moving fluids within complex 3D polymeric nonwoven materials.

REFERENCES

1.   Staudinger, H., Über Polymerisation. *Berichte der deutschen chemischen Gesellschaft (A and B Series)* **1920,** *53* (6), 1073-1085.
2.   Holger Frey and Tobias Johann, Celebrating 100 years of "polymer science": Hermann Staudinger's 1920 manifesto. . *Polymer Chemistry* **2020,** *11*, 8-14.
3.   Russell, S. J., *Handbook of Nonwovens*. Woodhead Publishing: 22 Dec 2006; p 544
4.   Pasquini, N., Polypropylene Handbook. *HANSER* **2005**, 491–569.
5.   Badrossamay, M.; Sun, G., Enhancing hygiene/antimicrobial properties of polyolefins. *Polyolefin Fibres* **2009**, 262-287.
6.   Zhu, C.; Jiang, W.; Hu, J.; Sun, P.; Li, A.; Zhang, Q., Polylactic Acid Nonwoven Fabric Surface Modified with Stereocomplex Crystals for Recyclable Use in Oil/Water Separation. *ACS Applied Polymer Materials* **2020,** *2* (7), 2509-2516.
7.   Goddard, J. M.; Hotchkiss, J. H., Polymer surface modification for the attachment of bioactive compounds. *Progress in Polymer Science* **2007,** *32* (7), 698-725.
8.   Gruber, E. D. G. a. J. V., *Principles of Polymer Science and Technology in Cosmetics and Personal Care*. **1999**.
9.   Namazi, H., Polymers in our daily life. *Bioimpacts* **2017,** *7* (2), 73-74.
10.   Unnikrishnan, S. K. N. S. M. L., *Trends and Applications in Advanced Polymeric Materials*. Scrivener Publishing LLC: **2017**.
11.   Motloung, M. P.; Ojijo, V.; Bandyopadhyay, J.; Ray, S. S., Cellulose Nanostructure-Based Biodegradable Nanocomposite Foams: A Brief Overview on the Recent Advancements and Perspectives. *Polymers* **2019,** *11* (8), 1270.
12.   Geyer, R., Jambeck, J. R., & Law, K. L., Production, use, and fate of all plastics ever made. *Science Advances* **2017**.
13.   Lascano, D.; Guillen-Pineda, R.; Quiles-Carrillo, L.; Ivorra-Martínez, J.; Balart, R.; Montanes, N.; Boronat, T., Manufacturing and Characterization of Highly Environmentally Friendly Sandwich Composites from Polylactide Cores and Flax-Polylactide Faces. *Polymers* **2021,** *13* (3), 342.
14.   Cichosz, S.; Masek, A., Thermal Behavior of Green Cellulose-Filled Thermoplastic Elastomer Polymer Blends. *Molecules* **2020,** *25* (6), 1279.
15.   Dutkiewicz, J., Some Advances in Nonwoven Structures For Absorbency, Comfort and Aesthetics. *Autex Research Journal* **2002,** *2* (3).
16.   Dey, S.; Purdon, M.; Kirsch, T.; Helbich, H.; Kerr, K.; Li, L.; Zhou, S., Exposure Factor considerations for safety evaluation of modern disposable diapers. *Regulatory Toxicology and Pharmacology* **2016,** *81*, 183-193.
17.   Bostik Adhesives in the Core System. https://www.bostik.com/global/en/markets-applications/disposable-hygiene-adhesives/adhesives-hygiene-manufacturing/core-needs-disposable-hygiene/core-materials/.
18.   Chen, J.-P.; Chiang, Y.-P., Surface modification of non-woven fabric by DC pulsed plasma treatment and graft polymerization with acrylic acid. *Journal of Membrane Science* **2006,** *270* (1), 212-220.
19.   Sanbhal, N.; Mao, Y.; Sun, G.; Xu, R. F.; Zhang, Q.; Wang, L., Surface modification of polypropylene mesh devices with cyclodextrin via cold plasma for hernia repair: Characterization and antibacterial properties. *Applied Surface Science* **2018,** *439*, 749-759.
20.   Tsai, P. P.; Wadsworth, L. C.; Roth, J. R., Surface modification of fabrics using a one-atmosphere glow discharge plasma to improve fabric wettability. *Textile Research Journal* **1997,** *67* (5), 359-369.
21.   Kwon, Y. A., Influence of the CF4 plasma treatments on the wettability of polypropylene fabrics. *Fibers and Polymers* **2002,** *3* (4), 174-178.
22.   Väänänen R., H. P., Tuominen M., Kuusipalo J., Harlin A. , Fast and efficient surface treatment for nonwoven materials by atmospheric pressure plasma. *AUTEX Research Journal* **2010,** *10* (1), 8-13.
23.   B, K., Plasma Surface Treatments of Nonwovens. **2016**.

24.   Liu, K.; Wei, J. F.; Zhou, X. Y.; Liu, N. N., Construction of amphiphilic segments on polypropylene nonwoven surface and its application in removal of endocrine disrupting compounds (EDCs) from aqueous solution. *Applied Surface Science* **2015,** *337*, 178-187.

25.   C, D.; K, Z., Surface modification of polyolefins by photografting of acrylic monomers. *Macromolecular Symposia* **1998,** *129* (1), 99-108.

26.   Chen, S.; Zhang, L.; Sun, M.; Zhang, X.; Chen, W., Surface modification of polypropylene nonwoven fabrics by grafting of polydopamine. *Advances in Polymer Technology* **2018,** *37* (8), 3519-3528.

27.   Yoo, S.; Barker, R. L., Moisture management properties of heat-resistant workwear fabrics - Effects of hydrophilic finishes and hygroscopic fiber blends. *Textile Research Journal* **2004,** *74* (11), 995-1000.

28.   Saffar, A.; Carreau, P. J.; Ajji, A.; Kamal, M. R., Development of polypropylene microporous hydrophilic membranes by blending with PP-g-MA and PP-g-AA. *Journal of Membrane Science* **2014,** *462*, 50-61.

29.   Xin, Z.; Yan, S.; Ding, J.; Yang, Z.; Du, B.; Du, S., Surface modification of polypropylene nonwoven fabrics via covalent immobilization of nonionic sugar-based surfactants. *Journal of Applied Surface Science* **2014,** *300,* 8-15.

30.   Sarmadi, A. M.; Kwon, Y. A.; Young, R. A., Wettability of nonwoven fabrics. 2. Effect of cationic surfactant treatment. *Journal of Industrial & Engineering Chemistry Research* **1993,** *32* (2), 287-293.

31.   Quincy, R. Nonwovens treated with surfactants having high polydispersities. United States Patent US6300258B1, 1999.

32.   Aviles, M. Absorbent Article with Topsheet Treated to Reduce Surfactant Migration. 2020.

33.   Website: Tiseo, I. Global plastic production 1950-2019. https://www.statista.com/statistics/282732/global-production-of-plastics-since-1950/.

34.   Billmeyer, F. W., *Textbook of Polymer Science*. Wiley: 1984.

35.   Amorphous State of Polymers. In *Fundamentals of Polymer Science for Engineers*, 2017; pp 59-102.

36.   Crystalline Polymers. In *Fundamentals of Polymer Science for Engineers*, 2017; pp 103-140.

37.   Polymer Molecular Weights. In *Fundamentals of Polymer Science for Engineers*, 2017; pp 167-188.

38.   Flexibility of Polymer Chains and Its Origin. In *Fundamentals of Polymer Science for Engineers*, 2017; pp 43-58.

39.   Hufenus, R.; Yan, Y.; Dauner, M.; Kikutani, T., Melt-Spun Fibers for Textile Applications. *Materials* **2020,** *13* (19), 4298.

40.   Ziegler, K. H., E; Breil; H; Martin, H, Polymerisation von Äthylen Und Anderen Olefinen. *Angewandte Chemie.* **1955,** *67* (16), 426–426.

41.   Maddah, H. A., Polypropylene as a Promising Plastic: A Review. *American Journal of Polymer Science* **2016,** *6* (1), 1-11.

42.   McKenna., J. L., *Polyolefin Reaction Engineering*. Wiley-VCH Verlag GmbH & Co. KGaA: 2012.

43.   Kavesh, S.; Schultz, J. M., Meaning and measurement of crystallinity in polymers: A Review. *Polymer Engineering & Science* **1969,** *9* (5), 331-338.

44.   Graziano, A.; Jaffer, S.; Sain, M., Review on modification strategies of polyethylene/polypropylene immiscible thermoplastic polymer blends for enhancing their mechanical behavior. *Journal of Elastomers & Plastics* **2018,** *51* (4), 291-336.

45.   Jia-Horng Lin, Y.-J. P., Chi-Fan Liu, Chien-Lin Huang, Chien-Teng Hsieh, Chih-Kuang Chen, Zheng-Ian Lin and Ching-Wen Lou, Preparation and Compatibility Evaluation of Polypropylene/High Density Polyethylene Polyblends. *Materials* **2015,** (8), 8850–8859.

46.   Mural, P. K. S.; Rana, M. S.; Madras, G.; Bose, S., PE/PEO blends compatibilized by PE brush immobilized on MWNTs: improved interfacial and structural properties. *RSC Advances* **2014,** *4* (31), 16250-16259.

47.   Teh, J. W.; Rudin, A.; Keung, J. C., A review of polyethylene–polypropylene blends and their compatibilization. *Journal of Advances in Polymer Technology* **1994,** *13* (1), 1-23.

48.   Ugbolue, S. C. O., Polyolefin Fibres *:* Structure, Properties and Industrial Applications. A volume in The Textile Institute Book Series, 2 ed.; Elsevier Science: **2017**.

49.   Rucker, G. Polypropylene ethylene-propylene copolymer blends and in-line process to produce them. **2014**.

50.   Shanks, R. A.; Li, J.; Yu, L., Polypropylene–polyethylene blend morphology controlled by time–temperature–miscibility. *Polymer* **2000,** *41* (6), 2133-2139.

51.   Crangle, A., 1 - Types of polyolefin fibres. In *Polyolefin Fibres (Second Edition)*, Ugbolue, S. C. O., Ed. Woodhead Publishing: **2017**; pp 3-32.

52.   Gong, R. H., 8 - Developments in 3D nonwovens A2 - Chen, Xiaogang. In *Advances in 3D Textiles*, Woodhead Publishing: **2015**; pp 183-203.

53.   Albrecht, W.; Fuchs, H.; Kittelmann, W., *Nonwoven Fabrics: Raw Materials, Manufacture, Applications, Characteristics, Testing Processes*. Wiley: **2006**.

54.   Hubbe, M. A.; Koukoulas, A. A., Wet-Laid Nonwovens Manufacture – Chemical Approaches Using Synthetic and Cellulosic Fibers. *Journal of BioResources; Vol 11, No 2 (2016)* **2016**.

55.   V.A. Wente et al., Manufacture of Superfine Fibers. **1954**.

56.   Lohkcamp, R. Melt-Blowing-A One-Step Process for New Nonwoven Products. *TAPPI* **1973,** *56* (4), 75.

57.   *Nonwoven Fabric Manufacturing and Applications*. Nova Science Publishers, Inc.: New York, **2020**.

58.   Adanur, S., *Wellington Sears handbook of industrial textiles*. Technomic Pub: Lancaster, Pa., **1995**.

59.   Cai, B.; Zheng, Q.-K.; Li, R.-X.; Wu, D.-C., Adsorption mechanism of surfactants on nonwoven fabrics. *Journal of Applied Polymer Science* **2003,** *89* (12), 3210-3215.

60.   Nemani, S. K.; Annavarapu, R. K.; Mohammadian, B.; Raiyan, A.; Heil, J.; Haque, M. A.; Abdelaal, A.; Sojoudi, H., Surface Modification of Polymers: Methods and Applications. *Advanced Materials Interfaces* **2018,** *5* (24), 1801247.

61.   Fabbri, P.; Messori, M., 5 - Surface Modification of Polymers: Chemical, Physical, and Biological Routes. In *Modification of Polymer Properties*, Jasso-Gastinel, C. F.; Kenny, J. M., Eds. William Andrew Publishing: **2017**; pp 109-130.

62.   Ozdemir, M.; Yurteri, C. U.; Sadikoglu, H., Physical Polymer Surface Modification Methods and Applications in Food Packaging Polymers. *Critical Reviews in Food Science and Nutrition* **1999,** *39* (5), 457-477.

63.   Hamada, K.; Ochiai, T.; Tsuchida, Y.; Miyano, K.; Ishikawa, Y.; Nagura, T.; Kimura, N., Eco-Friendly Cotton/Linen Fabric Treatment Using Aqueous Ozone and Ultraviolet Photolysis. *Catalysts* **2020,** *10* (11), 1265.

64.   Koo, G.-H.; Jang, J., Surface modification of poly(lactic acid) by UV/Ozone irradiation. *Fibers and Polymers* **2008,** *9*, 674-678.

65.   Kobayashi, T.; Arisawa, M.; Ngoc, N.; Trang, T.; Myoubudani, H., Surface Modification of Polymer Textiles by Thermally Dried Ozone. *Journal of Adhesion Science and Technology - J ADHES SCI TECHNOL* **2011,** *25*, 1849-1859.

66.   MacManus, L. F.; Walzak, M. J.; McIntyre, N. S., Study of ultraviolet light and ozone surface modification of polypropylene. *Journal of Polymer Science Part A: Polymer Chemistry* **1999,** *37* (14), 2489-2501.

67.   Vesel, A.; Mozetic, M., New developments in surface functionalization of polymers using controlled plasma treatments. *Journal of Physics D: Applied Physics* **2017,** *50* (29), 293001.

68.   Ferrero, F.; Periolatto, M., Modification of Surface Energy and Wetting of Textile Fibers. 2015.

69.   Liu, T. L.; Kim, C.-J. C., Turning a surface superrepellent even to completely wetting liquids. *Science* **2014,** *346* (6213), 1096-1100.

70.   Xu, Q. F.; Mondal, B.; Lyons, A. M., Fabricating Superhydrophobic Polymer Surfaces with Excellent Abrasion Resistance by a Simple Lamination Templating Method. *ACS Applied Materials & Interfaces* **2011,** *3* (9), 3508-3514.

71.   Jean Pinson, D. T., *Surface Modification of Polymers: Methods and Applications*. Wiley-VCH: 2020.

72.   Haridoss, S.; Perlman, M. M., Chemical modification of near-surface charge trapping in polymers. *Journal of Applied Physics* **1984,** *55* (5), 1332-1338.

73.   Pellegrino, L.; Cocchiola, R.; Francolini, I.; Lopreiato, M.; Piozzi, A.; Zanoni, R.; Scotto d'Abusco, A.; Martinelli, A., Taurine grafting and collagen adsorption on PLLA films improve human primary chondrocyte adhesion and growth. *Colloids and Surfaces B: Biointerfaces* **2017,** *158*, 643-649.

74.   Sheng, E.; Sutherland, I.; Brewis, D. M.; Heath, R. J., Effects of the chromic acid etching on propylene polymer surfaces. *Journal of Adhesion Science and Technology* **1995,** *9* (1), 47-60.

75.   Gilliam, M., Polymer Surface Treatment and Coating Technologies. In *Handbook of Manufacturing Engineering and Technology*, Nee, A., Ed. Springer London: London, **2013**; pp 1-23.

76.   Ebnesajjad, S., Chapter 4 - Surface and Material Characterization Techniques. In *Surface Treatment of Materials for Adhesive Bonding (Second Edition)*, Ebnesajjad, S., Ed. William Andrew Publishing: Oxford, 2014; pp 39-75.

77.   Jönsson, C.; Aronsson, M.; Rundström, G.; Pettersson, C.; Mendel-Hartvig, I.; Bakker, J.; Martinsson, E.; Liedberg, B.; MacCraith, B.; Ohman, O.; Melin, J., Silane-dextran chemistry on lateral flow polymer chips for immunoassays. *Lab Chip* **2008,** *8* (7), 1191-7.

78.   H. Yu, E. Liua and N. H. Loha, Low temperature and deformation-free bonding of PMMA microfluidic devices with stable hydrophilicity via oxygen plasma treatment and PVA coating. *RSC Advances* **2015,** *5*, 8377-8388.

79.   Peran, J.; Ercegović Ražić, S., Application of atmospheric pressure plasma technology for textile surface modification. *Textile Research Journal* **2020,** *90* (9-10), 1174-1197.

80.   Mather, R. R., 13 - Surface modification of textiles by plasma treatments. In *Surface Modification of Textiles*, Wei, Q., Ed. Woodhead Publishing: **2009**; pp 296-317.

81.   Tendero, C.; Tixier, C.; Tristant, P.; Desmaison, J.; Leprince, P., Atmospheric pressure plasmas: A review. *Spectrochimica Acta Part B: Atomic Spectroscopy* **2006,** *61* (1), 2-30.

82.   *Plasma Technologies for Textiles*. Woodhead Publishing: **2007**.

83.   PB., N. S. a. J., *Plasma Technologies for Textile and Apparel*
Woodhead Publishing: India, **2015**.

84.   Zhang, X.; Liu, J.; Zhang, H.; Hou, J.; Wang, Y.; Deng, C.; Huang, C.; Jin, X., Multi-Layered, Corona Charged Melt Blown Nonwovens as High Performance PM(0.3) Air Filters. *Polymers (Basel)* **2021,** *13* (4).

85.   Novák, I.; Pollák, V.; Chodák, I., Study of Surface Properties of Polyolefins Modified by Corona Discharge Plasma. *Plasma Processes and Polymers* **2006,** *3* (4-5), 355-364.

86.   Shim, E., 3 - Smart surface treatments for textiles for protection. In *Smart Textiles for Protection*, Chapman, R. A., Ed. Woodhead Publishing: **2013**; pp 87-126.

87.   Klemberg-Sapieha J.E., M. L., Sapieha S., Wertheimer M.R., *Control and Modification of Surfaces and Interfaces by Corona and Low Pressure Plasma*. Springer, Dordrecht: **1993**; Vol. 230.

88.   Borcia, C.; Punga, I. L.; Borcia, G., Surface properties and hydrophobic recovery of polymers treated by atmospheric-pressure plasma. *Applied Surface Science* **2014,** *317*, 103-110.

89.   Occhiello, E.; Morra, M.; Cinquina, P.; Garbassi, F., Hydrophobic recovery of oxygen-plasma-treated polystyrene. *Polymer* **1992,** *33* (14), 3007-3015.

90.   Radu C. D., K. P., Verschuren J., *Surface modification of textiles by plasma treatments.* Marcel Dekker: New York, **2001**.

91.   Kale K. H., D. A. N., Atmospheric pressure plasma treatment of textiles using nonpolymerising gases. *Indian Journal of Fibre and Textile Research* **2011,** *36* (3), 289–299.

92.   A., W. R., *Atmospheric plasma modification of textile surfaces.* John Wiley & Sons: **2012**.

93.   Fader, R.; Schmitt, H.; Rommel, M.; Bauer, A. J.; Frey, L.; Ji, R.; Hornung, M.; Brehm, M.; Vogler, M., Novel organic polymer for UV-enhanced substrate conformal imprint lithography. *Microelectronic Engineering* **2012,** *98*, 238-241.

94.   Kraus, E.; Baudrit, B.; Heidemeyer, P.; Bastian, M.; Stoyanov, O. V.; Starostina, I. A., Surface treatment of polymers by an ultraviolet laser to improve adhesion quality. *Polymer Science Series D* **2016,** *9* (1), 5-12.

95.   Liu, X. C., Naveen; Lee, Youn Suk., Polymer surface modification using UV treatment for attachment of natamycin and the potential applications for conventional food cling wrap (LDPE). *Applied Surface Science* **2016,** *386*, 276-284.

96.   Thomas, J. I.-P. S., *Printing on Polymers, Fundamentals and Applications*. 2015.

97.   Strobel, M.; Walzak, M. J.; Hill, J. M.; Lin, A.; Karbashewski, E.; Lyons, C. S., A comparison of gas-phase methods of modifying polymer surfaces. *Journal of Adhesion Science and Technology* **1995,** *9* (3), 365-383.

98.   Bhattacharyya, A.; Klapperich, C. M., Mechanical and chemical analysis of plasma and ultraviolet-ozone surface treatments for thermal bonding of polymeric microfluidic devices. *Lab Chip* **2007,** *7* (7), 876-82.

99.   Lin, T.-Y.; Pfeiffer, T. T.; Lillehoj, P. B., Stability of UV/ozone-treated thermoplastics under different storage conditions for microfluidic analytical devices. *RSC advances* **2017,** *7* (59), 37374-37379.

100.   Vig, J. R., UV/ozone cleaning of surfaces. *Journal of Vacuum Science & Technology A* **1985,** *3* (3), 1027-1034.

101.   Körlü, A., *Use of Ozone in the Textile Industry*. In book Textile Industry and Environment, **2018**.

102.   Eren HA, O. D., The evaluation of ozonation as an environmentally friendly alternative for cotton preparation. *Textile Research Journal.* **2011,** *81* (5), 512-519.

103.   Kihlman Oiseth, S.; Krozer, A.; Lausmaa, J.; Kasemo, B., Ultraviolet light treatment of thin high-density polyethylene films monitored with a quartz crystal microbalance. *Journal of Applied Polymer Science* **2004,** *92*, 2833-2839.

104.   Wang, Y.; Wiener, J.; Militky, J.; Mishra, R.; Zhu, G., Ozone Effect On the Properties of Aramid Fabric. *Autex Research Journal* **2016,** *17*.

105.   Robin, J. J., The use of ozone in the synthesis of new polymers and the modification of polymers. *Advances in Polymer Science* **2004,** *167*, 35-79.

106.   Samsudin, N.; Hashim, Y. Z. H.-Y.; Arifin, M. A.; Mel, M.; Salleh, H. M.; Sopyan, I.; Jimat, D. N., Optimization of ultraviolet ozone treatment process for improvement of polycaprolactone (PCL) microcarrier performance. *Cytotechnology* **2017,** *69* (4), 601-616.

107.   Huang, Q.; Xia, J.; Zhao, J.; Dong, G.; Liu, F.; Meng, H.; Liang, X., Ultraviolet/ozone and oxygen plasma treatments for improving the contact of carbon nanotube thin film transistors. *Science Bulletin* **2018,** *63* (12), 802-806.

108.   Hillborg, H.; Tomczak, N.; Olàh, A.; Schönherr, H.; Vancso, G. J., Nanoscale Hydrophobic Recovery: A Chemical Force Microscopy Study of UV/Ozone-Treated Cross-Linked Poly(dimethylsiloxane). *Langmuir* **2004,** *20* (3), 785-794.

109.   Cheneler, D.; Bowen, J., Degradation of polymer films. *Soft Matter* **2013,** *9* (2), 344-358.

110.   Riveiro, A.; Maçon, A. L. B.; del Val, J.; Comesaña, R.; Pou, J., Laser Surface Texturing of Polymers for Biomedical Applications. *Frontiers in Physics* **2018,** *6* (16).

111.   Riveiro, A.; Soto, R.; Comesaña, R.; Boutinguiza, M.; del Val, J.; Quintero, F.; Lusquiños, F.; Pou, J., Laser surface modification of PEEK. *Applied Surface Science* **2012,** *258* (23), 9437-9442.

112.   Lorusso, A.; Nassisi, V.; Paladini, F.; Torrisi, L.; Visco, A. M.; Campo, N., Comparison of the laser effects induced on ultra-high-molecular-weight polyethylene. *Radiation Effects and Defects in Solids* **2008,** *163* (4-6), 435-440.

113.   Kumar, S.; Bhattarai, A.; Chatterjee, S., *Applications of Surfactants in modern Science and Technology*. **2013**; p 147-158.

114.   Yu, D. I.; Doh, S. W.; Kwak, H. J.; Kang, H. C.; Ahn, H. S.; Park, H. S.; Kiyofumi, M.; Kim, M. H., Wetting state on hydrophilic and hydrophobic micro-textured surfaces: Thermodynamic analysis and X-ray visualization. *Applied Physics Letters* **2015,** *106* (17), 171602.

115.   Dadsetan, M.; Mirzadeh, H.; Sharifi, N., Effect of CO2 laser radiation on the surface properties of polyethylene terephthalate. *Radiat. Phys. Chem.* **1999,** *56* (5), 597-604.

116.   Riveiro, A.; Soto, R.; del Val, J.; Comesaña, R.; Boutinguiza, M.; Quintero, F.; Lusquiños, F.; Pou, J., Laser surface modification of ultra-high-molecular-weight polyethylene (UHMWPE) for biomedical applications. *Applied Surface Science* **2014,** *302*, 236-242.

117.   Laurens, P.; Sadras, B.; Decobert, F.; Arefi-Khonsari, F.; Amouroux, J., Enhancement of the adhesive bonding properties of PEEK by excimer laser treatment. *International Journal of Adhesion and Adhesives* **1998,** *18* (1), 19-27.

118.   Okoshi, M.; Inoue, N., Microfabrication of Polyethylene Using Femtosecond Ti:sapphire Laser and Nanosecond ArF Laser. *Japanese Journal of Applied Physics* **2003,** *42* (Part 1, No. 9A), 5642-5647.

119.   Riveiro, A.; Soto, R.; del Val, J.; Comesaña, R.; Boutinguiza, M.; Quintero, F.; Lusquiños, F.; Pou, J., Texturing of polypropylene (PP) with nanosecond lasers. *Applied Surface Science* **2016,** *374*, 379-386.

120.   Zhang, D.; Sun, C.; Xiao, J., Effect of Selected Additives on Surface Energy of Fibers and Meltblown Nonwovens. *Textile Research Journal* **2006,** *76* (3), 261-265.

121.   Antunes, L. F.; Simon, D. A.; Fiorio, R.; Francisquetti, E., Effects of polyether siloxane surfactant on the hydrophilic capacity of polypropylene films. *Polímeros* **2019,** *29*.

122.   Sun, Y.; Xing, Z.; Xue, Y.; Mustafa, K.; Finne-Wistrand, A.; Albertsson, A.-C., Surfactant as a Critical Factor When Tuning the Hydrophilicity in Three-Dimensional Polyester-Based Scaffolds : Impact of Hydrophilicity on Their Mechanical Properties and the Cellular Response of Human Osteoblast-Like Cells. *Biomacromolecules* **2014,** *15* (4), 1259-1268.

123.   Shamsuri, A. A.; Azid, M. K. A.; Ariff, A. H. M.; Sudari, A. K., Influence of Surface Treatment on Tensile Properties of Low-Density Polyethylene/Cellulose Woven Biocomposites: A Preliminary Study. *Polymers* **2014,** *6* (9), 2345-2356.

124.   Sudari, A. K.; Shamsuri, A. A.; Zainudin, E. S.; Tahir, P. M., Exploration on compatibilizing effect of nonionic, anionic, and cationic surfactants on mechanical, morphological, and chemical properties of high-density polyethylene/low-density polyethylene/cellulose biocomposites. *Journal of Thermoplastic Composite Materials* **2015,** *30* (6), 855-884.

125.   Shamsuri, A. A.; Md. Jamil, S. N. A., A Short Review on the Effect of Surfactants on the Mechanico-Thermal Properties of Polymer Nanocomposites. *Applied Sciences* **2020,** *10* (14), 4867.

126.   Mu, L.; Seow, P.-H.; Ang, S.-N.; Feng, S.-S., Study on surfactant coating of polymeric nanoparticles for controlled delivery of anticancer drug. *Colloid and Polymer Science* **2004,** *283* (1), 58-65.

127.   Wang, Z.; Yang, H.; Pan, N.; Li, W.; Xie, Y.; Liu, Z.; Fang, Y., Effect of Polyethylene Film Lamination on the Water Absorbency of Hydrophilic-finished Polypropylene Non-woven Fabric. *Fibers and Polymers* **2019,** *20* (7), 1404-1410.

128.   Fillon, B., Chapter 17 - Polymer Thin Films—Processes, Parameters and Property Control. In *Micromanufacturing Engineering and Technology (Second Edition)*, Qin, Y., Ed. William Andrew Publishing: Boston, **2015**; pp 393-424.

129.   Inc, N. E. C. M. An Overview of Roll Coating Methods, Capabilities and Limitations – Part 2 of 4. Website: https://neweraconverting.com/news/an-overview-of-roll-coating-methods-capabilities-and-limitations-part-2-of-4 (accessed 23.07.**2021**).

130.   Chmielewski, H. J. Synthetic Surfactant-Free Finish, Sheet Having Synthetic Surfactant-Free Finish, Articles Having Sheet With Synthetic Surfactant-Free Finish, And Related Methods. 20160136321, 05/19/**2016**.

131.   Khatwani, P. A.; Desai, K. S.; Thakor, U. S., Developments in the use of nonwovens in building and construction. In *Advances in Technical Nonwovens*, Kellie, G., Ed. Woodhead Publishing: **2016**; pp 385-401.

132.   Zhang, D., 6 - Nonwovens for consumer and industrial wipes. In *Applications of Nonwovens in Technical Textiles*, Chapman, R. A., Ed. Woodhead Publishing: **2010**; pp 103-119.

133.   Chen, J. Y., 10 - Nonwoven textiles in automotive interiors. In *Applications of Nonwovens in Technical Textiles*, Chapman, R. A., Ed. Woodhead Publishing: **2010**; pp 184-201.

134.   Ajmeri, J. R.; Ajmeri, C. J., 5 - Nonwoven personal hygiene materials and products. In *Applications of Nonwovens in Technical Textiles*, Chapman, R. A., Ed. Woodhead Publishing: **2010**; pp 85-102.

135.   Tabone, M. D.; Cregg, J. J.; Beckman, E. J.; Landis, A. E., Sustainability Metrics: Life Cycle Assessment and Green Design in Polymers. *Environmental Science & Technology* **2010,** *44* (21), 8264-8269.

136.   Swatee, D.; Dianna, K.; Mauricio, O.; Ioannis, H., Modern diaper performance: construction, materials, and safety review. *International Journal of Dermatology* **2016,** *55* (S1), 18-20.

137.   Kosemund, K.; Schlatter, H.; Ochsenhirt, J. L.; Krause, E. L.; Marsman, D. S.; Erasala, G. N., Safety evaluation of superabsorbent baby diapers. *Regulatory toxicology and pharmacology : RTP* **2009,** *53* (2), 81-9.

138.   S,B. Skin benefits from continuous topical administration of a zinc oxide/petrolatum formulation by a novel disposable diaper. *Journal of the European Academy of Dermatology and Venereology* **2001,** *15* (s1), 5-11.

139.   Porter, M. R., *Handbook of Surfactants*. Springer US: **1991**.

140.   Tanford, C., The Hydrophobic Effect: Formation of Micelles and Biological Membranes. *John Wiley & Sons* **1980**, 232.

141.   Nakama, Y., Chapter 15 - Surfactants. In *Cosmetic Science and Technology*, Sakamoto, K.; Lochhead, R. Y.; Maibach, H. I.; Yamashita, Y., Eds. Elsevier: Amsterdam, **2017**; pp 231-244.

142.   Joshib, N. D. T., A Concise Review on Surfactants and Its Significance. *International Journal of Applied Chemistry* **2017,** *13* (3), 663-672.

143.   Myers, D., *Surfactant Science and Technology*. Wiley: **2020**.

144.   Chinchalikar, A. J.; Aswal, V. K.; Kohlbrecher, J.; Wagh, A. G., Small-angle neutron scattering study of temperature vs. salt dependence of clouding in charged micellar system. *The European Physical Journal E* **2012,** *35* (7), 55.

145.   Schlienger, S.; Ducrot-Boisgontier, C.; Delmotte, L.; Guth, J.-L.; Parmentier, J., History of the Micelles: A Key Parameter for the Formation Mechanism of Ordered Mesoporous Carbons via a Polymerized Mesophase. *The Journal of Physical Chemistry C* **2014,** *118* (22), 11919-11927.

146.   Schramm, L.; N. Stasiuk, E.; Marangoni, G., *Surfactants and their Applications*. **2003**; Vol. 99, p 3-48.

147.   O'Rear, E. A., Review of An Introduction to Surfactants. *Journal of Chemical Education* **2015,** *92* (11), 1779-1780.

148.   Oliveira, M.; Magri, A.; Baldo, C.; Camilios-Neto, D.; Minucelli, T.; Antonia, M.; Celligoi, M. A., Review: Sophorolipids A Promising Biosurfactant and it's Applications. *International Journal of Advanced Biotechnology and Research (IJBR)* **2015,** *6*, 161-174.

149.   Guzmán, E.; Llamas, S.; Maestro, A.; Fernández-Peña, L.; Akanno, A.; Miller, R.; Ortega, F.; Rubio, R. G., Polymer–surfactant systems in bulk and at fluid interfaces. *Advances in Colloid and Interface Science* **2016,** *233*, 38-64.

150.   Lindman, B.; Nylander, T., Chapter 26 - Polymer–Surfactant Interactions. In *Cosmetic Science and Technology*, Sakamoto, K.; Lochhead, R. Y.; Maibach, H. I.; Yamashita, Y., Eds. Elsevier: Amsterdam, **2017**; pp 449-469.

151.   Patnaik, A.; Rengasamy, R. S.; Kothari, V. K.; Ghosh, A., Wetting and Wicking in Fibrous Materials. *Textile Progress* **2006,** *38* (1), 1-105.

152.   Khan, N.; Brettmann, B., Intermolecular Interactions in Polyelectrolyte and Surfactant Complexes in Solution. *Polymers* **2019,** *11* (1), 51.

153.   Bing, C.; Qing, Z., Adsorption mechanism of surfactants on nonwoven fabrics. *Journal of Applied Polymer Science* **2003,** *89* (12), 3210-3215.

154.	Grow, D. T.; Shaeiwitz, J. A., Surfactant adsorption dynamics. *Journal of Colloid and Interface Science* **1982,** *86* (1), 239-253.

155.	S.S. Dukhin, G. K., R. Miller, *Dynamics of Adsorption at Liquid Interfaces: Theory, Experiment, Application*. Elsevier, 11 Apr 1995 - Technology & Engineering: 11 Apr **1995**; p 600.

156.	Böhmer, M. R., Effects of Polymers on Particle Adsorption on Macroscopic Surfaces Studied by Optical Reflectometry. *Journal of Colloid and Interface Science* **1998,** *197* (2), 251-256.

157.	Ivanova, R.; Alexandridis, P.; Lindman, B., Interaction of poloxamer block copolymers with cosolvents and surfactants. *Colloids and Surfaces A: Physicochemical and Engineering Aspects* **2001,** *183-185*, 41-53.

158.	Meconi, G. M.; Ballard, N.; Asua, J. M.; Zangi, R., Adsorption and desorption behavior of ionic and nonionic surfactants on polymer surfaces. *Soft Matter* **2016,** *12* (48), 9692-9704.

159.	Needles, H. L.; Berns, R. S.; Lu, W.-C.; Alger, K.; Varma, D. S., Effect of nonionic surfactant and heat on selected properties of polyester. *Journal of Applied Polymer Science* **1980,** *25* (8), 1737-1744.

160.	Bengt KronBerg, K. H., Björn lindman, Adsorption of Polymers at Solid Surfaces. In *Surface Chemistry of Surfactants and Polymers*, Wiley: **2014**; pp 211-229.

161.	Fleming, B.; Wanless, E., Soft-contact Atomic Force Microscopy Imaging of Adsorbed Surfactant and Polymer Layers. *Microscopy and microanalysis : the official journal of Microscopy Society of America, Microbeam Analysis Society, Microscopical Society of Canada* **2000,** *6*, 104-112.

162.	Grosse, I.; Estel, K., Thin surfactant layers at the solid interface. *Colloid and Polymer Science* **2000,** *278* (10), 1000-1006.

163.	Zehev Tadmor, C. G. G., *Principles of polymer processing*. John Wiley: New York, **2006**; p 746.

164.	Griffiths, P. C.; Hirst, N.; Paul, A.; King, S. M.; Heenan, R. K.; Farley, R., Effect of Ethanol on the Interaction between Poly(vinylpyrrolidone) and Sodium Dodecyl Sulfate. *Langmuir* **2004,** *20* (16), 6904-6913.

165.	Flynn, J. H., A collection of kinetic data for the diffusion of organic compounds in polyolefins. *Polymer* **1982,** *23* (9), 1325-1344.

166.	Barton, A. F. M., *CRC Handbook of Solubility Parameters and Other Cohesion Parameters*. 2 ed.; Routledge: Boca Raton, 2013.

167.	Hansen, C. M., *Hansen solubility parameters: a user's handbook*. 2 ed.; CRC Press: United States, **2007**; p 519.

168.	Venkatram, S.; Kim, C.; Chandrasekaran, A.; Ramprasad, R., Critical Assessment of the Hildebrand and Hansen Solubility Parameters for Polymers. *Journal of Chemical Information and Modeling* **2019,** *59* (10), 4188-4194.

169.	Flory, P. J., Thermodynamics of High Polymer Solutions. *The Journal of Chemical Physics* **1942,** *10* (1), 51-61.

170.	J. H. Hildebrand, R. L. S., *The solubility of nonelectrolytes*. Dover Publications: New York, **1964**.

171.	J. Brandrup and E. H. Immergut, *Polymer handbook*. 4 ed.; Wiley-Interscience, : New York, **1989**; p 277-277.

172.	Hirata, Y.; Ducruet, V., Effect of temperature on the solubility of aroma compounds in polyethylene film. *Polymer Testing* **2006,** *25* (5), 690-696.

173.	Michaels, A. B.; Haussleix, R. W., Elastic factors controlling sorption and transport properties of polyethylene. *Journal of Polymer Science Part C: Polymer Symposia* **1965,** *10* (1), 61-86.

174.	Michaels, A. S.; Bixler, H. J., Solubility of gases in polyethylene. *Journal of Polymer Science* **1961,** *50* (154), 393-412.

175.	C. E. Rogers, V. S. a. M. S., The Sorption of Organic Vapors by Polyethylene. *The Journal of Physical Chemistry* **1959,** *63* (9)1406-1413.

176.	Malotky, D. L.; Dermody, D. L.; Schmidt, D.; Young, T. J.; Kalinowski, M., Chapter 1 Development, Characterization, and Application of Novel High Temperature Thermoplastic and Thermosetting Dispersions. In *Polymer Colloids: Formation, Characterization and Applications*, The Royal Society of Chemistry: **2020**; pp 1-29.

177.   Lanyi, F. J.; Wenzke, N.; Kaschta, J.; Schubert, D. W., A method to reveal bulk and surface crystallinity of Polypropylene by FTIR spectroscopy - Suitable for fibers and nonwovens. *Polymer Testing* **2018,** *71*, 49-55.

178.   Furukawa, T.; Sato, H.; Kita, Y.; Matsukawa, K.; Yamaguchi, H.; Ochiai, S.; Siesler, H. W.; Ozaki, Y., Molecular Structure, Crystallinity and Morphology of Polyethylene/Polypropylene Blends Studied by Raman Mapping, Scanning Electron Microscopy, Wide Angle X-Ray Diffraction, and Differential Scanning Calorimetry. *Polymer Journal* **2006,** *38* (11), 1127-1136.

179.   Hermans, P. H.; Weidinger, A., Quantitative investigation of x-ray diffraction by "amorphous" polymers and some other noncrystalline substances. *Journal of Polymer Science* **1950,** *5* (3), 269-281.

180.   Kong, Y.; Hay, J. N., The enthalpy of fusion and degree of crystallinity of polymers as measured by DSC. *European Polymer Journal* **2003,** *39* (8), 1721-1727.

181.   Ahmed, A. K.; Atiqullah, M.; Pradhan, D. R.; Al-Harthi, M. A., Crystallization and melting behavior of i-PP: a perspective from Flory's thermodynamic equilibrium theory and DSC experiment. *RSC Advances* **2017,** *7* (67), 42491-42504.

182.   Nguyen, H. G. T.; Horn, J. C.; Bleakney, M.; Siderius, D. W.; Espinal, L., Understanding Material Characteristics through Signature Traits from Helium Pycnometry. *Langmuir : the ACS journal of surfaces and colloids* **2019,** *35* (6), 2115-2122.

183.   Schawe, J. E. K., Remarks regarding the determination of the initial crystallinity by temperature modulated DSC. *Thermochimica Acta* **2017,** *657*, 151-155.

184.   Nurul Huda, M.; Dragaun, H.; Bauer, S.; Muschik, H.; Skalicky, P., A study of the crystallinity index of polypropylene fibres. *Colloid and Polymer Science* **1985,** *263* (9), 730-737.

185.   Nunes, C.; Mahendrasingam, A.; Suryanarayanan, R., Quantification of crystallinity in substantially amorphous materials by synchrotron X-ray powder diffractometry. *Pharm Res* **2005,** *22* (11), 1942-53.

186.   G.W.H. Höhne, W. H., H.-J. Flammersheim, *Differential Scanning Calorimetry*. Springer,: Berlin, Heidelberg, **1996**.

187.   Bonner, D. C., Solubility of supercritical gases in polymers—a review. *Polymer Engineering & Science* **1977,** *17* (2), 65-72.

188.   Sato, Y.; Fujiwara, K.; Takikawa, T.; Sumarno; Takishima, S.; Masuoka, H., Solubilities and diffusion coefficients of carbon dioxide and nitrogen in polypropylene, high-density polyethylene, and polystyrene under high pressures and temperatures. *Fluid Phase Equilibria* **1999,** *162* (1), 261-276.

189.   Palamara, J. E.; Mulcahy, K. A.; Jones, A. T.; Danner, R. P.; Duda, J. L., Solubility and Diffusivity of Propylene and Ethylene in Atactic Polypropylene by the Static Sorption Technique. *Industrial & Engineering Chemistry Research* **2005,** *44* (26), 9943-9950.

190.   Lee, J. K.; Yao, S. X.; Li, G.; Jun, M. B. G.; Lee, P. C., Measurement Methods for Solubility and Diffusivity of Gases and Supercritical Fluids in Polymers and Its Applications. *Polymer Reviews* **2017,** *57* (4), 695-747.

191.   Yao, Z.; Xu, L.-j.; Zhu, F.-j.; Zhang, Y.-f.; Zeng, C.; Cao, K., Solubility of Subcritical and Supercritical Propylene in the Semicrystalline Polyethylenes. *Journal of Chemical & Engineering Data* **2015,** *60* (10), 3033-3038.

192.   Wang, G. L. J.; Park, C. B., Measurement of N_2 Solubility in Polypropylene and Ethene/Octene Copolymer. *SAE Transactions* **2006,** *115*, 437-443.

193.   Michaels, A. S.; Parker Jr., R. B., Sorption and flow of gases in polyethylene. *Journal of Polymer Science* **1959,** *41* (138), 53-71.

194.   Klopffer, M. H.; Flaconneche, B., Transport Properties of Gases in Polymers: Bibliographic Review. *Oil & Gas Science and Technology - Revue d'IFP Energies nouvelles* **2001,** *56* (3), 223-244.

195.   Koros, W. J., Simplified analysis of gas/polymer selective solubility behavior. *Journal of Polymer Science: Polymer Physics Edition* **1985,** *23* (8), 1611-1628.

196.   Iwai, Y.; Ohzono, M.; Arai, Y., Gas Chromatographic Determination and Correlation Of Weight-Fraction Henry's Constant for Hydrocarbon Gases and Vapours in Molten Polymers. Journal of *Chemical Engineering Communications* **1985,** *34* (1-6), 225-240.

197.   Tsuboi, A.; Kolář, P.; Ishikawa, T.; Kamiya, Y.; Masuoka, H., Sorption and partial molar volumes of C2 and C3 hydrocarbons in polypropylene copolymers. *Journal of Polymer Science Part B: Polymer Physics* **2001,** *39*, 1255-1262.

198.   Podivinská, M.; Jindrová, K.; Chmelař, J.; Kosek, J., Swelling of polyethylene particles and its relation to sorption equilibria under gas-phase polymerization conditions. *Journal of Applied Polymer Science* **2017,** *134* (27), 45035.

199.   Mathlouthi, M., *Permeability and structure in polymeric packaging materials* 1ed.; Springer US: 1994.

200.   Buchhold, R.; Nakladal, A.; Gerlach, G.; Herold, M.; Gauglitz, G.; Sahre, K.; Eichhorn, K. J., Swelling behavior of thin anisotropic polymer layers. *Thin Solid Films* **1999,** *350* (1), 178-185.

201.   Ochiai, H.; Gekko, K.; Yamamura, H., Sorption properties of polypropylene. *Journal of Polymer Science Part A-2: Polymer Physics* **1971,** *9* (9), 1629-1640.

202.   Reynier, A.; Dole, P.; Fricoteaux, F.; Saillard, P.; Feigenbaum, A. E., Stabilization of aroma compounds through sorption-release by packaging polymers. *J Agric Food Chem* **2004,** *52* (18), 5653-62.

203.   Kim, M.-H.; Glinka, C. J., Correlation between Structure and Vapor Sorption in Semicrystalline Linear Polyethylene: One Dimensional Nano-Swelling Measured Using in Situ Vapor Sorption Small Angle Neutron Scattering (iVSANS). *Macromolecules* **2009,** *42* (7), 2618-2625.

204.   N, P., *Polypropylene – The Business*. Hanser: Munich, **2005**; p 491-569.

205.   Maghsoud, Z.; Rafiei, M.; Famili, M. H. N., Effect of processing method on migration of antioxidant from HDPE packaging into a fatty food simulant in terms of crystallinity. *Packaging Technology and Science* **2018,** *31* (3), 141-149.

206.   Castle, L., 1 - Chemical migration into food: an overview. In *Chemical Migration and Food Contact Materials*, Barnes, K. A.; Sinclair, C. R.; Watson, D. H., Eds. Woodhead Publishing: **2007**; pp 1-13.

207.   Ebnesajjad, S., 16 - A Survey of Regulatory Aspects of Food Packaging. In *Plastic Films in Food Packaging*, Ebnesajjad, S., Ed. William Andrew Publishing: Oxford, **2013**; pp 345-388.

208.   Guidance for Industry: Preparation of Food Contact Notifications for Food Contact Substances (Toxicology Recommendations). FDA, Ed. Center for Food Safety and Applied Nutrition: US, **2002**.

209.   Commission Regulation (EU) No 10/2011 on plastic materials and arti-cles intended to come into contact with food Annex V,Compliance Testing, Chapter 1, Testing for specific migrationof materials and articles already in contact with food. **2015**.

210.   Caner, C., Sorption Phenomena in Packaged Foods: Factors Affecting Sorption Processes in Package–Product Systems. *Packaging Technology and Science* **2011,** *24* (5), 259-270.

211.   Poças, M. F.; Oliveira, J. C.; Oliveira, F. A. R.; Hogg, T., A Critical Survey of Predictive Mathematical Models for Migration from Packaging. *Critical Reviews in Food Science and Nutrition* **2008,** *48* (10), 913-928.

212.   D.W. van Krevelen , K. t. N., *Properties of Polymers : Their Correlation with Chemical Structure; their Numerical Estimation and Prediction from Additive Group Contributions*. 4 ed.; Elsevier Science & Technology: Oxford, United Kingdom, **2009**.

213.   Alin, J.; Hakkarainen, M., Type of polypropylene material significantly influences the migration of antioxidants from polymer packaging to food simulants during microwave heating. *Journal of Applied Polymer Science* **2010,** *118* (2), 1084-1093.

214.   Neogi, P., *Diffusion in polymers*. Marcel Dekker: New York, **1996**.

215.   Galotto, M. J.; Torres, A.; Guarda, A.; Moraga, N.; Romero, J., Experimental and theoretical study of LDPE versus different concentrations of Irganox 1076 and different thickness. *Food Research International* **2011,** *44* (2), 566-574.

216.   Roy, S.; Ruckenstein, E.; Stroeve, P., Diffusion of a nonionic surfactant through polymeric nonporous and porous membranes. *Journal of Colloid and Interface Science* **1983,** *92* (2), 383-395.

217.   Transport phenomena, R. B. Bird, W. E. Stewart, and E. N. Lightfoot, John Wiley and Sons, Inc., New York (1960). 780 pages. $11.50. *AIChE Journal* **1961,** *7* (2), 5J-6J.

218.	Lindman, B.; Karlström, G., Nonionic polymers and surfactants: Temperature anomalies revisited. *Comptes Rendus Chimie* **2009,** *12* (1), 121-128.

219.	Pereira, A., Polymer-polymer miscibility in PEO/cationic starch and PEO/hydrophobic starch blends. *Express Polymer Letters -* **2010,** *4*, 488-499.

220.	Trifkovic, M.; Hedegaard, A.; Huston, K.; Sheikhzadeh, M.; Macosko, C. W., Porous Films via PE/PEO Cocontinuous Blends. *Macromolecules* **2012,** *45* (15), 6036-6044.

221.	*Surface Analysis Methods in Materials Science*. 2 ed.; Springer-Verlag Berlin Heidelberg: **2003**; Vol. 23.

222.	Wolstenholme, J. F. W., *An Introduction to Surface Analysis by XPS and AES*. John Wiley & Sons, Ltd: 28 January **2005**.

223.	Tang, X.; Wei, J.; Kong, Z.; Zhang, H.; Tian, J., Introduction of amino and rGO into PP nonwoven surface for removal of gaseous aromatic pollutants and particulate matter from air. *Applied Surface Science* **2020,** *511*, 145631.

224.	Vargha, V.; Chetty, A.; Sulyok, Z.; Mihaly, J.; Keresztes, Z.; Tóth, A.; Sajó, I.; Korecz, L.; Anandjiwala, R.; Boguslavsky, L., Functionalisation of polypropylene non-woven fabrics (NWFs). *Journal of Thermal Analysis and Calorimetry* **2011,** *109*, 1-14.

225.	Wei, Q. F.; Wang, X. Q., AFM Characterisation of Technical Fibres. *Journal of Industrial Textiles* **2004,** *34* (1), 51-60.

226.	Bastidas, J. C.; Venditti, R.; Pawlak, J.; Gilbert, R.; Zauscher, S.; Kadla, J. F., Chemical force microscopy of cellulosic fibers. *Carbohydrate Polymers* **2005,** *62* (4), 369-378.

227.	Decho, A. W., Imaging an alginate polymer gel matrix using atomic force microscopy. *Carbohydrate Research* **1999,** *315* (3), 330-333.

228.	Gould, S. A. C.; Schiraldi, D. A.; Occelli, M. L., Analysis of poly(ethylene terephthalate) (PET) films by atomic force microscopy. *Journal of Applied Polymer Science* **1997,** *65* (7), 1237-1243.

229.	Lim, C. T.; Tan, E. P. S.; Ng, S. Y., Effects of crystalline morphology on the tensile properties of electrospun polymer nanofibers. *Applied Physics Letters* **2008,** *92* (14), 141908.

230.	García, R., Dynamic Atomic Force Microscopy Methods. *Surface Science Reports* **2002,** *47*, 197-301.

231.	Nguyen-Tri, P.; Ghassemi, P.; Carriere, P.; Nanda, S.; Assadi, A. A.; Nguyen, D. D., Recent Applications of Advanced Atomic Force Microscopy in Polymer Science: A Review. *Polymers* **2020,** *12* (5), 1142.

232.	Edwards, N.; Best, E.; Connell, S.; Goswami, P.; Carr, C.; Wilcox, M.; Russell, S., Role of surface energy and nano-roughness in the removal efficiency of bacterial contamination by nonwoven wipes from frequently touched surfaces. *Science and Technology of Advanced Materials* **2017,** *18*.

233.	Homola, T.; Wu, Y.; Černák, M., Atmospheric Plasma Surface Activation of Poly(Ethylene Terephthalate) Film for Roll-To-Roll Application of Transparent Conductive Coating. *Journal of Adhesion* **2014,** *90*, 296-309.

234.	Lavoie, J. H.; Rojas, O. J.; Khan, S. A.; Shim, E., Migration Effects of Fluorochemical Melt Additives for Alcohol Repellency in Polypropylene Nonwoven Materials. *ACS Applied Materials & Interfaces* **2020,** *12* (32), 36787-36798.

235.	Annemie, A.; Luc, V. V.; Freddy, A., Static secondary ion mass spectrometry (S-SIMS) Part 2: material science applications. *Mass Spectrometry Reviews* **1999,** *18* (1), 48-81.

236.	Mogk, D. W. Time-of-Flight Secondary Ion Mass Spectrometry (ToF-SIMS). https://serc.carleton.edu/research_education/geochemsheets/techniques/ToFSIMS.html.

237.	Good, R. J., Contact angle, wetting, and adhesion: a critical review. *Journal of Adhesion Science and Technology* **1992,** *6* (12), 1269-1302.

238.	Webiste: Information on Contact Angle. http://www.ramehart.com/contactangle.htm (accessed 29.05.18).

239.	Yuan Y., L. T. R., Contact Angle and Wetting Properties. In: Bracco G., Holst B. (eds) Surface Science Techniques. Springer, Berlin, Heidelberg: **2013**; Vol. 51, pp 3-34.

240.	Williams, D. R., Particle engineering in pharmaceutical solids processing: surface energy considerations. *Curr Pharm Des* **2015,** *21* (19), 2677-94.

241.	Heng, J. Y. Y.; Pearse, D. F.; Thielmann, F.; Lampke, T.; Bismarck, A., Methods to determine surface energies of natural fibres: a review. *Composite Interfaces* **2007,** *14* (7-9), 581-604.

242.	Shen, H.; Nutt, S.; Hull, D., Direct observation and measurement of fiber architecture in short fiber-polymer composite foam through micro-CT imaging. *Composites Science and Technology* **2004,** *64* (13), 2113-2120.

243.	Collins, G. E., 11—A Surface Tension Method for Measuring the Perimetwers of Fibres and the Contact Angles of Liquids against Fibres. *Journal of the Textile Institute Transactions* **1947,** *38* (2), T73-T77.

244.	Wang, Z.; Li, Y.; Fang, Y.; Feng, G.; Xu, J., Aging behavior of nano-CaCO3-modified polypropylene nonwoven fabric composites. Journal of *Polymers and Polymer Composites* *2021*

245.	Young, J. R. C. a. C. L., Physicochemical measurement by gas chromatography. *Journal of Chromatography A* **1979,** *187* (1), 632.

246.	Williams, D., 5 - Inverse Gas Chromatography A2 - Ishida, Hatsuo. In *Characterization of Composite Materials*, Newnes: Boston, **1994**; pp 80-104.

247.	Voelkel, A., Chapter 2.5 Inverse gas chromatography in the examination of acid-base and some other properties of solid materials. In *Studies in Surface Science and Catalysis*, Dąbrowski, A.; Tertykh, V. A., Eds. Elsevier: **1996**; Vol. 99, pp 465-477.

248.	Berezkin, V. G., Interfacial Phenomena in Chromatography, Peffekorn, E., Ed., New York: Marcel Dekker, 1999,448 pp. *Journal of Analytical Chemistry* **2000,** *55* (10), 1003-1004.

249.	Etzler, F.; Gardner, D., Surface Free Energy Determination of Powders and Particles with Pharmaceutical Applications: A Critical Review. **2019**; pp 315-352.

250.	Storey, R. A.; YmΓ©n, I.; Heng, J. Y. Y.; Williams, D. R., *Vapour Sorption and Surface Analysis*. **2011**.

251.	Brunauer, S.; Deming, L. S.; Deming, W. E.; Teller, E., On a Theory of the van der Waals Adsorption of Gases. *Journal of the American Chemical Society* **1940,** *62* (7), 1723-1732.

252.	Voelkel, A.; Strzemiecka, B.; Adamska, K.; Milczewska, K., Inverse gas chromatography as a source of physiochemical data. *Journal of Chromatography A* **2009,** *1216* (10), 1551-1566.

253.	Rückriem, M.; Enke, D.; Hahn, T., Inverse gas chromatography (IGC) as a tool for an energetic characterisation of porous materials. *Microporous and Mesoporous Materials* **2015,** *209*, 99-104.

254.	Smith, R. R.; Williams, D. R.; Burnett, D. J.; Heng, J. Y. Y. A New Method To Determine Dispersive Surface Energy Site Distributions by Inverse Gas Chromatography *Langmuir* [Online], 2014, p. 8029-8035. http://dx.doi.org/10.1021/la500688d.

255.	Thielmann, F.; Butler, D. A.; Williams, D. R., Characterization of porous materials by finite concentration inverse gas chromatography. *Colloids and Surfaces A: Physicochemical and Engineering Aspects* **2001,** *187-188*, 267-272.

256.	Ylä-Mäihäniemi, P. P.; Heng, J. Y. Y.; Thielmann, F.; Williams, D. R. Inverse Gas Chromatographic Method for Measuring the Dispersive Surface Energy Distribution for Particulates *Langmuir* [Online], **2008**, p. 9551-9557. http://dx.doi.org/10.1021/la801676n.

257.	Kondor, A.; Quellet, C.; Dallos, A., Surface characterization of standard cotton fibres and determination of adsorption isotherms of fragrances by IGC. *Surface and Interface Analysis* **2015,** *47* (11), 1040-1050.

258.	Voelkel, A., Inverse Gas Chromatography: Characterization of Polymers, Fibers, Modified Silicas, and Surfactants. *Critical Reviews in Analytical Chemistry* **1991,** *22* (5), 411-439.

259.	Guillet, J. a. A. S., Z. Y., Inverse Gas Chromatography in Analysis of Polymers. In *Encyclopedia of Analytical Chemistry*, Provder, R. A. M. a. T., Ed. **2006**.

260.	R., M. J.; G., P. C., Inverse gas chromatography of wool. *Journal of Applied Polymer Science* **1982,** *27* (5), 1643-1654.

261.	Rjiba, N.; Nardin, M.; Dréan, J.-Y.; Frydrych, R., A study of the surface properties of cotton fibers by inverse gas chromatography. *Journal of Colloid and Interface Science* **2007,** *314* (2), 373-380.

262. Legras, A.; Kondor, A.; Heitzmann, M. T.; Truss, R. W., Inverse gas chromatography for natural fibre characterisation: Identification of the critical parameters to determine the Brunauer–Emmett–Teller specific surface area. *Journal of Chromatography A* **2015,** *1425* (Supplement C), 273-279.

263. Mohammadi-Jam, S.; Waters, K. E., Inverse gas chromatography applications: A review. *Advances in Colloid and Interface Science* **2014,** *212* (Supplement C), 21-44.

264. Bahners, T.; Gutmann, J., Procedures for the Characterization of Wettability and Surface Free Energy of Textiles - Use, Abuse, Misuse and Proper Use: A Critical Review. *Reviews of Adhesion and Adhesives* **2019,** *7*, 259-293.

265. Sing, K., The use of nitrogen adsorption for the characterisation of porous materials. *Colloids and Surfaces A: Physicochemical and Engineering Aspects* **2001,** *187-188*, 3-9.

266. Hernández-Aguirre, O. A.; Núñez-Pineda, A.; Tapia-Tapia, M.; Gómez Espinosa, R. M., Surface Modification of Polypropylene Membrane Using Biopolymers with Potential Applications for Metal Ion Removal. *Journal of Chemistry* **2016,** *2016*, 2742013.

267. Standardization:, ISO 12154 Determination of density by volumetric displacement — Skeleton density by gas pycnometry. Switzerland, 1 Eds. Switzerland, **2014**; p 11.

268. Dudić, D.; Kostoski, D.; Djoković, V.; Stojanović, Z., Recrystallization processes induced by accelerated ageing in isotactic polypropylene of different morphologies. *Polymer Degradation and Stability* **2000,** *67* (2), 233-237.

269. Munaro, M.; Akcelrud, L., Correlations between composition and crystallinity of LDPE/HDPE blends. *Journal of Polymer Research* **2008,** *15* (1), 83-88.

270. Chmelař, J.; Pokorný, R.; Schneider, P.; Smolná, K.; Bělský, P.; Kosek, J., Free and constrained amorphous phases in polyethylene: Interpretation of 1H NMR and SAXS data over a broad range of crystallinity. *Polymer* **2015,** *58*, 189-198.

271. Fujiwara, H. In *Spectroscopic Ellipsometry: Principles and Applications*, **2007**.

272. Ogieglo, W.; Wormeester, H.; Eichhorn, K.-J.; Wessling, M.; Benes, N. E., In situ ellipsometry studies on swelling of thin polymer films: A review. *Progress in Polymer Science* **2015,** *42*, 42-78.

273. Hajduk, B.; Bednarski, H.; Trzebicka, B., Temperature-Dependent Spectroscopic Ellipsometry of Thin Polymer Films. *The Journal of Physical Chemistry B* **2020,** *124* (16), 3229-3251.

274. Erber, M.; Tress, M.; Eichhorn, K.-J., Glass Transition of Polymers with Different Architectures in the Confinement of Nanoscopic Films. In *Ellipsometry of Functional Organic Surfaces and Films*, Hinrichs, K.; Eichhorn, K.-J., Eds. Springer Berlin Heidelberg: Berlin, Heidelberg, **2014**; pp 63-78.

275. Higuchi, R.; Hirano, M.; Ashaduzzaman, M.; Yilmaz, N.; Sumino, T.; Kodama, D.; Chiba, S.; Uemura, S.; Nishiyama, K.; Ohira, A.; Fujiki, M.; Kunitake, M., Construction and Characterization of Molecular Nonwoven Fabrics Consisting of Cross-Linked Poly(γ-methyl-l-glutamate). *Langmuir* **2013,** *29* (24), 7478-7487.

276. Kilpatrick-Liverman, L.; Polefka, T. G., Use of the dynamic vapor sorption meter to measure skin hydration properties, in vitro. *Skin research and technology : official journal of International Society for Bioengineering and the Skin (ISBS) [and] International Society for Digital Imaging of Skin (ISDIS) [and] International Society for Skin Imaging (ISSI)* **2006,** *12* (1), 36-42.

277. Young, P. M.; Price, R.; Tobyn, M. J.; Buttrum, M.; Dey, F., The Influence of Relative Humidity on the Cohesion Properties of Micronized Drugs Used in Inhalation Therapy. *Journal of Pharmaceutical Sciences* **2004,** *93* (3), 753-761.

278. Young, P. M.; Edge, S.; Staniforth, J. N.; Steele, D. F.; Price, R., Dynamic Vapor Sorption Properties of Sodium Starch Glycolate Disintegrants. *Pharmaceutical Development and Technology* **2005,** *10* (2), 249-259.

279. Hunter, N. E.; Frampton, C. S.; Craig, D. Q. M.; Belton, P. S., The use of dynamic vapour sorption methods for the characterisation of water uptake in amorphous trehalose. *Carbohydrate Research* **2010,** *345* (13), 1938-1944.

280. Heng, J. Y. a. W., D. R., Solid State Characterization of Pharmaceuticals. In *Solid State Characterization of Pharmaceuticals*, Blackwell Publishing: **2011**.

281. Sheokand, S.; Modi, S. R.; Bansal, A. K., Dynamic Vapor Sorption as a Tool for Characterization and Quantification of Amorphous Content in Predominantly Crystalline Materials. *Journal of Pharmaceutical Sciences* **2014,** *103* (11), 3364-3376.

282. Bley, O.; Siepmann, J.; Bodmeier, R., Characterization of moisture-protective polymer coatings using differential scanning calorimetry and dynamic vapor sorption. *J Pharm Sci* **2009,** *98* (2), 651-64.

283. Anderson, H. Advantages and Disadvantages in Imaging Components and Applications. https://www.microscopemaster.com/scanning-electron-microscope.html.

284. Wang, K.; Wang, W.; Yang, D.; Huo, Y.; Wang, D., Surface modification of polypropylene non-woven fabric using atmospheric nitrogen dielectric barrier discharge plasma. *Applied Surface Science* **2010,** *256* (22), 6859-6864.

285. Ghassemieh, E.; Acar, M.; Versteeg, H., Microstructural analysis of non-woven fabrics using scanning electron microscopy and image processing. Part 2: Application to hydroentangled fabrics. *Proceedings of the Institution of Mechanical Engineers Part L Journal of Materials Design and Applications* **2002,** *216*.

286. Sm, C.; Shah, T.; Anand, S. C.; Soin, N., Development and Characterisation of Nonwoven Fabrics for Apparel Applications. *Journal of Textile Science & Engineering* **2018,** *08*.

287. Fairbrass, S. A.; Williams, D. R., Laser surface profilometry: A novel technique for the examination of polymer surfaces. *ACS Symposium Series* **2001,** *779*, 202-211.

288. Jaglarz, J.; Sanetra, J.; Cisowski, J., Studies of polymer surface topography by means of optical profilometry. *Optica Applicata* **2010,** *40*.

289. Lamprecht, M. R.; Sabatini, D. M.; Carpenter, A. E., CellProfiler: free, versatile software for automated biological image analysis. *Biotechniques* **2007,** *42* (1), 71-5.

290. Cardamone, J. M.; Baker, M. T.; Society, A. C.; American Chemical Society. Cellulose, P.; Division, T.; Meeting, A. C. S., *Historic Textiles, Papers, and Polymers in Museums*. American Chemical Society: **2001**.

291. Norbert, M.; Chepur, P.; Myers, J.; Linz, J., Concrete Roughness Characterization Using Laser Profilometry for Fiber-Reinforced Polymer Sheet Application. *Transportation Research Record* **2001,** *1775*.

292. Choong, L. T.; Yi, P.; Rutledge, G. C., Three-dimensional imaging of electrospun fiber mats using confocal laser scanning microscopy and digital image analysis. *Journal of Materials Science* **2015,** *50* (8), 3014-3030.

293. Charcosset, C.; Cherfi, A.; Bernengo, J.-C., Characterization of microporous membrane morphology using confocal scanning laser microscopy. *Chemical Engineering Science* **2000,** *55* (22), 5351-5358.

294. Li, L.; Sosnowski, S.; Chaffey, C. E.; Balke, S. T.; Winnik, M. A., Surface morphology of a polymer blend examined by laser confocal fluorescence microscopy. *Langmuir* **1994,** *10* (8), 2495-2497.

295. Bagherzadeh, R.; Latifi, M.; Najar, S. S.; Tehran, M. A.; Kong, L., Three-dimensional pore structure analysis of Nano/Microfibrous scaffolds using confocal laser scanning microscopy. *Journal of Biomedical Materials Research Part A* **2013,** *101A* (3), 765-774.

296. Song, Y.; Srinivasarao, M.; Tonelli, A.; Balik, C. M.; McGregor, R., Laser Scanning Confocal Microscopy Study of Dye Diffusion in Fibers. *Macromolecules* **2000,** *33* (12), 4478-4485.

297. Lin, Y.-M.; Song, C.; Rutledge, G. C., Direct Three-Dimensional Visualization of Membrane Fouling by Confocal Laser Scanning Microscopy. *ACS Applied Materials & Interfaces* **2019,** *11* (18), 17001-17008.

298. Waldo-Mendoza, M. A.; Quiñones-Jurado, Z. V.; Pérez-Medina, J. C.; Yañez-Soto, B.; Ramírez-González, P. E., Fogging Control on LDPE/EVA Coextruded Films: Wettability Behavior and Its Correlation with Electric Performance. *Membranes* **2017,** *7* (1), 11.

299. Lichtman, J. W. C., José Angel, Fluorescence microscopy. *Nature Methods* **2005,** *2* (12), 910-919.

300. Valeur, B., Molecular Fluorescence. In *Digital Encyclopedia of Applied Physics*, Wiley-VCH Verlag GmbH & Co. KGaA (Ed.): **2009**; pp 477-531.

301. Lakowicz, J. R., *Principles of Fluorescence Spectroscopy*. 3 ed.; Springer US: **2006**.

302. Tiwari, G. Jablonski Diagram – Consequences of Light Absorption. https://gauravtiwari.org/.

303. Minsky, M., Memoir on inventing the confocal scanning microscope. Scanning. **1988**, *10* (4), 128-138.

304. Gramatikov, B., Modern technologies for retinal scanning and imaging: An introduction for the biomedical engineer. *Biomedical engineering online* **2014**, *13*, 52.

305. Mueller, L. N.; de Brouwer, J. F. C.; Almeida, J. S.; Stal, L. J.; Xavier, J. B., Analysis of a marine phototrophic biofilm by confocal laser scanning microscopy using the new image quantification software PHLIP. *BMC Ecology* **2006,** *6* (1), 1.

306. Alvarez-Román, R.; Naik, A.; Kalia, Y. N.; Fessi, H.; Guy, R. H., Visualization of skin penetration using confocal laser scanning microscopy. *European Journal of Pharmaceutics and Biopharmaceutics* **2004,** *58* (2), 301-316.

307. Pioch, T.; Stotz, S.; Staehle, H. J.; Duschner, H., Applications of Confocal Laser Scanning Microscopy to Dental Bonding. *Advances in Dental Research* **1997**, *11* (4), 453-461.

308. Kus, J., Application of confocal laser-scanning microscopy (CLSM) to autofluorescent organic and mineral matter in peat, coals and siliciclastic sedimentary rocks — A qualitative approach. *International Journal of Coal Geology* **2015,** *137*, 1-18.

309. Ilie, M. A., Caruntu, C., Lupu, M., Lixandru, D., Tampa, M., Georgescu, S. ... Boda, D., Current and future applications of confocal laser scanning microscopy imaging in skin oncology. Oncology Letters **2019,** *17* (5), 4102-4111.

310. Croix, C. M. S.; Shand, S. H.; Watkins, S. C., Confocal microscopy: comparisons, applications, and problems. *BioTechniques* **2005,** *39* (6S), S2-S5.

311. Hamada, H.; Bousfield, D.; Luu, W., Absorption Mechanism of Aqueous and Solvent Inks into Synthetic Nonwoven Fabrics. *Journal of Imaging Science and Technology* **2009,** *53* (5), 50201-1-50201-6.

312. Paddock, S. W.; Eliceiri, K. W., Laser Scanning Confocal Microscopy: History, Applications, and Related Optical Sectioning Techniques. In *Confocal Microscopy: Methods and Protocols*, Paddock, S. W., Ed. Springer New York: New York, NY, 2014; pp 9-47.

313. Cremer, C.; Cremer, T., Considerations on a laser-scanning-microscope with high resolution and depth of field. *Microscopica acta* **1978,** *81* (1), 31-44.

314. Jonkman, J.; Brown, C. M., Any Way You Slice It-A Comparison of Confocal Microscopy Techniques. *J Biomol Tech* **2015,** *26* (2), 54-65.

315. Conchello, J.-A.; Lichtman, J. W., Optical sectioning microscopy. *Nature Methods* **2005,** *2* (12), 920-931.

316. Murray, J. M.; Appleton, P. L.; Swedlow, J. R.; Waters, J. C., Evaluating performance in three-dimensional fluorescence microscopy. *J Microsc* **2007,** *228* (Pt 3), 390-405.

317. Nathan S. Claxton, T. J. F., and Michael W. Davidson, Laser Scanning Confocal Microscopy. In *Encyclopedia of Nanotechnology*, Bhushan, B., Ed. Springer Netherlands: Dordrecht, **2012**; pp 1192-1192.

318. Jonkman, J. E. N.; Swoger, J.; Kress, H.; Rohrbach, A.; Stelzer, E. H. K., Resolution in optical microscopy. In *Methods in Enzymology*, Academic Press: **2003**; Vol. 360, pp 416-446.

319. Jonkman, J.; Brown, C. M.; Wright, G. D.; Anderson, K. I.; North, A. J., Tutorial: guidance for quantitative confocal microscopy. *Nature Protocols* **2020**.

320. Davidson, T. J. F. a. M. W. Introduction to Confocal Microscopy.

321. Schindelin, J.; Arganda-Carreras, I.; Frise, E.; Kaynig, V.; Longair, M.; Pietzsch, T.; Preibisch, S.; Rueden, C.; Saalfeld, S.; Schmid, B.; Tinevez, J. Y.; White, D. J.; Hartenstein, V.; Eliceiri, K.; Tomancak, P.; Cardona, A., Fiji: an open-source platform for biological-image analysis. *Nat Methods* **2012,** *9* (7), 676-82.

322.   Heydorn, A.; Nielsen, A. T.; Hentzer, M.; Sternberg, C.; Givskov, M.; Ersboll, B. K.; Molin, S., Quantification of biofilm structures by the novel computer program COMSTAT. *Microbiology (Reading, England)* **2000,** *146 (Pt 10),* 2395-407.

323.   Otsu, N., A Threshold Selection Method from Gray-Level Histograms. *IEEE Transactions on Systems, Man, and Cybernetics* **1979,** *9* (1), 62-66.

324.   Egerton, R., *Physical Principles of Electron Microscopy: An Introduction to TEM, SEM, and AEM.* Springer US: 2011.

325.   Mohammed, A., Scanning electron microscopy (SEM): A review. **2018**.

326.   Karan, S., *Shape Based Characterization of Nanoparticles – A Fuzzy Mathematical Approach.* 2015; Vol. 81.

327.   Zygo Nexview 3D Optical Profiler. https://ywccleanroom.yale.edu/equipment/zygo-nexview-3d-optical-profiler (accessed April **2021**).

328.   Ho, R.; Heng, J. Y. Y., A Review of Inverse Gas Chromatography and its Development as a Tool to Characterize Anisotropic Surface Properties of Pharmaceutical Solids. *KONA Powder and Particle Journal* **2013,** *30,* 164-180.

329.   YI, K. A. a. Y., *Intermolecular Interactions in Gas Adsorption Chromatography.* Plenum Press: New York, **1969**; Vol. 26.

330.   Williams, D. In *Characterisation of Filler and Fibre Surfaces Using Inverse Gas Chromatography,* Controlled Interphases in Composite Materials, Dordrecht, Ishida, H., Ed. Springer Netherlands: Dordrecht, **1990**; pp 219-232.

331.   Nardin, M.; Papirer, E., *Powders and Fibers: Interfacial Science and Applications.* CRC Press: 2006.

332.   Hadjittofis, E. Interfacial phenomena in pharmaceutical process development. Imperial College London, Spiral, **2019**.

333.   Thommes, M.; Kaneko, K.; Neimark Alexander, V.; Olivier James, P.; Rodriguez-Reinoso, F.; Rouquerol, J.; Sing Kenneth, S. W., Physisorption of gases, with special reference to the evaluation of surface area and pore size distribution (IUPAC Technical Report). In *Pure and Applied Chemistry*, **2015**; Vol. 87, p 1051.

334.   Siemieniewska, T., Reporting Physisorption Data For Gas/Solid Systems with Special Reference to the Determination of Surface Area and Porosity. *International Union of Pure and Applied Chemistry* **1985,** *54* (4), 603-619.

335.   Fowkes, F. M., Attractive Forces at Interface. *Industrial & Engineering Chemistry* **1964,** *56* (12), 40-52.

336.   Schultz, J.; Lavielle, L.; Martin, C., The Role of the Interface in Carbon Fibre-Epoxy Composites. *The Journal of Adhesion* **1987,** *23* (1), 45-60.

337.   Dorris, G. M.; Gray, D. G., Adsorption of n-alkanes at zero surface coverage on cellulose paper and wood fibers. *Journal of Colloid and Interface Science* **1980,** *77* (2), 353-362.

338.   Shi, B.; Wang, Y.; Jia, L., Comparison of Dorris–Gray and Schultz methods for the calculation of surface dispersive free energy by inverse gas chromatography. *Journal of Chromatography A* **2011,** *1218* (6), 860-862.

339.   Van Oss, C. J.; Good, R. J.; Chaudhury, M. K., Additive and nonadditive surface tension components and the interpretation of contact angles. *Langmuir* **1988,** *4* (4), 884-891.

340.   Young, T., III. An essay on the cohesion of fluids. *Philosophical Transactions of the Royal Society of London* **1805,** *95,* 65-87.

341.   Fowkes, F. M., Dispersion Force Contributions to Surface and Interfacial Tensions, Contact Angles, and Heats of Immersion. In *Contact Angle, Wettability, and Adhesion,* American Chemical Society: **1964**; Vol. 43, pp 99-111.

342.   Mohos, M.; Románszki, L.; Telegdi, J.; Keresztes, Z.; Nyikos, L., A comparison of contact angle measurement results obtained on bare, treated, and coated alloy samples by both dynamic sessile drop and Wilhelmy method. *Periodica Polytechnica Chemical Engineering*, 58(Supplement), pp. 53–59, **2014**.

343.   Subedi, D. P., Contact Angle Measurement for The Surface Characterization of Solids. *Himalayan Physics* **2001,** *2*, 1-4.

344.   Wenzel, R. N., Resistance of Solid Surfaces to Wetting by Water. *Industrial & Engineering Chemistry* **1936,** *28* (8), 988-994.

345.   Cassie, A. B. D.; Baxter, S., Wettability of porous surfaces. *Transactions of the Faraday Society* **1944,** *40* (0), 546-551.

346.   Giacomello, A.; Chinappi, M.; Meloni, S.; Casciola, C. M., Metastable Wetting on Superhydrophobic Surfaces: Continuum and Atomistic Views of the Cassie-Baxter-Wenzel Transition. *Physical Review Letters* **2012,** *109* (22), 226102.

347.   Wbsite: (NPL), Introduction to XPS: X-ray Photoelectron Spectroscopy. http://www.npl.co.uk/science-technology/surface-and-nanoanalysis/surface-and-nanoanalysis-basics/introduction-to-xps-x-ray-photoelectron-spectroscopy (accessed June 2021).

348.   Yahia, L. H.; Mireles, L. K., 4 - X-ray photoelectron spectroscopy (XPS) and time-of-flight secondary ion mass spectrometry (ToF SIMS) In *Characterization of Polymeric Biomaterials*, Farè, S., Ed. Woodhead Publishing: **2017**; pp 83-97.

349.   Kot, M., *In-operando hard X-ray photoelectron spectroscopy study on the resistive switching physics of HfO2-based RRAM*. **2014**.

350.   Binnig, G.; Quate, C. F.; Gerber, C., Atomic Force Microscope. *Physical Review Letters* **1986,** *56* (9), 930-933.

351.   Group, N. F., Schematic illustrating the basic principles of AFM. https://www.nanofunction.org/commercial-afms, (accessed June 2021).

352.   Nisbet, D. R.; Rodda, A. E.; Finkelstein, D. I.; Horne, M. K.; Forsythe, J. S.; Shen, W., Surface and bulk characterisation of electrospun membranes: Problems and improvements. *Colloids and Surfaces B: Biointerfaces* **2009,** *71* (1), 1-12.

353.   Howland R, B. L., *A practical guide to scanning probe microscopy*. **1996**; Vol. 74.

354.   Kinney, J. H.; Balooch, M.; Marshall, S. J.; Marshall, G. W., Jr.; Weihs, T. P., Atomic Force Microscope Measurements of the Hardness and Elasticity of Peritubular and Intertubular Human Dentin. *Journal of Biomechanical Engineering* **1996,** *118* (1), 133-135.

355.   S. Maghsoudy-Louyeh, M. K., B. R. Tittmann*, Review of Progress in Atomic Force Microscopy. **2018,** *12* (1), 86.

356.   Meyer, G.; Amer, N. M., Simultaneous measurement of lateral and normal forces with an optical-beam-deflection atomic force microscope. *Applied Physics Letters* **1990,** *57* (20), 2089-2091.

357.   Krieg, M.; Fläschner, G.; Alsteens, D.; Gaub, B. M.; Roos, W. H.; Wuite, G. J. L.; Gaub, H. E.; Gerber, C.; Dufrêne, Y. F.; Müller, D. J., Atomic force microscopy-based mechanobiology. *Nature Reviews Physics* **2019,** *1* (1), 41-57.

358.   Brunauer, S.; Emmett, P. H.; Teller, E., Adsorption of Gases in Multimolecular Layers. *Journal of the American Chemical Society* **1938,** *60* (2), 309-319.

359.   Baumgarten, E.; Weinstrauch, F.; Höffkes, H., Adsorption isotherms of hydrocarbons on γ-alumina. *Journal of Chromatography A* **1977,** *138* (2), 347-354.

360.   Wesite: Barron, P. M. V. R.; Andrew, R., BET Surface Area Analysis of Nanoparticles. https://chem.libretexts.org/Bookshelves/Analytical_Chemistry/Physical_Methods_in_Chemistry_an d_Nano_Science_(Barron)/02%3A_Physical_and_Thermal_Analysis/2.03%3A_BET_Surface_Area_An alysis_of_Nanoparticles (accessed **2021**).

361.   Hilfiker, J.; Tompkins, H., *Spectroscopic Ellipsometry: Practical Application to Thin Film Characterization*. 2016.

362.   Woollam, J. A., Flow chart for ellipsometry data analysis. **2021**.

363.   Ogieglo, W. In-situ Spectroscopic Wllipsometry for Studies of Thin Film and Membranes. University of Twente, **2014**.

364.   Woollam, J.; Johs, B.; Herzinger, C.; Hilfiker, J.; Synowicki, R.; Bungay, C., *Overview of variable-angle spectroscopic ellipsometry (VASE): I. Basic theory and typical applications*. SPIE: **1999**; Vol. 10294.

365.   Herzinger, C. M.; Johs, B.; McGahan, W. A.; Woollam, J. A.; Paulson, W., Ellipsometric determination of optical constants for silicon and thermally grown silicon dioxide via a multi-sample, multi-wavelength, multi-angle investigation. *Journal of Applied Physics* **1998,** *83* (6), 3323-3336.

366.   Website: Dynamic Vapor Sorption (DVS). https://www.surfacemeasurementsystems.com/solutions/dynamic_vapor_sorption/ (accessed 29/11/2017).

367.   Stubberud, L.; Arwidsson, H. G.; Graffner, C., Water-solid interactions: I. A technique for studying moisture sorption/desorption. *International Journal of Pharmaceutics* **1995,** *114* (1), 55-64.

368.   Zografi, G., States of Water Associated with Solids. *Drug Development and Industrial Pharmacy* **1988,** *14* (14), 1905-1926.

369.   Garbalińska, H.; Bochenek, M.; Malorny, W.; von Werder, J., Comparative analysis of the dynamic vapor sorption (DVS) technique and the traditional method for sorption isotherms determination — Exemplified at autoclaved aerated concrete samples of four density classes. *Cement and Concrete Research* **2017,** *91*, 97-105.

370.   Vora, K. L.; Buckton, G.; Clapham, D., The use of dynamic vapour sorption and near infra-red spectroscopy (DVS-NIR) to study the crystal transitions of theophylline and the report of a new solid-state transition. *European Journal of Pharmaceutical Sciences* **2004,** *22* (2-3), 97-105.

371.   Li, W.; Buckton, G., Using DVS-NIR to assess the water sorption behaviour and stability of a griseofulvin/PVP K30 solid dispersion. *International Journal of Pharmaceutics* **2015,** *495* (2), 999-1004.

372.   Lane, R. A.; Buckton, G., The novel combination of dynamic vapour sorption gravimetric analysis and near infra-red spectroscopy as a hyphenated technique. *International Journal of Pharmaceutics* **2000,** *207* (1-2), 49-56.

373.   Sneha, S.; R., M. S.; K., B. A., Dynamic Vapor Sorption as a Tool for Characterization and Quantification of Amorphous Content in Predominantly Crystalline Materials. *Journal of Pharmaceutical Sciences* **2014,** *103* (11), 3364-3376.

374.   Gill, P.; Moghadam, T. T.; Ranjbar, B., Differential scanning calorimetry techniques: applications in biology and nanoscience. *J Biomol Tech* **2010,** *21* (4), 167-193.

375.   Akash, M. S. H.; Rehman, K., Differential Scanning Calorimetry. In *Essentials of Pharmaceutical Analysis*, Springer Singapore: Singapore, **2020**; pp 199-206.

376.   Ho, R.; Hinder, S. J.; Watts, J. F.; Dilworth, S. E.; Williams, D. R.; Heng, J. Y. Y., Determination of surface heterogeneity of d-mannitol by sessile drop contact angle and finite concentration inverse gas chromatography. *International Journal of Pharmaceutics* **2010,** *387* (1), 79-86.

377.   Wang, D. Advanced Physical Characterisation of Milled Pharmaceutical Solids. Imperial College London, London, **2012**.

378.   Evgeniya Lock, S. W., Richard Fernsler *Preparation of Ultra Thin Polystyrene, Polypropylene and Polyethylene Films on Si Substrate Using Spin Coating Technology*; Naval Research Laboratory, Washington, DC 20375-5320: 4 January **2008**.

379.   Ahmadi-Kandjani, S.; Mirershadi, S.; Nikniazi, A., Inorganic–Organic Perovskite Solar Cells. **2015**; Chapter 8, pp 223-246.

380.   International, A., Standard Test Method for Carbon Black—Total and External Surface Area by Nitrogen Adsorption. PA: West Conshohocken, **2021**.

381.   ISO 9277:**2010** - Determination of the specific surface area of solids by gas adsorption using the BET method.

382.   Duralliu, A. The Influence of Moisture Content and Temperature on Storage Stability of Freeze-Dried Biologics. Imperial College London, London, **2019**.

383.   Hadjittofis, E.; Zhang, G. G. Z.; Heng, J. Y. Y., Influence of sample preparation on IGC measurements: the cases of silanised glass wool and packing structure. *RSC Advances* **2017,** *7* (20), 12194-12200.

384.   Mittal, K. L.; International Sympsoium on Contact Angle, W.; Adhesion, *Contact angle, wettability and adhesion. Vol.3*. VSP: Utrecht, **2003**.

385.   Etzler, F. M., *Contact Angle, Wettability and Adhesion*. Ed: K. L. Mittal ed.; Leiden, Boston: **2003**; Vol. 3.

386.   Wenzel, R. N., Surface Roughness and Contact Angle. *The Journal of Physical and Colloid Chemistry* **1949,** *53* (9), 1466-1467.

387.   Goswami, A.; Pillai, S. C.; McGranaghan, G., Surface modifications to enhance dropwise condensation. *Surfaces and Interfaces* **2021,** *25*, 101143.

388.   Ström, G.; Fredriksson, M.; Stenius, P., Contact angles, work of adhesion, and interfacial tensions at a dissolving Hydrocarbon surface. *Journal of Colloid and Interface Science* **1987,** *119* (2), 352-361.

389.   Armagan, O.; B, K.; Karakaş, H.; Guner, S., Adhesion strength behaviour of plasma pre-treated and laminated polypropylene nonwoven fabrics using acrylic and polyurethane-based adhesives. *Journal of Industrial Textiles* **2012,** *43*, 396-414.

390.   Morent, R., Surface Modification of Non-woven Textiles using a Dielectric Barrier Discharge Operating in Air, Helium and Argon at Medium Pressure. *Textile Research Journal* **2007,** *77* (7), 471-488.

391.   Esmizadeh, E.; Tzoganakis, C.; Mekonnen, T. H., Degradation Behavior of Polypropylene during Reprocessing and Its Biocomposites: Thermal and Oxidative Degradation Kinetics. *Polymers* **2020,** *12* (8), 1627.

392.   Yeh, J.; Lai, Y., An improvement on the adhesion-strength of laminated ultra-high-molecular-weight polyethylene fabrics: surface-etching/modification using highly effective helium/oxygen/nitrogen plasma treatment. *Polymers for Advanced Technologies* **2011,** *22* (12), 1971-1981.

393.   Kiss, E.; Bertóti, I.; Vargha-Butler, E. I., XPS and wettability characterization of modified poly(lactic acid) and poly(lactic/glycolic acid) films. *J Colloid Interface Sci* **2002,** *245* (1), 91-8.

394.   Majchrzycka, K., Time-Dependent Antimicrobial Activity of Filtering Nonwovens with Gemini Surfactant-Based Biocides. *Molecules (Basel, Switzerland)* **2017,** *22* (10), 1620.

395.   Černáková, L., Surface Modification of Polypropylene Non-Woven Fabrics by Atmospheric-Pressure Plasma Activation Followed by Acrylic Acid Grafting. *Plasma Chemistry and Plasma Processing* **2005,** *25* (4), 427-437.

396.   Bardestani, R., Experimental methods in chemical engineering: specific surface area and pore size distribution measurements—BET, BJH, and DFT. *The Canadian Journal of Chemical Engineering* **2019,** *97* (11), 2781-2791.

397.   Serilevy, A., Effects of heterogeneous surface geometry on adsorption. *Langmuir* **1993,** *9* (11), 3067-3076.

398.   Zdziennicka, A.; Jańczuk, B.; Wójcik, W., Wettability of polytetrafluoroethylene by aqueous solutions of two anionic surfactant mixtures. *Journal of Colloid and Interface Science* **2003,** *268* (1), 200-207.

399.   Costa, S.; Richter, A.; Schmidt, U.; Breuninger, S.; Hollricher, O., Confocal Raman microscopy in life sciences. *Morphologie* **2018**.

400.   Cho, L. L., Identification of textile fiber by Raman microspectroscopy. *Forensic Sci. J.* **2007,** *6* (1), 55-62.

401.   Sharikova, A.; Foraida, Z. I.; Sfakis, L.; Peerzada, L.; Larsen, M.; Castracane, J.; Khmaladze, A., Characterization of nanofibers for tissue engineering: Chemical mapping by Confocal Raman microscopy. *Spectrochimica Acta Part A: Molecular and Biomolecular Spectroscopy* **2020,** *227*, 117670.

402.   Rydz, J.; Šišková, A.; Andicsová Eckstein, A., Scanning Electron Microscopy and Atomic Force Microscopy: Topographic and Dynamical Surface Studies of Blends, Composites, and Hybrid Functional Materials for Sustainable Future. *Advances in Materials Science and Engineering* **2019,** *2019*, 6871785.

403.   Song, C. L.; Kazarian, S. G., Three-dimensional depth profiling of prostate tissue by micro ATR-FTIR spectroscopic imaging with variable angles of incidence. *Analyst* **2019,** *144* (9), 2954-2964.

404.   Chan, C.-M.; Weng, L.-T.; Lau, Y.-T. R., Polymer surface structures determined using ToF-SIMS. *Reviews in Analytical Chemistry* **2014,** *33* (1), 11-30.

405.   Garcea, S. C.; Wang, Y.; Withers, P. J., X-ray computed tomography of polymer composites. *Composites Science and Technology* **2018,** *156*, 305-319.

406.   Nair, S.; Gao, J.; Otto, C.; Duits, M. H. G.; Mugele, F., In-situ observation of reactive wettability alteration using algorithm-improved confocal Raman microscopy. *Journal of Colloid and Interface Science* **2021,** *584*, 551-560.

407.   Zhang, H. W.; Hu, X. B.; Qin, Y.; Jin, Z. H.; Zhang, X. W.; Liu, Y. L.; Huang, W. H., Conductive Polymer Coated Scaffold to Integrate 3D Cell Culture with Electrochemical Sensing. Jounal of *Analytical Chemistry* **2019,** *91* (7), 4838-4844.

408.   Cho, S.; Jung, M.; Ju, D.; Lee, Y.-H.; Cho, K.; Okabe, S., Anammox biomass carrying efficiency of polyethylene non-woven sheets as a carrier material. *Environmental Technology* **2017,** *39*, 1-34.

409.   Kiel, S.; Klein, M.; Kroupitski, Y.; Peiper, U. M.; Sela Saldinger, S.; Poverenov, E., Air-ozonolysis activation of polyolefins versus use of laden finishing to form contact-active nonwoven materials. *Scientific Reports* **2021,** *11* (1), 10798.

410.   Gao, J.; Nie, Y.; Lim, B. H.; Zhai, X.; Kedir, N.; Chen, W., In-situ observation of cutting-induced failure processes of single high-performance fibers inside a SEM. *Composites Part A: Journal of Applied Science and Manufacturing* **2020,** *131*, 105767.

411.   Ekoi, E. J.; Dickson, A. N.; Dowling, D. P., Investigating the fatigue and mechanical behaviour of 3D printed woven and nonwoven continuous carbon fibre reinforced polymer (CFRP) composites. *Composites Part B: Engineering* **2021,** *212*, 108704.

412.   Muniz, N. O.; Vechietti, F. A.; Anesi, G. R.; Guinea, G. V.; dos Santos, L. A. L., Blend-based fibers produced via centrifugal spinning and electrospinning processes: Physical and rheological properties. *Journal of Materials Research* **2020,** *35* (21), 2905-2916.

413.   Analytical Currents: Kindling proteins light a fluorescent "fire". *Analytical Chemistry* **2003,** *75* (7), 139 A-139 A.

414.   Yin, J.; Deng, J.; Wang, L.; Du, C.; Zhang, W.; Jiang, X., Detection of Circulating Tumor Cells by Fluorescence Microspheres-Mediated Amplification. *Analytical Chemistry* **2020**.

415.   O'Connor, N. A.; Sakata, S. T.; Zhu, H.; Shea, K. J., Chemically Modified Dansyl Probes: A Fluorescent Diagnostic for Ion and Proton Detection in Solution and in Polymers. *Organic Letters* **2006,** *8* (8), 1581-1584.

416.   Deng, W.; Goldys, E. M., Plasmonic Approach to Enhanced Fluorescence for Applications in Biotechnology and the Life Sciences. *Langmuir* **2012,** *28* (27), 10152-10163.

417.   S. B., Fingerprint Source Book – Chapter 3: Chemical and Physical Processes. 2 ed.; (CAST), Ed. **2017**.

418.   Russell, R. A.; Adams, N. M.; Stephens, D. A.; Batty, E.; Jensen, K.; Freemont, P. S., Segmentation of Fluorescence Microscopy Images for Quantitative Analysis of Cell Nuclear Architecture. *Biophysical Journal* **2009,** *96* (8), 3379-3389.

419.   R., L., *The Quantum Theory of Light*. Oxford Press: London, **2003**.

420.   L., S. C., Basic Confocal Microscopy. *Current Protocols in Molecular Biology* **2008,** *81* (1), 14.11.1-14.11.18.

421.   Knapczyk-Korczak, J.; Szewczyk, P. K.; Ura, D. P.; Bailey, R. J.; Bilotti, E.; Stachewicz, U., Improving water harvesting efficiency of fog collectors with electrospun random and aligned Polyvinylidene fluoride (PVDF) fibers. *Sustainable Materials and Technologies* **2020,** *25*, e00191.

422.   Duprat, C.; Protière, S.; Beebe, A. Y.; Stone, H. A., Wetting of flexible fibre arrays. *Nature* **2012,** *482* (7386), 510-3.

423.   Aydin, O.; Emon, B.; Cheng, S.; Hong, L.; Chamorro, L. P.; Saif, M. T. A., Performance of fabrics for home-made masks against the spread of COVID-19 through droplets: A quantitative mechanistic study. *Extreme Mechanics Letters* **2020,** *40*, 100924.

424.   Konda, A.; Prakash, A.; Moss, G. A.; Schmoldt, M.; Grant, G. D.; Guha, S., Aerosol Filtration Efficiency of Common Fabrics Used in Respiratory Cloth Masks. *ACS Nano* **2020,** *14* (5), 6339-6347.

425.   Hu, D.; Li, X.; Li, L.; Yang, C., Designing high-caliber nonwoven filter mats for coalescence filtration of oil/water emulsions. *Separation and Purification Technology* **2015,** *149*, 65-73.

426.   Graham, T., LV. On the absorption and dialytic separation of gases by colloid septa. *The London, Edinburgh, and Dublin Philosophical Magazine and Journal of Science* **1866,** *32* (218), 401-420.

427.   Budzien, J.; McCoy, J.; Weinkauf, D., Solubility of Gases in Amorphous Polyethylene. *Macromolecules* **1998,** *31*, 3368.

428.   Palkopoulou, S.; Joly, C.; Feigenbaum, A.; Papaspyrides, C. D.; Dole, P., Critical review on challenge tests to demonstrate decontamination of polyolefins intended for food contact applications. *Trends in Food Science & Technology* **2016,** *49*, 110-120.

429.   Miller-Chou, B. A.; Koenig, J. L., A review of polymer dissolution. *Progress in Polymer Science* **2003,** *28* (8), 1223-1270.

430.   Hansen, C. M., Polymer additives and solubility parameters. *Progress in Organic Coatings* **2004,** *51* (2), 109-112.

431.   Tolinski, M., Overview of Polyolefins and Additives. In *Additives for Polyolefins (Second Edition)*, Tolinski, M., Ed. William Andrew Publishing: Oxford, **2015**; pp 3-7.

432.   Shamey, R., 12 - Improving the coloration/dyeability of polyolefin fibres. In *Polyolefin Fibres (Second Edition)*, Ugbolue, S. C. O., Ed. Woodhead Publishing: **2017**; pp 359-388.

433.   Hao, W.; Wang, M.; Zhou, F.; Luo, H.; Xie, X.; Luo, F.; Cha, R., A review on nanocellulose as a lightweight filler of polyolefin composites. *Carbohydrate Polymers* **2020,** *243*, 116466.

434.   Schlotter, N. E.; Furlan, P. Y., A review of small molecule diffusion in polyolefins. *Polymer* **1992,** *33* (16), 3323-3342.

435.   Chang, S.-S., Migration of low molecular weight components from polymers: 1. Methodology and diffusion of straight-chain octadecane in polyolefins. *Polymer* **1984,** *25* (2), 209-217.

436.   K., U., *The solution process* Academic Press: New York, **1986**.

437.   Blackadder, D. A.; Le Poidevin, G. J., Dissolution of polypropylene in organic solvents: 1. Partial dissolution. *Polymer* **1976,** *17* (5), 387-394.

438.   Blackadder, D. A.; Le Poidevin, G. J., Dissolution of polypropylene in organic solvents: 2. The steady state dissolution process. *Polymer* **1976,** *17* (9), 768-776.

439.   Blackadder, D. A.; Le Poidevin, G. J., Dissolution of polypropylene in organic solvents: 3. Effect of molecular weight of polymer. *Polymer* **1977,** *18* (6), 547-550.

440.   Blackadder, D. A.; Le Poidevin, G. J., Dissolution of polypropylene in organic solvents: 4. Nature of the solvent. *Polymer* **1978,** *19* (5), 483-488.

441.   Experiments In Polymer Science Edward A. Collins, Jan Bares and Fred Billmeyer, Jr. John Wiley and Sons, New York-London-Sydney-Toronto, 1973. 530 pp. *Journal of Chromatographic Science* **1975,** *13* (7), 12A-12A.

442.   Khalifeh, S., Introduction to Polymers for Electronic Engineers. In *Polymers in Organic Electronics*, Khalifeh, S., Ed. ChemTec Publishing: **2020**; pp 1-31.

443.   Michaels, A. S.; Vieth, W. R.; Alcalay, H. H., The solubility parameter of polypropylene. *Journal of Applied Polymer Science* **1968,** *12* (7), 1621-1624.

444.   Qin, Y.; Rubino, M.; Auras, R.; Lim, L.-T., Impact of polymer processing on sorption of benzaldehyde vapor in amorphous and semicrystalline polypropylene. *Journal of Applied Polymer Science* **2008,** *110* (3), 1509-1514.

445.   Park, J. C. a. G. S., *Diffusion in polymers*. Academic Press, London and New Yorrk: **1968**.

446.   Peacock, A. J., *Handbook of polyethylene : structures, properties, and applications*. Marcel Dekker: New York, 2000.

447.   Mandelkern, L., *Crystallization of Polymers*. McGraw-Hill: **1964**.

448.   Sharples, A., *Introduction to polymer crystallization*. Edward Arnold: London, **1966**.

449.   Alamo, R.; Mandelkern, L., Origins of endothermic peaks in differential scanning calorimetry. *Journal of Polymer Science Part B: Polymer Physics* **1986,** *24* (9), 2087-2105.

450.   . Thermal Analysis Application No. UC 134- Determination of polymer crystallinity with DSC measurements **2010**.

451.   Mandelkern, L.; Fatou, J. G.; Denison, R.; Justin, J., A calorimetric study of the fusion of molecular weight fractions of linear polythylene (1). *Journal of Polymer Science Part B: Polymer Letters* **1965,** *3* (10), 803-807.

452.   Li, D.; Zhou, L.; Wang, X.; He, L.; Yang, X., Effect of Crystallinity of Polyethylene with Different Densities on Breakdown Strength and Conductance Property. *Materials* **2019,** *12* (11), 1746.

453.   Fischer, E. W.; Goddar, H.; Schmidt, G. F., Determination of degree of crystallinity of drawn polymers by means of density measurements. *Journal of Polymer Science Part A-2: Polymer Physics* **1969,** *7* (1), 37-45.

454.   Robertson, R. E.; Paul, D. R., Stress–strain behavior of polyolefin blends. *Journal of Applied Polymer Science* **1973,** *17* (8), 2579-2595.

455.   Orwoll, R. A. *Densities, Coefficients of Thermal Expansion, and Compressibilities of Amorphous Polymers: Datasheet from · Volume : "Physical Properties of Polymers Handbook" in SpringerMaterials (https://doi.org/10.1007/978-0-387-69002-5_7)*, Springer Science+Business Media, LLC.

456.   Koszinowski, J., Diffusion and solubility of n-alkanes in polyolefines. *Journal of Applied Polymer Science* **1986,** *32* (5), 4765-4786.

457.   Kong, Y.; Hay, J. N., The measurement of the crystallinity of polymers by DSC. *Polymer* **2002,** *43* (14), 3873-3878.

458.   Manley, T. R., Calorimetry and thermal analysis of polymers, edited by V. B. F. Mathot. Hanser, Munich, **1994**. pp. 377, price £59.00. ISBN 3-446-17511-3. *Polymer International* **1995,** *37* (1), 83-83.

459.   Sato, Y.; Yurugi, M.; Yamabiki, T.; Takishima, S.; Masuoka, H., Solubility of propylene in semicrystalline polypropylene. *Journal of Applied Polymer Science* **2001,** *79* (6), 1134-1143.

460.   Jahn, N. H. Hydration phenomena in concentrated protein solutions. Imperial College London, 2015.

461.   Chapman, W. G.; Gubbins, K. E.; Jackson, G.; Radosz, M., SAFT: Equation-of-State Solution Model for Associating Fluids. *Fluid Phase Equilibria* **1989,** *52*, 31-38.

462.   Felipe J, B.; Lourdes F, V., Thermodynamic behaviour of homonuclear and heteronuclear Lennard-Jones chains with association sites from simulation and theory. *Molecular Physics* **1997,** *92* (1), 135-150.

463.   Amparo Galindo Lowri A. Davies Alejandro Gil-Villegas George, J., The thermodynamics of mixtures and the corresponding mixing rules in the SAFT-VR approach for potentials of variable range. *Molecular Physics* **1998,** *93* (2), 241-252.

464.   Gross, J.; Sadowski, G., Application of perturbation theory to a hard-chain reference fluid: an equation of state for square-well chains. *Fluid Phase Equilibria* **2000,** *168* (2), 183-199.

465.   Lafitte, T.; Apostolakou, A.; Avendaño, C.; Galindo, A.; Adjiman, C. S.; Müller, E. A.; Jackson, G., Accurate statistical associating fluid theory for chain molecules formed from Mie segments. *The Journal of Chemical Physics* **2013,** *139* (15), 154504.

466.   Papaioannou, V.; Lafitte, T.; Avendaño, C.; Adjiman, C. S.; Jackson, G.; Müller, E. A.; Galindo, A., Group contribution methodology based on the statistical associating fluid theory for heteronuclear molecules formed from Mie segments. *The Journal of Chemical Physics* **2014,** *140* (5), 054107.

467.   Dufal, S.; Papaioannou, V.; Sadeqzadeh, M.; Pogiatzis, T.; Chremos, A.; Adjiman, C. S.; Jackson, G.; Galindo, A., Prediction of Thermodynamic Properties and Phase Behavior of Fluids and Mixtures with the SAFT-γ Mie Group-Contribution Equation of State. *Journal of Chemical & Engineering Data* **2014,** *59* (10), 3272-3288.

468.   Dufal, S.; Lafitte, T.; Haslam, A. J.; Galindo, A.; Clark, G. N. I.; Vega, C.; Jackson, G., The A in SAFT: developing the contribution of association to the Helmholtz free energy within a Wertheim TPT1 treatment of generic Mie fluids. *Molecular Physics* **2015,** *113* (9-10), 948-984.

469.   Fischer, E. W., Das Grenzflächenschmelzen der Kristallite in teilkristallisierten Hochpolymeren. *Kolloid-Zeitschrift und Zeitschrift für Polymere* **1967,** *218*, 97-114.

470.   Zachmann, H., Peterlin, A., Influence of the surface morphology on the melting of polymer crystals. I. Loops of random length and adjacent reentry. *Journal of Macromolecular Science Part B.* **1969,** *3*.

471.   Albrecht, T.; Strobl, G., Temperature-Dependent Crystalline-Amorphous Structures in Linear Polyethylene: Surface Melting and the Thickness of the Amorphous Layers. *Macromolecules* **1995,** *28* (17), 5827-5833.

472.   Minelli, M.; De Angelis, M. G., An equation of state (EoS) based model for the fluid solubility in semicrystalline polymers. *Fluid Phase Equilibria* **2014,** *367*, 173–181.

473.   Kofinas, P.; Cohen, R. E.; Halasa, A. F., Gas permeability of polyethylene/poly(ethylene-propylene) semicrystalline diblock copolymers. *Polymer* **1994,** *35* (6), 1229-1235.

474.   Griffin, W. C., Classification of Surface-Active Agents by "HLB". *Journal of Cosmetic Science* **1949,** *1*, 311-326.

475.   WC, G., Calculation of HLB Values of Non-Ionic Surfactants. *Journal of Cosmetic Science* **1954,** *5*, 259.

476.   EEC, Directive 90/128/EEC. Commision Directive of 23 February **1909** relating to plastics materials and articles intended to come into contact with foodstuff. **1990**; Vol. L349, p 26.

477.   Malkan, S. R., Improving the use of polyolefins in nonwovens. In *Polyolefin Fibres (Second Edition)*, Ugbolue, S. C. O., Ed. Woodhead Publishing: 2017; pp 285-311.

478.   Simoneau, M. A. P. a. C. *OLC002 2013 - Identification of Polymeric Materials*; European Commission Joint Research Center: European Comission Repository, **2013**.

Appendix A

(Chapter 4 supplementary information)

<u>FT-IR</u>

Characterization of nonwovens using FT-IR was also attempted since it's a simple quick and inexpensive method. The FTIR spectra acquired for the base nonwoven, coated nonwoven, and the neat surfactant for both Core Cover, (100 % PP) and Top Sheet (50:50 % PP/PE) nonwovens are presented in Figure A. 1 and Figure A. 2 respectively. Observing the initial uncoated Core Cover nonwoven spectra, it is possible to define this nonwoven polymer as polypropylene. The FTIR spectrum of polypropylene[45, 478] features the stretching vibration of –C–H at 2985–2810 and that of –CH_2 at 2950–2850 cm^{-1} which are present all our nonwoven samples. It also contains the bending vibrations of –CH_2 and –CH_3 are 1475–1440 cm^{-1} confirming that our nonwoven core cover is made of polypropylene. However, the spectra for uncoated and surfactant coated nonwovens appear to be identical suggesting that FTIR is unable to distinguish between these samples. Typically, for use in commercial products surfactants are applied to nonwovens in the loading range of 0.4-0.6 % wt/wt.[130] Such small amounts of surfactants seem to be unable to be detected by FTIR technique.
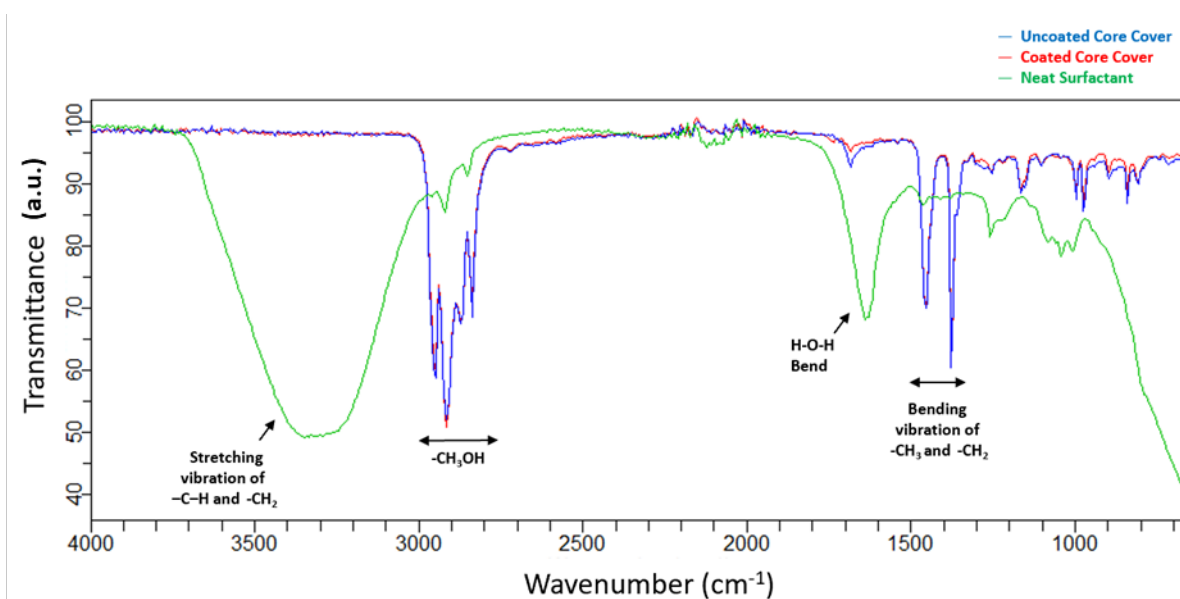
Figure A. 1 FTIR spectra of original uncoated Core Cover nonwoven, surfactant treated nonwoven and the neat surfactant, (PHP).

Figure A. 1 shows the frequency range as related to different vibration types of methyl (PP/HDPE): the stretching vibration of –C–H is 2985–2810 cm^{-1} (PP) and that of –CH_2 is 2950–2850 cm^{-1} (HDPE); the bending vibrations of –CH_2 and –CH_3 are 1475–1440 cm^{-1} (PP) and 1380–1370 cm^{-1} (PP), respectively, and that of –CH_2 is 1470–1460 cm^{-1} (HDPE); and the

rocking vibration of -CH$_2$ is 730–700 cm^{-1} (HDPE). It is difficult to differentiate polyethylenes by FTIR[478]. The main difference with LDPE is seen in 1380 cm^{-1} peak. For LDPE, the band region 1400- 1330 cm^{-1} consists in three peaks, while that for HDPE consists in two peaks. If no individual peak is observed at 1742 cm^{-1}, then the material is likely to be HDPE. In our sample there is no peak at 1742 cm^{-1} therefore, suggesting that the nonwoven is HDPE base. Like the Core Cover nonwovens the spectra for uncoated and surfactant coated Top Sheet nonwovens appear to be identical suggesting that FTIR is unable to distinguish between these samples either. Similar as before, the reason could be the low sensitivity of FTIR on detecting such low surfactant coatings, (0.4-0.6 % wt/wt)[45].
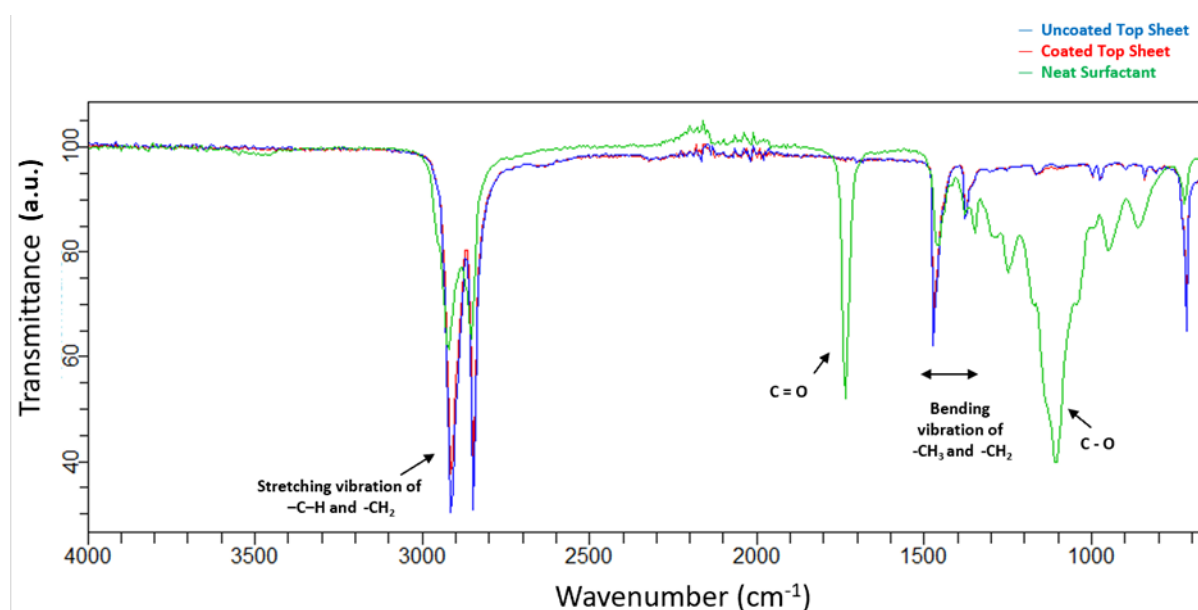
Figure A. 2 FTIR spectra of original uncoated Top Sheet nonwoven, surfactant treated nonwoven and the neat surfactant, (Stantex).

Surface chemical composition analysis (XPS)

Surface chemical analysis using XPS was conducted to measure elemental composition of surfactant coated and uncoated reference PP based nonwoven fibres. Figure A. 3 shows the survey scan spectra for the PP fibers; coated (CC-A) and uncoated (CC-B). There are the two specific energy peaks present in the spectra observed on the survey scan and some traces of other peaks featuring mostly on the coated sample. The expected carbon (1s) peak existed at 285 eV and oxygen (1s) peak existed at 531eV. After surfactant treatment, the intensity of oxygen-related peak dramatically increased while the intensity of carbon related peak decreased. The increased oxygen content ratio on the surfactant-coated surface, Table 4.16, indicated the improvement of surface wettability as was also observed in wetting and IGC results. Carbon content (C1s) of the uncoated PP fabric was ideally expected to be 100% due to the PP molecular structure. However, a low oxygen content (O1s) of 2.78% on the uncoated

fabric was detected which could be due to finishing agents or surface contamination on the fibers[389]. The presence of oxygen on the surface of the uncoated PP nonwoven suggests that the material contains some contamination or probably surface oxidation[390]. Degradation/oxidation of polymers during the fibre production might be another reason for presence of oxygen on the surface[391, 392].
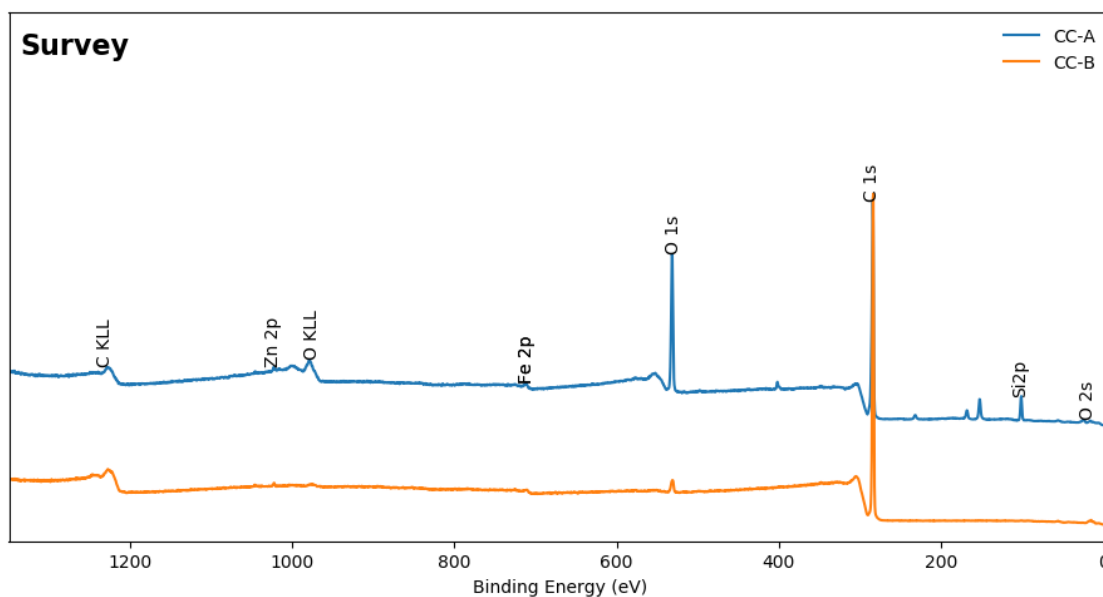

Figure A. 3 XPS survey scan spectra of the three months aged polypropylene (PP) nonwoven (a) CC-A coated and (b) CC-B uncoated.

To gain a greater insight into the surface composition of nonwovens coated with surfactants, high-resolution spectra were acquired in the regions of C1s and O1s core levels. As shown in Figure A. 4 (a), carbon is found at lower binding energy to the standard adventitious carbon (284.8 eV) which could arise from silicon oxycarbide SiO-C type. Also, Figure A. 4 (b) shows Si 2p found in its SiO-C (oxycarbide) form at 531.8 eV. Although the composition of the surfactant coating is not fully identified for proprietary reasons, it is known that it is a mixture of fatty acid quaternary ammonia compounds and cationically modified poly-dimethyl siloxanes which is in line with the results shown here.
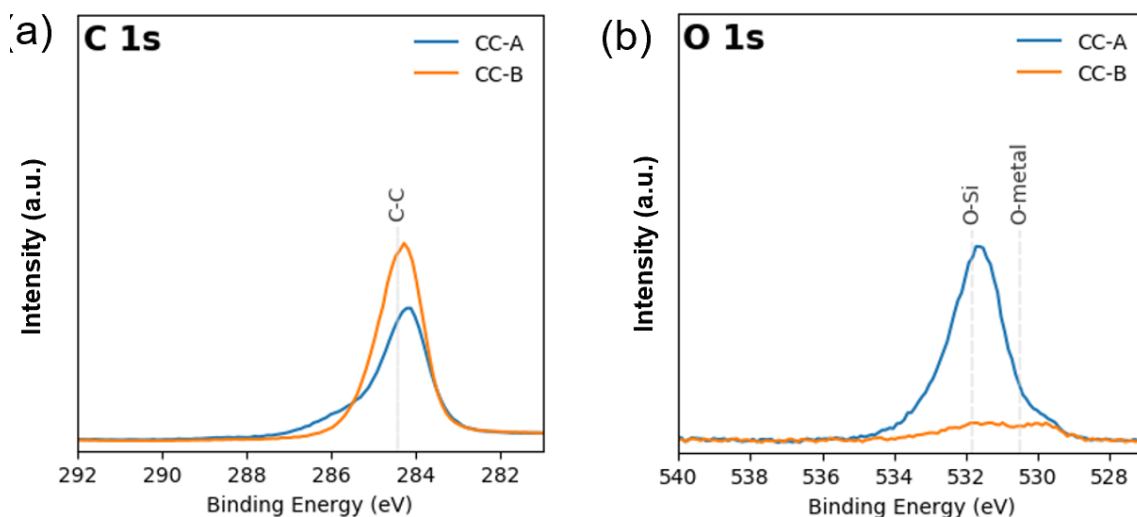
Figure A. 4 Core level spectra of CC-A coated and CC-B uncoated PP nonwoven, both three-month-old (a) C1s (b) O1s.

The peak fitting and knowledge concerning relative peak positions in the C1s and O1s signals were obtained from literature[393]. The C1s and O1s signal were deconvoluted into Gaussian peak components and evaluating the areas of these peaks allowed to obtain the quantitative information. One-year-old samples of surfactant coated, and uncoated PP based nonwoven fibres were also analysed using XPS. Figure A. 5 indicates the survey scan spectra for the elements on the PP fibers, coated (PTC-A) and uncoated (PTC-B). There are specific peaks present for the expected carbon (1s) peak at 285 eV for both samples and only a small oxygen (1s) peak at 531 eV, for the surfactant coated sample, PTC-A. These results suggest potential aging of the sample and loss of surface surfactant as a function of time.
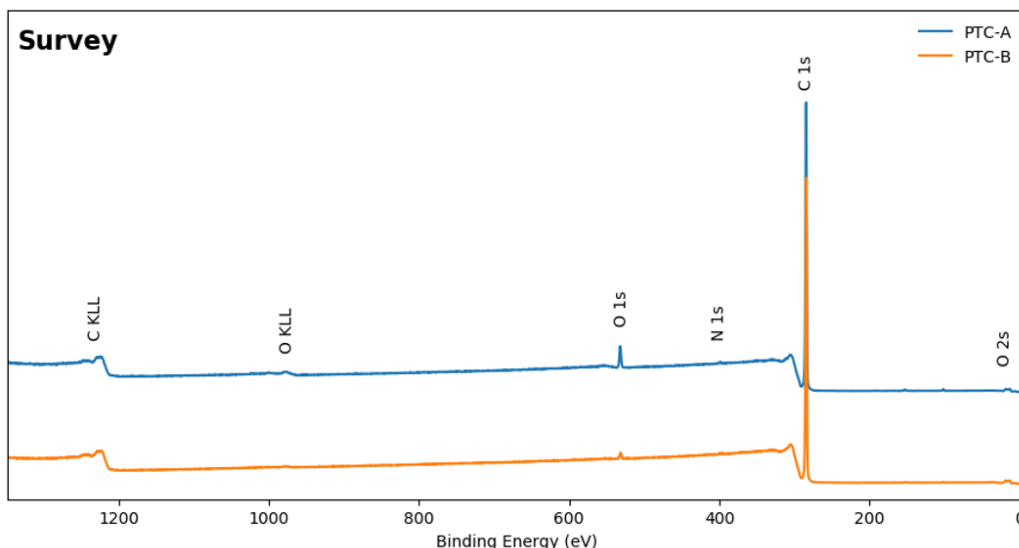
Figure A. 5 X-ray photoelectron spectroscopy (XPS) survey scan spectra of the one-year-old polypropylene (PP) nonowoven (a) PTC-A coated and (b) PTC-B uncoated.

As seen with the previous samples the carbon, is found at lower binding energy to the standard adventitious carbon (284.8 eV) suggesting presence of silicon oxycarbide SiO-C type bonds and the Si 2p is found in its SiO-C (oxycarbide) form at 531.8 eV. However, these are present at trace levels and there isn't a noticeable chemical difference between the surface of coated and uncoated one year old nonwoven samples suggesting lack/ loss of surfactants from surface of coated samples. This supports what the industry have experienced with surfactant coated nonwoven samples, an aging process which is detected by XPS.
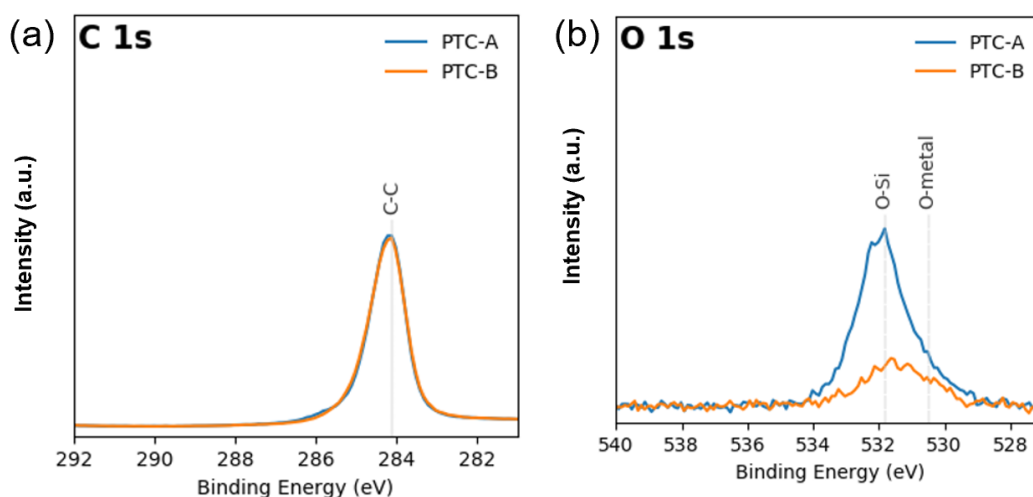
Figure A. 6 Core level spectra of PTC-A coated and PTC-B uncoated PP nonwoven, both one year old (a) C1s (b) O1s.

The relative chemical composition determined by XPS of surfactant coated and uncoated nonwovens are reported, as a percentage, in Table A. 1. The results for both one year old

nonwoven samples and the three-month-old samples are shown in Table A. 1. The surfactant coated one-year older sample appears to have significantly less oxygen and nitrogen present at its surface than the three months old, coated sample. Again, the aging affect is confirmed and the result support the theory that surfactant surface concentrations are reduced as a function of time. Imaging with XPS is possible but this is a lengthy and expensive process, and it was not explored as part of this thesis.

Table A. 1 Relative chemical composition determined by XPS for uncoated and surfactant coated PP based nonwovens, three months old.

% Atomic Abundance	Sample Type			
	3 months		1 year	
	Surfactant Coated	Uncoated Control	Surfactant Coated	Uncoated Control
Carbon	72.3 (4)	96.5 (1)	96.1 (3)	98.5 (2)
Oxygen	17.2 (6)	2.7 (8)	3.0 (6)	0.9 (3)
Nitrogen	1.5 (3)	—	0.3 (3)	0.3 (2)
Silicon	7.0 (3)	0.1 (1)	0.4 (8)	0.2 (3)
Iron	0.3 (0)	0.3 (1)	—	—
Zinc	0.0 (9)	0.1 (2)	—	—

Overall, the XPS analysis showed that surfactant treatment of polypropylene fibre surface results in a significant increase in atomic percentage of oxygen species which are responsible for the hydrophilic surface. The intensity of C–C related binding energy levels decreased while oxygen-related binding energy levels increased and expanded for the surfactant coated samples. However, the results from the aged samples show that the surfactant treatment is not permanent, and the surface concentrations are significantly reduced after one year, rendering the sample hydrophobic. Similar aging effects of hydrophilic nonwovens have been documented in the literature[394, 395].

TOF-SIMS characterization of nonwoven surfaces

XPS cannot give absolute information about the specific surface chemical functionalities on a fiber surface because this technique includes subsurface contributions (up to 5nm). Surface characterization using ToF-SIMS method has unique advantages compared with XPS due to its high molecular specificity, extreme surface sensitivity (about 1nm), and high-mass resolution, and therefore qualitative interpretation from ToF-SIMS are most suitable for characterising the changes in the surface chemistry with a high degree of accuracy.

TOF-SIMS was used to image the surfactant distribution on polymer-based nonwovens and to verify the "patchwise" hydrophilic heterogeneity phenomena observed with contact angle measurement. TOF-SIMS provides semi-quantitative mass spectrum analysis of the outmost ~ 3nm of the sample's surface. Five different positions, (non-bonding areas, 500x500µm^2, 256x256 pixels), of a surfactant treated top sheet nonwoven were analysed and the results are shown in Figure A. 7. TOF-SIMS images were normalised and standardised at the same pseudo-color scale for sample-to-sample comparison. For each image shown, going from left to right, the silicon distribution is featured on the 1st image, then the second image shows surfactant, (stantex), distribution, followed by erucamide distribution shown on the 3rd image. Erucamide is commonly used as a slip agent in polyolefin resins, like those used to manufacture nonwovens used in hygiene industry. Images on the fourth column represent an overlay image of the three chemicals, (silicon, surfactant and erucamide).

Figure A. 7 showed presence of surfactants on the treated sample, with high variation of surfactant distribution featured between the different sample positions. The silicone and stantex distribution appears relatively uniform within 500x500 µm^2 area, but variation is observed between area to area within the same sample. Images display heterogeneous distribution of surfactants across the surface of the nonwoven which aligns with the findings from the wettability studies. The heterogeneity is displayed by the different local intensities observed in the images. TOF-SIMS observations of silicone and erucamide distribution showed uneven distribution between area to area, with local unevenness likely resulting from the natural fiber network structure.
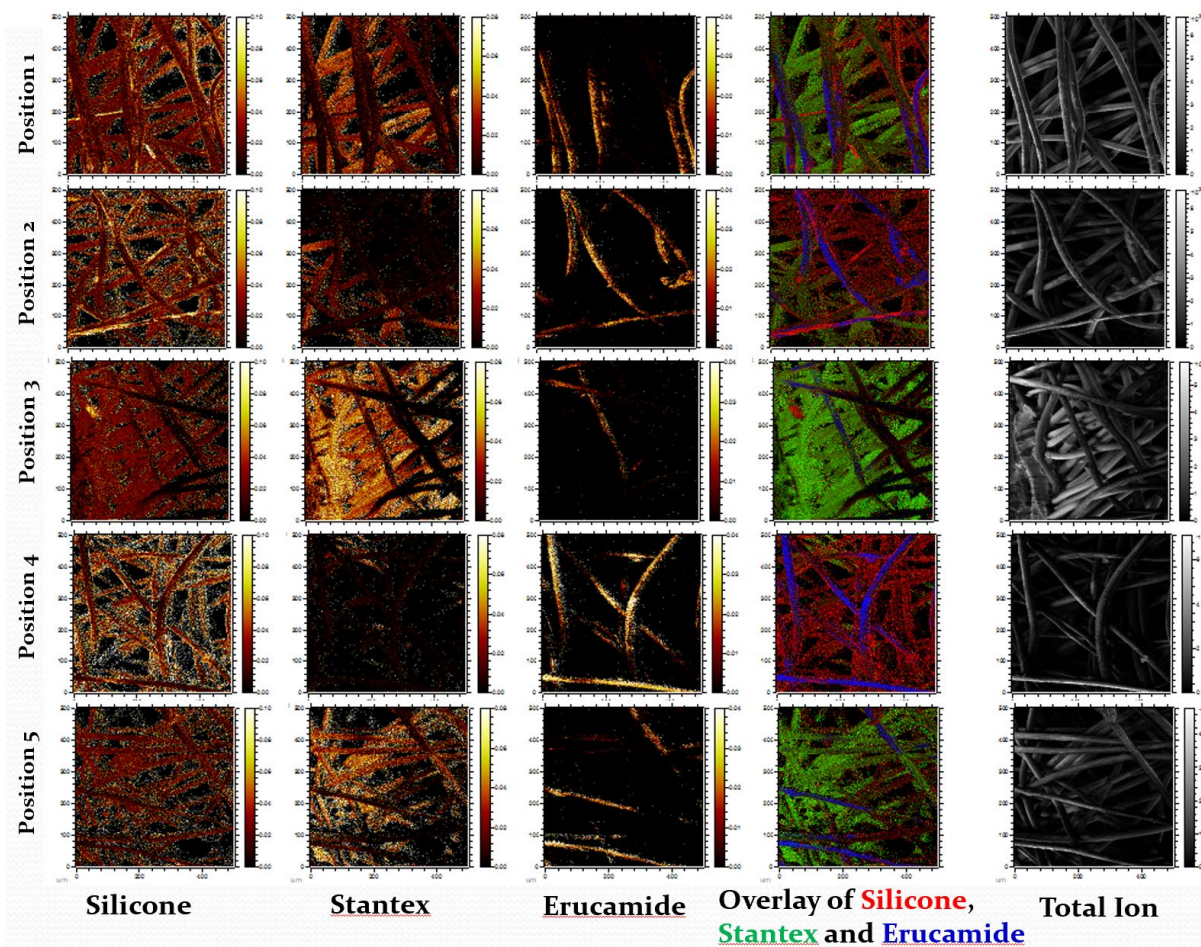
Figure A. 7 ToF-SIMS elemental mapping of 5 different positions on a top sheet nonwoven treated with surfactant.

The results for the reference, untreated, sample are displayed in Figure A. 8. In the same way as for the treated sample, the data, going from left to right, show the silicon distribution on the first image, the surfactant, (Stantex), distribution on the second image, followed by erucamide distribution the third image. The fourth column represent the overlay image of the three chemicals, (silicon, surfactant and erucamide). Comparing the distribution and location of the components on the fibre surface before and after treatment informs on the surface chemical composition. The data in Figure A. 8 clearly shows that:

- there is no surfactant present on the untreated sample,
- and the silicon and erucamide distributions observed appear the same as for the treated sample suggesting these are components of the nonwoven base sample.

286
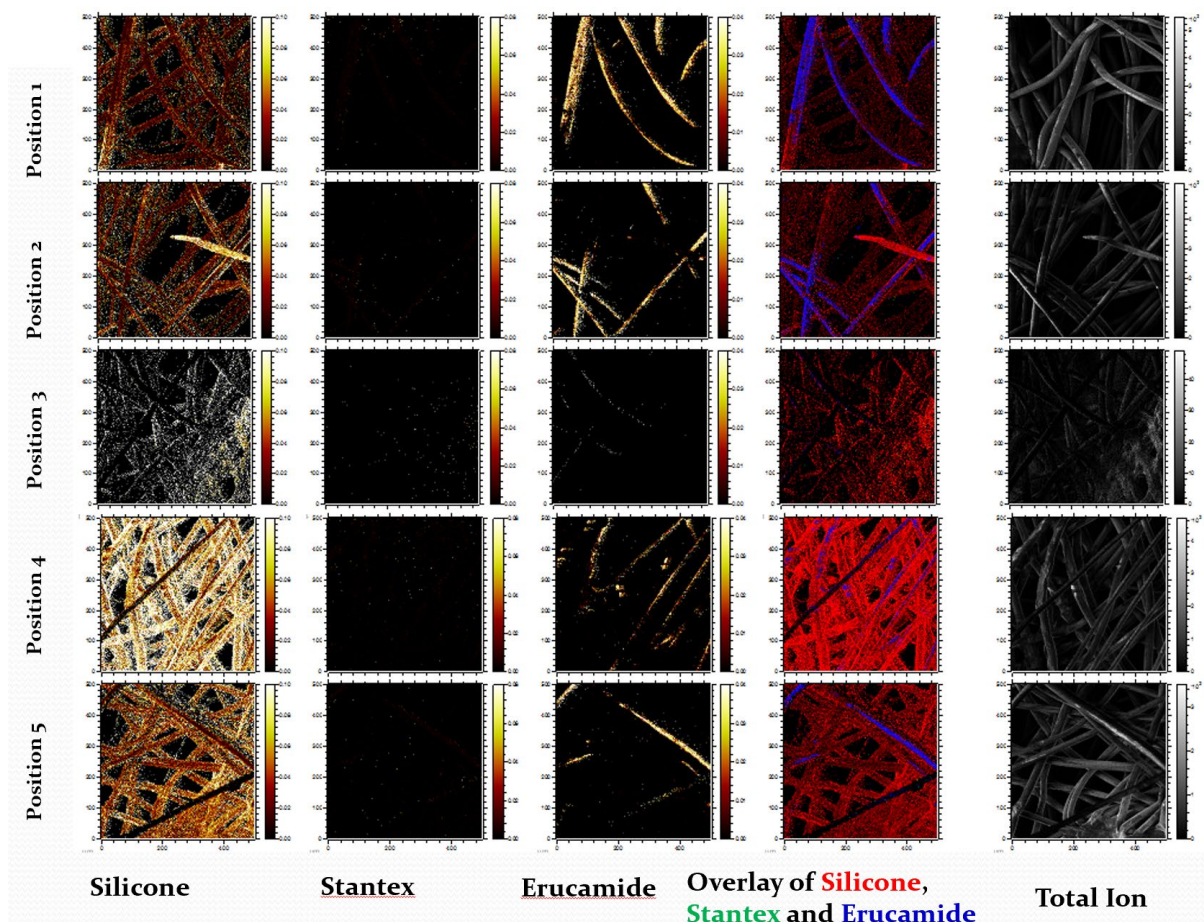
Figure A. 8 . ToF-SIMS elemental mapping of surface components on 5 different locations on a top sheet untreated reference nonwoven.

Overall, the uneven surfactant distribution, the presence of "spotty" erucamide, and the existence of silicone could all contribute to the non-uniformity and variation of contact angle measurement observed. The study confirms that TOF-SIMS was able to identify and chemically distinguish between surfactant treated and nontreated nonwovens. However, this method is not quantitative. Furthermore, the logistics associated with this instrument not being located at the college meant intensive studies using this method were not feasible.

AFM analysis of thin films

Analysis method and instrument calibration:

The following samples were tested with the AFM, (JPK AFM – Bruker) to establish differences between surfactant coated and uncoated thin polymer films. Inert silicon wafers were used for casting the films via spin coating method.

1. Blank
2. Surfactant
3. PE FILM
4. PE FILM + Surfactant

287

The AFM was calibrated at the beginning of experiment, in contact-free mode.

Sensitivity: 31.03 nm/V

Spring Constant: 25.294 N/m

Resonance Frequency: 267.9 kHz

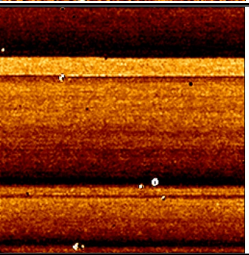Tip (cantilever used): PPP-NCHAuD from APEX Probes
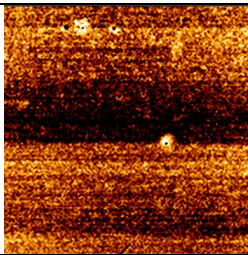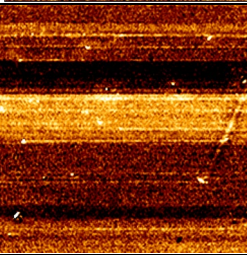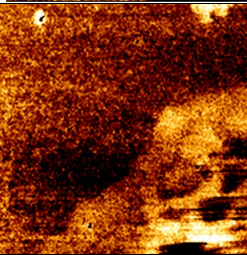
Tip Width: 30 µm
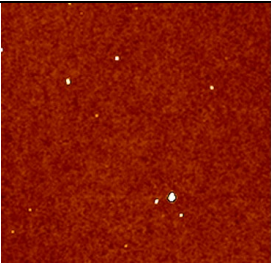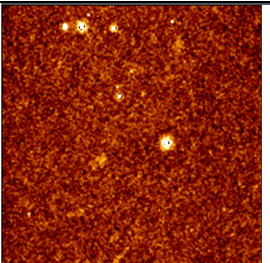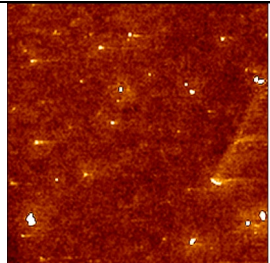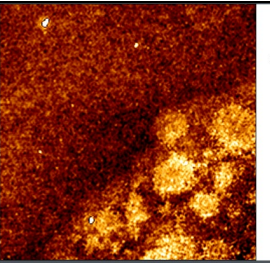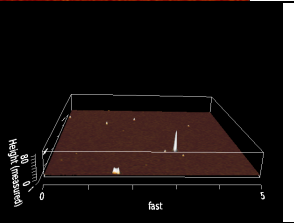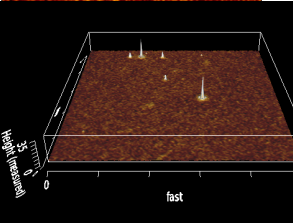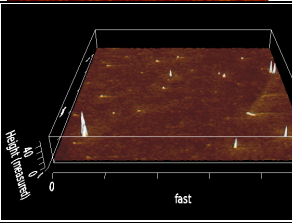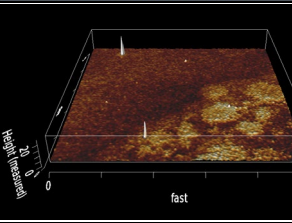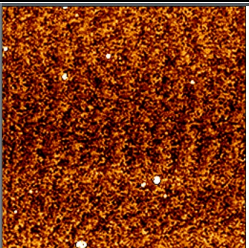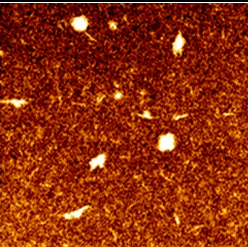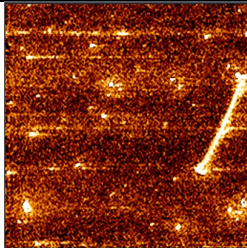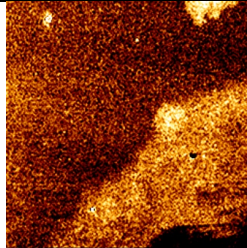
Length: 125 µm

Set point, Z length, Z speed and resolution was adjusted accordingly based on the material to achieve a decent force distance curve.

Scan size was set at 5 um x 5 um (256 x 256 resolution).

Images were analysed using JPK processing software.

Table A. 2 AFM analysis of thin films

AFM Images	Blank SiO$_2$ wafer 5 x 5 μm	SiO$_2$ wafer + PE film 5 x 5 μm	SiO$_2$ wafer + surfactant/PHP film 5 x 5 μm	SiO$_2$ wafer +PE film + PHP film 5 x 5 μm
Height	4.77 nm / 0 nm	1.98 nm / 0 nm	3.4 nm / 0 nm	1.67 nm / 0 nm
Height 3D				
Slope (stiffness)	31.6 nN/μm / -133 nN/μm	252 nN/μm / -106 nN/μm	454 nN/μm / -194 nN/μm	462 nN/μm / -194 nN/μm
Adhesion	6.81 nN / -2.9 nN	3.24 nN / -1.37 nN	7.91 nN / -3.39 nN	8.2 nN / -3.43 nN
Stats/other	Ra:150.8pm Resolution: 256 x 256	Ra:153pm Resolution: 256 x 256	Ra:188.2pm Resolution: 256 x 256	Ra:210.1pm Resolution: 256 x 256

289

Optical profilometry of nonwoven fibre

To study the effect of surfactants on surface morphology of polymeric based nonwoven fibre profilometry was explored. It want possible to determine any differences between coated and uncoated nonwoven fibres. Roughness average (Sa), root mean square (Sq) roughness and average of the height difference between five highest peaks (Sz) were calculated and are included in the image below. An example of an optical image of nonwoven fibre obtained using profilometry has been shown in Figure A. 10.
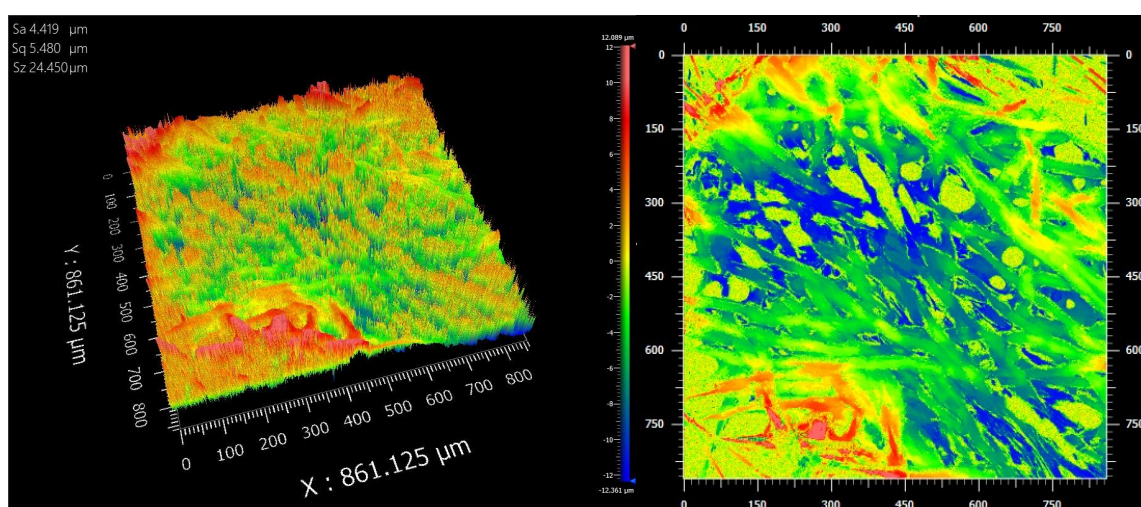

Figure A. 9 Optical profilometry images showing 3D (left) and 2D (right) surface morphology of surfactant coated, (0.8% w/v PHP) polymeric based nonwoven fibre.

Surface energy determination using IGC with alkane vapours

Normally, to measure the dispersive component of surface energy, a minimum sequence of three linear alkanes having different carbon chain lengths are used in an IGC experiment. However, preliminary BET analysis, (discussed above) suggested that alkanes are absorbed into the bulk by the nonwoven samples therefore, they are not suitable as test probes for IGC measurements of polyolefins, be they for surface area or surface energy.

Table A39 presents the IGC measurements for a surfactant treated nonwoven, (0.75% surfactant loading), conducted using n-alkanes at 303.15 K and subsequent calculations by the Dorris–Gray method of γ_s^D for different adsorbate surface coverages. The net retention volumes (V_N) were calculated using Eqn A. 1[245]:

$$V_N = jt_R F \left(\frac{T}{273.15}\right) - jt_0 F \left(\frac{T}{273.15}\right) \qquad \textbf{Eqn A. 1}$$

where j stands for the James–Martin pressure drop correction factor, allowing for the pressure drops along the column. F is the carrier gas flow rate, usually given in standard cubic centimetres per minute (sccm). The t_R stands for the retention time of the interacting probe and t_0 stands for the dead time determined via methane injections. Finally, T corresponds to the experiment's temperature and 273.15 K is the reference temperature. The London dispersive surface free energy γ_s^D was calculated following Eqn A. 2 as proposed by Dorris-Gray et al.[337,][338]

$$\gamma_S^D = \frac{1}{4\gamma_{CH_2}} \left(\frac{-\Delta G^{CH_2}}{N \cdot a_{CH_2}}\right)^2 = \frac{1}{4\gamma_{CH_2}} \left(\frac{RT \cdot \ln\left(\frac{V_{N,n+1}}{V_{N,n}}\right)}{N \cdot a_{CH_2}}\right)^2 \qquad \textbf{Eqn A. 2}$$

where N is the Avogadro's constant, $V_{N,n}$ is the retention volume of n-alkanes/alcohols and R and T have the same meaning as in the ideal gas equation. The $a^2 CH_2$ is the surface area of a methylene group which has been assumed by Gray et al. to be 6 $\mathring{A}^2$ and γ_{CH_2} is the surface free energy of the methylene group as given by Eqn A. 3:

$$\gamma_{CH_2} = 35.6 - 0.058\,(T - 20)\, mJm^{-2} \qquad \textbf{Eqn A. 3}$$

The Gibbs free energy of adsorption ΔG_a is related to the net retention volume as follows:

$$\Delta G_a = -R\,T\,\ln V_N + K \qquad \textbf{Eqn A. 4}$$

γ_s^D plots of the calculated RTlnV$_N$ values from IGC measurements for a surfactant treated nonwoven, (with 0.75% surfactant loading) are presented in Figure A. 11. The graph showed lack of linearity especially for the high coverages which stems from the fact that n-alkane feature nonsymmetric peaks caused by not only surface adsorption but dissolution of the probe into the test material and a slow desorption of the test probes.

Table A. 3 IGC measurements for a surfactant treated nonwoven, (0.75% surfactant loading), using a series of n-alkanes at 303.15 K and subsequent calculations by the Dorris–Gray method for different fractional surface coverages using both peak maximum and peak COM methods.

Retention Volume (Vn)				Retention Volume (Vn)			
P.Max	Fractional Surface coverage			_P.COM_	Fractional Surface coverage		
	0.05	0.1	0.2		0.05	0.1	0.2
Heptane	2.5	1.4	1.5	Heptane	6.8	7.7	3.9
Octane	8.3	7.7	7.0	Octane	22.1	21.8	21.7
Nonane	38.8	35.5	33.1	Nonane	67.1	66.2	65.6

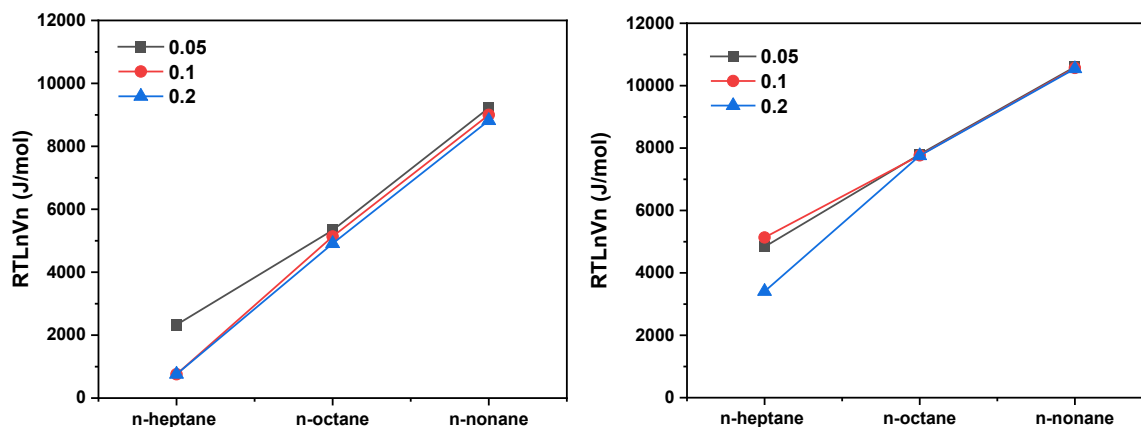| RTLnVn (J/mol)				RTLnVn (J/mol)			
P.Max	Fractional Surface coverage			_P.COM_	Fractional Surface coverage		
	0.05	0.1	0.2		0.05	0.1	0.2
Heptane	2329.5	756.4	756.4	Heptane	4835.1	5134.8	3404.2
Octane	5333.8	5134.8	4911.6	Octane	7799.8	7765.3	7754.9
Nonane	9219.3	8999.5	8817.9	Nonane	10599.7	10566.4	10543.9
slope	3444.9	4121.5	4030.8	**slope**	2882.3	2715.8	3569.4

Figure A. 10.Plot of calculated RTlnV$_N$ values from IGC measurements using n-alkanes for testing surfactant treated nonwoven, (0.75% loading) using peak maximum, (left) and peak COM (right).

Calculated dispersive surface energy values for the surfactant treated nonwoven, (0.75% surfactant loading), using Dorris–Gray method, are presented in Table A. 4. The calculated γ_s^D values appeared exaggerated, > 40 J/m^2. This is believed to be a result of bulk sorption of the probes and a slow desorption phenomenon caused by the dissolution of the n-alkanes into the polyolefin based nonwoven material.

Table A. 4 Calculated dispersive surface energy for surfactant coated nonwoven, (0.75% surfactant loading), using Dorris–Gray method, from measurements at 303.15 K for different fractional surface coverages.

Fractional Surface Coverage (n/nm)	γ_s^D (J/m^2)	
	P.Max	P.COM
	n-Alkanes	n-Alkanes
0.05	**64.9**	**45.4**
0.1	**92.9**	**40.3**
0.2	**88.8**	**69.7**

The effect of temperature and flow rate were investigated to optimise the method. Figure A. 12 shows the IGC chromatograms for heptane measured at different temperatures (left) and at different flow rates (right) on a typical polyolefin nonwoven material. The results show temperature having a greater effect on the elution of test probes as a function of time. As the temperature increased the peaks became wider and the FID signal decreased. This reflected the bulk sorption of these probes which was accelerated by the higher temperatures. Increasing the flow improved peak symmetry and the FID signal increased.
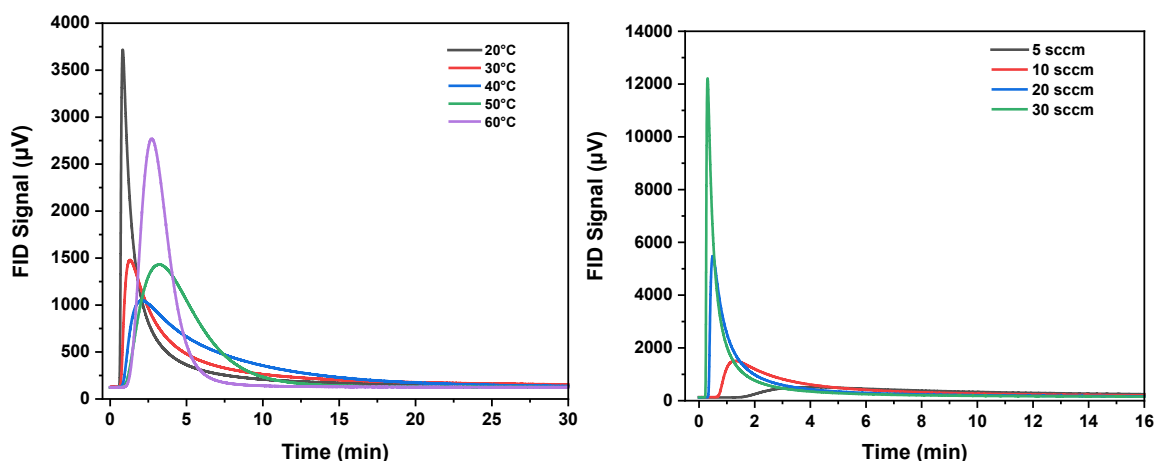

Figure A. 11 The effect of temperature, (left) and flow rate, (right) on the elution chromatograms of heptane, for a PP based nonwoven sample.

Optimum conditions appeared to be 60°C and 30sccm flow rates. These extreme conditions of 60°C temperature and higher flow rates, 30 sccm, produced improved results. The raw data are shown in Figure A. 13. The results demonstrated improved peak symmetry and faster desorption with minimal peak tailing. It appeared that increasing both the temperature and the flow rate produced symmetrical peaks with minimal tailing within reasonable times.
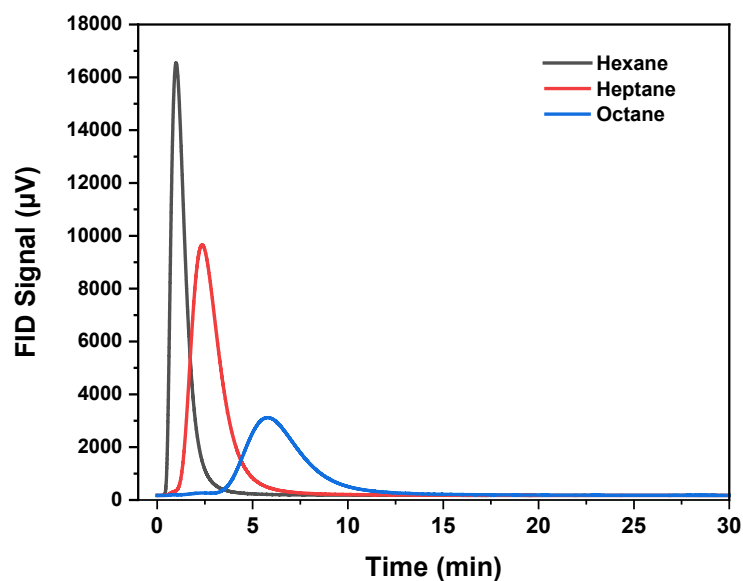
Figure A. 12 Elution chromatograms for a homologues series of n-alkanes measured at 60°C and 30sccm flow rate for PP based nonwoven sample using IGC.

Surface energy measurements of two types of nonwovens were performed with IGC using the standard alkanes method at these optimum conditions. Each column was pre-conditioned for 2 hours at 30°C and 0% RH with helium carrier gas to remove any physiosorbed water. All experiments were carried out at 60°C with 30sccm total flow rate of helium, using methane for dead volume corrections. Samples were run at a series of surface coverages with alkanes. For the analysis, the Dorris and Gray method was employed. The samples measured included a freshly treated surfactant nonwoven and a two-year-old surfactant treated nonwoven and the surfactant free nonwoven control samples. The results shown in Figure A. 14 demonstrated more reasonable γ_s^D values than previously obtained for these materials under normal conditions. There was no significant difference observed between the surfactant treated and untreated controls for either freshly coated surfactant nonwovens samples, or for the aged 2-year-old samples. Plausible explanations for the results are a) the surfactants do not change the surface energy of the nonwoven, (although these do change the surface tension of the liquid coming into contact with the surfactant coated surface, see contact angle result) and b) the method doesn't work because of the extreme conditions used the surfactants could have been lost before their contribution was measured.
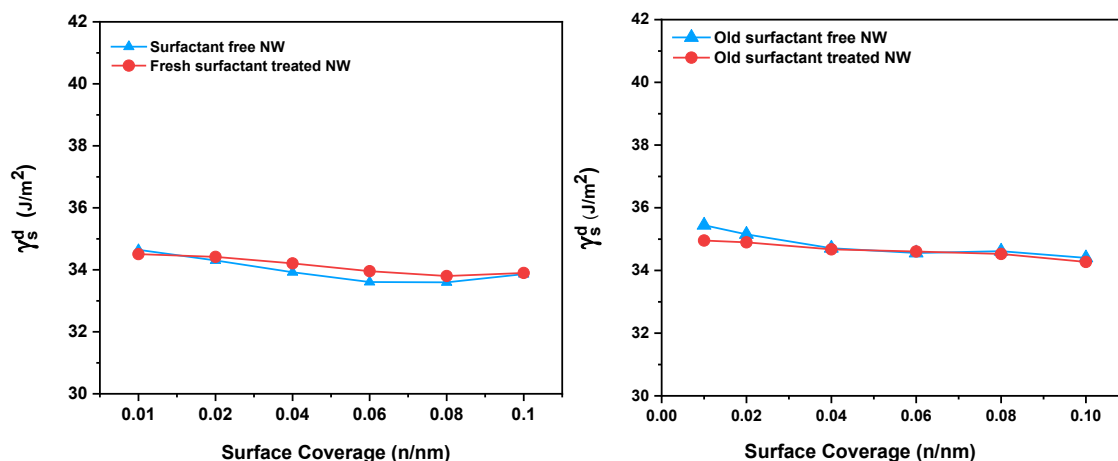
294

Figure A. 13 Dispersive surface energies for top sheet nonwovens, (left) freshly surfactant treated, and (right) aged samples, 2 years old, and their corresponding surfactant free control samples, calculated using Dorris and Gray method and measured with alkanes at optimum conditions.

All the calculations were carried out using iGC Surface Energy Analyzer (SMS, Alperton, UK). The software gives an option to determine the acid-base (short range forces) component of the surface energy of solid materials, γ_s^{ab}. This is sometimes also termed the specific surface energy. Two mono-polar probes, dichloromethane and toluene, were injected to determine this parameter. The specific surface energies were determined based on the van Oss methodology using the Della Volpe scale. More details about these calculations and the corresponding theories can be found in Chapter 3. The results shown in Figure 8. A15 and Figure 8. A16 demonstrated that the dispersive surface energy contributed the most to the total surface energy, which was expected for these polyolefin-based materials. The data shown in Figure 8. A15 and Figure 8. A16 demonstrated that there was no significant difference between the values calculated for the γ_s^{ab} either for the surfactant treated and the surfactant free controls for either freshly coated surfactant nonwovens samples, or the agreed 2-year-old samples.

Surface energy of polymer without surfactants should only contain a dispersion component due to its hydrocarbon base and therefore the calculated values for γ_s^{ab} obtained were unrealistically high for the hydrophobic, (surfactant free) control samples. The expectation was that the presence of the surfactants would introduce a polar component of the surface energy of the polymer, but this has not been observed, not even for the freshly surfactant coated samples and therefore these results could be arguable. The samples used were industrial samples and therefore the surfactant loadings could be very low, (<1% by weight of the nonwoven fabric to which it is applied) so one could argue that IGC is not sensitive enough to detect such low loadings as another explanation for the results.
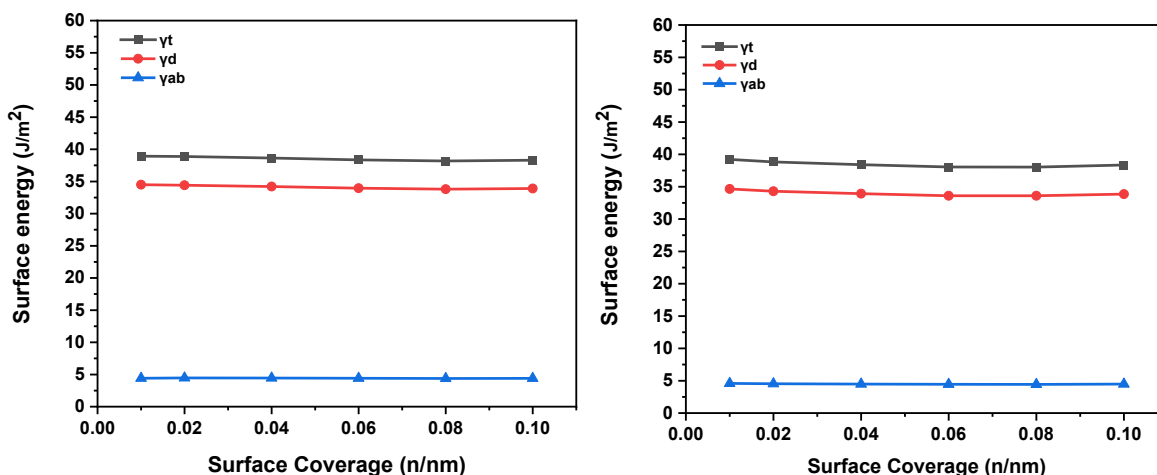
Figure A. 14 Surface energy components of nonwovens, (left) freshly treated with surfactants and (right) the untreated control, measured using toluene and dichloromethane for the acid-base component using the Della Volpe approach and alkanes at optimum conditions.
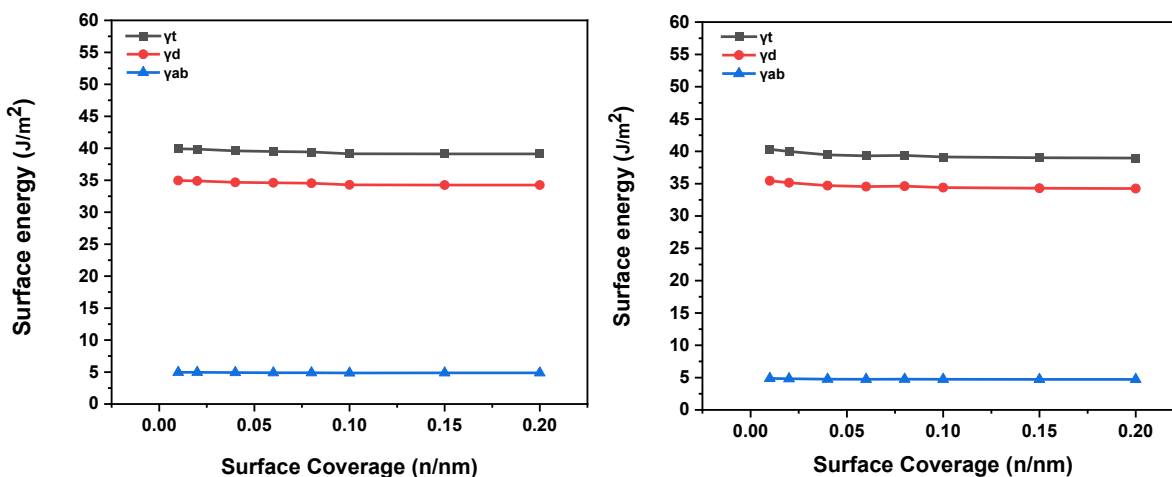

Figure A. 15 Surface energy components of nonwovens, (left) aged samples, 2 years old, with surfactants and (right) the untreated control, measured using toluene and dichloromethane for the acid-base component by the Della Volpe approach and alkanes at optimum conditions.

Conducting measurements at such extreme conditions is not always suitable, for thermally sensitive samples which could be damaged during the analysis. Such elevated conditions also do not represent relevant industrial environmental conditions where these materials are used, and therefore, the behaviour of the industrial nonwovens of interest cannot truly be replicated under these conditions. So, the bulk sorption of the alkanes into the polyolefin nonwoven test material measured with IGC at normal environment conditions and the insensitive measurements for surfactant treated nonwovens at elevated temperatures undermines the measurement of the surface adsorption processes needed for a reliable surface energy determination. This subsequently instigated the need for the development of an alternative method for the analysis of polymeric nonwoven materials using IGC.

296

Appendix B

(Chapter 7 supplementary information)

HDPE-PHP film "in-situ" aging studies

A set of samples, a silicon wafer and an aluminium foil, coated with HDPE-PHP were analysed simultanesly using a typical 0-90-0%RH cycle in a DVS coupled with an ellipsometer. The analysis were repeated 4 times sequentially without removing the samples from the instrument between each run. The results are shown in Figure B. 1, and Table B. 1. The data shows that the amount of water dissolved in the material decreases as a function of time and this suggested a decrease of surfactant amount in the material over time and therefore water dissolution is reduced.
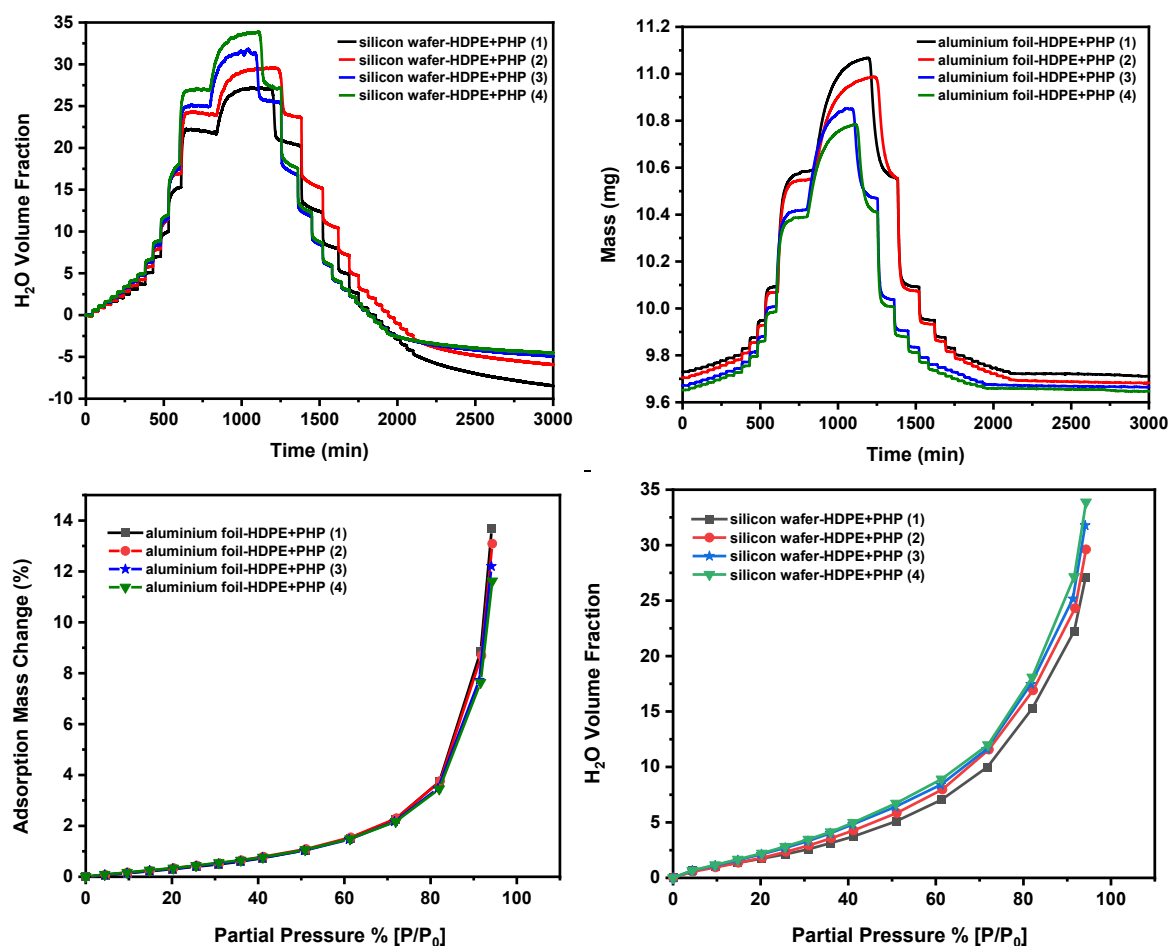

Figure B. 1 Ellipsometry (left) and DVS (right) data of HDPE+PHP films coated onto silicon wafer and aluminium foil and the and corresponding water vapour sorption isotherms (bottom) for each substrate.

Table B. 1 Mass changes of HDPE-PHP films for consecutive experiments of water vapour measurements with a DVS

DVS Run	Initial Mass (mg)	Final Mass (mg)	Mass Difference (µg)	Mass Loss (%)
1	9.7297	9.711	-18.70	0.1922
2	9.7055	9.682	-23.50	0.2421
3	9.6722	9.6644	-7.80	0.0806
4	9.6522	9.6463	-5.90	0.0611
total			-83.40	0.5761

Aging of iPP-PHP films coated onto a silicon wafer and an aluminium foil

A set of samples, a silicon wafer, and an aluminium foil coated with iPP-PHP were analysed simultanesly using a typical 0-90-0%RH cycle in a DVS coupled with an ellipsometer. The analysis were repeated 4 times sequentially without removing the samples from the instrument between each run. The results are shown in Figure B. 2, Table B. 2. The data shows that the amount of water dissolved in the material decreases as a function of time and this suggested a decrease of the amount of surfactant in the material over time.
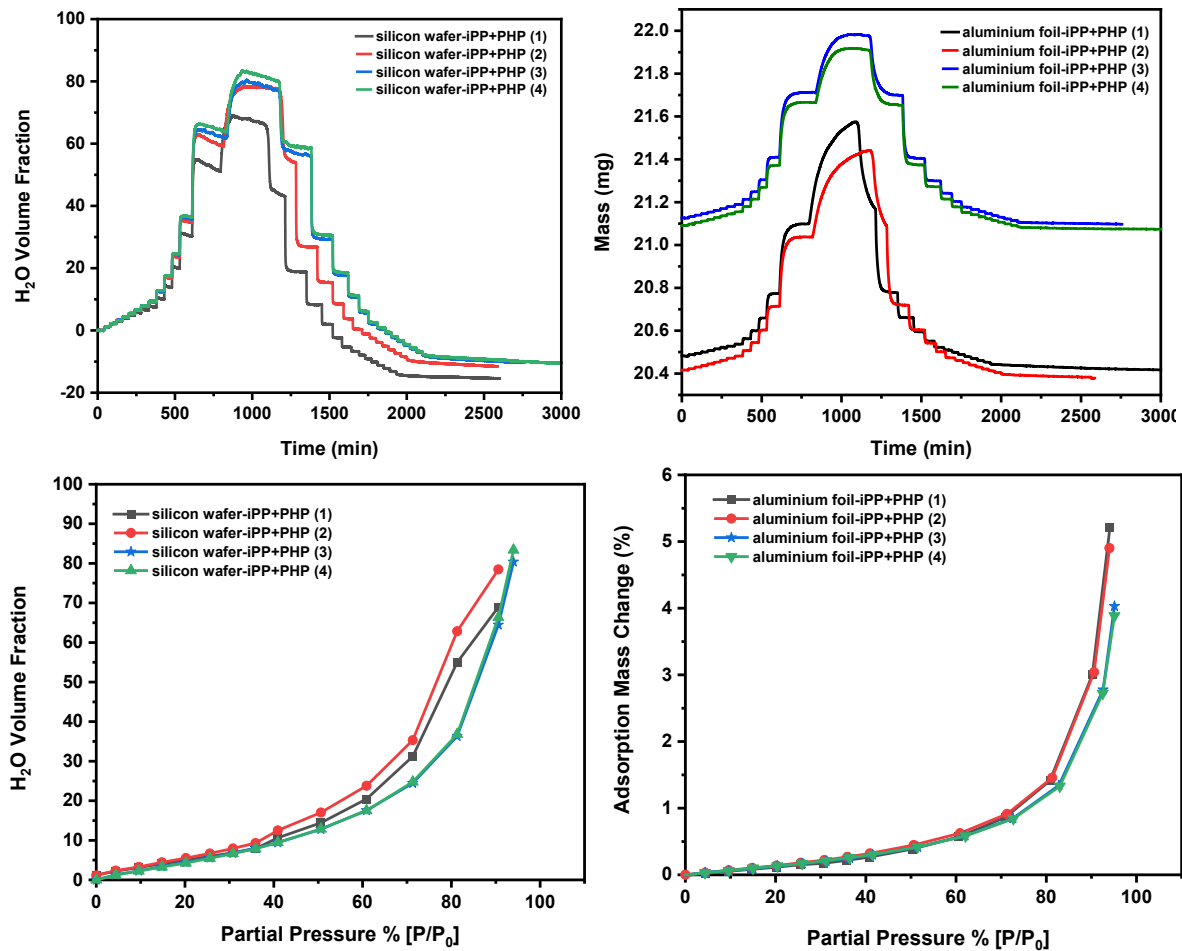

Figure B. 2 Ellipsometry (left) and DVS (right) data of iPP+PHP films coated onto silicon wafer and aluminium foil and the and corresponding water vapour sorption isotherms (bottom) for each substrate.

Table B. 2 Mass changes of iPP-PHP films for consecutive experiments of water vapour measurements with a DVS

DVS Run	Initial Mass (mg)	Final Mass (mg)	Mass Difference (μg)	Mass Loss (%)
1	20.4831	20.4239	-59.20	0.2890
2	20.4162	20.3783	-37.90	0.1860
3	21.1260	21.0990	-27.00	0.1280
4	21.0916	21.0754	-16.20	0.0770
total			592.3	0.6790

Thin film thickness measurements

The film thickness measurements of model substates were performed using both ellipsometry and reflectometry, (Filmetrics®). Comparisons of some of these results are shown in Table B. 3 and Figure B. 3 to Figure B. 6.

Table B. 3 Comparison of ellipsometry and reflectometry results.

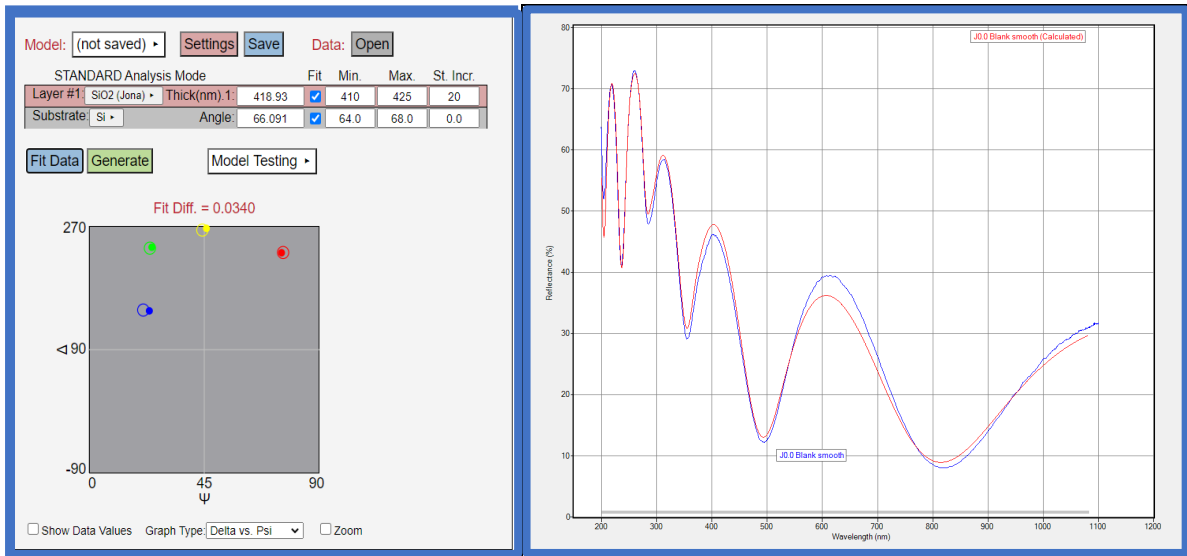| Sample No.	Sample Type	Ellipsometry Thickness (nm)	Fit Difference	Reflectometry Thickness (nm)	Goodness of fit
1	SiO_2 layer	418.93	0.0340	419.7	0.9883
2	LDPE film	18.46	0.0276	517.7	0.6271
3	MDPE film	353.09	0.0189	351.5	0.9868
5	PPi film	41.15	0.0370	59.77	0.9658

Figure B. 3 Comparison between ellipsometry (left) and reflectometry (right) measurements for thickness for SiO$_2$ film on Si substrate, and the reflectance estimated by the model.
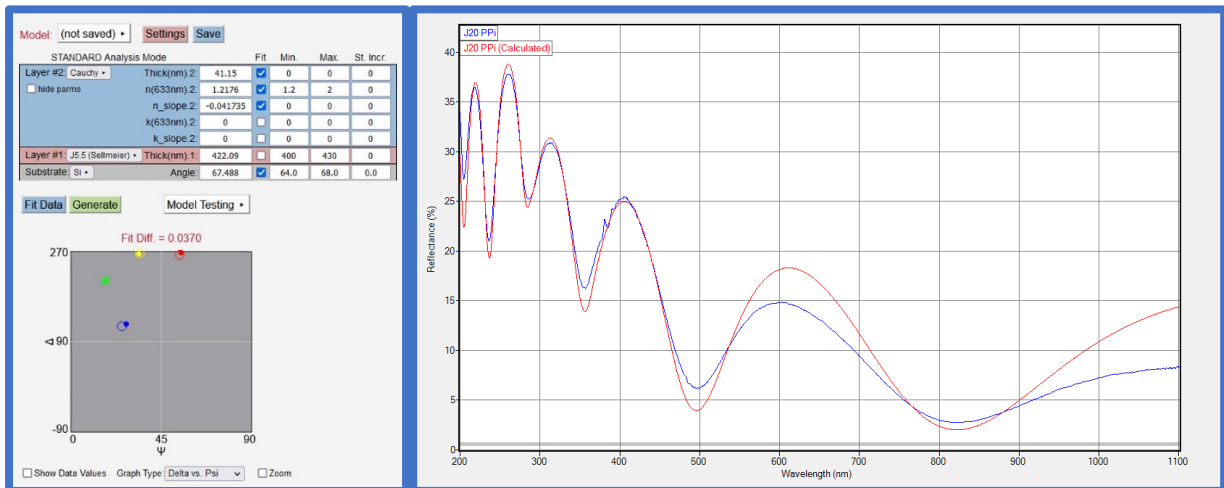

Figure B. 4 Comparison between ellipsometry (left) and reflectometry (right) measurements for thickness for PPi film on Si substrate, and the reflectance estimated by the model.
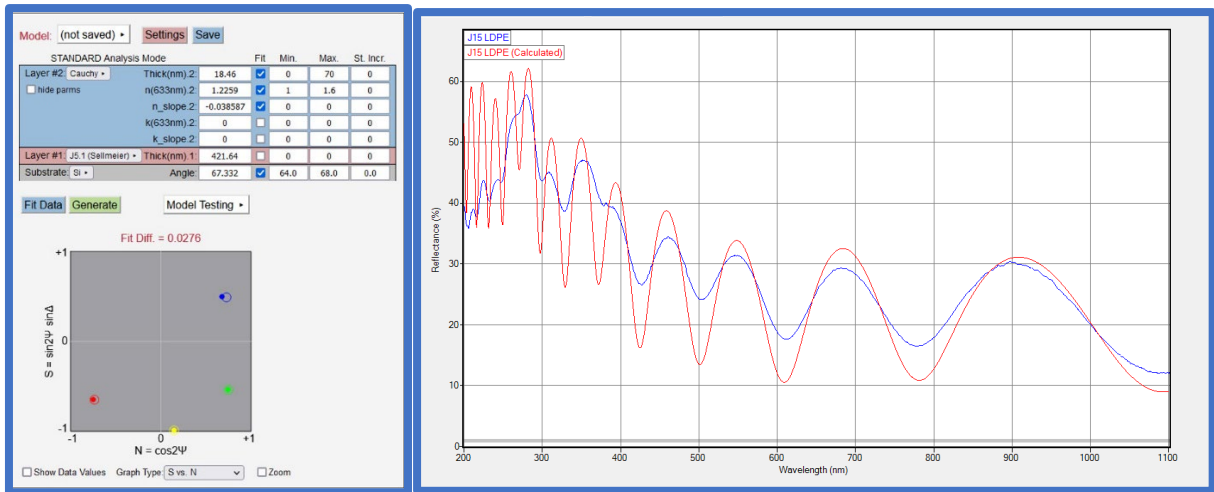
Figure B. 5 Comparison between ellipsometry (left) and reflectometry (right) measurements for thickness for LDPE film on Si substrate, and the reflectance estimated by the model.
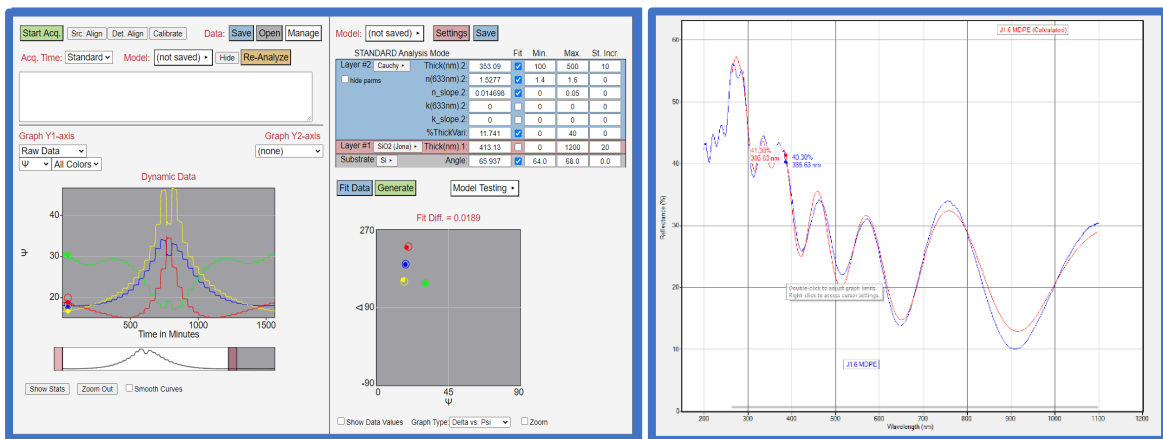

Figure B. 6 Comparison between ellipsometry (left) and reflectometry (right) measurements for thickness for MDPE film on Si substrate, and the reflectance estimated by the model.